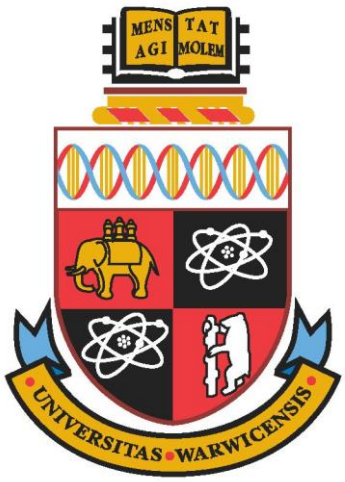

Processing bodies are dynamically localised and associate with multiple organelles throughout the replicative lifespan of the yeast cell

by

Oliver Paul Sinfield

Thesis

for the degree of

Doctor of Philosophy

To

MRC Doctoral Training Partnership, Warwick Medical School, University of Warwick

---

Supervisors: Prof. John E G McCarthy and Prof. Robert Cross

September 2018

Table of Contents

1 Table of Figures

Acknowledgements

Firstly, I would like to thank Professor John McCarthy for the opportunity to perform this work in his laboratory and his assistance and guidance throughout the work. I would also like to thank Professor Robert Cross for his valuable advice, scientific and otherwise, throughout his study.

Special thanks go to the members of the McCarthy Lab at the University of Warwick. Dr Helena Firczuk who has trained me since my initial bachelor's project and taught me all the yeast techniques I know, Dr John Duncan who taught me peaked my interest in microscopy and Dr Mark Walsh for his assistance with image analysis coding. Dr Estelle Dacheux was a continuous source of support in all areas both scientific and personal. Thanks also go to the Warwick Integrative Synthetic Biology Centre for use of their equipment and facilities to conduct this work.

I would like to thank the original designers of the microfluidic chips used in this study. Dr Sandrine Morlot and Gilles Charvin of IGBMC, France, for the use of their unpublished CliC 2 device. Professor Peter Swain and Dr Matthew Crane of Edinburgh University for the designs of the ALCATRAS 2. Dr Weiwei Dang of Baylor College of Medicine and Dr's Lidong Qin and Myeong Chan Jo of Houston Methodist Hospital for the designs of the HYAA device. Finally, Dr Matthias Heinemann of the University of Groningen who provided the designed from Lee et. Al.

I would also like to thank Dr Marco Polin and Dr Raphael Jeanneret of the University of Warwick Physics department who produced the microfluidic moulds for this study.

Finally, I would like to thank the administration team for the MRC DTP, especially Samantha Plumb for her assistance during my write up period, and to the MRC and University of Warwick for funding this work.

Declaration

This thesis is submitted to the University of Warwick in support of my application for the degree of Doctor of Philosophy. It has been composed by myself and has not been submitted in any previous application for any degree.

The work presented (including data generated and data analysis) was carried out by the author.

Abbreviations

RNA	ribonucleic acid
mRNA	messenger ribonucleic acid
mRNP	messenger ribonucleoprotein
GTP	Guanosine triphosphate
poly-A	poly-adenosine
DNA	Deoxyribonucleic acid
ER	endoplasmic reticulum
tRNA	Transfer ribonucleic acid
GDP	Guanosine diphosphate
LLPS	liquid liquid phase separation
NMD	nonsense mediated decay
NSD	non-stop decay
NGD	No-go decay
PB	processing body
SG	stress granule
RLS	replicative lifespan
CLS	chronological lifespan
rDNA	ribosomal DNA
ERC	Extrachromosomal rDNA circles
DR	dietary restriction
TOR	target of rapamycin
PKA	protein kinase A
PDMS	polydimethylsiloxane
PCC	Pearson's correlation coefficient
MCC	Manders' correlation coefficient

Abstract

Processing bodies (p-bodies) are cytoplasmic messenger ribonucleoprotein granules containing components of the mRNA degradation machinery, that form during stress conditions in the budding yeast *Saccharomyces cerevisiae*. P-bodies are conserved in eukaryotes and are related to other mRNP granules such as stress granules and neuronal granules. mRNP granules and their components self-assemble through a process of liquid-liquid phase separation, facilitated by protein-protein interaction by low complexity regions. Errors in this assembly process can cause a build-up of aggregated protein and have been implicated in the pathology of human neurodegenerative diseases such as amyotrophic lateral sclerosis. The exact role of p-bodies in normal cellular function is not known, but p-bodies are induced in conditions of stress, and can store mRNA that later re-enters translation, leading to the theory that they are sites of mRNA storage. A contrasting theory suggests them as sites of mRNA decay, due to the presence of deadenylation, decapping and exonuclease complexes within p-bodies. In this work, time-lapse fluorescence microscopy, using optimised high brightness, low photobleaching fluorescent protein fusions, was used to allow long term imaging of p-body localisation throughout the cell cycle of *S. cerevisiae*. Imaging was combined with microfluidic dissection of mother and daughter cells, to track single mother cells over their entire replicative lifespan (RLS) while continuing to monitor p body localisation. P-bodies were found to be localised in proximity to multiple different organelles with changes to localisation occurring through the cell cycle. Advanced replicative aged altered the profile of p-body localisation causing p-bodies to localise heavily to the mitochondria. P-bodies were also found to be inherited by daughter cells in a process dependent on the mRNA transport machinery and the p-body protein Dcp1. This inheritance was multigenerational with a single p-body moving between multiple daughter cells and was not lost in cells of advanced replicative age.

2 Introduction

2.1 Foreword

Through all the advances in modern medicine over the past century, we now live longer and more prosperous lives that we ever have before. The advent of germ theory, modern hygiene standards and powerful interventions such as antibiotics, have made the infectious diseases of the past largely insignificant to mortality statistics in the developed world. But with this newfound longevity previously unrecognised ailments have arisen, caused in part by our own body's lack or preparedness for life beyond historical limits. The most widely publicised of these conditions are the cancers, diseased of uncontrolled cellular proliferation triggered by the build-up of genetic mutations and therefore exacerbated in their prevalence by virtue of our lengthening lifespans. Large amounts of research investment have gone into understanding the mechanisms of cancer development and pathogenesis over the last few decades. This has led to a significant reduction in the morbidity and mortality caused by cancers, due to successful interventions and early screening programmes.

While cancers affect all parts of the body, the recent shift in media and academic attention has been towards the brain, with projects such as the BRAIN initiative in the US and the Human Brain Project in Europe hoping to significantly advance our understanding of the human brain. What, one might ask, is the point of living to our 100s, curing our various physical maladies along the way, only to lose our identities long before that due to neurodegeneration of the brain? Understanding the pathology of neurodegenerative diseases, such as Alzheimer's and Parkinson's disease, is therefore integral to the improvement of quality of life in an ever ageing population.

As well as the focus on this new avenue of research, the age-linked conditions, neurodegenerative diseases of the general population also benefit from the new-found attention due to their reported similarities at the molecular level. For example, many neurodegenerative diseases, both age-related and not, show an increase in the prevalence of aberrant protein aggregation. mRNP granules are a key element. These granules are made up of various combinations of mRNA binding and other proteins, as well as ribonucleic acids, and have been found to be over-represented in diseased cells in conditions such as Amyotrophic Lateral Sclerosis (ALS). One possible model of disease pathology involves the

sequestration of mRNA and proteins within these granules leading to changes in gene expression and cellular function that ultimately lead to the death of the cell. mRNP granules have also been implicated in a range of cancers, highlighting their potential as agents of disease.

Although clearly an important factor in a range of statistically important diseases, the structure and function of mRNP granules has only recently started to become clearer, and much still remains unexplained. Here, I describe new aspects of the dynamics of mRNP granules in the yeast *S. cerevisiae*.

2.2 The mRNA life cycle in yeast

The creation and utilisation of mRNA plays a fundamental role in the central dogma of molecular biology, in which DNA is transcribed to mRNA which is subsequently translated into proteins.

2.2.1 Transcription and nuclear processing of mRNA

In eukaryotes, mRNA is created in the nucleus in a process called transcription, in which RNA polymerase II catalyses the polymerisation of ribonucleotides complementary to the sequence of DNA being transcribed to create a single stranded RNA molecule. This process is facilitated by proteins known as transcription factors. Once sequence transcription is complete, the RNA undergoes a series nuclear processing events (T. I. Lee & Young, 2000).

A 5′ cap consisting of a 7′methylguanosine is added at the 5′ end of the mRNA molecule, which stabilises the mRNA and prevents exonuclease degradation. The capping process occurs while transcriptional elongation is still taking place and involves 3 steps. The exposed triphosphate of the first nucleotide in the RNA sequence is hydrolysed by RNA triphosphatase and a guanosine monophosphate nucleotide derived form GTP is fused to the exposed phosphate through a 5′-5′ triphosphate bond by mRNA guanylyl transferase. Finally, the N7 position nitrogen of the guanosine nucleotide is methylated by mRNA (guanine-N7-)-methyltransferase (Fong, 2001). Non-coding regions of the RNA, called introns, are removed in a process called splicing carried out by a ribonucleoprotein complex known as the spliceosome. The spliceosome contains catalytically active RNA that recognises intronic sequences within the mRNA and catalyses their removal. As with 5′ capping this

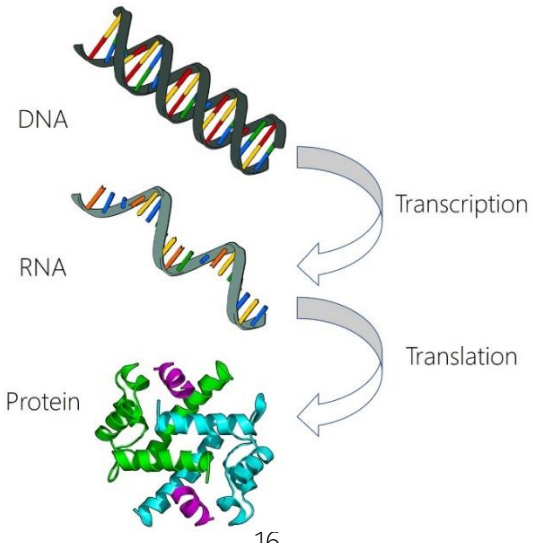

Figure 1: The central dogma of molecular biology, DNA is transcribed to mRNA which is translated into protein.

process happens co-transcriptionally, while the mRNA is still attached to RNA polymerase 2 (Görnemann et al., 2011).

Once transcription of the sequence is complete, a poly-A tail, consisting solely of adenosine nucleotides is attached completing the maturation of the mRNA. Almost all coding mRNAs in yeast contain a poly-A tail comprising on average 70 poly-adenosines at the 3' end of the sequence. Poly-A polymerases add these adenosine monophosphate nucleotides after mRNA has been cleaved at the 3' end in a processes that is instigated by the cis regulatory elements in the DNA sequence (Ares & Proudfoot, 2005; Bentley, 1999).

mRNA is exported from the nucleus where it can be recognised by components of the mRNA translation machinery and translated to produce proteins. The export process is controlled by the nuclear pore complex (NPC) made up of nucleoporin proteins that form a channel in the nuclear membrane (C. Smith et al., 2015a). To facilitate mRNA export, mRNAs combine with export factors to form ribonucleoproteins that then translocate across the NPC into the cytoplasm. These mRNPs can be remodelled to regulate directionality and nuclear export rate (C. Smith et al., 2015b).

2.2.2 Localisation of mRNA

Translation can occur freely in the cytoplasm or can be localised to specific areas of the cytoplasm or compartmentalised in specific organelles. The advantage of limiting translation to localised positions within the cell are numerous; for example, localised translation can be used to introduce polarity and facilitate polarised cell growth. It could also be used to facilitate asymmetric cell division as in budding yeast. Other examples of localised translation include production of protein involved in neuronal processes and daughter cell specific transcription inhibition (Niessing et al., 2018).

To achieve localised translation, mRNAs must be transported to the required destination by an mRNA transport system or linked to an existing organelle transport system by adapters. In budding yeast, examples of both mechanisms have been observed. Direct transport of mRNA in yeast is facilitated by myosin motor proteins, specifically Myo4 which translocates along actin filaments (Bohl, 2000; Rodriguez et al., 2006). The best-known example

of this process is that of the Ash1 mRNA which encodes a transcription inhibitor that

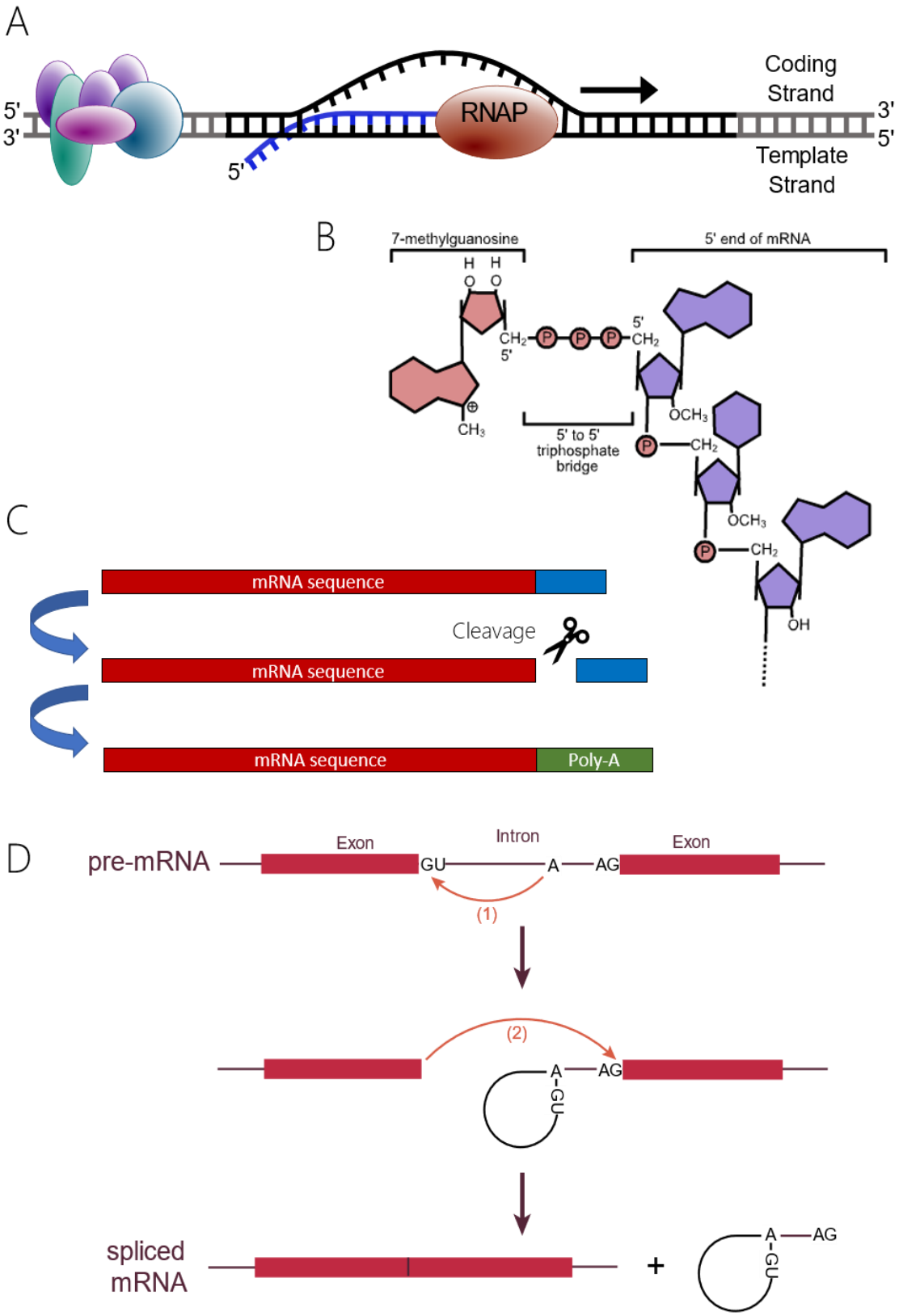

Figure 2: The main processes involved in transcription. A - The elongation of the mRNA transcript by RNA polymerase II. B – Addition of the 5' methyl guanosine cap. C – Splicing of introns in the mRNA. D cleavage of the 3' region and addition of a Poly-A tail. Reproduced under Creative commons licence, see Appendix for details.

prevents mating type switching when present. Ash1 is trafficked to the tip of the emerging bud during cell division and prevents mating type switching in the daughter cell by localised translation, while the mother cell retains the ability to switch mating types (Bobola et al., 1996). ASH1 mRNA has several localisation elements contained in both the coding region and 3' untranslated region (Bohl, 2000). These regions are recognised by the mRNA binding protein She2 in the nucleus, with a relatively low affinity that is enhanced by the addition of a second protein, She3, upon nuclear export. She3 binds both She2 and the mRNA to stabilise the interaction and increase its specificity (Edelmann et al., 2017; Marisa Müller et al., 2011). She3 also binds constitutively to the myosin motor protein Myo4. Together the 3 proteins form a messenger ribonucleoprotein complex capable of transport along actin filaments (Bohl, 2000; M. Müller et al., 2007).

She2 has also been shown to bind to the membrane of the endoplasmic reticulum, specifically the cortical ER which in yeast is transported to the bud tip. The observation that cortical ER transport is dependent on the Myo4/She3 complex revealed an associated role in mRNA transport (Genz et al., 2013; Schmid et al., 2006). Multiple mRNAs have been shown to be co-transported with the cortical ER into the budding daughter cell with all these mRNAs capable of being bound by She2 (Fundakowski et al., 2012). Although the specific mechanism of ER binding by She2 is not known the association with the ER has been shown to be specific to the ER and no other organelle membranes (Genz et al., 2013).

In order to prevent translation of mRNA during transportation, the She2/She3/Myo4 mRNP is complexed with translation inhibitors such as the p-body component Dhh1 (Zhang et al., 2017). Release on inhibition by the local environment at the destination then allows translation initiation to take place.

Translation can also occur on the outer membrane of the ER. Translation on ER membranes mainly produces membrane proteins or those destined for secretion (Shao & Hegde, 2011). Translation begins in the cytoplasm, after which the emergence of a targeting domain on the extending amino-acid sequence triggers a pause in translation and relocation of the ribosome to the ER membrane. The ribosome is bound by a membrane complex called the translocon and insertion of membrane proteins then occurs co-translationally.

2.2.3 Translation of mRNA

Translation of mRNA to produce proteins is a multistep process. The major conserved proteins in eukaryotic translation are outlined below. Translation begins with initiation, the formation of 80S ribosomes capable of elongating amino acid sequences, via the joining of a 48S initiation complex to a 60S ribosomal subunit (Jackson et al., 2010). The 5′ cap of the mRNA is initially bound by the cytoplasmic cap binding complex, composed of initiation factors 4E, 4G and 4A. The cap binding complex works to unwind secondary structures in the 5′ region of the mRNA and create a circular mRNA structure through binding to the poly-A binding protein associated with the 3′ poly-A region. The cap-binding complex associated mRNA is then bound by the 43S pre-initiation complex of the 40S ribosome and ternary complex of eIF2-GTP Met-tRNA^{met} to form a 48S initiation complex before scanning the mRNA to identify a start codon.

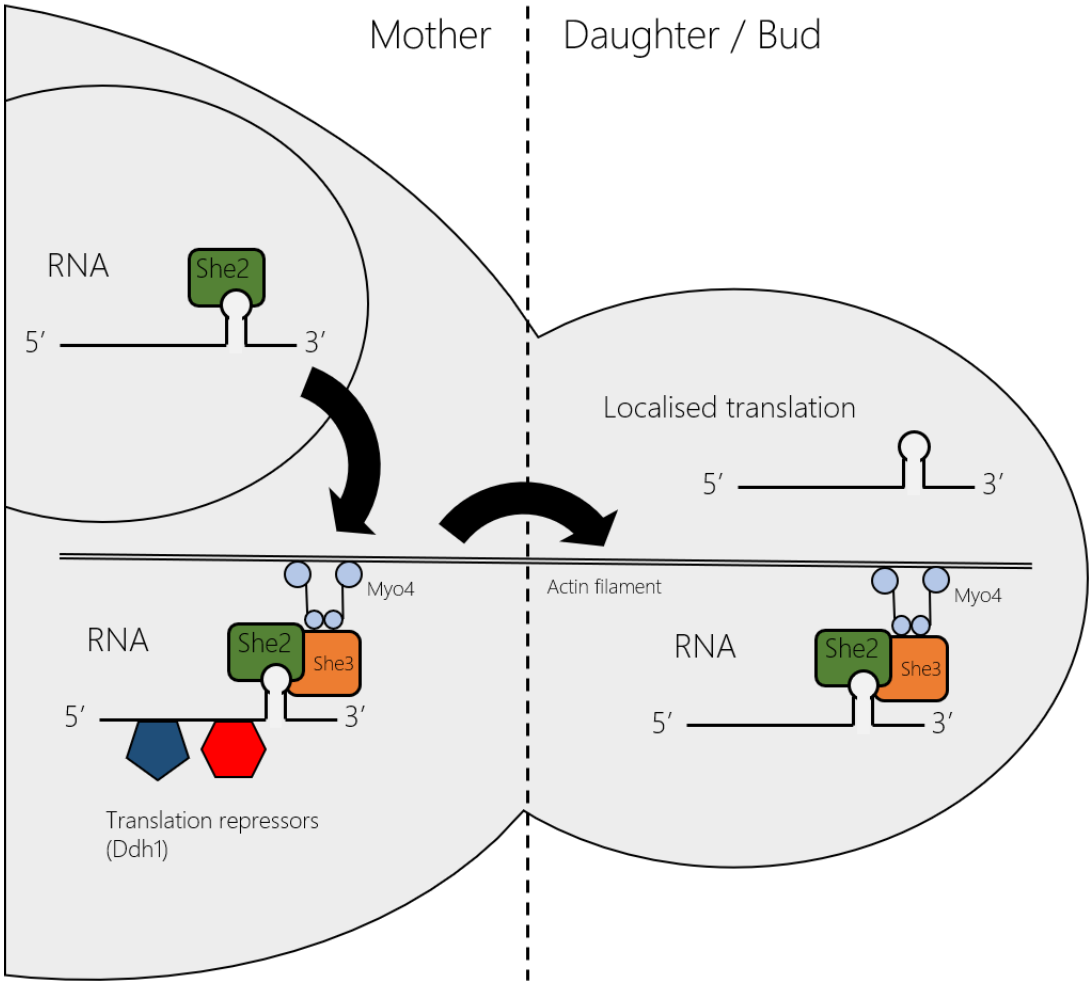

Figure 3: mRNA is transported through the cell by the "locasome" complex, made up of She2, She3 and Myo4 as well as translational repressors. She2 and She3 proteins link the mRNA to the actin cytoskeleton via the class V myosin motor protein Myo4. mRNAs are transported from mother to daughter cells to enable bud localised translation.

Upon recognition of the start codon at the P-site of the 40S ribosome, the GTP bound to

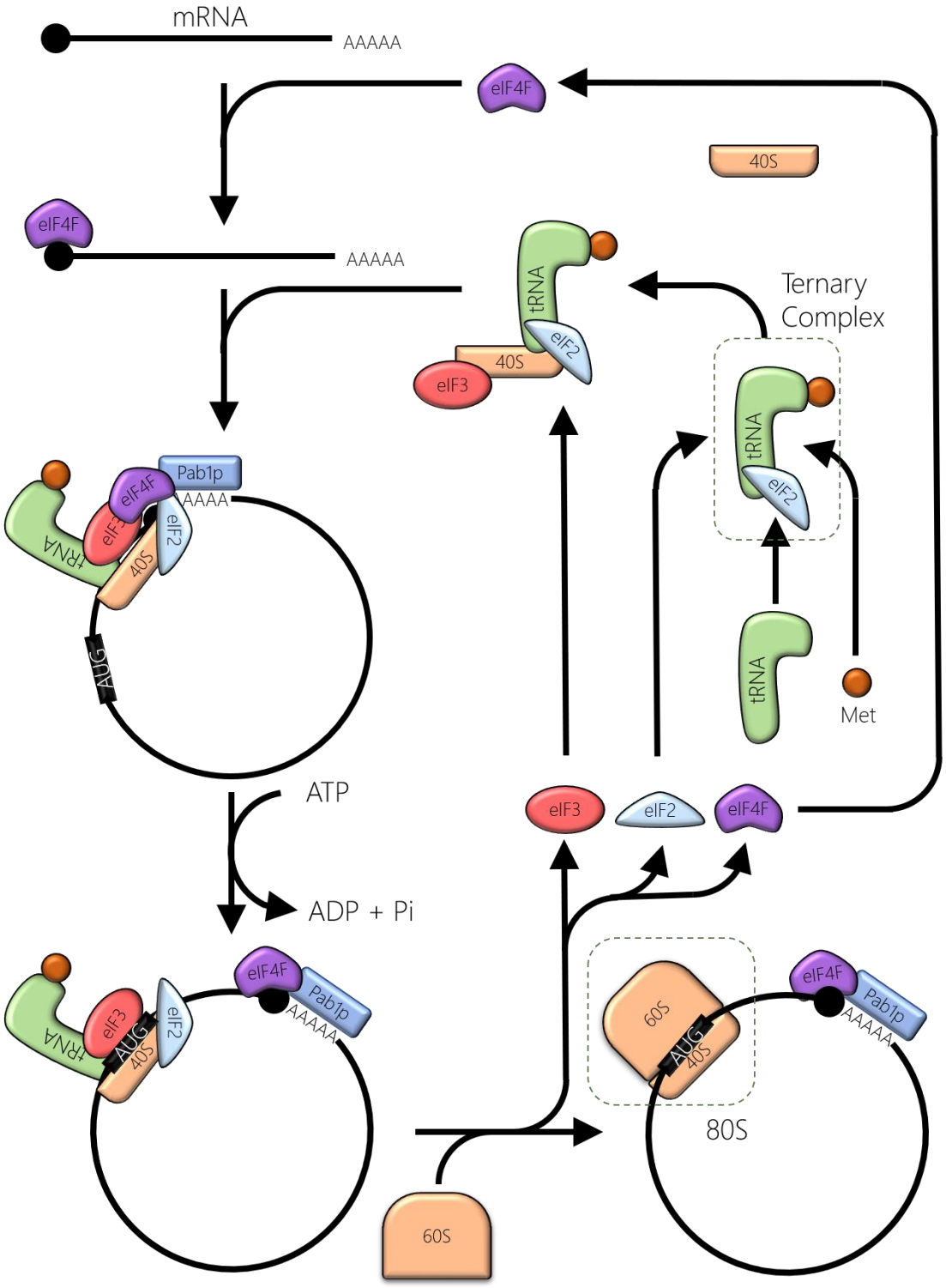

Figure 4: The initiation of Eukaryotic translation. The mRNA 5' cap is initially bound by the cap binding complex eIF4F, followed by mRNA circularisation by Pab1 binding to the cap complex and poly-A tail. The 48S complex associated bind to the cap complex and scans the mRNA for the start codon, after which the 60S subunit binds to form an elongation competent 80S ribosome.

eIF2 is hydrolysed to GDP, releasing it, along with the other initiation factors (Dever et al., 2016; Wilson et al., 2000).

To begin elongation of the peptide, the A site of the ribosome is populated with a eEF1A-GTP-aminoacyl-tRNA complementary to that of the mRNA sequence, and the eEF1A-GTP is hydrolysed to eEF1A-GDP. A peptide bond is formed between the two amino acids and movement of the ribosome shifts acceptor ends of these tRNAs into the E and P sites respectively. Hydrolysis of eEF2-GTP provides the energy for movement of the anticodon ends into the same sites. The E site tRNA is released and a new eIF1A-GTP-aminoacyl-tRNA populates the A site to begin the process again. Eventually a stop (or nonsense) codon is reached and translation termination is initiated (Dever et al., 2016).

Once the A site of the ribosome is populated with a stop codon, eRF1, a functional tRNA mimic binds the ribosome along with eRF3-GTP. Hydrolysis of the GTP of eRF3-GTP causes its dissociation and accelerates peptide release from the ribosome (Eyler et al., 2013). The ATPase Rli1 then binds eRF1 and catalyses the hydrolysis of the peptide-tRNA bond to release the nascent polypeptide. Further hydrolysis by Rli1 releases the 60S subunit from the mRNA and further ribosome associated proteins promote the dissociated of the 40S unit. This release process is known as recycling and these ribosomal subunits can then re-enter translation using the same or new mRNAs.

2.2.4 mRNA Decay in Yeast

A key stage in the control of gene expression in *Saccharomyces cerevisiae*, as in other eukaryotic cells, is the turnover of cytoplasmic mRNA. mRNA may be subject to decay due to regulatory processes influencing the decay of particular mRNA species, or due to quality control mechanisms identifying aberrant sequences and targeting them for decay. The multiple pathways for mRNA decay in yeast have been elucidated in numerous studies and proteins and mechanisms involved in mRNA degradation have been identified. In yeast, two general mRNA decay pathways are present and act on cytoplasmic mRNA. Both pathways begin with the process of deadenylation, in which the 3' poly(A) tail of the mRNA is shortened or removed by a deadenylation complex consisting of Pan2/Pan3 (Brown & Sachs, 1998) or Ccr4/Not/Pop2 (M Tucker et al., 2001). Following deadenylation, mRNA can

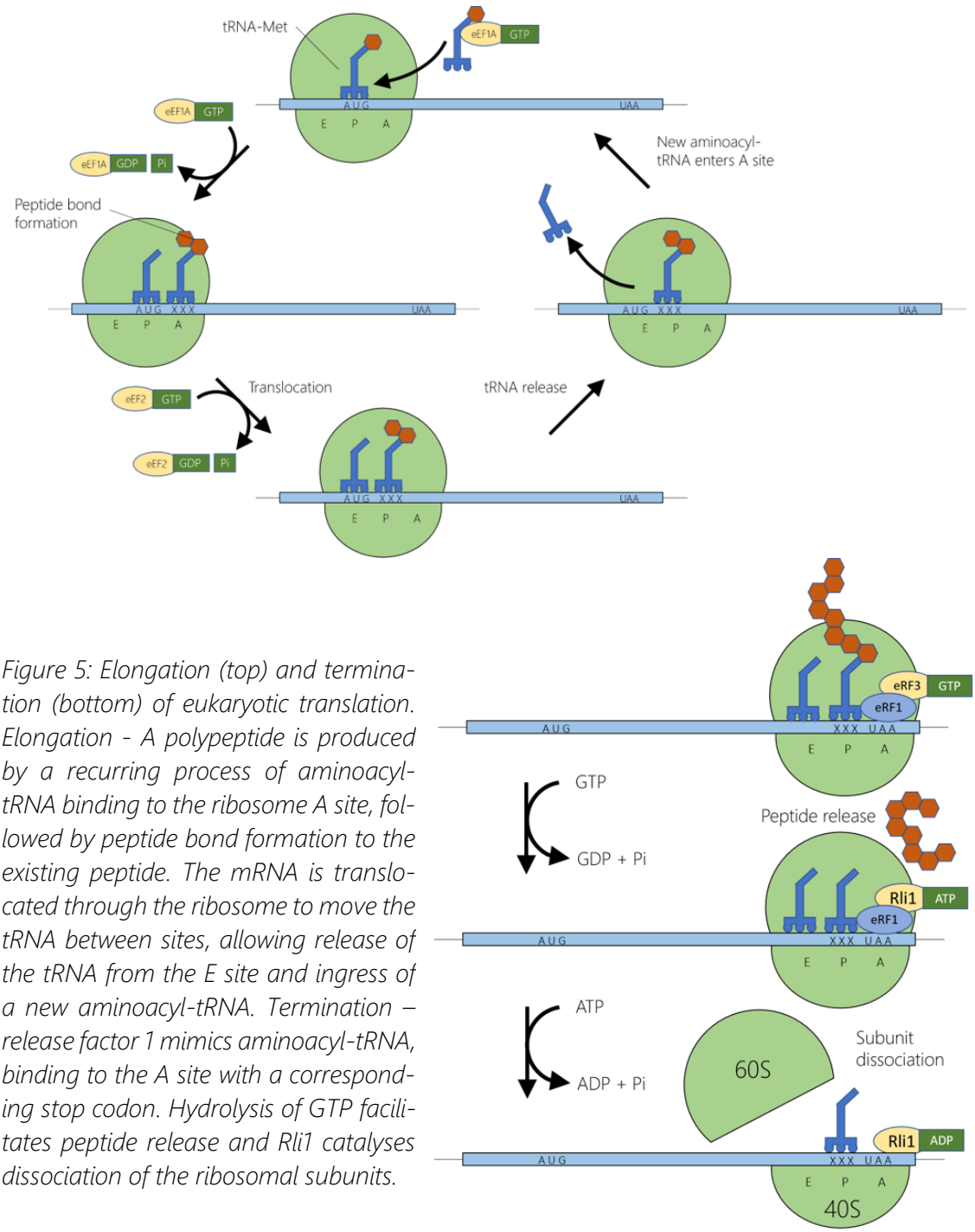

Figure 5: Elongation (top) and termination (bottom) of eukaryotic translation. Elongation - A polypeptide is produced by a recurring process of aminoacyl-tRNA binding to the ribosome A site, followed by peptide bond formation to the existing peptide. The mRNA is translocated through the ribosome to move the tRNA between sites, allowing release of the tRNA from the E site and ingress of a new aminoacyl-tRNA. Termination – release factor 1 mimics aminoacyl-tRNA, binding to the A site with a corresponding stop codon. Hydrolysis of GTP facilitates peptide release and Rli1 catalyses dissociation of the ribosomal subunits.

undergo either 3′ to 5′ exonuclease degradation by the exosome (J. S. J. Anderson & Parker, 1998) or decapping by the decapping complex consisting of Dcp1/Dcp2 followed by 5′ – 3′ exonuclease degradation by Xrn1 (Travis Dunckley & Parker, 1999; Hsu & Stevens, 1993; Kenna et al., 1993; D Muhlrad et al., 1995; Denise Muhlrad & Parker, 1994; E. Van Dijk et al., 2002). The exosome is also capable of endonuclease activity, although the mapping of endonuclease sites in *S. cerevisiae* to mRNA sequences showed that very few are

degraded in this way (Parker, 2012).

Decapping followed by degradation by Xrn1 is thought to be the major pathway for mRNA degradation in yeast due to both observations of mutant strains and direct measurement of degradation rates. Mutations in the 5′-3′ exonuclease or decapping factors show significant changed in mRNA decay rates compared with mutants in the 3′-5′ pathway (Beelman et al., 1996; X. He & Moore, 2005) indicating that the decapping pathway may influence the degradation of a greater volume of mRNA. Mutations in the decapping proteins also cause severe growth restrictions and are lethal in some strains of yeast (Beelman et al., 1996; Travis Dunckley & Parker, 1999; Giaever et al., 2002). Computation modelling of the degradation pathways also implied that deadenylation had the largest influence on mRNA levels and changing the rate of deadenylation had a larger effect on levels than changing the activity of the 3′-5′ exonuclease pathway (Cao & Parker, 2001).

For the non-standard degradation of mRNA, for example in cases of aberrant mRNA sequences, yeast also possess quality control mechanisms capable of acting independently of the usual degradation pathways that allow specific targeting and degradation of these mRNAs. These pathways can act by bypassing the usual restriction of deadenylation through deadenylation-independent decapping, such as in nonsense-mediated decay, or through rapid 3′-5′ exonuclease (non-stop decay) or endonuclease cleavage (no-go decay) of the mRNA (Doma & Parker, 2006, 2007; D Muhlrad et al., 1994; Van Hoof et al., 2002).

2.2.4.1 As deadenylation, decapping and Xrn1 degradation factors have been shown to accumulate in cytoplasmic p-bodies, this pathway is explored further below.

Deadenylation

Deadenylation is the process of removing adenine nucleobases from the 3′ UTR of an mRNA. This process is carried out by 3′ – 5′ exonucleases known as deadenylases with the Ccr4/Pop2/Not1 complex being the major yeast deadenylase (M Tucker et al., 2001). Ccr4 has been shown to be the catalytically active subunit of this complex (Goldstrohm et al., 2007) with Pop2 promoting Ccr4 activity, but still retaining an exonuclease activity, demonstrated in vitro, that may be active under certain conditions (Thore et al., 2003; Viswanathan

et al., 2004). The Not proteins may function in adapting the complex to different mRNAs, as mutations in these proteins can affect the deadenylation of specific subsets of mRNA (Morgan Tucker et al., 2002). A secondary deadenylase complex consisting of Pan2, the catalytic subunit, and Pan3, thought to bind the poly-A tail region via a zinc finger domain (Schäfer et al., 2014) is also present in yeast. This complex is promoted by the poly-A binding protein, Pab1 (Boeck et al., 1996), which also inhibits Ccr4 activity, and may be responsible for the initial shortening of exposed poly-A tails bound to Pab1, as deletion mutants of Pan2 lead to longer poly-A tails (Brown & Sachs, 1998). A partial redundancy exists between these 2 deadenylase complexes, as deletion of either does not lead to fatal phenotypes, but growth defects in which growth rate is limited. Pan2 can continue past its initial 25 nucleotide region in a Ccr4 deletion mutant but arrests at around 20-25 remaining adenine nucleotides. No further deadenylases are known and none are likely to exist given

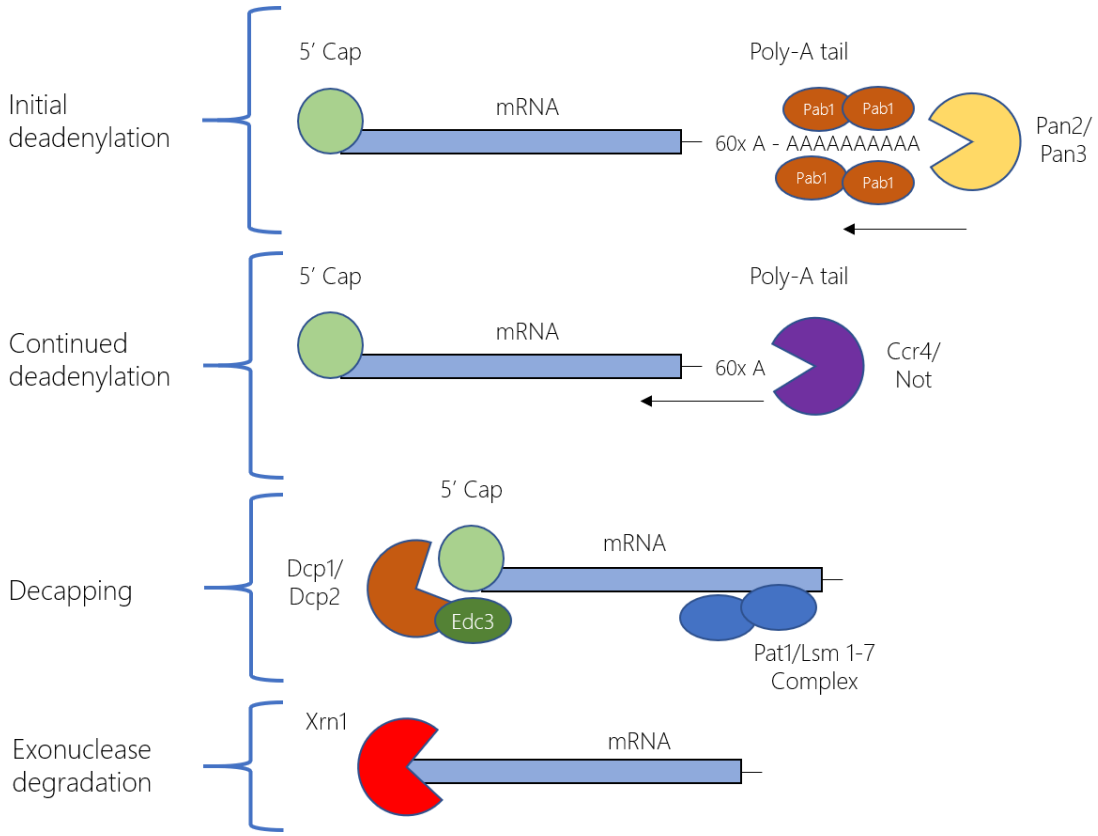

Figure 6: Simplified progression of mRNA decay in budding yeast and eukaryotes. The Pan2/Pan3 complex is responsible for initial deadenylation, followed by continued deadenylation by the Ccr4/Not1 complex. Decapping proteins Dcp1 and Dcp2 catalyse the removal of the 5′ mRNA cap, in a process enhanced by Edc3. Finally, Xrn1 exonuclease activity degraded the exposed 5′ mRNA in a 5′ – 3′ direction.

that a double deletion of Ccr4 and Pan2 results in the loss of deadenylation activity (M Tucker et al., 2001).

Regulation of deadenylation rate has been shown to occur via three general mechanisms. First, as previously mentioned, the binding of Pab1 to mRNA promotes Pan2 activity as Pab1 plays an important part in translation initiation through the binding of eiF4G. There is therefore an intrinsic link between translation and degradation. Many of the mutations and events in translation that affect degradation could be explained by changes in the binding of Pab1 to the Poly-A tail, causing a decrease in Pan2 activity and an increase in Ccr4 activity leading to a greater overall rate of deadenylation (Parker, 2012). Second, translation termination also impacts deadenylation rates, possibly through the direct interaction of eRF3 with Pab1 (Cosson et al., 2002) as inhibiting this interaction leads to changes in deadenylation (Kobayashi et al., 2004). Deadenylation can also be influenced by external environmental factors, although current knowledge in this area is limited. Deadenylation reduces in response to stress (Hilgers et al., 2006), most likely to compensate for the concurrent inhibition of translation initiation and maintain required mRNA levels. Although translation initiation complexes and other mRNPs can be packaged in cytoplasmic granules (see below) during stress events, and Ccr4 has been shown to localise to one such granule, the p-body, this process is not necessary for the general reduction in deadenylase activity. Cycloheximide treatment, which inhibits granule formation, has no effect on the inhibition of deadenylation during stress. Deadenylation can also be influenced by the kinases Pkh1 and Pkh2, which are also regulators of p-body formation (G. Luo et al., 2011). These kinases are activated by sphingolipids, important signalling molecules, that can also influence p-body formation (Cowart et al., 2010). Finally, deadenylation can be influenced by the mRNA structure. The sequence of mRNA can influence its secondary structure by creating stem loops and other structures that can inhibit or enhance the binding of mRNA binding proteins such as Pab1. Deadenylation is particularly susceptible to 3′ UTR structures that recruit other mRNA binding proteins. Puf5, a member of the Puf family of 3′ UTR binding proteins, has been shown to recruit the Ccr4 deadenylase complex through the direct biding of Pop2 (Goldstrohm et al., 2006, 2007). Other mRNA binding proteins such as the helicase Dhh1 also influence Ccr4 recruitment, and it has recently been shown that transcripts

bound by Ccr4/Dhh1 (Dhh1 again being a p-body component) during normal growth are subject to regulation during starvation (J. E. Miller et al., 2017).

To summarise, deadenylation is a two-stage process in which the Pan2/Pan3 complex first shortens the initial nucleotides and then has its activity is promoted by the presence of Pab1, introducing a point of regulation. The Ccr4/Not complex removes the remaining poly-A nucleotides not bound by Pab1 triggering either the decapping process or 3′-5′ degradation by the exosome. Multiple factors affect Ccr4/Not complex binding to the mRNA, and sequence specific features can regulation the specific decay rates of individual mRNAs. This process can be globally regulated by environmental factors with some environmental factors such as nutrient starvation having specific effects on distinct mRNA populations.

Decapping

2.2.4.2 Active eukaryotic mRNAs feature a 5′ structure called the cap, a methylated guanine nucleotide that is linked to the 5′ end of the mRNA by its own 5′ carbon. This unique structure stabilises the mRNA, preventing 5′-3′ exonuclease activity. For complete degradation of mRNA via the 5′-3′ pathway this 5′ cap must therefore be removed to allow access to the exonuclease Xrn1. The process of removing this 5′ cap, known as decapping, involves the hydrolysis of the cap structure, leaving an exposed 5′ monophosphate that is targeted by Xrn1. In yeast decapping is performed by the decapping complex, made up of the catalytic pyrophosphatase Dcp2 (E. Van Dijk et al., 2002) and the decapping promotor subunit Dcp1 (Deshmukh et al., 2008; She et al., 2004). The first 300 amino acids of Dcp2 are responsible for the hydrolysis of the phosphate bond (Travis Dunckley & Parker, 1999), and fold into a 2 domain structure which closes into a more active structure when associated with Dcp1 (Deshmukh et al., 2008; Floor et al., 2010; She et al., 2008). Dcp2 also features binding sites for other activators of decapping such as the Edc3 (Harigaya et al., 2010).

Regulatory functions of decapping fall into three categories, the catalytic action of Dcp2, the removal of the cap-binding complex eIF4F to allow access to the cap and the recruitment of the decapping complex to the cap.

In vitro observations showed that Edc3 and Pat1 directly bind to and enhance Dcp2

catalysis (Harigaya et al., 2010; Nissan et al., 2010), Edc1 and its paralog Edc2 bind instead to Dcp1, and have been shown *in vitro* to enhance Dcp2's catalytic activity in this complex (Borja et al., 2011). During log phase, stress free growth, the catalytic activity of Dcp2 is not rate limiting for decapping, as demonstrated by the lack of decapping-deficient phenotypes in Edc1/2/3 deletion mutants (T Dunckley et al., 2001; Kshirsagar & Parker, 2004). Other mutations affecting Dcp2 catalysis give similar phenotypes showing little loss of decapping activity, including Pat1 C-terminal domain deletion (Nissan et al., 2010; Pilkington & Parker, 2008) and mutations in Dcp1 and Dcp2 themselves (Steiger et al., 2003; Tharun & Parker, 1999).

Further regulatory proteins can increase the rate of decapping by promoting the binding of the decapping complex to the 5' cap or recruiting additional enhances of decapping. Protein interaction studies have identified 2 major groups of proteins that interact to form decapping complexes. One complex binds to the 3' end of deadenylated mRNAs in vitro and consists of Pat1, the sub complex of Lsm1-7 and the Xrn1 exonuclease (Chowdhury et al., 2007). This complex is important in maintaining the order to degradation, ensuring that decapping enhancement occurs only after deadenylation by binding to oligoadenylated rather than polyadenylated mRNA. It also preferentially activates the decapping and 5'-3' degradation pathway, as a Pat1 or Lsm1 deletion causes exonuclease activity at the 3' end of the mRNA indicative of exosome activity (W. He & Parker, 2001)). The Dcp1/Dcp2 complex can also recruit or be recruited by additional proteins including Edc3, Scd6 and Dhh1 (Parker, 2012). Several of the proteins involved in these complexes, including Lsm4 and Edc3 contain low complexity domains that can lead to aggregation of these mRNP complexes into larger structures such as p-bodies.

Given the need to remove the cap-binding complex before decapping can occur, translation initiation can be thought of as being in competition with decapping, with the fate of the mRNA factors determining access of the respective proteins (McCarthy, 1998; C. Vilela et al., 2000). The observation that a decrease in translation initiation rate, achieved through various means, lead to an modulation of the decapping rate support this theory (LaGrandeur & Parker, 1999; Linz et al., 1997; D Muhlrad et al., 1995; Schwartz & Parker, 1999; Cristina Vilela et al., 1999) although this relationship is complex (McCarthy, 1998;

Ramirez et al., 2002). The proteins regulating this competition are diverse in function and many are also involved in the formation of, or localise to, cytoplasmic p-bodies during cellular stress (Nissan & Parker, 2008). Enhancers of decapping in yeast are summarised in table x. For enhancers that work by inhibiting translation, the exact mechanism that leads to an increase in decapping rate is not clear. It could be a simple matter of increasing the time available for the dissociation of the cap binding complex or may be a more complex remodelling of the mRNP (Parker, 2012). This set of proteins would be classed under the final category of 'removing the 5' cap binding complex'. Further evidence that the cap binding complex is the key inhibitor of decapping comes from studies of mutants with aberrant copies of its constituent proteins, in which mRNA stability is significantly reduced (Linz et al., 1997; McCarthy, 1998; Ramirez et al., 2002; Schwartz & Parker, 1999, 2000; C. Vilela et al., 2000; Cristina Vilela et al., 1999).

In the 5'-3' pathway, the initiation of decapping is triggered by the completion of dead-enylation. As the poly-A tail is reduced it loses the ability to bind to Pab1 but increases its affinity for the Pat1/Lsm complex as demonstrated by the *in vitro* studies of Pat1/Lsm and Pab1 poly-A binding (Chowdhury et al., 2007; Sachs et al., 1987). This reliance on Pab1 is supported by the observation that decapping and deadenylation are uncoupled in Pab1 deletion mutants (Caponigro & Parker, 1995).

Individual mRNAs can show different rates of decapping. In the same way that mRNA sequence can influence the rate of deadenylation, mRNA sequence can recruit additional proteins to either increase or decrease the rate of decapping. Many sequence features that influence the rate of decapping have concurrent effects on the rate of deadenylation (Caponigro et al., 1993; D Muhlrad et al., 1995; D Muhlrad & Parker, 1992; Olivas & Parker, 2000), pointing towards a general model in which translating mRNPs are remodelled into repressed and then decaying mRNPs through the exchange of translation initiation factors for decay factors. mRNA features that reduce translation will have an opposite effect on decapping. In early work studying the decay rates of both stable and unstable mRNA, features that were found to inhibit translation such as poor AUG context (LaGrandeur & Parker, 1999) in the case of the MFA2 mRNA enhance mRNA instability and cause faster decay rates.

Once exposed by the decapping process, the 5′ monophosphate can be recognised by the Xrn1 exonuclease, beginning a process of rapid 5′-3′ exonuclease degradation (Kenna et al., 1993; Stevens & Poole, 1995; E. L. Van Dijk et al., 2011).

2.3 Processing bodies

Processing Bodies (p-bodies) are non-membranous cellular compartments, part of a family of similar bodies/granules known as mRNP granules, consisting of an aggregated mixture of mRNA and proteins, some conserved and others variable depending on the state of the cell. Similar mRNP granules are present in a variety of organisms and hold different roles for cellular development and survival, these include Stress Granules (P. Anderson & Kedersha, 2008) Germ Granules (Gallo et al., 2008) and Neuronal Granules (Kiebler & Bassell, 2006). The structure, composition and function of p-bodies has been studied in both human cell lines as well as multiple model organisms such as the yeast *Saccharomyces cerevisiae*.

2.3.1 Discovery

P-bodies were originally observed as cytoplasmic foci of mRNA decay and decapping proteins, identified by fluorescent protein fusions and immunofluorescence experiments initially in mammalian cells (Kedersha et al., 2005) and subsequently in yeast and other eukaryotes (U Sheth & Parker, 2003). Fluorescence microscopy represents an invaluable tool for the study of p-bodies given the difficulty of purifying or reproducing them *in vitro*. The highly conserved XRN1 exonuclease was shown to form discrete foci in mouse fibroblasts (Bashkirov et al., 1997) while both Dcp1 and Dcp2 decapping proteins were found to exhibit similar localisations in HEK293 cells (E. Van Dijk et al., 2002). The inclusion of both exonuclease and decapping factors led to the initial idea that these foci were sites of mRNA decay. Further studies of yeast identified a wider range of proteins involved in decapping and mRNA decay that also localised to cytoplasmic foci, as well as co-localising these proteins to confirm they form a single compartment (J. R. Buchan et al., 2011). The term Processing Bodies was coined as a name to describe these foci, indicating their role in mRNA processing. Genetic studies also showed that deletion mutants of the identified constituent proteins caused various effects on PB size and number (summarised in Table X)(U Sheth & Parker, 2003).

Around the same time as the discovery of p-bodies, a closely related mRNP known as a stress granule was also identified and has been shown to be conserved in a similar range of model organisms and cell lines (P. Anderson et al., 2015; Nover et al., 1989). Stress granules are not constitutive components of cells and instead are induced by a range of cellular stresses including heat shock, starvation and other translation inhibiting factors (J. R. Buchan et al., 2011). Although initially proposed to be formed from existing p-bodies, further work has highlighted key distinctions between the composition and function of these two mRNPs. For simplicities sake this section focuses only on p-bodies, but their relationship with stress granules should be kept in mind given their various similarities which are highlighted throughout.

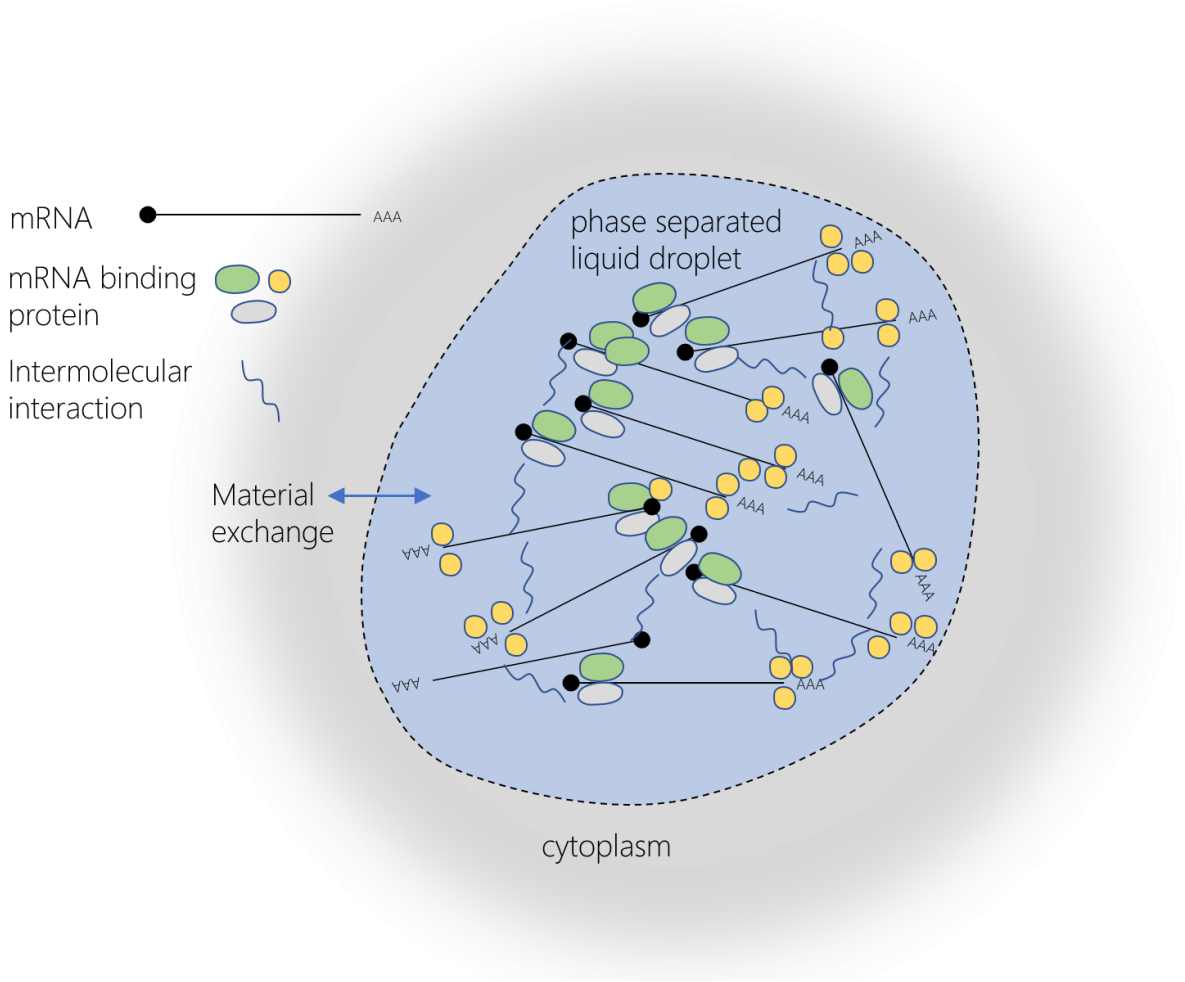

Figure 7: Simplified representation of a processing body, a liquid droplet made up of mRNA and mRNA binding proteins. The processing body is a phase separated liquid droplet that assembles due to multiple intermolecular interactions, Van der Waals forces and hydrogen bonds between mRNA and mRNA binding proteins. These interactions lead to increased density separating the body from the cytoplasm.

2.3.2 Structure and Composition

Studies using electron microscopy to investigate the ultrastructure of stress granules and p-bodies found that they are often closely associated with one another in HeLa cells. However, the two mRNPs have distinct, non-overlapping structures, with p-bodies showing a fibrillar ultrastructure compared with a fibrillo-granular stress granule ultrastructure (Souquere et al., 2009). These results point to distinct functions for SGs and p-bodies that are backed up by their differing protein composition.

There are also differences between the p-bodies observed in mammalian cells and in the budding yeast *Saccharomyces cerevisiae*, in which a large number of studies have been conducted. Mammalian p-bodies are constitutive components of most cells but vary in number and composition depending on the cell type. In contrast, yeast p-bodies have been observed to form only under certain conditions, similar to SGs, such as starvation or caloric restriction (Decker & Parker, 2012). Mammalian p-bodies disassemble during mitosis in a similar fashion to some other organelles and reform in G1, whereas in yeast, p-bodies can be present throughout mitosis if the inducing conditions remain in place (Garmendia-Torres et al., 2014; Yang, 2004). The composition of yeast p-bodies has been extensively documented since their initial discovery. With further immunofluorescence experiments and fluorescent protein fusions, a wide range of proteins have been observed to localise to p-bodies, some constitutively while others only during certain stresses.

In yeast, the components of p-bodies fall in to 3 general groups. A core group of proteins are conserved in p-bodies across organisms in which the decapping and deadenylation factors are heavily enriched, with the decapping complex proteins Dcp1 and Dcp2 forming core constituents and the enhancer of decapping Edc3 having a role in their formation and regulation(Franks & Lykke-Andersen, 2008). CCR4 and other components of the CCR4-NOT deadenylation complex have also be shown to localise to p-bodies in both yeast and other organisms (Doma & Parker, 2007). Secondly a number of mRNA-binding, translation-repressing proteins have been observed to localise to p-bodies such as the repressor of translation initiation SCD6. Interestingly, while SCD6 binds to eIF4G to repress translation initiation, and eIF4G appears to localise to both p-bodies and SGs in yeast (Brengues & Parker, 2007; Frydryskova et al., 2016), no other translation initiation factors are found in

yeast p-bodies. Finally, yeast p-bodies contain a currently unknown group of mRNAs, although some mRNAs have been individually identified to localise to p-bodies (Aizer et al., 2014). mRNA is a requisite component of p-bodies, and when translation is blocked experimentally using cycloheximide) leading to a reduction in mRNA abundance, p-bodies disassemble, presumably into smaller mRNP complexes. More recently, a study of human p-bodies, in which a sorting method similar to fluorescence associated cell sorting (FACS) was used to purify p-bodies, the mRNA content of p-bodies in human cells was obtained through mRNA sequencing (Hubstenberger et al., 2017). This study showed that almost 1/3 of coding mRNA transcripts could be found within the constitutive p-bodies of the human cell line, mainly made up of highly abundant but poorly translated sequences. As well as this it was also found that another 1/3 of coding mRNAs, and the majority of non-coding mRNAs were significantly excluded from p-bodies indicating that mRNA entry into p-bodies was a specific rather than a global phenomenon. This study also discovered a number of new protein components of human p-bodies via mass-spectrometry based analysis of the purified bodies. Many of these fell into the traditional categories of mRNA repression and decay, but some new components were identified including a number of myosin proteins of which one example was shown to localise to p-bodies *in vivo*. A full list of the yeast PB components as derived from the *Saccharomyces* Genome Database can be found in in the Appendix.

How mRNAs are targeted to PBs has not been fully elucidated but recent work in yeast shows that it may be linked to transcription. Linking the transcriptional promotor of an mRNA, known to localise to PBs during glucose restriction, to a reporter mRNA results in its targeting to p-bodies during that stress. Elements of the promoter known as Heat-shock elements (HSEs) were important in limiting localisation and chimeric promotors containing HSEs were able to replicate the observed effects. mRNAs may therefore be co-transcriptionally loaded with proteins that direct their localisation to p-bodies upon glucose stress. The timing of transcription was also shown to influence localisation, as translation was upregulated, and focus formation downregulated when transcription was started during stress, rather than before (Zid & O'Shea, 2014).

2.3.3 Assembly and regulation

Although PB regulation appears to vary between organisms, with yeast p-bodies being stress-induced and metazoan p-bodies always present, the proteins involved in the regulation of size and abundance appear to be conserved across species. Assembly of p-bodies depends on the concentrations of their constituent proteins (Franks & Lykke-Andersen, 2008; Y. Luo et al., 2018), with low complexity region of Edc3 and Lsm4 being particularly important in yeast p-bodies (Decker et al., 2007; Reijns et al., 2008). These regions of low complexity have been shown to be involved in both protein-protein interaction and RNA binding and are thought to contribute to a process of liquid-liquid phase separation (LLPS), in which non-membranous aggregates of proteins become phase separated into a dense inner core and aqueous outer layer(Schutz et al., 2017). A complex of Dcp1/Dcp2, mRNA and Edc3 has been shown to undergo LLPS in vitro.

The idea of p-body proteins undergoing LLPS is consistent with previous observations of p-bodies in various organisms. Firstly, the conservation of proteins with low complexity regions capable of forming a high number of protein or RNA interactions indicates a requirement for this type of protein for the formation of these granules. The appearance of p-bodies, as spherical, non-membranous, structures is also consistent with a granule that is held together by the surface tension of multiple intermolecular interactions (Kroschwald et al., 2015). P-bodies have been shown to undergo fusion events with other p-bodies, and similar docking events with the related mRNPs stress granules (J. R. Buchan et al., 2008). Further support is provided by the observations that many p-body protein interactions appear to show redundancy and can be compensated by overexpression of other factors, indicating a non-specific regulation of assembly (Rao & Parker, 2017). Together with the in vitro evidence, this provides a strong argument that p-bodies assemble sporadically due to LLPS, and that regulation is likely to occur by increasing or decreasing the intermolecular interactions necessary for this process.

Multiple p body associated proteins have also been shown to be susceptible to aberrant protein aggregation when the normal mRNA surveillance mechanisms are disrupted. In a study of the composition of wild type protein aggregates and those formed in mutants of the mRNA surveillance pathways, multiple p-body components were identified (Jamar et al., 2018). Two major p-body components, Dhh1 and Xrn1, were found to commonly form protein aggregates in wild type cells, and Dhh1, a regulator of p-body assembly and disassembly (J. R. Buchan et al., 2008; Mugler et al., 2016) also aggregated in NMD, NSD and NGD mutants. The p-body components Pat1, Ccr4 and Dcp2 were also shown to form protein aggregates in cells deficient in NSD, NMD and MD respectively. This propensity to form aggregates can be seen as both advantageous, in the formation of phase separated p-bodies, and potentially dangerous, as uncontrolled aggregation can lead to cellular damage.

Yeast p-bodies differ from mammalian p-bodies in their regulation during the cell cycle. While mammalian p-bodies appear to be dissolved during mitosis (Yang, 2004), yeast p-bodies are maintained, and trafficked into the emerging bud in a unidirectional manner that appears to confer a selective advantage on the daughter cells, at least under conditions of caloric restriction (Garmendia-Torres et al., 2014). Outside of mitosis regulation of p-bodies appears similar across species, with increases in their numbers under conditions that generally inhibit translation such as oxidative stress and starvation. In yeast, Dcp2 is

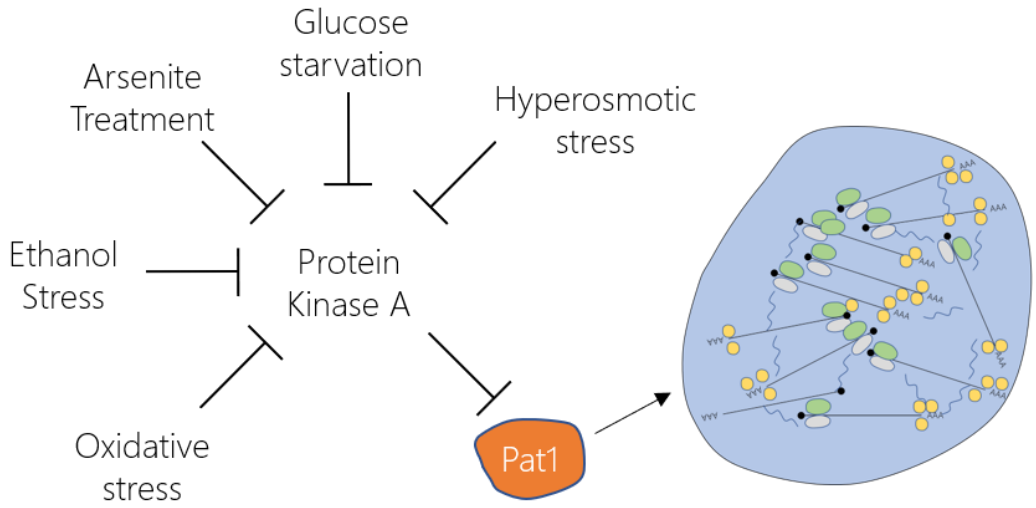

Figure 8: Conditions inducing processing body formation. Conditions of cellular stress cause inhibition of protein kinase A signalling, which may link them to processing body assembly. Pat1, a processing body scaffolding protein is phosphorylated by PKA and a subsequent reduction in phosphorylation of Pat1 allows processing body assembly.

phosphorylated in response to stress which causes its localisation to p-bodies while also stabilising a set of mRNAs encoding ribosomal proteins (Yoon et al., 2010). Mammalian DCP1a is also phosphorylated in response to stress, affecting its p-body localisation, as is human DCP1a during cellular differentiation (Chiang et al., 2013; Rzeczkowski et al., 2011).

2.3.4 Function

The function of p-bodies has been much debated in the decades since their discovery. While the initial evidence pointed towards a clear role as hubs of mRNA degradation, further investigation has cast doubt on that role, and a more general function in mRNA storage and regulation of translation has taken shape.

The initially observed composition of P-bodies was the main driver of the theory that p-bodies were sites of cytoplasmic mRNA degradation. This was backed up by the observation that the inhibition of 5′ – 3′ mRNA decay by removal of the Xrn1 exonuclease caused a build-up of p-bodies that were also larger than wild type p-bodies and were thought to contain mRNAs stalled in degradation (U Sheth & Parker, 2003) and in human cells were shown to be enriched in polyA mRNA (Cougot et al., 2004). It was also found that mRNA decay intermediates localised to p-bodies in Xrn1-deficient yeast strains (U Sheth & Parker, 2003) supporting the theory of degradation occurring in p-bodies. The inhibition of translation, through the stabilisation of mRNA complexes using cycloheximide, caused a marked decrease in p-bodies. This supported their role in mRNA decay, as a reduction in available mRNA, due to mRNA becoming trapped on in polysomes rather than available for binding, would likely reduce the size of p-bodies reliant on mRNA for their formation. The lack of translation initiation factor in p-bodies also points to a role outside general storage of mRNAs, unlike SGs where translation factors are found during stress conditions and mRNAs are thought to be stored ready to re-enter translation (Brengues et al., 2005).

Further studies presented a contrasting role for p-bodies, focused on the storage rather than degradation of mRNA. mRNA localised to p-bodies was shown to be able to re-enter translation after amino-acid starvation-induced p-body accumulation was removed, while mRNA's entering p-bodies were not immediately degraded (Aizer et al., 2014). The mRNA-Seq study mentioned earlier (Hubstenberger et al., 2017) also found a lack of mRNA decay

intermediates in p-bodies, while a study using a new imaging technique to image mRNA decay as it occurs showed a lack of mRNA degradation events in p-bodies (Horvathova et al., 2017). It has also been shown that the inhibition of PB formation by removal of core formation regulator DDX6 (human, Ddh1 in yeast) has little effect on RNA stability for p-body localised transcripts (Hubstenberger et al., 2017), and that nonsense-mediated mRNA decay does not require p-bodies to occur (Stalder & Mühlemann, 2009). An alternative approach to mRNA degradation analysis identified both stabilisation and degradation of mRNAs that were localised to p-bodies on glucose starvation in yeast (Wang et al., 2018).

The structure of p-bodies could also be an influencing factor in their function. Recent studies into LLPS showed that enzyme activity of the core PB component Dcp2 is reduced in an *in vitro* model of LLPS, as is the activity of RNAse A. This could imply that the dense liquid droplet core of the PB reduces the activity of decay factors enough for them to function as storage sites and protect their mRNA components from decay, either for storage or possible for mRNA transport.

Overall the true function of p-bodies still remains unclear. There is a large body of evidence supporting the fact that they are site of mRNA decay, but more recently work has begun to question this, and a role in mRNA storage has also emerged. Given that the initial work on PB function, as well as some of the later work supporting its role in decay, was performed in yeast whereas the bulk of the evidence for storage comes from metazoan studies, it could be that p-bodies have taken on divergent roles, with yeast p-bodies only functioning as storage sites during cellular stress and functioning as sites of decay under normal conditions. This is supported by the findings that highly expressed mRNA accumulate in yeast p-bodies during various stresses (Lavut & Raveh, 2012) and that p-bodies are required for long-term survival of stationary phase yeast cells (Ramachandran et al., 2011), while also not contradicting the earlier studies of p-bodies that indicate their role in mRNA decay. Further work is clearly required to elucidate the full function of p-bodies.

2.3.5 Transport within the cell

To date, no functions have been reported that relate p-bodies to the transport of mRNA or proteins. However, multiple lines of evidence point towards this as a possibility. In both

mammals and unicellular organisms, association of p-bodies with the cytoskeleton has been reported.

In mammalian cells, p-bodies have been shown to move along microtubules in a directional manner and change microtubule tracks implying association with motor proteins. It was suggested that this association with microtubules could be facilitated by binding to organelles such as mitochondria, which are known to move on microtubules; although the adaptor proteins or cellular motors involved were not identified (Aizer & Shav-Tal, 2008). Microscopic observation of fluorescently tagged p-bodies showed both spatially confined movement and linear translocation across small regions of the cell. Various p-body components have also been shown to co-localise and bind to the class V myosin motor Myosin Va in mammalian cells, and siRNA knockdown of Myosin Va inhibits p-body assembly. Overexpression of Myosin Va tails also limits the movement of p-bodies in vivo (Lindsay & McCaffrey, 2011). Recently, Nesprin-1 has been identified as a link between p-bodies and microtubules and expression of the Nesprin-1 microtubule binding region disrupts p-body transport on microtubules (Rajgor et al., 2014).

In plants, p-body motion appears to be actin, rather than microtubule based. P-bodies were observed to translocate along actin filaments, with movement inhibited by the overexpression of myosin XI tails. Myosin XI was shown to bind to the p-body component atDCP1, and the Dcp1 myosin interaction was conserved across species, with Yeast Myo2 binding yeast Dcp1, and Mouse MyoVa binding both yeast and human Dcp1 homologues (Alexandra Steffens et al., 2014).

Less work has been undertaken in budding yeast, although all current evidence supports an actin-based mechanism of movement. Myo2 was found in a sucrose gradient fraction containing multiple p-body components as well as multiple mRNAs (Chang et al., 2008). Myo2 showed partial co-localisation with p-bodies in live cell imaging and a temperature sensitive Myo2 protein appeared to inhibit p-body disassembly. A study of a related mRNP containing RNase mitochondrial RNA processing factor (MRP) and Xrn1 showed a preferential localisation in the daughters of budding yeast cells (Gill et al., 2006) which was dependent on the mRNA transport machinery or "locasome" of She2/She3/Myo4. Further

work using live cell observation of the p-body marker Edc3 in a microfluidic device showed that p-bodies are directionally trafficked into emerging buds, lingering at the bud site before budding begins. This deliberate inheritance was again dependent on the locasome machinery and a drop in velocity of p-bodies during budding was also inhibited by this loss of the locasome. The inheritance of the p-body was also shown to confer a selective advantage on the daughter cell, whereby cells inheriting a p-bodies reached a larger size before budding, although this study was carried out in conditions of dietary restriction.

2.4 Replicative ageing in budding yeast

Ageing is the continuing change and development of an organism over time, and on a cellular level takes the form of an eventual breakdown in key maintenance systems leading to the eventual death of the cell, and the organism. In budding yeast, ageing is described in terms of replicative or chronological ageing. Replicative ageing refers to the breakdown in cellular function as a mother cell spawns an increasing number of daughter cells, whereas daughters are "reset" in terms of age and capable of producing daughter cells of their own. Chronological ageing is the process in which yeast cells deteriorate when not dividing, under conditions such as starvation. Replicative ageing in yeast represents an attractive model for eukaryotic ageing research, as the mother and daughter cell relationship is easily defined, simplifying the tracking of inherited molecules and damaged proteins. The genetic tractability of budding yeast and its ease of growth, short cell cycle/lifespan and well-developed toolkit of laboratory techniques mean that it has featured heavily in ageing research over the past 30 years.

2.4.1 Conserved mechanisms of extended lifespan

Using budding yeast as a model for research into eukaryotic ageing processes would make little sense unless these mechanisms were conserved in general amongst eukaryotes. Research to date has identified a number of genetic and environmental factors that impact RLS in yeast, with these effects being conserved in higher eukaryotes, (Wasko & Kaeberlein, 2014). A recent high-throughput study of replicative lifespan (RLS) extension in *S. cerevisiae* identified a large number of deletion mutants capable of extending lifespan, and confirmed a previous observation that lifespan-influencing genes in the nematode worm

Caenorhabditis elegans were 5 times more likely to influence lifespan in yeast, implying a high degree of conservation in ageing pathways (McCormick et al., 2015; E. D. Smith et al., 2008). These longer-lived mutants are not necessarily fitter than the wild type strains, in fact in most cases they appear to have reduced fitness in a competitive environment, due to the gene deletion having an impact on systems vital for normal cell growth (Kyryakov et al., 2016). Whether or not interventions against these identified targets in humans could yield lifespan extensions remains to be seen, but the conservation of pathways across species and the biologically uncompetitive environment that we now inhabit suggest potential interventions may be possible (C. He et al., 2018). The factors affecting replicative lifespan in budding yeast can roughly be split into physical-environmental and genetic, with significant crosstalk between the two, in that genetic modifications to the pathways sensing the environment may yield similar lifespan extensions in response to changes in the environment itself. Many of these factors were initially identified in budding yeast and the main areas of past and existing research are discussed here.

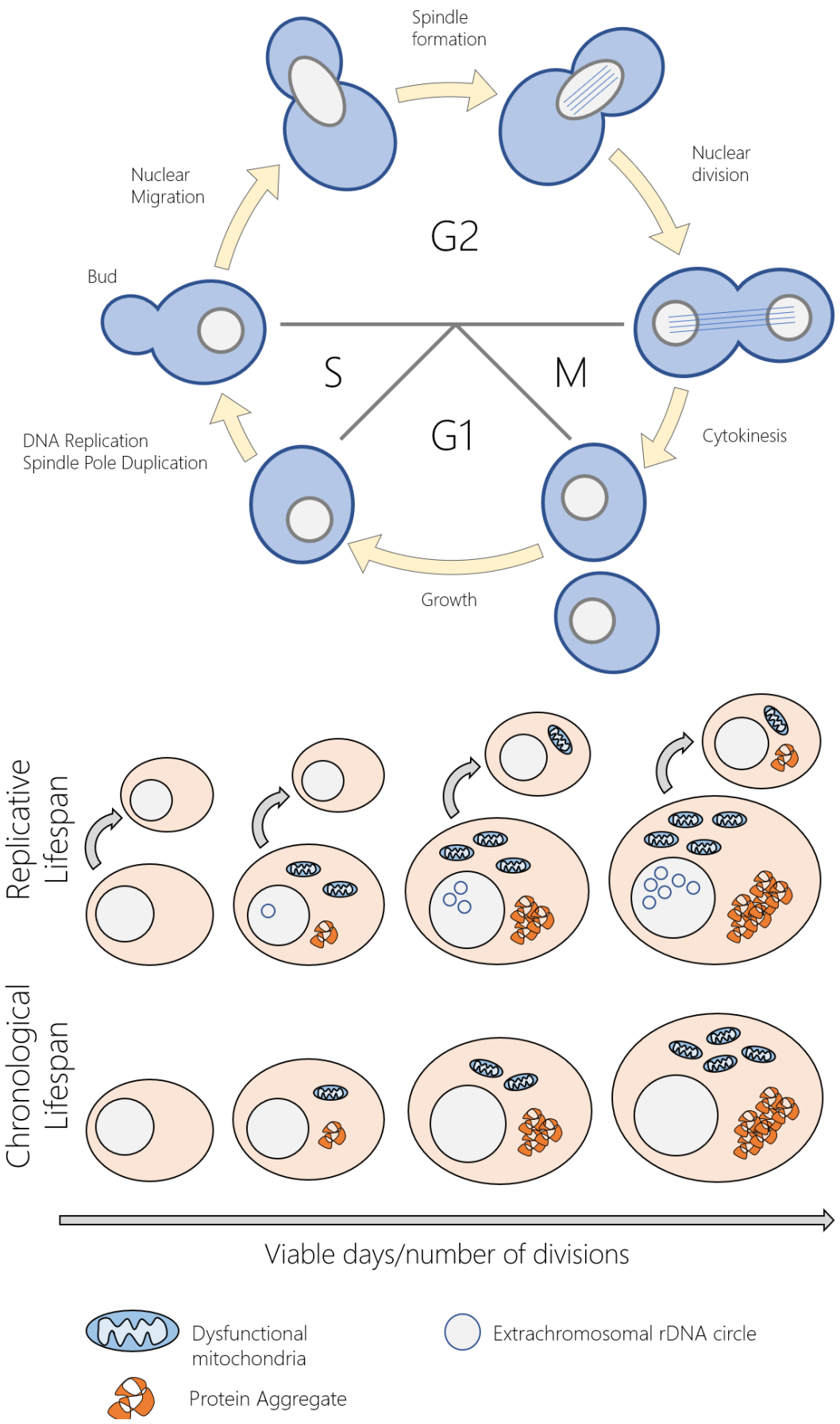

Figure 9: Cell cycle progression (upper) and measures of ageing (lower) in budding yeast. The yeast cell cycle follows a defined morphological pattern, as shown above. Replicative lifespan is the ageing process due to repeated cell divisions. Chronological ageing is the ageing process due to extended non-replicative survival.

2.4.2 Sirtuins and ERCs

The first group of proteins found to extend lifespan in yeast were the Sirtuins. Sirtuins are a group of protein deacetylases that deacetylate their targets in response to signalling pathways. For example, the namesake of the group, Sir2, deacetylates histones to silence certain genetic loci (Finkel et al., 2009). Only Sir2 is highly conserved across species, having homologues in bacteria, yeast, flies, worms and mammals (Brachmann et al., 1995). Over-expression of Sir2 robustly extends replicative lifespan in budding yeast, and a null mutant significantly reduced RLS, an effect which has been replicated in chronological lifespan studies from worms and flies (Kaeberlein et al., 1999; Brian K Kennedy et al., 1997; Rogina & Helfand, 2004; Tissenbaum & Guarente, 2001). This lifespan-extending effect is thought to be due to the activity of Sir2 in promoting genomic stability via chromatin silencing, preventing extensive recombination of DNA and limiting global transcription levels (Dang et al., 2009). As yeast mother cells age, reduced levels of Sir2 caused increased histone acetylation, opening up chromatin and causing increased levels of recombination and a global rise in transcription rate that may lead to an aberrant proteome (Dang et al., 2009).

A further function of Sir2 is to limit recombination at the yeast rDNA locus which encodes rRNA. This locus is highly repetitive and therefore subject to increased levels of recombination compared to the rest of the yeast genome (Kaeberlein et al., 1999; Lindstrom et al., 2011). Recombination in this locus can cause the excision of so called extrachromosomal rDNA circles (ERCs), circular regions of DNA that can accumulate in the nucleus of mother cells (Ganley & Kobayashi, 2014). The impact of ERCs on replicative ageing is highly debated (C. He et al., 2018), but a large body of evidence shows a strong correlation between the accumulation of ERCs and the shortening of RLS. Live cell imaging of fluorescently tagged ERC DNA (using a DNA binding protein fused to a fluorescent protein) showed that ERCs are preferentially retained in mother cells during the asymmetric cell division in budding yeast (Denoth-Lippuner et al., 2014) in a process dependent on the SAGA complex that facilitated anchoring to nuclear pore complexes (NPCs) (Denoth-Lippuner et al., 2014). Only ERCs that are bound to NPCs appear to be retained in the mother cell, in an NPC Cap structure, while unbound ERC can be inherited with limited efficiency. Another study suggested that the true reason for this asymmetric segregation was not necessarily

an active mechanism, but a passive one, in which ERCs bound or unbound to NPCs are prevented from moving into the daughter nucleus due to the geometry of the bud neck and limited timespan of mitosis (Gehlen et al., 2011). This passive mechanism might also explain how cytoplasmic structures are partitioned asymmetrically, in cases were their active transport to the daughter cell has not been selected for throughout evolution in a kind of "default" segregation to the mother cell. The observation that other centromere-lacking DNA constructs such as plasmids are also retained in the mother cell seems to support this idea, as they may lack the sequence or epigenetic features required for NPC binding. Further support comes from a study demonstrating that a relaxing of the diffusion barrier, caused by mild heat shock, can allow a more symmetrical partitioning of ERCs, extends lifespan of mother cells (Baldi et al., 2017) and is reliant on changes in the activity of protein kinase A (PKA) and target of rapamycin (TOR) signalling pathways, which have also been shown to influence lifespan (see below).

The number of ERCs can be influenced by lifespan-extending genetic changes as well as environmental factors. For example, deletion of the Fob1 gene, involved in DNA replication of rDNA regions, extends replicative lifespan and appears to reduce recombination in the rDNA locus, thereby reducing ERCs (Defossez et al., 1999). rDNA instability can also be decreased through dietary restriction (DR) in yeast, or by inhibiting the downstream signalling target or DR, TOR (Ha & Huh, 2011; Riesen & Morgan, 2009). Taken together it is clear that at least in yeast, ERCs play some role in the progression of replicative ageing.

2.4.3 Asymmetric inheritance of protein aggregates

ERCs are not the only features that are asymmetrically inherited in yeast. Protein aggregates made up of misfolded proteins, co-ordinated by chaperones such as Hsp104 also appear to be selectively retained within mother cells. This observation is of particular importance to research on human neurodegenerative diseases, as many of these diseases are characterised by aberrant protein aggregation and subsequent cell death during ageing (Di Gregorio & Duennwald, 2018). In yeast, damaged and misfolded proteins are deposited in aggregates such as the IPOD, Insoluble Protein Deposit and JUNQ, JUxta Nuclear Quality control compartment (Spokoini et al., 2012). These aggregates sequester potentially toxic proteins and allow for their bulk retention in aging mother cells(Nyström &

Liu, 2014). Cells lacking Hsp104 fail to form these compartments, leading to a breakdown in inheritance of aggregated proteins, with smaller aggregates passing through the bud neck to the daughter cell (Spokoini et al., 2012). Sir2 has also been implicated in the asymmetric partitioning of aggregated proteins highlighting a potential role in ageing for these aggregates (Sampaio-Marques et al., 2012).

Whether aggregates are actively or passively retained in mother cells remains to be proven. Modelling of aggregate motility suggested that similarly to ERCs, the geometry of the budding yeast cell prevents the inheritance of aggregates due to their slow diffusion rate. Bud neck diameter and mitosis time were found to be key factors in the model of aggregate inheritance (Zhou et al., 2011) although this modelling was based on an average of the diffusion coefficients of observed aggregates. For larger aggregates such as JUNQ and IPOD that are attached to organelles, evidence of active transport supporting retention in mother cells has been reported. Large scale genetic screens identified the actin cable nucleating polarisome machinery as an essential component for protein aggregate retention (Liu et al., 2010; Tessarz et al., 2009) and Sir2 may be affecting the function of actin when regulating retention. Protein aggregates have also been shown to localise with actin in live cell imaging experiments (Liu et al., 2011). Multiple studies have also shown that aggregates may associate with various organelles and could be co-trafficked to ensure their retention (Kaganovich et al., 2008; S. B. Miller et al., 2015; Specht et al., 2011; Zhou et al., 2014).

Functional protein aggregates, that are related to inclusions in neurodegenerative diseases (such as stress granules and p-bodies) have not been thoroughly investigated during replicative ageing. P-bodies, unlike damaged protein aggregates, have been shown to be inherited by daughter cells, rather than retained in the mother (Garmendia-Torres et al., 2014). The mechanism of this inheritance has not been confirmed but appears to rely on the mRNA transport machinery, as deletion mutants for components of this machinery showed a reduction in p-body inheritance. Another possibility is that the conditions in which p-bodies are induced, dietary restriction or mild heat shock, have some impact on the diffusion barrier at the bud neck, enabling transport of these aggregates.

2.4.4 Dietary restriction and downstream signalling pathways

Dietary restriction (DR), in which the caloric intake of an organism is restricted to below usual levels, acts through a number of signalling pathways. DR has been shown to increase replicative lifespan in yeast and lifespan in a number of multicellular organisms (B. K. Kennedy et al., 2007; Omodei & Fontana, 2011). The downstream effects of DR are thought to prolong lifespan in different ways, including a reduction in protein synthesis and associated misfolding of proteins (Kaeberlein, 2013), a general increase in autophagy of damaged cellular components (Johnson et al., 2013) and changes in mitochondrial respiration (Hempenstall et al., 2012). DR appears to work by influencing nutrient sensing signalling pathways within the cell, to decrease activities associated with cell growth and increase activities associated with the response to stress.

An increase in mitochondrial aerobic respiration compared to anaerobic respiration appears to be conserved across species, although there is contradictory evidence in yeast, in that a lack of mitochondrial DNA does not remove the impact of DR on replicative life span (Hempenstall et al., 2012; Kaeberlein et al., 2005). An increase in aerobic respiration appears to contradict the long held theory that reactive oxygen species (ROS) from aerobic respiration are one of the main drivers of cellular ageing, causing damage to many components of the cell (Harman, 2006). It may be that a breakdown of the asymmetrical inheritance of damage could extend mother lifespan while reducing overall fitness, although how this would work in multicellular organisms remains unclear. Another possibility is that the associated upregulation of autophagy compensates for the increase in ROS, as autophagy normally diminishes with age (Cuervo, 2008). Surprisingly, an increase in autophagy alone does not increase RLS in yeast (Wasko & Kaeberlein, 2014).

Dietary restriction influences nutrient sensing signalling pathways that are responsible for the downstream effects that increase RLS. TOR signalling is responsible for a wide range of regulatory functions in eukaryotic cells and is conserved from yeast to humans. Genetic strategies to inhibit TOR signalling in yeast, worms, flies and mice have all been shown to increase lifespan (Kapahi et al., 2004; Lamming et al., 2012; Vellai et al., 2003) and the use of the immunosuppressant drug rapamycin has a similar effect (Bjedov et al., 2010; Harrison et al., 2009; Medvedik et al., 2007; Robida-Stubbs et al., 2012). In Yeast, the TOR

homolog,TORC1 regulates global mRNA translation rates as well as autophagy and the response to stress and an ortholog of the yeast substrate of TORC1, the serine threonine protein kinase, Sch9 has similar activity in multicellular organisms (Jorgensen et al., 2002; Stanfel et al., 2009; Urban et al., 2007). Inhibition of TOR signalling can also increase mitochondrial biogenesis leading to increased respiration (Wasko & Kaeberlein, 2014).

Dietary restriction also inhibits signalling via Protein Kinase A, a cyclic AMP dependent kinase complex (Lin et al., 2000; Toda et al., 1987). PKA signalling is similar to TOR, in that it negatively regulates the stress response, including stress responsive transcription factors. Reducing PKA signalling genetically mimics the effect of dietary restriction in yeast (Lin et al., 2000), and has a corresponding effect on replicative lifespan which cannot be enhanced by dietary restriction in the same strain. Interestingly, both PKA and TOR signalling have been found to be important in the regulation and assembly of mRNP granules including p-bodies and stress granules during the response to stress in yeast (Ramachandran et al., 2011; Sfakianos et al., 2018; Vindry et al., 2017).

The underlying pathways of ageing appear to be conserved from single-celled eukaryotes such as budding yeast to multicellular eukaryotes. Factors such as genome instability, nutrient signalling, mitochondrial dysfunction and proteostasis all appear to play roles in contributing to the ageing process. Interestingly the mechanisms by which ageing can be interrupted, including TOR and PKA signalling also promote the activity of stress responsive elements such as p-bodies within the cell. Although the interventions that increase RLS in yeast (and general lifespan in higher eukaryotes) do not necessarily equate to improvements in selective fitness, they may not be of great importance in the treatment and/or prevention of neurodegenerative diseases that appear later in life. Understanding the relationship between the ageing process and the stress response, including the function of p bodies, will help us develop a systems level view of eukaryotic ageing, the beginnings of which are outlined in figure 10.

2.5 Objectives

It is clear from the existing literature that there exists some form of relationship between the progression of ageing in eukaryotic cells and the response to stress in the cellular

environment. Signalling pathways, in which interventions can lengthen lifespan in model organisms, control the transcriptional and post-transcriptional response to stress, including the formation and regulation of cytoplasmic mRNP granules. The full functionality of these mRNP granules remains elusive. They may play a role in mRNA decay and/or storage, and more recently they have been implicated in the transport of mRNA in dividing cells. Few data have been gathered on the changes that may occur to p-bodies during the ageing process.

Saccharomyces cerevisiae represents an attractive model organism for the study of ageing and age-related effects on organelles/cellular compartments such as p-bodies. The easy of creating genetic modifications such as introducing fluorescent protein fusions makes live cell imaging possible and many other genetic tools have been developed to aid research in this organism. Recently, age related research in yeast has been greatly facilitated by the introduction and use of microfluidic devices capable of selectively retaining yeast mother cells while removing the daughters. This allows cells to be monitored for the duration of their replicative lifespan.

This study aimed to take advantage of the recent advances in fluorescence microscopy and microfluidics as powerful tools for use in the investigation of the impact of age on the

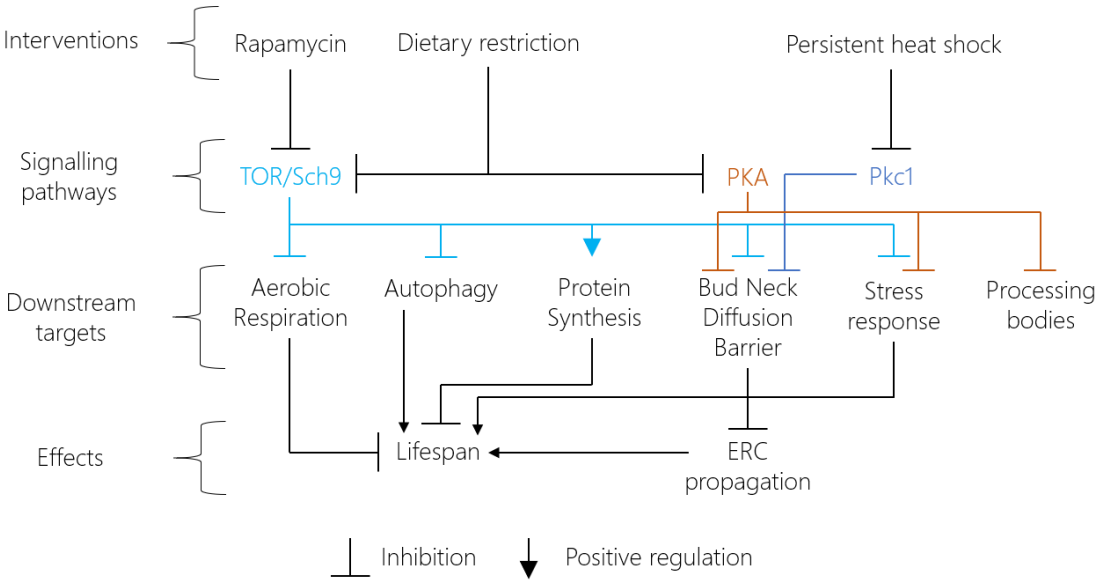

Figure 10: Regulatory interactions affecting cellular ageing in budding yeast. Interventions are shown with the signalling pathways they are thought to effect. Signalling pathways target specific cellular processes that have been shown to affect the lifespan of budding yeast cells.

localisation and function of p-bodies in the budding yeast *Saccharomyces cerevisiae*. Modern fluorescent proteins, with improved brightness and reduced photobleaching were used to allow longer-term imaging of p-bodies alongside other organelles. Automated time-lapse microscopy was used to capture images at defined intervals and track individual p-bodies as they moved within and between cells. Additionally, a series of microfluidic dissection platforms were evaluated for their use in the study of p-bodies during replicative ageing of budding yeast. The-best suited platform was then utilised to study changes in localisation and dynamics of p-bodies in yeast cells of advanced replicative age. Finally, the inheritance of p-bodies was investigated further with focus on the role of the decapping protein Dcp1.

3 Materials and Methods

3.1 Molecular Cloning

Multiple plasmids were constructed for this work using a number of molecular cloning methods, making it unfeasible to describe the construction of each in detail. Instead a detailed summary of each technique is presented as well as the necessary oligonucleotide primers and plasmid descriptions (Appendix).

3.1.1 DNA Manipulation

Restriction Cloning

3.1.1.1 For plasmids constructed using traditional restriction cloning, DNA fragments were generated in one of 2 ways. Either the fragment was directly excised from an existing plasmid using restriction enzymes, or the fragment was amplified from a template using PCR with oligonucleotide primers containing restriction sites, which were then digested.

For directly excised fragments, 1 µg of the source plasmid was incubated with the required restriction enzymes (New England Biolabs, ThermoFisher Scientific) and suitable buffer solution at a temperature and time according to the manufacturer's recommendations in a total volume of 40 µl. After incubation the reaction mixture was mixed with a 6X DNA Loading Dye (New England Biolabs) at a ratio of 5:1. Agarose gels were prepared using 1% w/v agarose (Sigma) dissolved in 1X TAE Buffer (see appendix for composition) containing 0.5µg/ml ethidium bromide. DNA fragments were loading in their entirety into the wells of the agarose gels and electrophoretic separation was performed at 100V constant voltage for 45 minutes in a horizontal electrophoresis gel tank (Bio-Rad) alongside a marker of standard dsDNA lengths. After separation, DNA fragments of the correct size were excised from the gel using gel excision pipette tips under UV light illumination and the DNA was purified using a spin column-based DNA recovery kit (Zymo Research). Finally, the eluted DNA concentration was measured using an automated UV-Vis Spectrophotometer (Nanodrop 2000 - Thermo Scientific).

For fragments generated via PCR, oligonucleotide primers were designed, by standard design principles, that complemented the ends of the desired region of amplification, and also included a suitable restriction site at each end. Where the plasmid was to yield an open reading frame, restriction sites were placed so that the final sequence would be in

frame with the existing ORF. PCR amplification was performed using a high fidelity proof reading polymerase (Q5 - New England Biolabs) with buffer and nucleotide concentrations as well as thermal profiles according to the manufacturers recommendations in an automated thermocycler (T100 - Bio-Rad) at a total volume of 50 µl. After amplification PCR products were purified using a spin column based DNA purification kit (Zymo Research) and DNA concentration was measured via a spectrophotometer as with restriction digest fragments.

Destination plasmids were digested, isolated and purified in the same manner as restriction fragments, but were further treated with alkaline phosphatase before isolation to remove phosphate groups from the DNA ends to prevent re-annealing of the plasmid. 1 µl alkaline phosphatase (Calf intestinal – New England Biolabs) was added to the digestion reaction mixture and incubated at 37°C for 30 minutes after which the isolation and purification steps proceeded as previously.

After generation, DNA fragments were annealed by incubating with T4 DNA ligase and a corresponding buffer system (New England Biolabs) for 20 minutes at room temperature, after which they were placed on ice. Fragments were ligated in a molar ratio of 3 parts insert to 1-part destination plasmid forming a total of 100ng of DNA. 5 µl of the ligation mixture was used directly as the DNA for bacterial transformation (see Bacteria Transformation).

3.1.1.2 Gibson assembly

For plasmids constructed via Gibson assembly, there were again 2 methods of fragment generation. Gibson assembly requires overlapping ends between fragments; the required overlap can be introduced on both, or a single fragment depending on the convenience of adding overlaps via PCR. When joining multiple fragments from different sources, oligonucleotide primers for the PCR fragments can be designed that include the necessary overlaps, making it possible to include restriction only fragments in the assembly as well. For an overview of the assembly process see Figure 11.

Fragments generated for plasmids in this project fall into 3 categories; PCR fragments for ligating to other PCR fragments (Type 1), PCR fragments for ligating to restriction fragments

(Type 2) and restriction fragments (Type 3).

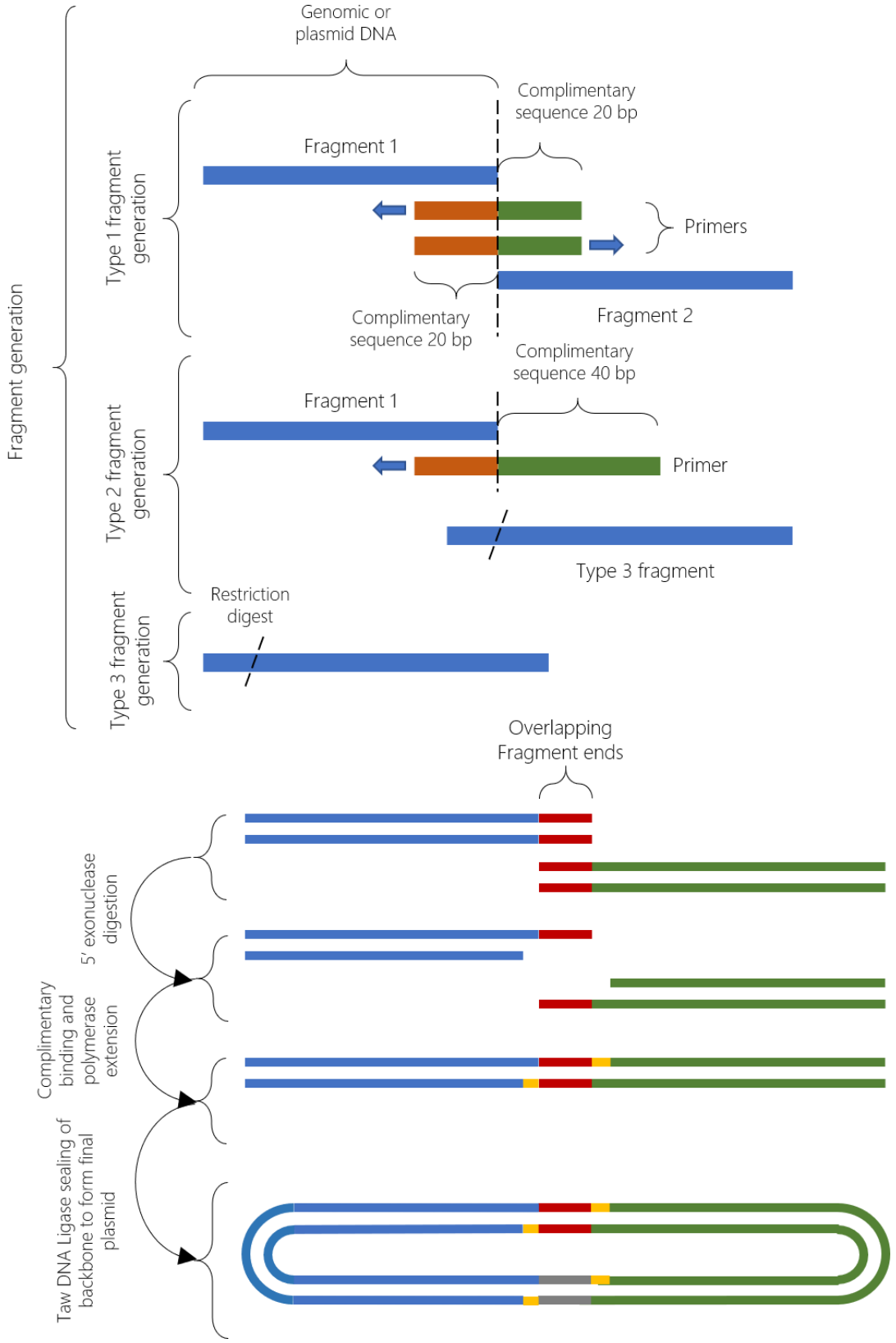

Figure 11: An overview of the Gibson assembly cloning process used to create plasmids in this study. Gibson assembly allowed the ligation of multiple fragments in a single reaction to simplify and speed up the cloning process. 3 fragment types were generated as outline in the upper panel. These fragments underwent 5' digestion, followed by overlapping complimentary ends, and polymerase extension and ligation to create complete plasmids.

For Type 1 fragments, 40 nucleotide primers were designed according to standard design principles and included 20 bp tails, complementary to the primer sequence of the adjacent PCR fragment in the assembly so that the primers for adjacent fragments are reverse complements of each other. Fragments were amplified from template DNA using a high-fidelity proofreading polymerase (Expand High-Fidelity PCR System – Roche) with buffer and nucleotide concentrations as well as thermal profiles according to the manufacturers recommendations in an automated thermocycler (T100 - Bio-Rad) at a total volume of 50 µl. After amplification PCR products were purified using a spin column-based DNA purification kit (Zymo Research) and DNA concentration was measured using an automated UV-Vis Spectrophotometer (Nanodrop 2000 - Thermo Scientific).

For Type 2 fragments, 60 nucleotide primers were designed according to standard design principles and included 40 bp tails, complementary to the DNA sequence of the adjacent DNA fragment in the assembly. PCR was performed as with type 1 fragments.

For Type 3 fragments, restriction digest and gel extraction were performed identically to the process for restriction cloning.

After fragment generation, assembly was performed using 2X Gibson assembly master mix (New England Biolabs). Fragments were mixed with ddH2O in a ratio according to the manufacturer's recommendations to a total volume of 10 µl. The fragment mixture was then mixed with 10 µl of 2X Gibson assembly master mix and incubated at 50°C for 60 minutes before placing on ice prior to bacterial transformation.

3.1.1.3 Bacterial Transformation

Bacterial transformation with plasmid DNA was performed using chemically competent Escherichia coli. Top10 Competent cells were created using the following protocol:

Seed stocks were first prepared as follows: Top10 cells were streaked for single colonies on SOB Agar media (see appendix for composition) plates and incubated overnight at room temperature. Single colonies were picked using a sterile pipette tip and inoculated into 2 ml SOB liquid media (see appendix for composition) and incubated overnight at room temperature. After incubation, 60% glycerol was added to 15% and 1ml aliquots were dispensed into cryo-tubes and placed at -80˚C for storage.

To prepare competent cells, 250ml SOB was inoculated with a single 1 ml seed stock and incubated at room temperature until the culture reached OD600 0.3, approximately 14 hours (usually overnight). Cells were centrifuged at 3000 rpm in pre-chilled centrifuge tubes at 4˚C for 10 minutes. Supernatant was discarded, and cells were resuspended in a total volume of 80 ml CCMB80 buffer (see appendix for composition) before incubating on ice for 20 minutes. Cells were again centrifuged as previously and resuspended in a total volume of 10 ml CCMB80 buffer. Chilled CCMB80 buffer was added until an OD of 1 – 1.5 was achieved when 50 µl cells were mixed with 200 µl SOB media. Competent cells were aliquoted in 50 µl volumes in Eppendorf tubes and stored at -80˚C. Competence was tested using 1 µl of standard pUC19 plasmid (Invitrogen).

To transform chemically competent cells with plasmid DNA, 1 50 µl aliquot of cells per transformation was thawed on ice. 1 - 5 µl of ligation/Gibson mixture, derived from a mixture of the previously described fragment types, was added to the cells before incubation on ice for 30 minutes. Cells were then heat shocked for 45 – 60 seconds at 42˚C in a dry heat block (Eppendorf) before returning to ice for 2 minutes. 250 µl SOB liquid media was added per tube and then incubated at 37˚C for 2 hours in a shaking incubator at 200 rpm. Cells were plated on appropriate antibiotic containing media (see appendix for details) at 1 µl, 10 µl and 289 µl volumes on 3 separate plates and incubated overnight at 37˚C.

3.1.1.4 Clone Screening

Bacterial clones were screened in multiple ways to ensure the correct plasmid sequence was present. Where suitable primers were available, cloned were screened using colony PCR. To further confirm that plasmids were correct, or where colony PCR was not suitable, plasmids were purified using a commercial miniprep kit and digested with restriction enzymes and compared to expected digestion profiles. Finally, purified plasmids were sent for DNA sequencing with suitable primers to a commercial DNA sequencing service (GATC, Cologne, Germany).

To perform colony PCR, a 20 µl PCR master mix was prepared with 2X DreamTaq Green PCR Master Mix (Thermo Fisher Scientific) according to the manufacturers recommendations but replacing template DNA with ddH2O. Primers were selected to amplify a region

of the plasmid so that it would be distinguishable from the original insert and vector plasmids. Single colonies were picked using a sterile pipette tip and dipped into the PCR master mix, after which the tip was deposited into 2ml LB media (see appendix for composition) + appropriate antibiotic. PCR was performed using thermal profiles according to the manufacturer's recommendations in an automated thermocycler (T100 - Bio-Rad), while the inoculated media was incubated overnight at 37˚C. 10 µl of the PCR products were loaded directly onto a 1% agarose gel and observed under UV illumination as described previously. Gels were imaged using a gel documentation system (Gel Doc XR+, Bio-Rad) and documented via image acquisition. Colonies showing the expected PCR profile were selected for further confirmation, by purification of the plasmid from the overnight culture.

Before further confirmation, either restriction digest or sequencing, plasmid DNA was purified using a commercial plasmid purification (miniprep) kit (Thermo Fisher Scientific). Briefly, the 2 ml culture was harvested by centrifugation in a 2ml Eppendorf tube at 13,000 g for 1 minute. Supernatant was discarded, and cells were resuspended in 250 µl resuspension buffer. 250 µl lysis buffer was added and mixed by inversion 4 – 6 times. 350 µl neutralization buffer was added to the tube and mixed by inversion 4 – 6 times. The tube was then centrifuged at 13,000 g for 5 minutes before adding the supernatant to the spin column. The spin column was centrifuged for 1 minute discarding the flow through before addition of 500 ml wash buffer, followed by a further centrifugation of 1 minute, discarding the flow through and centrifuging for a further 2 minutes to clear residual wash buffer. 50 µl ddH2O was added to the spin column and it was placed in a fresh 1.5 ml Eppendorf before centrifugation for 1 minute at 13,000 g. DNA concentration was measured using an automated UV-Vis Spectrophotometer (Nanodrop 2000 - Thermo Scientific).

Purified plasmids were confirmed as correct by restriction digest. Digests were performed as with restriction cloning, and fragments were analysed via agarose gel electrophoresis and images captured as previously. Restriction profiles were compared to those expected from the desired and source plasmids to confirm the correct insertion or modification had been made.

Speculatively correct plasmids were finally confirmed via DNA sequencing. DNA sequencing primers were designed that would ensure coverage of the entire modified region and prepared for sequencing along with the plasmid according to the requirements from the DNA sequencing service (GATC Lightrun). Sequence files were analysed with a DNA sequence manipulation software (Snapgene) to compare to the desired sequence. Plasmid with the correct sequence were retransformed into bacterial hosts and stocked as both DNA and bacterial stocks.

Plasmid Stocking

3.1.1.5 Confirmed plasmids were stocked in both DNA and bacterial format. For DNA stocks, 10 µl of the purified plasmid was directly stored at -80˚C. For bacterial stocks; the retransformed bacterial culture was mixed with 60% glycerol to a final percentage of 15% in 2ml cryo tubes before storage at -80˚C.

3.1.2 Yeast Strain construction

Yeast integration

Modifications to the genome of various *Saccharomyces cerevisiae* background strains were made using standard yeast integration methods. DNA fragments for insertion were synthesized by PCR from source DNA in the form of plasmids. Oligonucleotide primers were designed using standard design principles for binding to the source DNA and including a 40 bp region complementary to the desired insertion site within the yeast genome. PCR was performed using a high-fidelity proofreading polymerase (Expand High-Fidelity PCR System – Roche) with buffer and nucleotide concentrations as well as thermal profiles according to the manufacturers recommendations in an automated thermocycler (T100 -

3.1.2.1

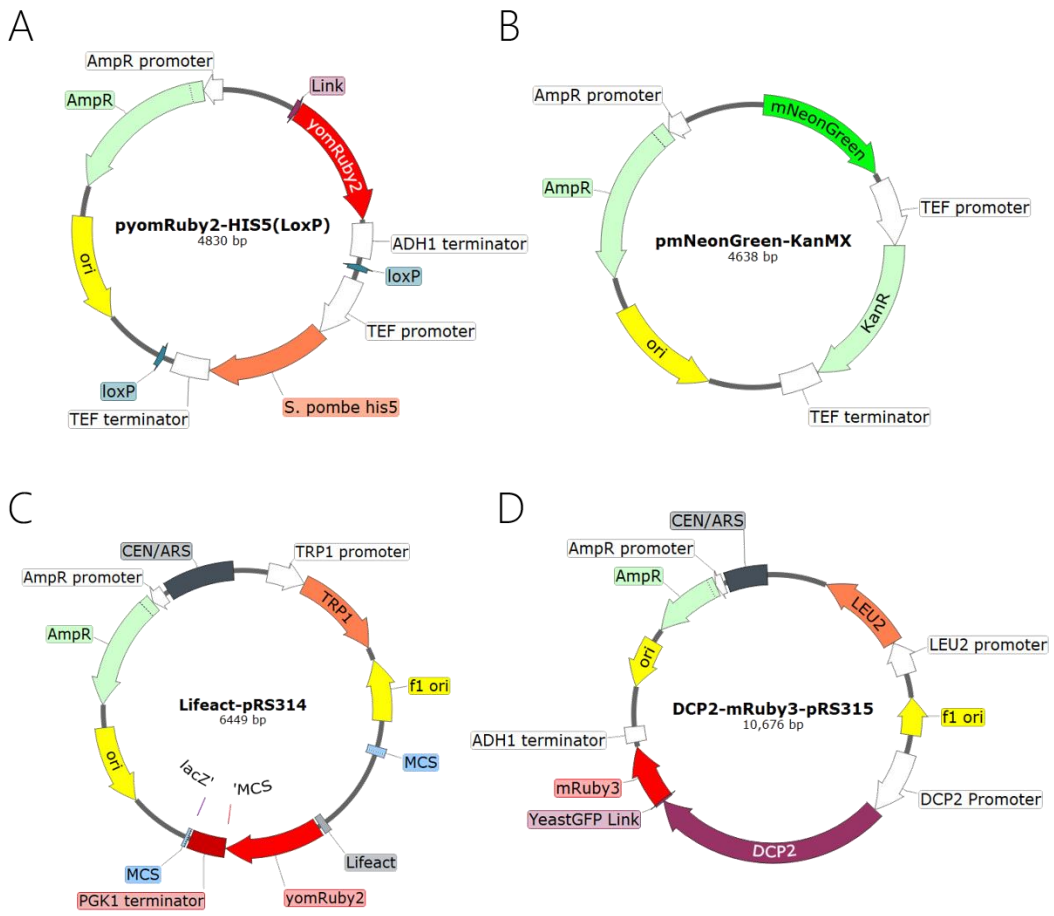

Figure 12: The main plasmids used in this study,
Top Row – A & B, plasmids for integrating fluorescent proteins to create fusion with endogenous yeast proteins. C - Lifeact plasmid created from mRuby2 fluorescent protein and yeast actin binding protein sequence used to visualise actin in live yeast cells. D – DCP2-mRuby 2 expressing plasmid used for the visualisation of p-bodies when combined with yeastGFP collection strains.

Bio-Rad) at a total volume of 50 µl. 5 µl of the PCR product was run on an agarose gel as previously to confirm amplification of the target sequence. Multiple PCR reactions were performed to produce the quantity of DNA required for yeast integration. DNA was purified by ethanol precipitation; 2.5 volumes of 100% ethanol were added to the completed PCR reaction along with 0.1 volumes of Sodium Acetate. This mixture was incubated at -20˚C for 20 minutes and then centrifuged at 13,000 g for 10 minutes. The supernatant was discarded, and the DNA pellet was washed once with 1ml 70% ethanol before drying in a laminar flow hood and resuspension in 10 µl ddH2O.

Integration into the yeast genome was performed using a protocol adapted from Gietz & Woods, 2002. Briefly, a 5 ml culture of yeast growth media, either YPAD or SC lacking specific nutrients (see appendix for compositions), was inoculated with the yeast strain to be transformed from either glycerol stock or agar plate. The culture was incubated overnight at 30˚C in a shaking incubator at 200 rpm. The following day, 50 ml pre-warmed 2X YPAD or SC media was inoculated with the culture to give an OD600 of 0.2 as measured by a spectrophotometer. The culture was incubated at 30˚C for 3-4 hours until the OD600 reached 0.6. Cells were then harvested by centrifugation at 4000 rpm in a bench top centrifuge (5810R, Eppendorf) using 50 ml centrifuge tubes. Cells were washed once in 25 ml ddH2O and then resuspended in 1 ml ddH2O and transferred to 2 ml Eppendorf tubes. Cells were centrifuged again at 13,000 g for 30 seconds and washed in 1.5 ml freshly prepared 1X TE/Lithium Acetate buffer (see appendix for details) before resuspension in a final volume of 200 µl 1X TE/Lithium Acetate buffer. For a single transformation, 2 µg of DNA for integration was mixed with 10 µl salmon sperm DNA (Invitrogen). Salmon sperm DNA was pre-boiled at 95˚C for 10 minutes and placed on ice for at least 10 minutes before transformation. 50 µl cells in buffer were added to the mixture, followed by 240 µl of PEG/TE/Lithium Acetate buffer (see appendix for details) and the mixture was topped up to 360 µl with ddH2O. The transformation mix was first incubated for 30 minutes at 30˚C followed by 45 minutes at 42˚C after which 1 ml YPD was added to the mixture and it was transferred to a loose top 12 ml growth tube. The transformation mix was incubated overnight at 30˚C then transferred back to a 2ml Eppendorf tube before centrifugation at 13,000 g for 1 minute. The cell pellet was then washed once in 1 ml ddH2O, resuspended in 1 ml

ddH2O and then plated onto the appropriate selection media + agar (see appendix for compositions) at volumes of 10 µl, 100 µl and 890 µl and incubated for 3 days at 30˚C. Colonies appearing on plates after this time were screened for positive integrations as described below.

Yeast plasmid transformation

3.1.2.2 Plasmid transformation of *Saccharomyces cerevisiae* strains was performed following the same protocol as DNA integration, with slight modification. Plasmid DNA was used instead of PCR products, in a total quantity of 100 – 500 ng. The step in yeast integration of refreshing the yeast culture to OD600 0.2 was omitted, and cultures were processed directly from overnight growth. Plasmid transformations of yeast strains were assumed to be successful if the colonies grew on selective media after streaking for single colonies from the original selection plate.

CRISPR Yeast integration

3.1.2.3 For certain experiments it was desirable to integrate a DNA sequence into the yeast genome without a selection marker in order to maintain the 3' UTR of the modified ORF. To achieve this marker-less integration, CRISPR based genome editing was employed as described in Dicarlo et al., 2013. Cas9 and gRNA plasmids were constructed as described in

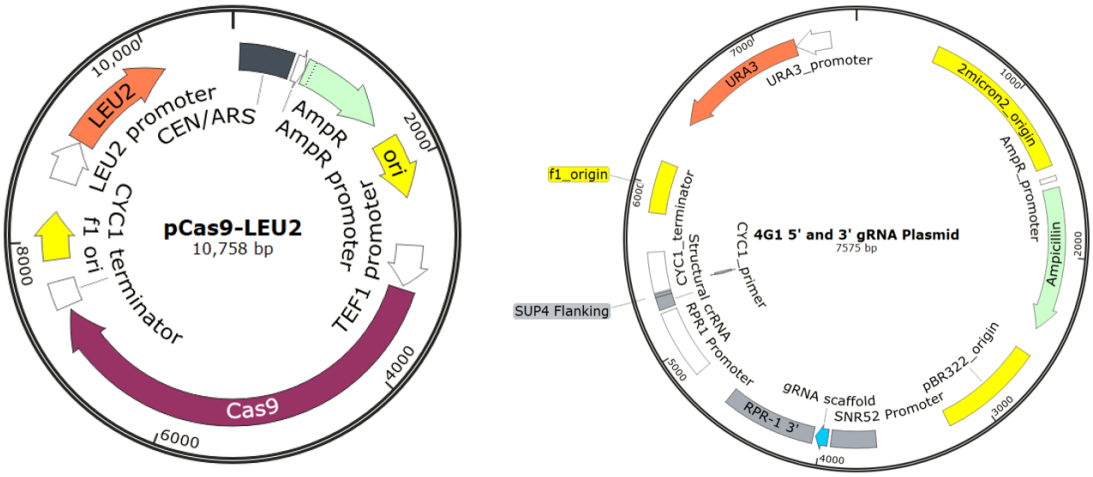

Figure 13: Plasmids used in the CRISPR-Cas9 Genome modification process.
Left – the Cas9 protein was carried on a yeast centromeric plasmid for constant expression in yeast cells. Right – A yeast 2-micron plasmid was used to express 2 different gRNA constructs, cutting at 2 separate locations within the yeast genome. Target strains were transformed with both plasmids to allow Cas9 targeting of the gRNA sequence. Strains were co-transformed with homologous DNA to replace the excised fragment.

the Molecular Cloning section of this document. The gRNA plasmid was modified to include 2 gRNA target sequences, one at the start of the desired insertion site and one at the end, in order to induce 2 double stranded DNA breaks. Donor DNA was synthesized via PCR as described previously for yeast integration, but any marker region was omitted from the target sequence. The Cas9 expression plasmid was first transformed into the target strain and confirmed, followed by a dual transformation with the gRNA plasmid and donor DNA. Selective media was used to select for both the Cas9 and gRNA plasmid after which colonies were screened for the integration product as described below. Confirmed colonies were then grown for several generations in liquid rich media (YPD – see appendix for composition) in order to remove the Cas9 and gRNA plasmids. The plasmids involved in this process are shown in Figure 13.

3.1.3 GFP Library replication

Multiple strains that were to be used in this study were derived from the Yeast GFP library described in Huh, W.K. et al. (2003), purchased from Invitrogen. To safely retrieve these strains from the library without risk of contamination, the library collection was replicated using a liquid handling robot (Freedom EVO 200, Tecan). This robot was equipped with a 96 well plate carousel; plate handling arm and 96 well pipetting head. A script was created (see appendix) in the robot's accompanying software to replicate plate with the following protocol: 96 well plates containing the yeast strains were retrieved from the carousel and shaken for 1 minute, followed by 3 empty 96 well plates using, the plate handling arm. The empty plates were filled with 150 µl sterile SC – His media per well (see appendix or composition) using the 96 well pipetting head, after which 5 µl of culture from the yeast plate was added to the corresponding well in the 3 new plates, using fresh pipette tips for each new source plate. Plates were returned to the carousel, after which the source plate was returned to -80˚C for storage. The 3 replicate plates were incubated, without shaking at 30˚C for 2 days, after which 60% glycerol was added to each well to a final percentage of 15% using an electronic pipette in a bio-containment hood. These replica plates were then stored at -80˚C and used as the source for the desired clones. Before use in experiments, clones were confirmed via PCR as described below.

High throughput plasmid transformation

3.1.3.1 Where strains from the GFP collection were augmented with plasmids, a modified yeast plasmid transformation protocol was used to increase throughput. For each well in a 96 well plate, the plasmid transformation protocol was reduced in scale, with a starting culture of 150 µl. After centrifugation in a plate centrifuge (5810R, Eppendorf) and 2 washes in 150 µl ddH2O, cells were resuspended in a transformation mixture of 25 µl TE/Lithium Acetate Buffer, 100 ng plasmid DNA, 5 µl pre-boiled salmon sperm DNA (prepared as described previously), and 120 µl PEG/TE/Lithium Acetate buffer, topped up to a total of 180 µl with ddH2O. The 96 well plate was incubated at 42˚C for 45 minutes after which the plate was centrifuged, and the cell pellets were resuspended ddH2O. Cells from individual wells were spotted onto selective media using a multichannel pipette and incubated for 3 days at 30˚C after which the spots were restreaked onto segments of selective agar media plates and assumed to be correctly transformed if growth was observed after 2 days incubation at 30˚C.

3.1.4 PCR Clone screening

To verify correct integration of genomic construct, or transformation of plasmid into the S. *cerevisiae* strains, PCR was used to amplify regions present only in the desired modified strains. Before PCR amplification, genomic and plasmid DNA was purified from the potential clones using the following protocol; from a selective plate following transformation, a single colony was picked using a sterile pipette tip and resuspended in 100ul of yeast Lysis Buffer (see appendix for composition) in an Eppendorf tube. The tube was placed in a dry heat block at 70˚C for 15 minutes before the addition of 300 µl 100% ethanol and centrifugation at 15 000 g for 12 minutes. The supernatant was discarded, and the pellet resuspended in 50 µl of ddH2O before centrifuging at 13,000 g for 1 minute after which the supernatant was used as the template for PCR. PCR was performed as with colony PCR for bacterial strain confirmation, briefly; primers were selected to amplify a region present in the genomic construct or plasmid so that it would be distinguishable from the original strain. An 18 µl PCR master mix was prepared with 2X DreamTaq Green PCR Master Mix (Thermo Fisher Scientific) according to the manufacturer's recommendations, including relevant primers. 2 µl of purified yeast DNA was added so the final PCR volume was 20 µl.

PCR was performed using thermal profiles according to the manufacturer's recommendations in an automated thermocycler (T100 - Bio-Rad) after which 10 µl of the reaction mixture (that included a DNA loading dye in the master mix) was loaded directly onto an agarose gel and analysed as described previously. Strains showing the expected DNA product were restreaked onto fresh selective media plates and carried forward for further confirmation. Example gel images are shown in Figure 14.

3.1.5 DNA Sequencing

For some genome modifications it was necessary to confirm the exact sequence of the integrated product. Genomic DNA extraction was performed as described previously, after which PCR was used to amplify the region for sequencing. PCR was performed using a proofreading DNA polymerase and appropriate buffer system (Q5 – New England Biolabs) with buffer and nucleotide concentrations as well as thermal profiles according to the manufacturers recommendations in an automated thermocycler (T100 - Bio-Rad) at a total volume of 50 µl. After amplification PCR products were purified using a spin column based DNA purification kit (Zymo Research) and DNA concentration was measured via a

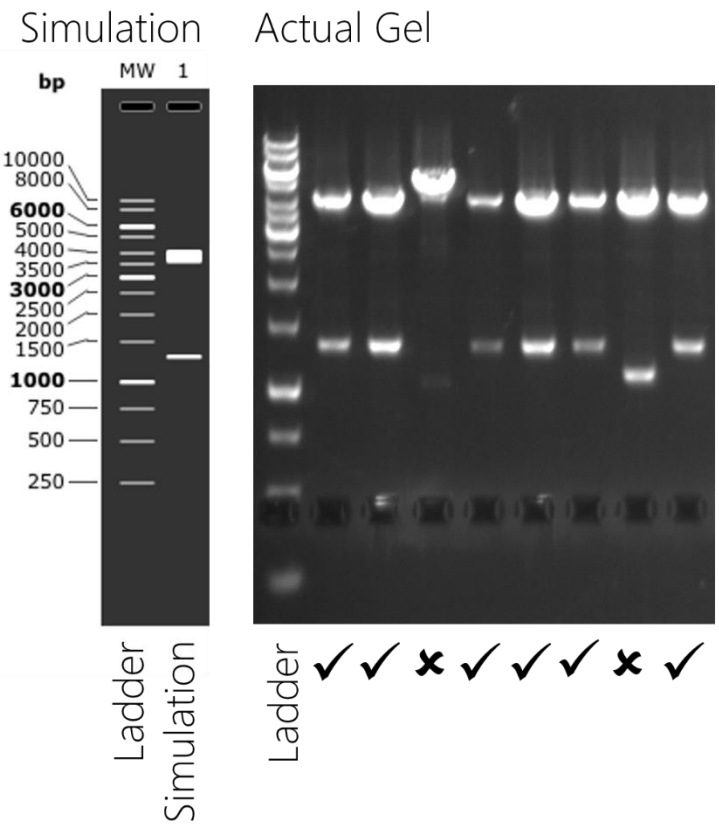

Figure 14: Example of DNA agarose gel. Gel results were first simulated in a software (Snapgene, GSL Biotech, USA) to calculate the expected band pattern. After running samples on agarose gels, they were compared with the simulation to find correct integrations or plasmid constructs. Correct results were carried forward for further experimentation.

spectrophotometer as with restriction digest fragments. The purified PCR product was sent for DNA sequencing to a commercial DNA sequencing service (GATC Lightrun) in a mixture according to the service's specification. Primers were designed to be 10-20 bp downstream of the PCR amplification primers. Multiple PCR and sequencing runs were performed where the region to be sequenced exceeded the maximum run length for the DNA sequencing service (roughly 1.2 kb). After confirmation by sequencing, strains were either stocked as described below or further analysed by fluorescence microscopy.

3.1.6 Fluorescence screening

As a final confirmation measure for strains that were designed to express a fluorescent protein, either as a fusion or individual protein, a fluorescence microscope was used to ensure that cells were indeed expressing the desired protein, and that the localisation of proteins was not altered by the fusion of the fluorescent tag. To prepare cells for microscopy, a single colony of cells was picked with a sterile pipette tip and inoculated into 10ml low fluorescence media (see appendix for composition) then grown overnight at 30˚C in a shaking incubator at 200 rpm. In the morning cells were diluted to an OD600 of 0.2 and grown in the same manner as previously until the OD600 reached 0.6. 1 ml of cells were then centrifuged at 13,000 g for 1 minute and resuspended in 100 µl low fluorescence media. 3 µl of the concentrated yeast suspension was placed on a standard glass microscope slide and covered with a 22 x 22 mm #1.5 glass coverslip, which sealed to the slide through capillary action. The prepared slide was analysed using an inverted fluorescence microscope (Axio Vert.A1 – Zeiss) equipped with a 60X NA 1.4 oil objective lens. Fluorescence illumination was achieved with a metal halide light source (HXP 120 – Zeiss) and filtered through appropriate excitation and emission filter sets for the fluorophore in question. Images were captured using a monochrome CCD camera (Axiocam ICm – Zeiss) using the Zeiss Zen software. Clones were selected for further experimentation if the fluorescent protein was visible as expected, and the localisation of the fusion protein corresponded to the established literature. Example images are shown in Figure 15.

For fluorescent tags of proteins involved in p-body or stress granule formation, where stress conditions such as glucose deprivation were expected to cause a change in localisation, further confirmation was performed to ensure the fluorescent tag had no effect on the ability to enter these mRNP granules. Cells were grown overnight as with standard fluorescence screening and refreshed to OD600 0.2 in the morning. After achieving an OD600 of 0.6, cells were centrifuged at 13,000 g for 1 minute before 3 washes in low fluorescence media lacking glucose. Cells were resuspended to the original volume in low fluorescence media lacking glucose and incubated at 30˚C, shaking at 200 rpm, for 60 minutes before proceeding with microscopy as previously.

3.1.7 Yeast strain stocking

After confirmation yeast strains were stocked for use in further experimentation. 2 ml overnight cultures were grown at 30˚C, shaking at 200 rpm, in appropriate media. After growth, 750 ml of each culture was mixed with 250 ml 60% glycerol in a cryo tube and stored at -80˚C until use.

3.2 Microfluidic system fabrication

3.2.1 Microfluidic mask design

To create digital designs for use in the production of microfluidic moulds, a 3D design software (AutoCAD) was used to create accurate scaled drawings. The polyline tool was used for drawing the outlines of the desired shapes, and all drawings were confined in a design template corresponding to the size of the microfluidic mask. A summary of each of the designs used in this study is shown in Figure 16. Completed designs were sent to a commercial printing service (Micro Lithography Services Ltd) for production of acetate or chromium masks depending on the required feature size. Further details of the designs

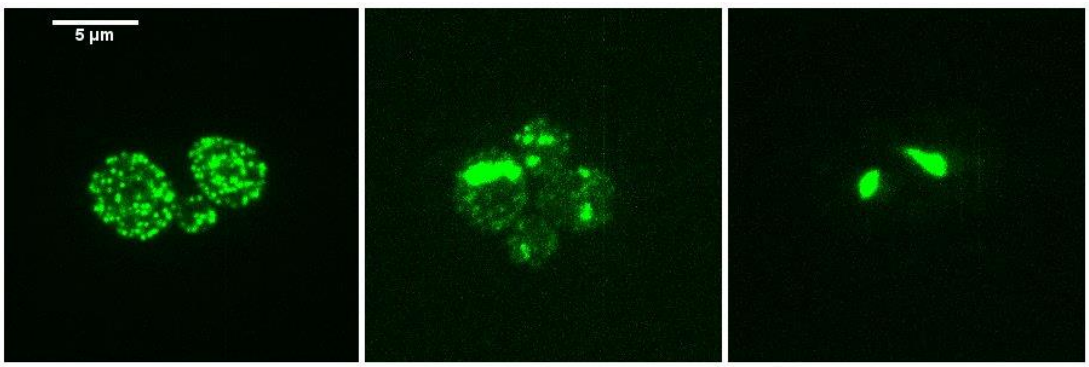

Figure 15: Example micrographs of transformed yeast strains. These images show examples of positive integrations of mNeonGreen into organelle markers.

used in this study are outlined in the subsequent sections.

3.2.2 Su-8 Mould fabrication

Su-8 moulds for this study were obtained from 2 separate sources. Originally, moulds were purchased from a commercial mould making service (MicroLiquid – Spain). For some of these moulds it was found that the resolution was insufficient for the size of trap structure used in the desired microfluidic chips, leading to failure to trap cells of *Saccharomyces cerevisiae*. Therefore, collaboration was sought with a group at the university with the capability to more accurately produce the moulds. For the chips used in this study Su-8 moulds were produced by the research group of Marco Polin, University of Warwick, Department of Physics. Production was carried out as performed in Jo et al. (2015). Briefly, Su-8 2005 (MicroChem) was spun onto a 4" silicon wafer (Si-Mat Silicon Materials) at the recommended rpm, time and acceleration to achieve a 5 µm thick layer, according to the manufacturer. Wafers were then soft baked at 65˚C for 1 minute followed by 3 minutes at 95˚C. UV light exposure was used to pattern the wafer with the desired mask design; the wafer was exposed to 150 mJ/cm2 UV light using a mask aligner (SÜSS Microtec AG, Model MJB4). Post exposure baking was performed at 65˚C for 1 minute and 95˚C for 2 minutes, followed by developing in Su-8 developer for 3 minutes and a final hard bake at 150˚C for 30 minutes. These wafers were then used as the moulds to produce PDMS microfluidic chips.

3.2.3 PDMS Chip fabrication

PDMS chips were fabricated using established procedures. All steps were carried out in a laminar flow hood. Sylgard 184 base and catalyst (Dow Corning) were mixed thoroughly in a ratio of 10:1 before degassing in a vacuum chamber. The wafer mould was placed in an aluminium foil lined 120mm borosilicate glass petri dish and the mixture was poured onto the wafer to a depth of 0.5 – 1 mm before degassing again. The petri dish was then covered with its corresponding glass lid and placed in a 65˚C oven for 2 hours. Once cured, the PDMS slab was diced into individual chips (see figure 16). Inlet/outlet holes were punched using blunted and polished 21 Gauge needles to give smooth sided channels for making connections. Where inlet/outlet channels were ripped during punching, the channel was abandoned due to the possibility of leakage. After punching, excess PDMS debris was

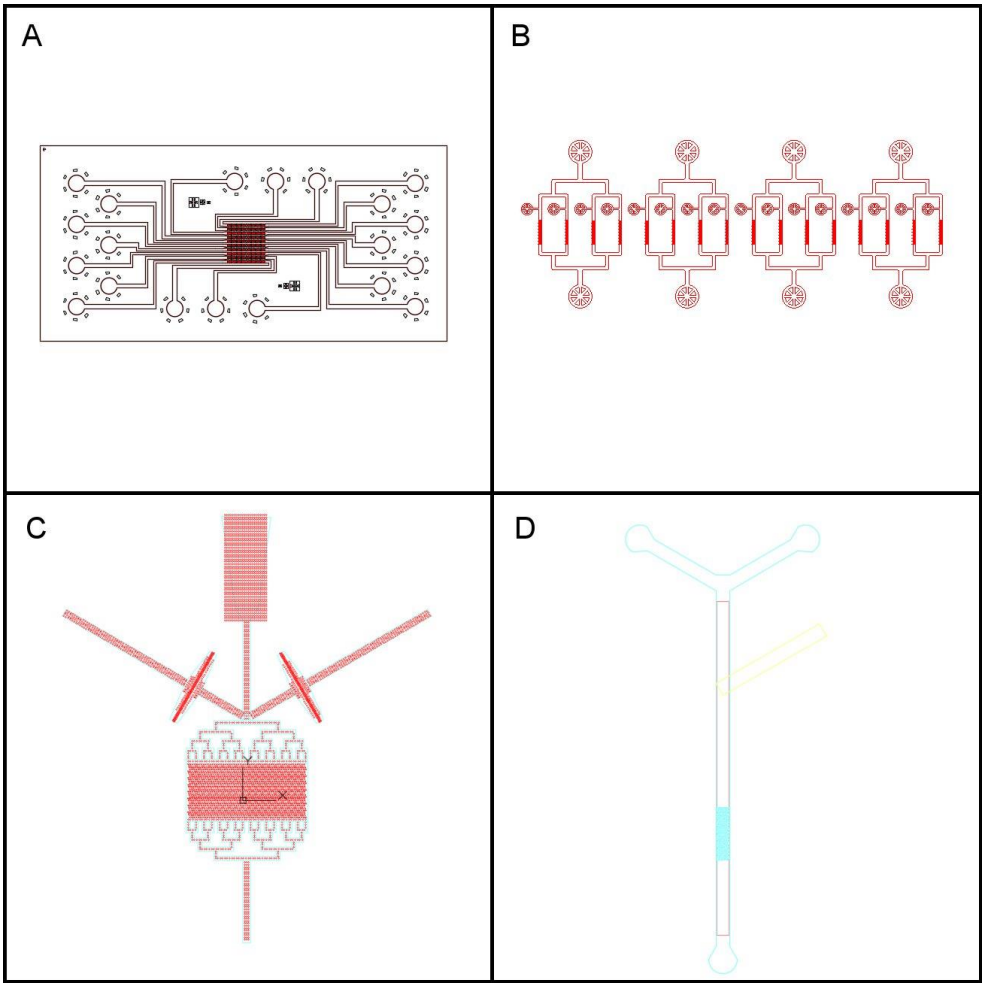

Figure 16: Designs of microfluidic masks fabricated for this study.
A, CliC 2 device, B – HYAA device, C, ALCATRAS device, D – Lee et al microfluidic dissection device. See figures 19 -22 for further detail.

cleaned off using scotch tape (3M) after which individual PDMS chips were rinsed in 100% ethanol before 3 washes in 0.2 µm filtered ddH2O and drying pattern side up on whatman paper. Punched and cleaned PDMS chips were then bonded to coverslips. 24 x 60 mm #1.5 glass coverslips (Scientific Laboratory Supplies) were washed in isopropanol before drying with filtered compressed air. Both the coverslip and PDMS chip were cleaned on the bonding side with scotch tape before placing in a plasma cleaner (Expanded table top Plasma Cleaner - Harrick Plasma). The plasma cleaner chamber was purged with 100% oxygen before evacuation with a vacuum pump to a pressure of 300 mTorr. The plasma cleaner was run for 60 seconds on its highest setting, before re-pressurising the chamber. The bondable sides of the coverslip and PDMS chip were immediately placed in contact and incubated on a hotplate for 20 minutes at 65˚C, completing the fabrication process. Bonding was tested after 1 hour by attempting to peel the coverslip from the chip to ensure the bond would hold under pressure.

3.2.4 Epoxy/Polyurethane replica moulding

To preserve the original Su-8 master moulds in optimal condition, an un-bonded chip was used to create a replica mould that was used for all subsequent mouldings. A diced PDMS chip was placed pattern side up in a 50 x 70 mm silicon cake mould and held in place by the native silicon-silicon bond. A 2-part polyurethane casting resin (Fast Cast – easycomposites) was mixed in the manufacturers recommended ratio and poured into the mould, degassing was unnecessary due to the low viscosity of the resin. The resin was cured at room temperature until solid, after which the resin block was removed from the mould, and the now embedded chip removed from the block. The resin block was then used as a mould for the fabrication of further PDMS chips, as described previously, although curing of the PDMS was carried out overnight at room temperature and no degassing of the PDMS took place after pouring.

3.2.5 Fluid reservoir fabrication

Due to the expense of commercial microfluidic reservoirs, custom reservoirs were constructed to allow the operation of multiple microfluidic channels simultaneously. Reservoirs were created in volumes of 2 ml, 50 ml and 100 ml for use in various experiments.

To create 2 ml reservoirs a 5 mm layer of 2-part polyurethane resin (mixed as previously) was poured into a 50 x 70 mm silicon cake mould. 8 x 2 ml screw cap tubes (Sarstedt) were then placed open end down onto the cured resin block. A further layer of polyurethane resin, sufficient only to cover the thread of the 2 ml tubes was poured into the mould and allowed to cure. Once cured, the 2 ml tubes were removed by unscrewing from the resin block and an appropriately sized O-ring was placed into each formed cavity. Inlet and outlet holes were created by heating a 21-gauge needle and inserting it into the top of the cavities to form 2 holes spanning the 5 mm polyurethane layer. A 21-gauge leur lock needle was then place into one of the holes of each cavity and sealed using a small amount of polyurethane resin. A 3-inch length of 21-gauge tubing was inserted into the second of the holes to a depth corresponding to the bottom of the 2 ml tube and again sealed with polyurethane resin. These completed resin blocks were then used as microfluidic reservoir manifolds, able to hold 8 fresh, sterile 2 ml tubes and be connected to a pressure source via the luer lock needle and pump fluid using the 3" tubing outlet. The manifold was sterilized with 70% ethanol before each new experiment.

50 ml reservoirs were created in a similar fashion to 2 ml reservoirs. An initial 5 mm layer of polyurethane resin was poured and cured in the cake mould. 2 x 50 ml polypropylene centrifuge tubes (Centristar - Corning) were placed, open end down onto the resin layer. A further layer of polyurethane resin, sufficient only to cover the thread of the 50 ml tubes was poured into the mould and allowed to cure. The tubes were then removed from the resin block and the block was removed from the cake mould and inverted before replacing it into the mould. 2 x 1/4"- 28 male threaded Teflon connectors (Elveflow) were placed thread down over the locations of each cavity at even spacing. A third layer of polyurethane resin was then poured to cover the threads of these connectors. The time between pouring/curing of these 3 layers was minimised to maximise the bonding between layers. Once cured the connecters were removed by unscrewing them from the resin block. In the cavities formed by these connectors, a 1.6 mm hole was drilled in the original layer. To allow the passage of microfluidic tubing into the 50 ml tubes. The completed reservoirs were removed from the cake mould and into one of the threaded cavities, a 1/4"- 28 male threaded 3/32" OD hose barb was inserted, sealed with PTFE tape. For experiments,

pressure was provided via flexible silicon tubing connected to the hose barb, while microfluidic tubing was connected via the second cavity using a 1/4"- 28 male threaded Teflon connector and associated ferule (Elveflow). Fresh 50 ml sterile tubes were used for each experiment, while the reservoirs were sterilized with 70% ethanol.

100 ml reservoirs were created using GL45 threaded bottle caps. Bottle caps with 20 mm apertures designed for septa (Duran Group) were placed top down in a silicon cake mould (described previously). 2-part polyurethane resin was poured into the cap at a depth of 5 mm and allowed to set until rigid enough to move. The cap was then inverted and a 25 mm diameter x 20mm plastic tube was placed over the setting polyurethane. 2 x 1/4"- 28 male threaded Teflon connectors (Elveflow) were placed thread down evenly spaced inside the tube and 2-part polyurethane resin was poured to cover the threads. Once both resin parts were fully set, a 1.6 mm hole was drilled through the initial layer to allow for tubing to be inserted. For experiments, pressure was provided via flexible silicon tubing connected to the hose barb, while microfluidic tubing was connected via the second cavity using a 1/4"- 28 male threaded Teflon connector and associated ferule (Elveflow). Fresh 100 ml media bottle (Duran Group) were sterilized by autoclaving with media already inside, and then attached to the fabricated lids for experiments, while the lids were sterilized with 70% ethanol. These reservoirs were also used for larger media bottles with GL45 threads for longer experiments.

3.2.6 Fluidic connection fabrication

Connectors to bridge the gap between microfluidic tubing and PDMS microfluidic chips were fabricated using 21-gauge 316L stainless steel tubing (Coopers Needle Works). Tubing was cut to 2-inch lengths using a diamond edge blade on a rotary tool. Openings at each end were polished and cleaned using a sanding disk and burr attached to a rotary tool. A 90˚ bend was then introduced 2/3 of the way along the length. These metal connectors were inserted one end into the punched inlet of the PDMS chip, lubricated using isopropanol, and one end into 1/32" ID PTFE Tubing (Sigma), inserted into the media reservoirs. Both tubing and connectors were sterilized by autoclaving before experiments.

3.3 Microscopy

3.3.1 CellASIC microfluidic platform set-up

For experiments using the CellASIC microfluidic platform, CellASIC Y04C plates were used to trap cells in a single focal plane. To prepare the cells and plates for imaging, cells were grown overnight in 10 ml YEP with 2 % glucose followed by re-inoculation to and OD600 of 0.2. Cells were then allowed to grow for several hours until reaching an OD600 of 0.6 or above. CellASIC plates were removed from their packaging on the morning of the experiment and allowed to equilibrate with in a 30˚C incubator until use. The storage buffer (present in the packaging) was removed from all wells and they were washed 3 times with filter-sterilized ddH_2O. Wells were then filled with the relevant media to the maximum allowed volume, 300 µl for wells 1 – 6. Well 7 was left empty for waste collection and well 8, the cell loading well, was loaded with 50ul 2 % glucose version of the media to be used in the experiment. The CellASIC plate was connected to the controller and wells 1 – 6 were infused for 5 minutes at 5 µl/hour to remove residual storage buffer from the microfluidic channels. Well 8 was then infused for 5 seconds at 8 µl/hour to remove residual buffer from that channel. The plate was disconnected from the controller and the media was removed from well 8 and replaced with 50 µl of log phase cell culture. The plate was reloaded onto the controller and cells were infused into the imaging area at 8 µl/hour in 5 second bursts until sufficient cells were visible to begin the experiment. Once cells were loaded, the relevant infusion program was started, and imaging was initiated.

3.3.2 Microfluidic chip platform set-up

For experiments using the aforementioned microfluidic chips, a customized microfluidic platform was used to provide constant media to the cells. The set-up was split into 3 steps, priming, cell loading and running. In the priming step, media was flown into the chips to remove any debris present and fill the channels with liquid. Cells were then loaded into the chip, using different methods depending on the chip in use. Finally, conditions for the experiment were set and media was infused at a constant rate for the duration or the experiment.

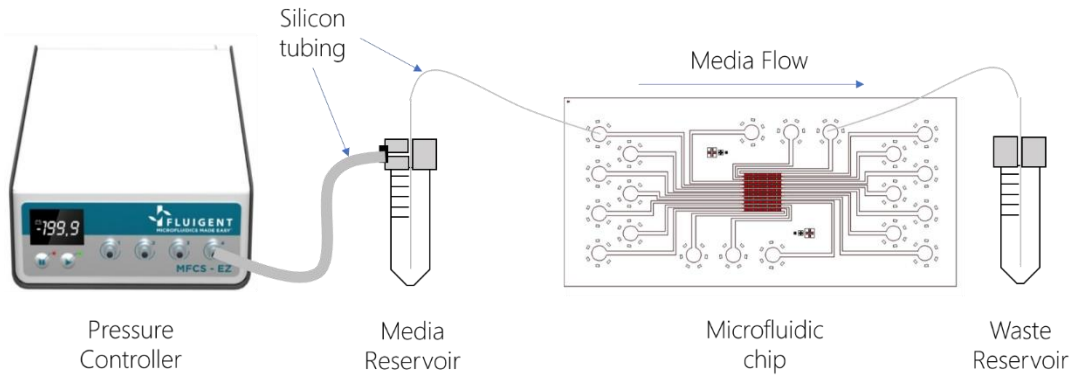

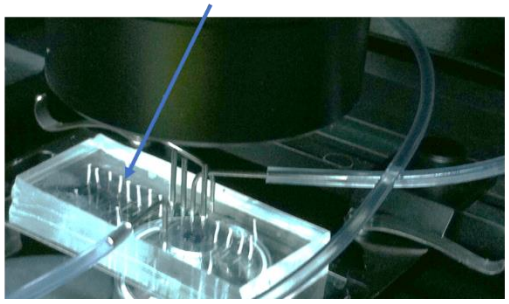

Figure 17: Diagram of the microfluidic platform as used in this study. Media flow to the microfluidic chips was controllerd with an air pressure controller. The chips were placed above the objective lens of an inverted microscope to alow observation of cells during growth.

Before priming the chips, all necessary connections were made between the chip, the media source and the waste outlet. To simplify the running process of multichannel chips, a single pneumatic pressure source (MFCS-EZ – Fluigent) was split into multiple outputs using t-shaped push in connectors and used to provide the pressure to drive media flow. Each positive pressure output was connected to a media reservoir (as previously described) using a 1/4"- 28 threaded 3/32" OD hose barb (Elveflow) via silicon tubing (Sigma). Connection to the chips was made using 1/16" ID / 1/32" OD PTFE Tubing (Sigma) inserted into the fabricated holes in the reservoirs and sealed using 1/4"- 28 male threaded Teflon connectors and associated ferules (Elveflow). Air pressure was increased to a level where visible movement of the media could be seen in the PTFE tubing, and halted when the media reached the open end of the tubing. At this point, the tubing was connected to the stainless-steel connector at the main inlet in the microfluidic chip by plugging the connector into the internal part of the tubing. Air pressure was then dramatically reduced so as not to damage the internal structure of the chip. At the outlets of the chip, further lengths of PTFE tubing were connected to the stainless-steel connectors and fed into a 500 ml glass Duran bottle acting as a waste reservoir. Between one of these tubing lengths and the waste reservoir, a microfluidic flow rate monitor (Fluigent) was connected using the supplied connectors in order to monitor the flow rate through one channel as a proxy for

every channel. A pressure limit of 1 bar was then set in the control software to prevent over pressurization of the microfluidic chip and flow rate identification, the software process in which the flow rate/unit pressure is calculated, was performed.

The chips were then sealed to a 3D printed support, designed to add rigidity to the coverslip, using rubber cement (Fixogum), which was attached to a microscope stage insert (ASI) with a single circular opening for access by an inverted microscope objective lens.

Once the fluidic connections were made and the chips were primed with media, cells were loading into the imaging areas of each chip. This process varied between chip designs. For the HYAA chips, a second inlet is available for cell loading; this inlet was blocked using a stainless-steel pin (Linton Instrumentation) connected to PTFE tubing during priming. Once the pin and tubing were removed, media flow followed the path of least resistance through this inlet connector in order to remove any bubbles. Cells were vortexed to create a homogenous cell suspension before loading into a syringe for infusion into the microfluidic chips. Cells were loaded using 1 ml syringes (Plastic Sterile - BD) tipped with 20-gauge luer stubs (Linton Instrumentation) and connected to a short length of PTFE tubing. Gentle pressure was applied until the cell culture reached the end of the tubing, after which the tubing was threaded around the inlet connector. Further pressure was applied while observing the chip under phase contrast microscopy until cells occupied > 80% of traps in the targeted channel. Media flow was kept constant at 5 µl/min during this process so as not to over pressurize the chip. Once loading was complete the syringe was disconnected from the chip and media was allowed to flow through the loading inlet for around 2 minutes to purge any settled cells that may have casued clogging at a later stage. The pin/tubing block was then reinserted to force media flow through the main channel. This process was repeated for each channel until the required channels were occupied with cells, after which the flow rate was increased to the published optimum of 8 µl/min.

As the second device used for experiments, the CliC 2, has only an inlet and outlet, the loading procedure was somewhat different. After the chip was primed, the main inlet tubing was disconnected from the chip, leaving only the stainless-steel connector pin. A 1 ml syringe was loaded in the same manner as for the HYAA chips but connected directly to

the main inlet of the CliC 2 chip. Pressure was then applied until several cells were visible in each trapping area (no the cavities) after which the syringe was disconnected, and the main inlet reconnected. This method was chosen over the recommendation of the developers of this chip to use the outlet for loading, as it was observed that large quantities of cells would accumulate in the inlet tubing when loading form the outlet which often caused clogging of the tubing leading to a build-up of pressure but no increase in flow rate. As the inlet was used for loading, flow rate was not measured, and the pressure source was not active during the loading process. Once cells were loaded, the priming process of moving the media to the end of the tubing before connecting was repeated to minimize bubble formation, and the flow rate was set to the recommended rate of 8 µl/min.

Once priming and cell loading were complete, the pressure was maintained at a level to provide the appropriate flow rate, which was determined by the control software of the pressure controller (Fluigent). The desired imaging protocol was then started on the microscope platform.

3.3.3 Microscope Set-up

3 types of microscopy were used for this study, either widefield fluorescence microscopy or spinning disk confocal fluorescence microscopy. The microfluidic chip set-up for each microscope did not vary as they were based on the same platform, a Nikon Ti-E. The chip was placed within a temperature-controlled incubator (Okolab) set to 30˚C at least 2 hours before the experiment in order to acclimatize, after which the priming process was carried out and the chip left for a further hour. Once cells were loaded and the proper flow rates were established, imaging was started. Control of the microscope hardware and imaging protocols was performed using Nikon Elements AR (Nikon) software.

Spinning disk imaging was carried out using Nikon/Andor imaging system-combining equipment from multiple manufacturers. Excitation was achieved using a Laser stack providing 50 mW lasers at 488 and 561 nm (Andor) directed through 60 or 100 x NA 1.4 phase contrast objective lenses (Nikon). Emission filtering was performed using an Automated filter wheel (Andor) and appropriate optical filters (Semrock). For mRuby2 an RFP filter set was used, while for mNeonGreen, a filter set for GRP was used. Light was further

directed through a Yokogawa CSU-X1 Spinning Disk Unit to produce confocality. Images were then captured using a 1024 x 1024 pixel EMCCD camera (Andor iXon 888). Sample position was controlled with an automated XY stage with Piezo Z control (ASI). A white led excitation module (CoolLED) was used to illuminate the sample through a condenser to capture phase contrast images of cells, all lenses used were phase contrast compatible. Focus was maintained using an infrared LED based automatic focusing (Nikon PFS) system that kept the coverglass at the specified from the objective lens.

For widefield fluorescence microscopy, images were captured as in spinning disk microscopy, with the following changes in equipment; Excitation was achieved using a multi-wavelength LED illumination device (Xcite XLED1), with both 488 and 560 nm LEDs, filtered through filter cubes containing both excitation filter, dichroic mirror and emission filter for the selected fluorophore. Images were captured on a 2048 x 2048 sCMOS camera (Andor Zyla 4.2).

3.4 Image analysis

3.4.1 Segmentation of Cells

In order to analyse the microscopy images produced in this study on a single cell level, it was necessary to segment each image into mask that could be used to direct analysis at specific regions of the image, i.e. individual cells. To segment individual cells, an image processing protocol was developed using the image analysis software ImageJ (NIH), making use of the inbuilt macro language to automate the process. A summary of the outputs of each section are shown in Figure 18. Entire folders of images were processed by looping through each image in the folder and performing the analysis/image processing tasks before saving to a new location. Images were first opened using the "Bio-formats importer" plugin, that allowed importing of many different file types, in this case ND2 files as they were produced using the Nikon Elements AR software. Where images were a time-lapse series, each time point was opened separately for individual processing.

Images were split into their individual channels, e.g. green, red, Phase and the fluorescence channels were closed as segmentation was based on the phase contrast images. The smooth function was used to reduce noise in this image. A binary image of the phase

contrast channel was then produced using the inbuilt automatic thresholding tool with the method set to "Otsu". This produced a rough outline of the cells requiring further processing, the watershed function was used to split and adjoining cells to create a binary image of cell outlines and surrounding areas. The fill tool was then used, with the colour set to white, to manually remove the area outside the cells that was included in the thresholding limit. This produced a binary image in which the cell areas were represented as black shapes (pixel value 255) and the background/empty regions were white (pixel value 0).

To create a list of cell areas, the "Analyze Particles" tool was used, this selects the outline of each black shape in the image and adds it to a list of "Regions of Interest". This list was saved for each image and served as the list of cell outlines when performing analysis on the fluorescence channels.

3.4.2 Counting p-bodies

To count the number of p-bodies within the cell, a second macro was written in imageJ to automate the process, again entire directories of images were analysed automatically. This time only the channel with the p-body protein was used for analysis. For each segmented ROI (cell) in the specified images, the "Find Maxima" tool was used to find points of local maximum intensity, which correlated to P-bodies. Several values for noise reduction were

trialled until a final value of 200 was selected as it gave a consistently similar output to

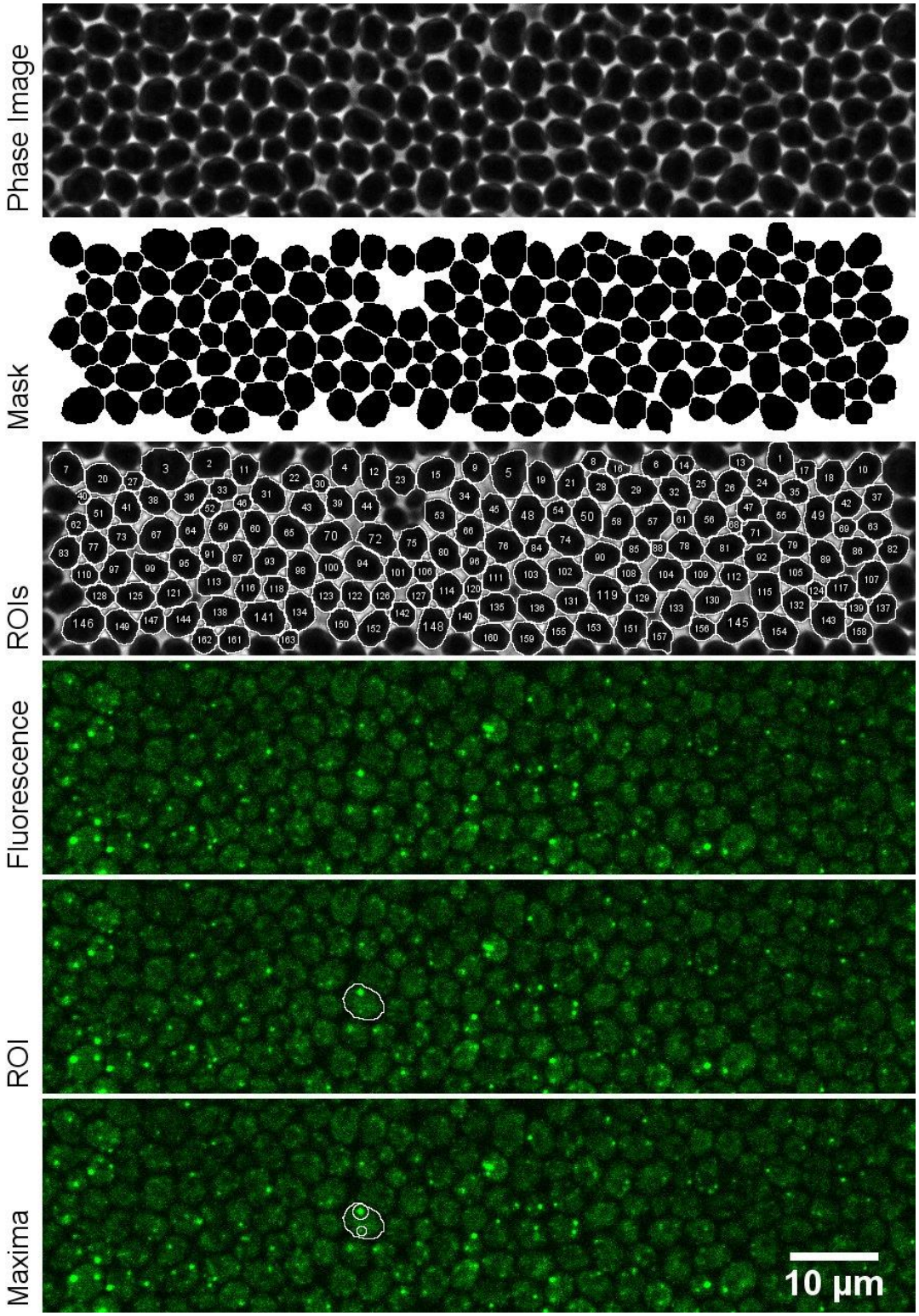

Figure 18: Demonstration of the cell segmentation and p-body analysis routine.
Cells are first segmented from a bulk image into individual cells. Next an individual ROI, correlating to a cell is further segmented in the fluorescence channel using the find maxima algorithm to identify p-bodies (local fluorescence maxima) within the cell. The identified maxima are analysed for size and intensity to register differences in morphology under various conditions.

manual selection. The total number of these maxima was recorded in a list for each cell.

3.4.3 Measuring p-body size and intensity

To measure the size and intensity of p-bodies within each cell the p-body counting script was adapted to include further processing steps. After using the "Find Maxima" tool, the sections were output as a binary image with single pixel dots representing the locations of p-bodies. These dots were expanded by 8 pixels and added to the list of ROIs using the "Analyze Particles" tool. This list was then used to cycle through the p-bodies and perform further analysis. For each p-body the ROI was duplicated from the main image, giving just an image of the body. This p-body image was then segmented using the "Otsu" thresholding method to give a binary image of the p-body. This binary image was converted to an ROI, once again using the "Analyze Particles" tool and this ROI was overlaid onto the image of the p-body. Finally, the ROI measure function was used to measure the area of the ROI, and hence the p-body, as well as the fluorescence intensity of the p-body based on the total grey value present with in the ROI.

3.4.4 Manual Curation

Each step in this automated imaging analysis protocol was manually curated by pausing the macro at certain points and checking the images for accurate segmentation. P-body selections were also checked for each image to ensure validity of the automated process.

3.4.5 Replicative age quantification

Automated counting of replicative ageing proved difficult using ImageJ due to the limited programming functions available in the standard macro language. Instead of automated counting, a semi-automated process was employed, where images were presented automatically and manually input was required for fully processing. For each time lapse series, the series was split into individual time points and saved as separate files. Files were opened in sequence and a user prompt was given instructing the user to select the relevant cell by clicking on it. After clicking on the cell, an image crop containing the cell and a small border was saved in a specified directory. Each cropped image was processed using the above outlined processing methods to produce a series of segmented images with p-body

location and quantification for each image. The segmented images were used to manually quantify the replicative age of the cells by counting the number of buds per cell.

3.4.6 P-body inheritance

To quantify p-body inheritance, the same processing steps as with replicative ageing were performed, except that the target for the crop was the p-body rather than the mother cell. Once segmentation and processing were complete, the segmentation masks and p-body spot locations were then overlaid to produce a diagrammatic representation of the p-body movement between cells. These overlays were observed when combined as a time-lapse movie and the movement between cells was quantified manually. Inheritance was recorded as positive when the p-body moved between cells without returning to the mother cell before cytokinesis. For each p-body, the number of inheritance events was recorded by following the p-body for the duration of the time lapse acquisition.

3.4.7 Cell cycle phase determination

To determine the position of p-bodies within the cell at various points within the cell cycle, segmentation of cells was performed as previously described. Each segmented image was then manually categorized based on the cellular morphology following the guide (Figure 19). For truly automated analysis of cell cycle stage based on morphology, a nuclear signal is needed to determine the transition from S to G2 to M phase, however not all of the images in this study contained a nuclear tag, and so more simple features were used to

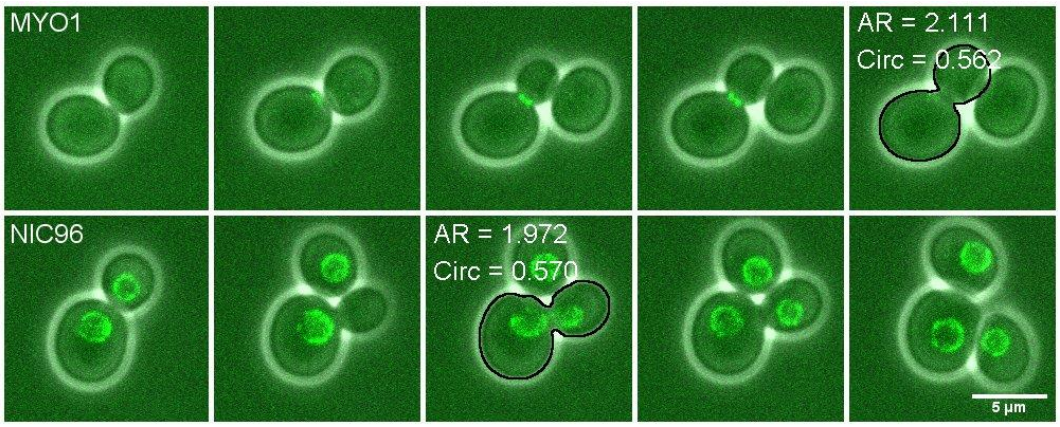

Figure 19: Cell cycle phase was determined based on shape characteristics of phase contrast cell images. AR represents the aspect ratio of the segmented cell; a higher aspect ratio means a later stage cell. Circ represents the circularity of the cell, a greater value represents a more circular shape, and hence an earlier cell cycle stage. Cells with fluorescent tags of the Myosin ring and nucleus were used to determine the values of AR and Circ for each transition point in the cell cycle.

estimate cell cycle stage. The 2 features chosen to indicate cell cycle stage were aspect ratio, where higher values indicated progression further towards cytokinesis, and circularity, where the lower values indicated a progression further into the cell cycle. For each cell/cell-bud these feature values were calculated to give an estimate of cell cycle stage, this was then correlated to p-body position within the cell. Cells with buds were identified manually, after which the aspect ratio and circularity were used to distinguish S and G2/M phase cells with a cut-off of AR = 1.8 and Circ = 0.62

3.4.8 Co-localization of p-bodies and organelles

To determine the p-body's most common position at various stages of the cell cycle, 2-colour images were subjected to co-localization analysis. Cells were segmented as described previously, then combined into one large image. The ImageJ Coloc2 plugin was used to analyses these large images, using the segmented image masks as an ROI for this analysis, i.e. the analysis was only performed within the cell boundaries. Coloc2 reports several different measures of co-localization. The co-localization analysis was performed on only subsets of the images corresponding to the different cell-cycle stages as outlined above.

The metric used to analyse p-body colocalisation with the specified organelles was the Mander's correlation coefficient as outlined below:

$$M_1 = \frac{\sum_i R_{i,colocal}}{\sum_i R_i}$$

where $R_{i,\text{colocal}} = R_i$ if $G_i > 0$ and $R_{i,\text{colocal}} = 0$ if $G_i = 0$. This represents the fractional overlap of red and green signals. In simple terms, it measures the intensity of red pixels, where the corresponding green pixel value is not equal to 0. The corresponding measure for green signal is:

$$M_2 = \frac{\sum_i G_{i,colocal}}{\sum_i G_i}$$

where $G_{i,\text{colocal}} = G_i$ if $R_i > 0$ and $G_{i,\text{colocal}} = 0$ if $R_i = 0$.

As this metric measures only values with a non-zero pixel value for the colocalisation marker, the subtraction of background signal is important in order to accurately identify pixels with signal as opposed to background.

Due to the small size and diffuse nature of some of the markers used in this study, the ideal method of thresholding (background subtraction to give 0 values), known as the Costes method proved ineffective as M values were consistently 0 using this method and thresholds gave por segmentation compared to manual observation where clear overlap was visible in micrographs. Instead, an automated threshold level was set by implementing the Otsu threshold in ImageJ (NIH). This algorithm sets the threshold by maximising the inter-class (black vs white) variance and was found to accurately represent the imaged compartments when compared to manual observation. Using this method eliminates bias in threshold setting that could otherwise influence the Mander's coefficients.

As a control, each analysed image was re-analysed, rotating one channel by 90 degrees, and re-running the analysis using the same threshold value as in the original analysis. This creates a control dataset in which there is only expected to be overlap due to chance. These two data sets were then compared by students t test to assess the significance of the overlap in the experimental set.

3.4.9 P-body tracking and velocity measurement

To follow the movement of p-bodies through the cell-cycle and calculate the changes in their velocity over these periods, the ImageJ plugin MTrackJ as utilized. MTrackJ allows the user to add tracks to a time-lapse image based on mouse clicks and calculate associated values. Fast time-lapse Images were cropped into small sections containing just a few cells, with a central cell in G1 phase of the cell cycle, and MTrackJ was used, clicking on a single p body and overlaying a track only the image after which the results for velocity were calculated using the distance between clicks and frame time interval. Velocities were then correlated to the time that they happened during the cell-cycle based on the recorded time point in the image and manual classification of the cell-cycle stage at that point.

4 Development of a robust protocol for analysis of p-bodies in *Saccharomyces cerevisiae* during replicative ageing

4.1 Existing imaging methodologies

The traditional method of p-body analysis in *Saccharomyces cerevisiae* involves growth of the cells in liquid rich media, containing sufficient glucose or other carbon source (normally YEP 2% glucose w/v) to allow optimal growth for at least 2 cell divisions following re-inoculation from an overnight culture. This would be followed by centrifugation of the culture to pellet cells and replacement of the media with a synthetic minimal media for a specified time period. The cells would them be placed on glass microscope slides, covered with a glass coverslip and imaged using a fluorescence microscope to visualise fluorescently tagged proteins (Nissan & Parker, 2008). This method has been used extensively for the in vivo visualisation of p-bodies and while it has provided much data on the numbers, localisation and protein composition of p-bodies (J. R. Buchan et al., 2008, 2011; Teixeira et al., 2005) it limits investigations to a few minutes after mounting cells. Due to these limitations researchers have developed multiple new methods for mounting cells for fluorescent microscopy.

As p-bodies, as well as some other mRNP granules, are often seen as a product of cellular stress, there are particular considerations that must be made when designing any new experimental technique relating to their analysis. In terms of microscopic analysis, any mounting/immobilisation devices for prolonged visualisation must be capable of delivering sufficient nutrients to the cells at an even rate over the experiment. This means that any new technique needs to be robustly evaluated before use in the study of p-bodies, as any change in conditions bought about by the technique could potentially bias results towards a certain conclusion. Single plane microfluidic devices such as the P-body 3.0 device (Garmendia-Torres et al., 2014) and commercially available CellASIC system have been used successfully in the study of p-bodies, as it is possible to finely tune the nutrient levels within the device to achieve reproducible results.

For this study, an experimental technique known as microfluidic dissection was used to study the changes in p-body morphology and movement during the replicative ageing process of *Saccharomyces cerevisiae*. Microfluidic dissection involves the immobilisation of

single cells of *Saccharomyces cerevisiae* in microfluidic traps, constructed as described pre-

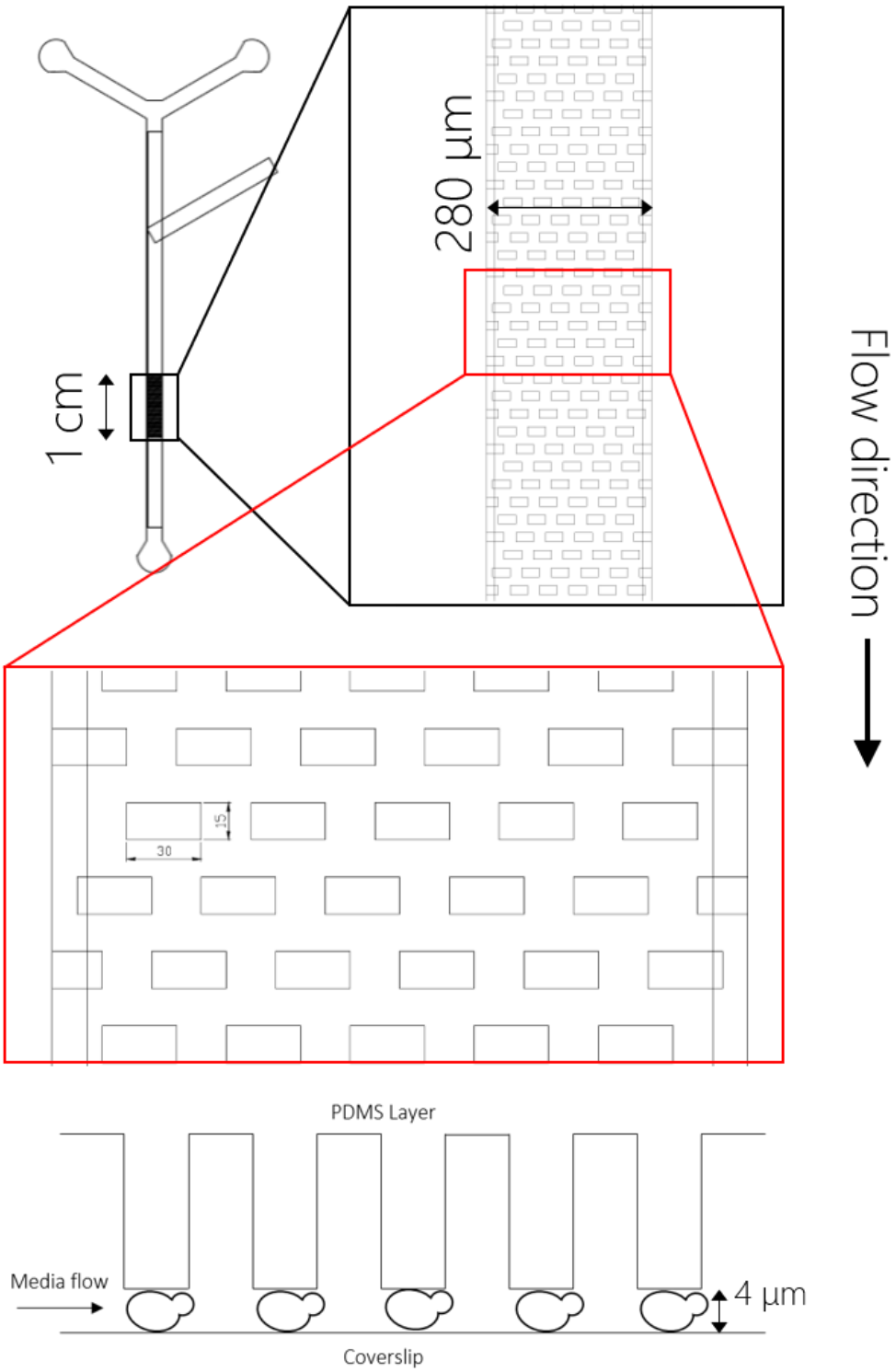

Figure 20: Microfluidic Dissection Device of Lee et al. Shown top left is the overall design of the chip. Inlets are punched at the 2 forks of the Y shape as well as the secondary side channel. Outlet is punched at the base of the Y shape. An array of pads (shown top right) is used to trap multiple cells. The size of the pads, shown centre are engineered to account for slight movements in cells, units are in micrometres. Cells are trapped beneath these pads due to the close proximity (4 µm depending on fabrication) to the coverslip glass.

viously, followed by the application of media flow to remove the daughter cells and observe only the replicatively ageing mother. These trapping devices are then placed above the objective of an inverted fluorescence microscope, which is used to visualise the cells and any fluorescently labelled proteins within them. Microfluidic dissection devices are necessary due to the exponential nature of yeast cell growth, meaning that without removing daughter cells, an imaging field would be completely filled with cells in a matter of hours, making replicative age analysis impossible. While multiple designs for these trapping devices have been published (Jo & Qin, 2016), none had previously been applied to the study of p-bodies, or any other stress induced mRNP aggregates, so no data was available on the suitability of these devices for such a study. It was therefore necessary to evaluate multiple design options to find the most suitable device for the analysis of p-bodies over the Saccharomyces cerevisiae replicative lifespan.

4.2 Microfluidic dissection devices available for evaluation

Four different device designs were obtained from the original publishers in order to evaluate their suitability for the study of p-bodies. The design principles of each of these devices can be seen in Figure 20 to Figure 23.

The microfluidic dissection device of S. Lee et al., 2012, is a multilayer single channel device that retains cells below multiple columns attached to the roof of the channel (imagine a stalactite). This column ends approximately 4 µm from the glass coverslip, while the channel roof is significantly higher. Mother cells are loaded below the columns by flowing cells into the device above the normal operating pressure, pushing the columns upwards and trapping cells when the pressure is released. Media is then flowed through at a reduced pressure, cells begin to grow, and daughter cells are removed in the media flow as they grow beyond the area of the base of the column.

The ALCATRAS (Crane et al., 2014) and HYAA (Jo et al., 2015) devices use similar concepts in order to trap the mother yeast cells. Either V shape or cup shaped traps are placed in an array within a microfluidic channel, and cells are flowed through the channel in a unidirectional manner. Mother cells become trapped against/within the trapping structures due to the pressure of the media flow and daughter cells, budding either above or through

the gaps in the trap structure, are washed away. One of the main advantages of these devices is that they are single layer of 5 - 6 µm, making the fabrication process significantly

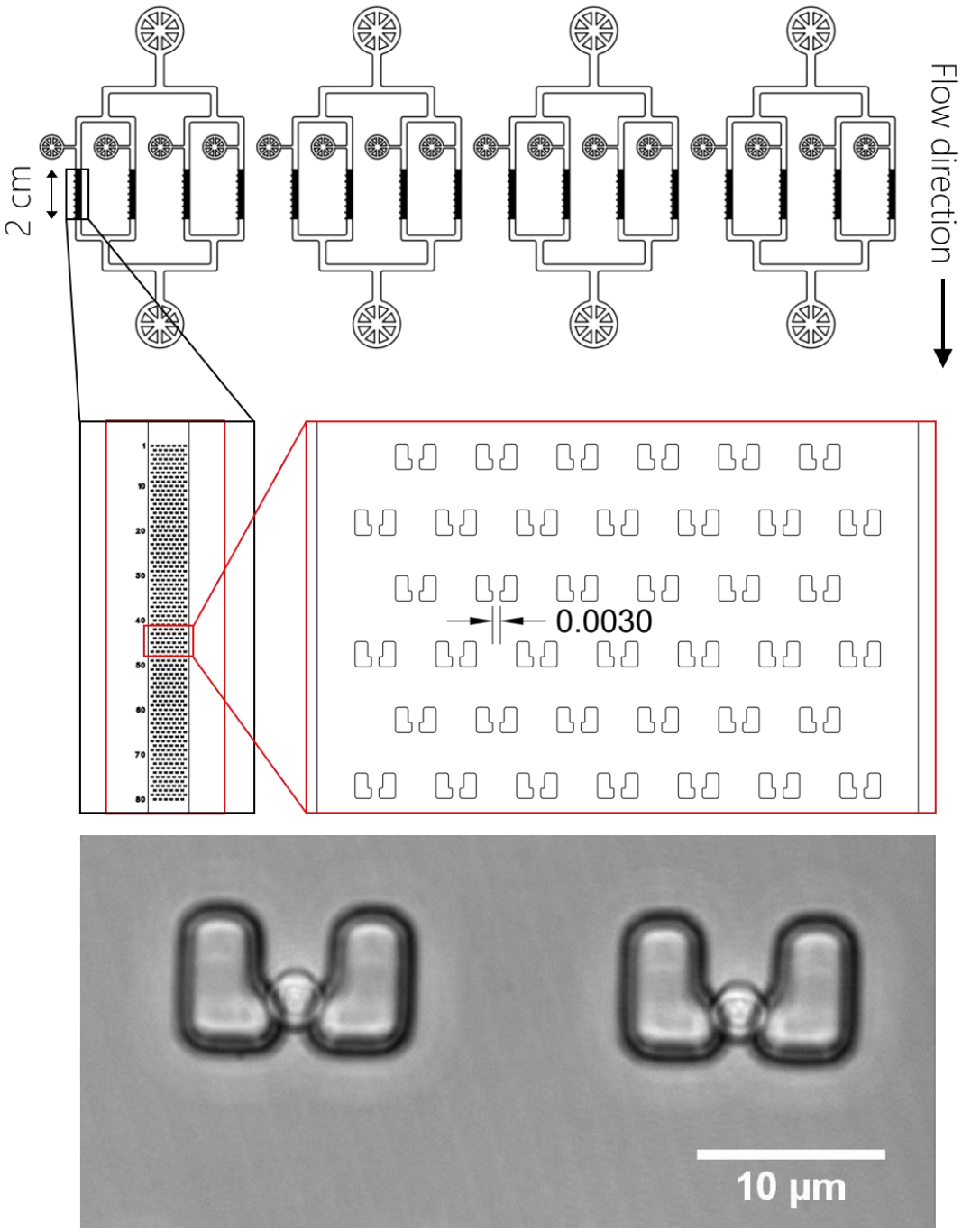

Figure 21: The High throughput Yeast Ageing Array device can accommodate up to 16 strains simultaneously via separate loading and media flow channels. Cells are held in place by the force of media flow and buds are removed in this flow by budding either through or above the traps. The distance between the 2 trap elements is optimised to allow budding of cells while retaining mother cells.

simpler and less time consuming. The HYAA device also allows multiple strains to be processed on the same device, greatly increasing throughput.

The final device considered was the CliC (Cell loaded into cavity) device (Fehrmann et al., 2013). While this device was originally published as a single channel, low throughput device, the designers of the chip have recently developed a high throughput 10-channel version that was used in this study. This device works in a similar way to the single plane microfluidic devices mentioned previously, with a few key differences. In the CliC device the imaging plane is a 3.3 µm tall, in order to trap the yeast cells when sufficient pressure is applied to raise the channel roof during loading. Around this single plane imaging area there is a much deeper channel for media flow, which also allows for cells growing beyond the imaging area to be washed away and prevent clogging of the device. Finally, inside the imaging plane, there are a series of long cavity structures, formed by a layer of PDMS (the construction material) that contacts the glass coverslip. As cells grow across the imaging plane, they fill these cavities. When a cell begins to bud in the direction of the cavity opening, it pushes all subsequent daughter cells out of the cavity, and they are eventually washed away into the deeper media channel. As most wild type yeast strains bud in a

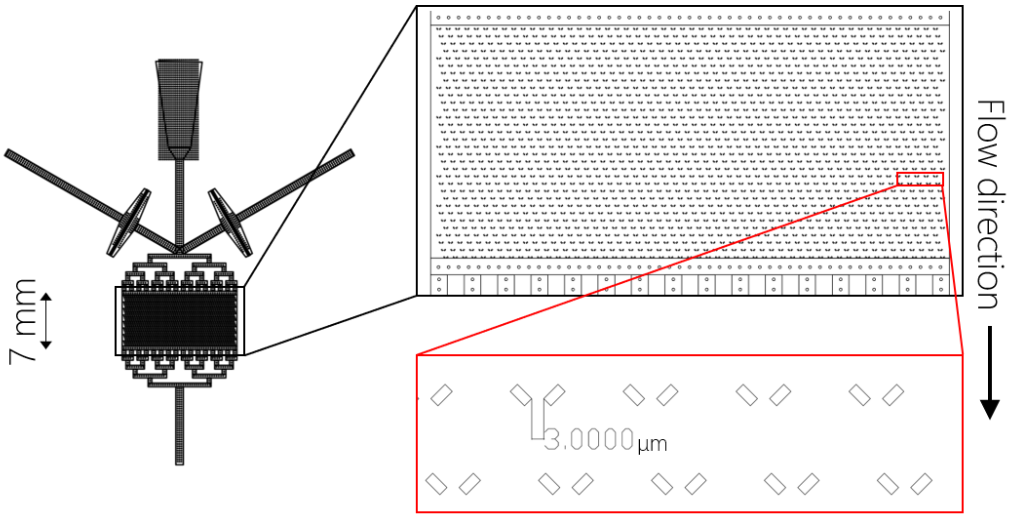

Figure 22: The ALCATRAS microfluidic device uses the same trapping concept as the HYAA chip, although a single channel is used rather than multiple channels, and a higher number of inlet channels allows for variation of media conditions during the experiment with aster switching times than external control methods.

unipolar manner for their replicative lifespan, this allows the mother cell to be trapped within the cavity while all daughter cells are removed. The advantage of this chip design is

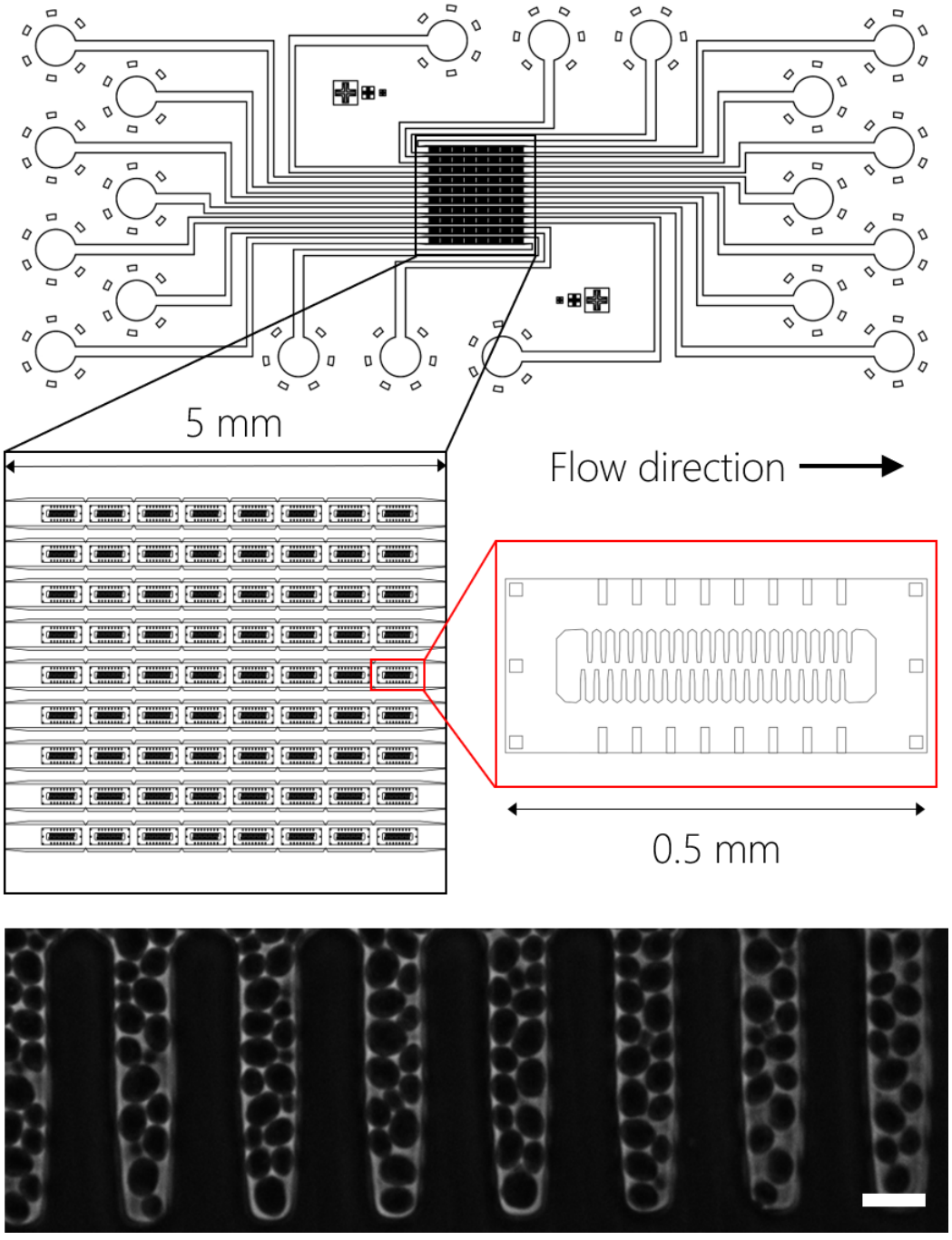

Figure 23: The CliC High throughput ageing device uses cavities within a PDMS trapping area to trap cells on a single focal plane. Mother cells are then immobilised within the cavities as daughter cells bud towards the entrance putting pressure on the mother cells. This design has the advantage of multiple independent channels allowing several strains to be analysed in one imaging cycle, as well as a reduced possibility of clogging due to the variation in chamber height between the trapping and flow areas.

that it is not dependent on the media flow to trap the cell, and once within the cavity, the mother cell is trapped by the presence of other dividing yeast cells. This allows the media flow rate to be adjusted across a much larger range of values for various studies and make the CliC device the most similar to those used in the past for p-body analysis.

For the Lee et al device, the ALCATRAS and the HYAA, CAD design files were obtained from the original authors. The CAD files were used to create Su-8 moulds for PDMS casting as described previously. For the CliC device, an unbonded PDMS chip was obtained from the authors and reverse moulded as described previously.

4.3 Testing and evaluation of microfluidic dissection devices

Due to the triple layer structure of the Lee et al design, as well as the difficulty in adhering it to the coverslip while ensuring the columns remained unattached after plasma bonding, this design was not used in the design comparison. Furthermore, as the ALCATRAS and HYAA designs use essentially the same trapping concept, while the HYAA allows significantly more strains to be tested at one time, only the HYAA chip was compared. This meant the comparison was between the HYAA and CliC chips. Figure 20 to 23 show the various attributes of these chips, including the number of strains and method of retention that informed the choice to compare these chips.

The most suitable device for this study was assessed through testing the devices after optimisation of a protocol for each device, and comparing data on retention rates, p-body number in low and high glucose conditions as well as average body intensity and size. In the latter comparisons, involving p body numbers and characteristics, each chip was also compared to a the cellASIC, in which cells were grown under optimised protocols for low and high glucose conditions.

Both the HYAA and CliC microfluidic devices were loaded with *Saccharomyces cerevisiae* cells as described in the Methods. The cells used had been previously transformed with a genomic integration construct that created a fusion protein of Edc3p, one of the major components of p-bodies used as a marker protein, with a yeast-optimised mRuby2 fluorescent protein. Following loading cells were grown under constant media conditions for 60 hours. The devices and the cells within them were observed by spinning-disk confocal

microscopy as described in the Methods, with images captured every 10 minutes in the phase contrast channel, and every 2 hours in the fluorescence channels to minimize photo bleaching and photo toxicity. Cells grown in the CellASIC device were imaged in the same manner.

4.3.1 CliC retains cells longer than HYAA

Retention rates in hours were calculated for each device and are shown in Figure 24. For the HYAA device, retention rates were based on 100 cells that were trapped within the cup-shaped traps at the start of the imaging run. For the CliC device, cells were grown overnight with phase contrast imaging only, allowing cells to populate the cavities, followed by 60 hours as previously described. Retention rates for the CliC device were then based on 100 cells that were budding in the correct orientation after entering a cavity. Retention rates for both devices were based on 100 cells over 3 separate experiments. Media flow rates for the devices were based on those used in the published materials.

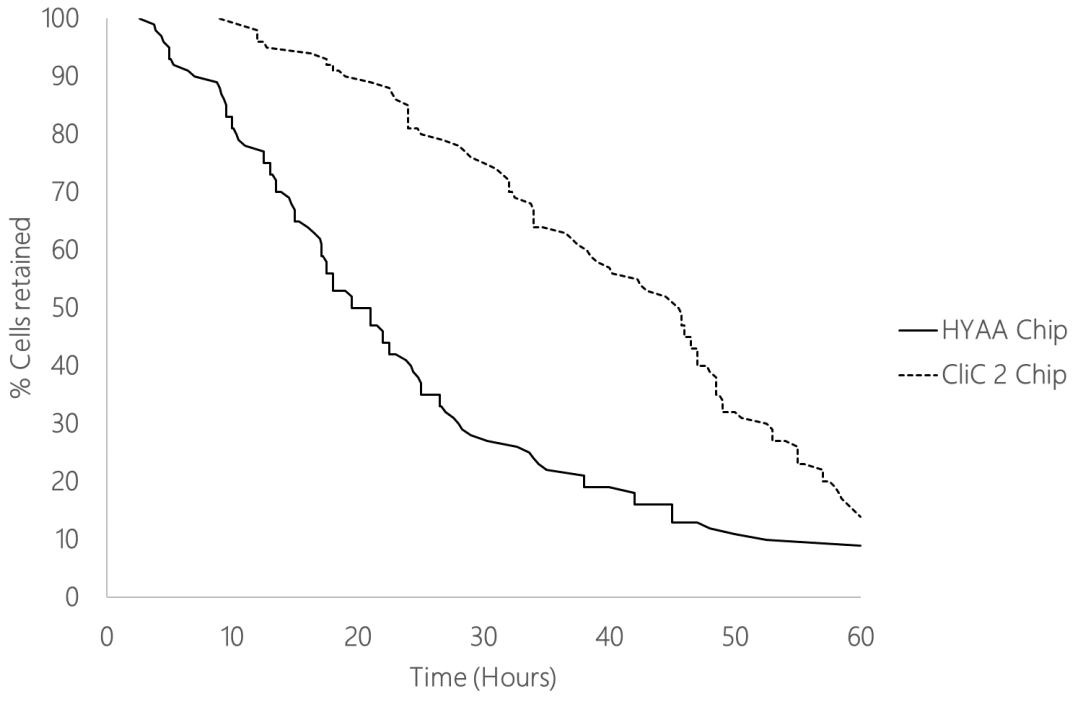

Figure 24: Cell retention in the Clic2 and HYAA microfluidic dissection devices. 100 cells across 3 individual experiments were followed for retention in the trapping structures of the two chip designs. Exact retention numbers over time are plotted. Clic2 retained a greater number of cells after 60 hours of growth.

The CliC device showed a better average retention rate over the 60 hour tests than the HYAA device, although both devices retention rates were well below the reported values of 65% cells retained over their replicative lifespan for CliC (Fehrmann et al., 2013) and approx. 90% over 96 hours for HYAA. For the CliC device the retention rate at 60 hours was 14% and the average retention rate was 40 hours, for HYAA the retention rate at 60 hours was only 9% (as shown in figure 24), 1/10th of the reported rate, and the average retention rate was only 24 hours. These differences in retention rates could be due to optimisation of protocols in the originating laboratories, although multiple cells were observed to leave the trap structures in the same manner in these tests.

Figure 25 shows how cells were commonly lost in the HYAA device. As the cell buds, the bud pushes against the internal sides of the trap, due to the budding orientation, rather than budding above or below the trap as intended. This causes the mother cell to be pushed upwards out of the trap, with any further buds exacerbating the issue and eventually leading to loss of the mother cell in the media flow. While tolerances in the fabrication process, for example, in the gap between the 2 trap elements, could cause this effect, it was observed over multiple chips from 3 wafers in which this gap was varied by 0.5 µm from 2 to 3 µm. This points to the overall design being at fault.

For the CliC device, there were 2 issues preventing maximum retention. Firstly, cells were often rotated to bud into the cavity due to the budding action of cells around them, this

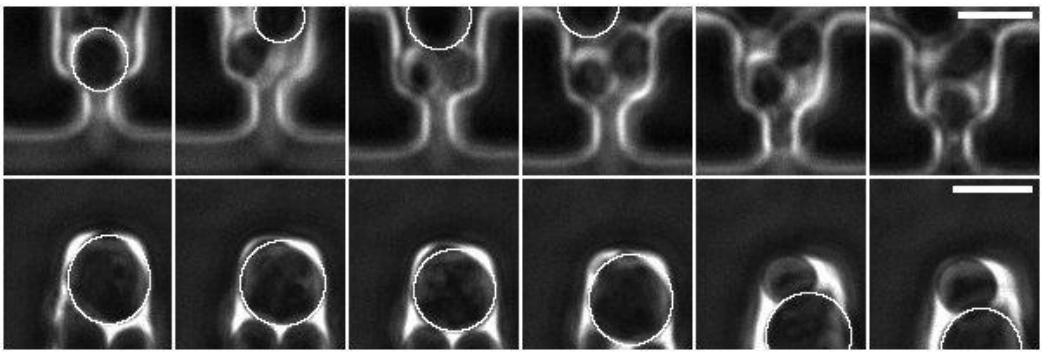

Figure 25: Loss of retention in the HYAA (top row, 20-minute intervals) and CliC 2 (bottom row, 10-minute intervals). In the HYAA device, buds often emerged oriented towards the inside corner of the trap design, causing the mother cell to be pushed out of the trap upon bud growth, resulting in loss of tracking. In the CliC device, a change in budding polarity could cause the same effect, where a mother cell is pushed from the trap. Scale bar 5 µm.

then forced the mother cell out of the cavity as it, and its progeny, continued to bud. This is not likely to be due to experimental set-up, as the budding direction of cells was not determined by media flow due to their location with the cavity. Secondly, on occasion, cells did switch bud site across the axis of the cell, causing a trapped cell to begin budding into the cavity and be forced out. This loss of retention is visualised in Figure 25. Even with these issues the CliC device was still superior to the HYAA in terms of cell retention.

4.3.2 P-body numbers and morphology

As well as their ability to retain cells, the 2 device designs were tested for their ability to reproduce the conditions that induce p-bodies while allowing continued cell growth. Cells were first grown in 2 % glucose to check that the microfluidic devices did not intensify p-body expression under optimal growth conditions. After confirmation that cells reproduce the p-body numbers of established methods in rich media, the media was then switched to a low glucose equivalent and the experiments repeated. In the CellASIC device, media flow of 8-10 µl per hour using synthetic media and 0.1 % glucose produces bright p-bodies, mostly 1 per cell with some smaller bodies sometimes visible. Under these conditions cells still divide at a similar rate to rich media conditions and the inheritance events can be observed. This would not directly translate to growth in other microfluidic devices, although the glucose concentration used in the CellASIC produces p-bodies at practically any flow rate. Given that the HYAA chip must be fed at a certain flow rate in order to effectively trap cells, the standard published flow rate of 8 µl/min was used for this device. The standard flow rate of 8 µl/min was used for the CliC device.

For each device, cells were grown overnight, allowing them to adapt to the conditions within the microfluidic device, and in the case of the CliC 2 device, grow into the cavities, where actual replicative ageing would take place. For each device, single time point images were then captured in both phase contrast and fluorescence channels. Once again the cells used contained the Edc3p-mRuby2 fusion construct. For each chip design, and the CellASIC, images were processed as described in the methods section to identify both the number of p-bodies per cell, as well as the size and fluorescence intensity (Edc3p protein content) of each body (figure 26, middle and last panels).

Plots of the p-body number per cell for each device are shown in Figure 266. In rich media

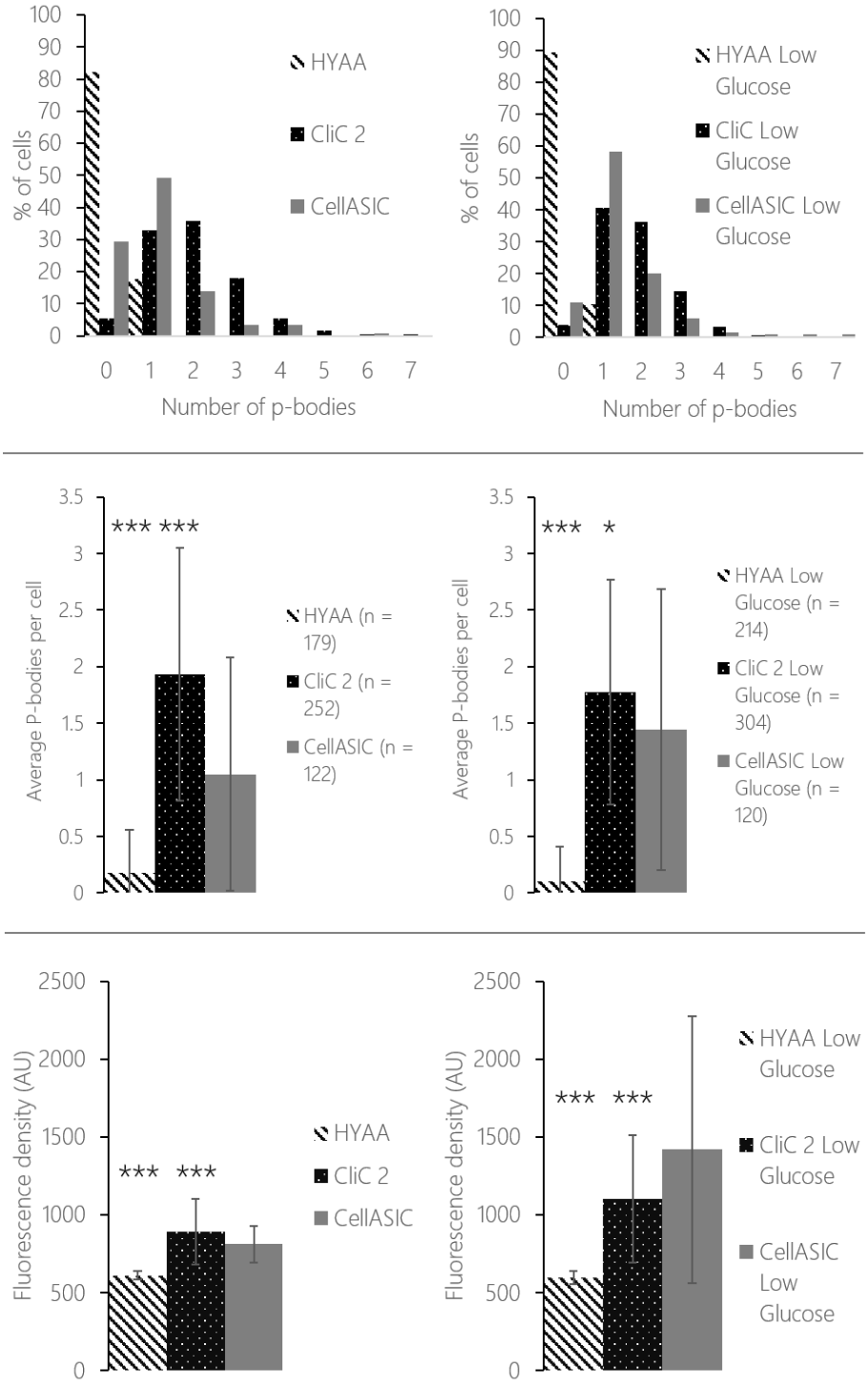

*Figure 26: Analysis of p-body numbers and fluorescence density in the HYAA, CliC 2 and CellASIC Devices. Top row – frequency distributions of p-body numbers per cell in rich media (left) and low glucose (right conditions). Middle row – Average p-body numbers per cell for each device in rich media (left) and low glucose (right), error bars represent standard deviation. Bottom row – Average fluorescence density of each p-body analysed in all cells present in each device under rich media conditions (left) and low glucose conditions (right). Error bars represent standard deviation. (***, p = 0.001, * p = 0.05, two tailed t-test), n = number of cells, indicated in second row for the shared dataset*

conditions, the majority of the cells contain either 1 or 2 p-bodies, upwards of 60 % for the CellASIC and CliC2 devices. However, for the HYAA device a stark lack of p-bodies was detected with over 80 % of cell containing no p-bodies, and the rest only ever containing a maximum of 1 body per cell. This observation is inconsistent with the idea that p-bodies are present during log phase growth in smaller and less concentrated foci (Ujwal Sheth & Parker, 2003) and points towards a bias in previous preparation protocols for microscopy that may induce p-bodies in such rapid fashion that they are perceived to be ubiquitous through all growth conditions. In either case the lack of p-bodies in the HYAA chip during growth in rich media differentiated it from established methods and introduced the further issue of how to induce p-body formation effectively for observation. In contrast, cells within the CliC 2 cavities displayed similar, although not identical p body induction to the established method of the CellASIC device.

In glucose restrictive conditions, i.e. 0.1 % glucose media, the results were similar to those of rich media conditions. Cells growing in both the CellASIC and CliC 2 device generally contained a single, or double p-body with less than 10% displaying no p-body formation. There was also an increase in the percentage of cells with a single p-body, consistent with the idea that glucose restriction, as a form of cellular stress, induces the aggregation of p-bodies into larger structures with greater protein and mRNA content. In the HYAA device, there was again a very limited number of cells displaying p-bodies, with an even higher percentage, 89 %, displaying no p-body induction. When p-bodies were present in cells in the HYAA device, they were only ever single foci.

To further test the suitability of the CliC and HYAA chips for the study of p-bodies, p-body morphology was assessed in terms of size and fluorescence intensity. Under similar conditions, cells were expected to produce p-bodies of similar size and fluorescence intensity, as the available scaffolding proteins should be at similar levels, although some degree of stochastic noise should be expected. P-bodies identified previously were segmented and measured as outlined in the methods section and each chip was compared for similarity to the CellASIC as the established method of observation. Rather than using size or fluorescence intensity as a single measure, the fluorescence density of each p-body was calculated as the intensity/area and used to compare the p-body morphology induced in

each device. Using fluorescence density rather than size or intensity alone gives a more accurate picture of p-body induction, as variations in cell size and cell-cycle stage can affect the total protein available for incorporation into p-bodies (Nissan & Parker, 2008).

Shown in Figure 26 (lower panel) are the average p body densities for each p-body in all of the cells analysed over the 3 repeat experiments. In rich media conditions, in the few p-bodies that were formed, the HYAA device showed significantly lower p-body fluorescence density than either the CliC 2 device or the CellASIC when measured by two-tailed t-test. Although the density of p-bodies in CliC 2 was significantly higher than in the CellASIC, the mean density was considerably closer to the CellASIC than the HYAA chip. Increased density in the CliC 2 device could be due to limited nutrient exchange within the cavity regions as they fall outside the main area of flow, causing the possibility of increase nutrient restriction induce aggregation of p-bodies.

In restricted glucose conditions, p-body density in both the CellASIC and CliC 2 devices was markedly increased, however p-bodies in the HYAA device showed reduced fluorescence density (figure 26, lower panel). P-body fluorescence density in the HYAA device in conditions of rich media and restrictive glucose media showed no significant difference (Students t-test, two-tailed, $p = 0.36$), when combined with the results of p-body counts per cell, this indicates that there was no significant induction of p-bodies in the experimental conditions used. Even in conditions of further reduced glucose level (0.05 %), cells growing within the HYAA device showed a similar lack of p-body induction. CliC 2 on the other hand showed a significant increase in p-body density while numbers decreased when grown in glucose restrictive media. These results indicate an induction of p-bodies in the CliC 2 device when exposed to conditions of restrictive glucose and the aggregation of components proteins into denser but less abundant structures as previously reported (Decker & Parker, 2012).

The flow rates used for each device were the same, but the structure of the channels in the devices was significantly different, with the channels for the HYAA device having a much smaller cross section, and hence a much faster refreshing rate in which the media is replaced. This fast refresh rate combined with the sparse spacing of cells in the HYAA device

may have meant that the glucose levels available to the cells was never limiting to the point of inducing p-bodies. Given that this flow rate is required to retain the cells in their traps in this device, a considerably lower glucose level may be required to induce p-bodies reproducibly. The larger channels in the CliC 2 device give a slower refresh rate, as they have a higher total volume, this would allow cells closer to the main channels to consume more of the available glucose, limiting that available to cells further inside the device, in particular inside the cavities. The higher cell density within the trapping area would compound this effect, as a larger population of cells would consume the available glucose quicker and may also release waste products that would contribute to cellular stress and induction of p-bodies. Overall the clear induction of p-bodies in the CliC 2 device, along with the ability of cells to continue to grow while under induction conditions, and the greater retention of ageing cells, made the CliC 2 device the preferred choice for further experimentation.

4.4 Improved designs for microfluidic dissection devices to observe p-bodies

The CliC 2 device was capable of inducing p-bodies in low glucose conditions and retaining cells during replicative ageing. However, the level of retention and disparity of the environment between the cavities and the rest of the trapping area (in which cells received faster media flow and hence increased glucose levels) means the device was still not ideal.

As an addition to the available repertoire of microfluidic dissection devices, a new device was designed, guided by the above results, in order to better study the impact of ageing on p-body kinetics and morphology. The principal design features for this device were the simplicity of construction and ability to retain cells while still inducing p-body formation effectively in established media conditions of 0.1 % glucose. Designs drew on aspects of

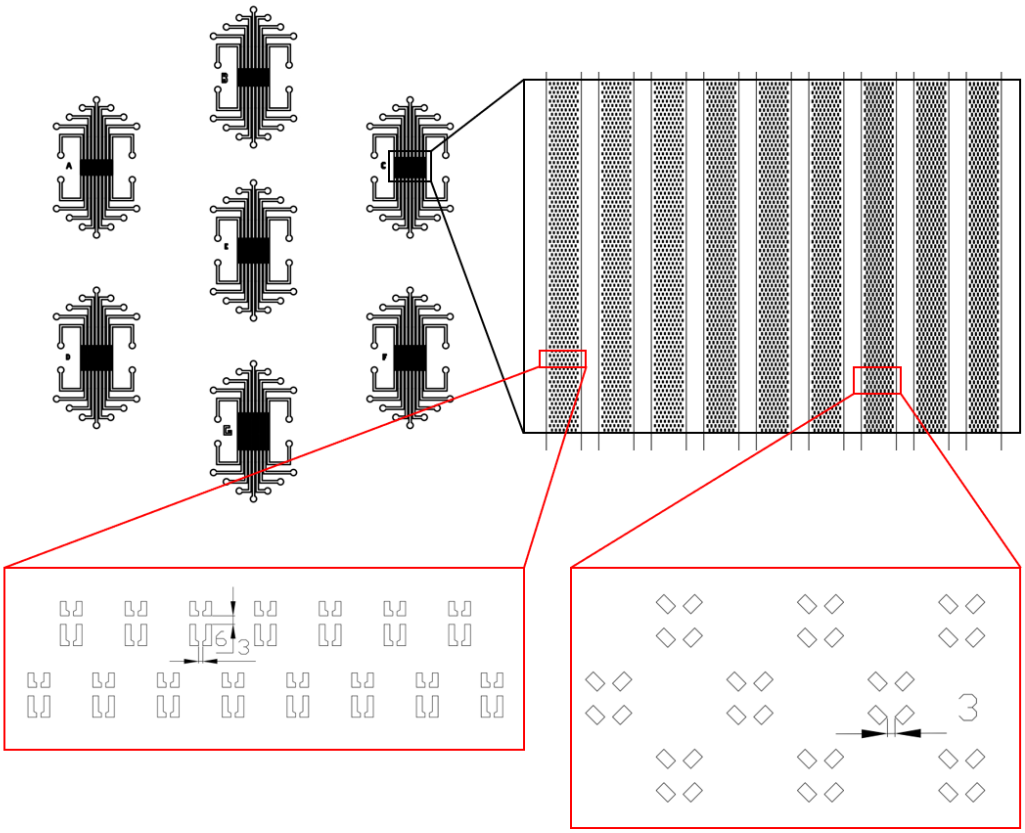

Figure 27: New Microfluidic dissection device designs. Left – full mask outline showing the 7 chips, containing variations of the designs. Top right – illustration of the channels, containing multiple trapping structures. Bottom right – The first trap structure design, containing 2 V shaped trap structures to capture the first virgin cell and allow growth inside a smaller region without limiting size. Bottom left – The second trap structure design used a size exclusion trap followed by a cavity/exclusion hybrid to trap the first virgin daughter cell. And allow growth without excessive media flow.

both the HYAA device, in that they contained only a single layer for fabrication and allowed cell budding through size exclusive gaps in the trap structures, and the CliC 2 device, by elongating the trapping areas into cavity like structures no allow cells to be retained under lower media flow rates. The proposed designs for these microfluidic chips are shown in Figure 27.

An Su-8 microfluidic mould, containing variations of these designs, based on alteration of the gaps between trapping elements, was produced as outlined in the methods section. Each individual chip contained 9 variations of one of 2 trapping structures. Variations were made in the distance between the 2 trap elements, the distance between the upper and lower traps, and the density of traps in the channel. These chips were designed to optimise these parameters and settle on the most suitable in terms of retention and p-body induction Unfortunately due to the time limitations of this study it was not possible to test these microfluidic chips, and it remains to be seen how effective the new designs are in retaining cells and replicating the correct conditions for the study of p-bodies. Further work therefore needs to be undertaken in order establish the suitability of these designs, based on the testing principles outlined above.

5 Processing body localisation during growth and ageing

5.1 Analysis of processing body localisation and morphology over the cell cycle.

While multiple studies have explored the composition and function of p-bodies (J. R. Buchan et al., 2011), there is still limited information on their role(s) within the cell. Compositional information such as the presence of translation initiation factors, decapping factors and Xnr1 exonuclease indicate a role in the degradation and storage of mRNA (Kedersha et al., 2005). The presence of mRNA within these granules, and the demonstration that this mRNA can re-enter translation upon relief of cellular stress also points towards their function as points of mRNP remodelling during these stress events (Brengues et al., 2005).

In yeast, the majority of these studies have been conducted under conditions of translational arrest. Conditions such as severe heat shock and total removal of carbon source cause the arrest of translation and subsequent induction of p-bodies. Other studies introduced the relief of stress via refreshing of media or re-introduction of nutrients after starvation to study the disassembly of p-bodies and the fates of the mRNA and proteins within them (Aizer et al., 2008). Although these stress induction studies have revealed many aspects of p-body formation and disassembly, they have a potential flaw in that they do not accurately represent the conditions that cells would experience in their natural environment. In the example of *Saccharomyces cerevisiae*, the conditions in which cells live are unlikely to change in such a drastic fashion as simulated in these stress induction experiments. Instead, cells are likely to undergo a transition from high to low nutrient levels as they consume the available nutrients, and very rarely would they experience the plentiful conditions of a laboratory made rich medium.

This leaves a gap in the existing knowledge of yeast p-body function, as the majority of studies take place either in rich media, or conditions of complete arrest of growth via depletion of nutrients or introduction of other stress factors. The behaviour of p-bodies in terms of their formation and function within the cell under conditions that induce their formation, but permit cell growth, is yet to be fully understood. One recent study (Garmendia-Torres et al., 2014) in S. cerevisiae showed that with a level of 0.1 % glucose in synthetic media, p-bodies are robustly induced as single granules, while cells continue to grow. Not only were p-bodies induced, but they were also shown to be transferred from

mother to daughter cells during the budding process. This inheritance of p-bodies was reliant on the established mRNA transport machinery in yeast, outlined in the introduction. The fact that p-bodies can be actively transported between mother and daughter cells indicates that they are not static entities reliant solely upon exchange of protein and mRNA for their function, and that they may have previously unidentified functions that require movement around the cell to interact with different cellular compartments. Given that localisation of mRNA, and the translation of mRNA in certain locations can have a key role in certain cellular process (Bertrand et al., 1998), including budding in *S. cerevisiae*, p-bodies may play an important role in regulating this process during conditions of restricted nutrition.

While studies have been performed in other organisms to show the interaction of p-bodies with various organelles (Cougot et al., 2012; Huang et al., 2011), information in yeast is still lacking. This means that the advanced techniques for studying age related changes in function that are applicable to budding yeast, such as microfluidic dissection, cannot be applied until these interactions are verified in S. cerevisiae. It was therefore necessary to establish that these interactions exist before moving on to study them at points of advanced replicative age.

5.2 Colocalisation of processing bodies and cellular compartments

To assess the possible interactions of processing bodies and other cellular compartments over the cell cycle, fluorescence microscopy was used to analyse the colocalisation of a range of these compartments, with a marker protein that is a core components of p-bodies, Edc3p. S. cerevisiae strains were genetically modified to express fluorescent proteins fused to markers for the cellular compartments in question, while co-expressing a non-overlapping fluorescent protein fused to Edc3p.

Initially, the commonly used fluorescent proteins eGFP and mCherry were used to create these protein fusions, but it was found that, in the case of mCherry, fluorescence depletion through bleaching was too high to image cells at sufficient time resolution and duration. eGFP was stable over a longer period of time, but the level of illumination using blue light (eGFP excitation peak is at 488nm) required to view some of the lesser-expressed proteins

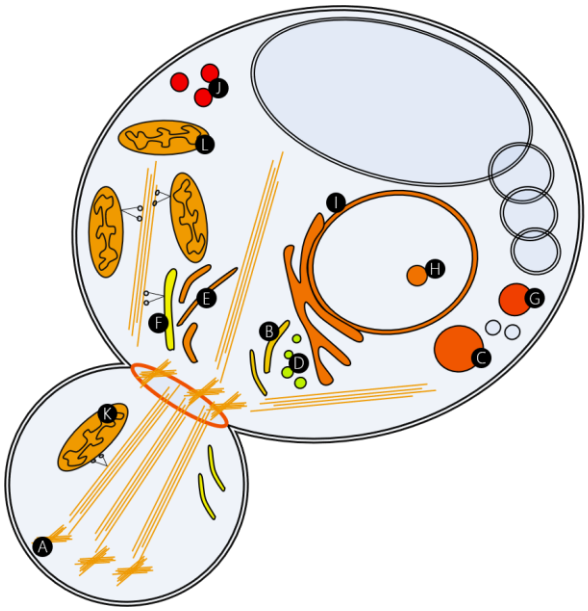

Compartment	Marker Protein
Actin (A)	Sac6
Early Golgi (B)	Cop1
Endosome (C)	Snf7
ER Golgi Vesicle (D)	Sec13
Golgi (E)	Anp1
Late Golgi (F)	Chc1
Lipid particle (G)	Erg6
Nucleolus (H)	Nop56/Sik1
Nucleus/ Nuclear periphery (I)	Nic96
Peroxisome (J)	Pex3
Actin-myosin ring (K)	Myo1
Mitochondrion (L)	Mitotag/Tom70 SS

Figure 28: Overview of structures tagged in this study. Each structure was tagged with a marker protein fused to mNeonGreen and co-expressed with Edc3-mRuby2 via a genomic integration.

caused damage to the cells through photo-toxicity. After testing a range of fluorescent proteins, it was found that, in the red range, mRuby2 had sufficient longevity of fluorescence and brightness to be imaged for the required period. In the green range, mNeonGreen was selected due to its high level of brightness, requiring lower illumination levels, which worked well for the required time-lapse experiments and did not induce noticeable photo-toxicity in the cells (Sidae Lee et al., 2013; Shaner et al., 2013). The target compartments and tagged proteins are outlined in Figure 28.

Each fluorescently tagged strain was grown overnight, using the CellASIC microfluidic platform to restrict growth to a single horizontal imaging plane, and imaged using an inverted spinning disk fluorescence microscope as described in the methods section. Cells were grown in synthetic complete media containing 0.1% glucose as the carbon source. This resulted in induction of p-bodies while cell growth occurred at a reduced rate. Cells were imaged in phase contrast as well as green and red fluorescent channels in a single z-plane. Images were segmented and analysed as described previously, and colocalisation analysis was performed in ImageJ after thresholding to include only areas of fluorescence. For each strain, cell images were split, depending on their morphology, into groups representing their cell cycle position; G1, S or G2/M. Analysis was performed on each set of images for

each cell cycle position as a group. Mander's M1 and M2 coefficients were calculated to evaluate the level of colocalisation of the 2 marker proteins as outlined in the methods. Mander's coefficients measure the fraction of one signal overlapping with the second (Dunn et al., 2011). Images were also manually analysed to check for points of colocalisation and are represented as merged colour images. Given that p-bodies appear as distinct foci within cells at high signal intensity, the relationship between fluorophore intensities is unlikely to be linear, Mander's coefficients were therefore used in interpretation of the results. All micrographs shown are presented as raw unscaled images, without background subtraction to show the full range of fluorescence signal. For automated analysis images were thresholded as described in the Methods section.

5.2.1 Sac6 / Actin patches

P-bodies were originally shown to be motile in HeLa cells using fluorescence time-lapse microscopy to show their interaction with stress granules (P. Anderson & Kedersha, 2006). Further studies revealed that in mammalian cells, p-bodies are directly linked to the microtubule cytoskeleton via static linker proteins including Myosin-Va and nesprin-1 (Lindsay & McCaffrey, 2011; Rajgor et al., 2014). P-body motion was identified to follow microtubule motion, rather than actively moving along the fibres via motor proteins or attaching to the microtubule tip. The motor protein Dynein has also been shown to colocalise with p-bodies under certain stress conditions (Loschi et al., 2009). This overall picture in mammalian cells therefore points to a model in which p-bodies rely upon microtubule attachment in order

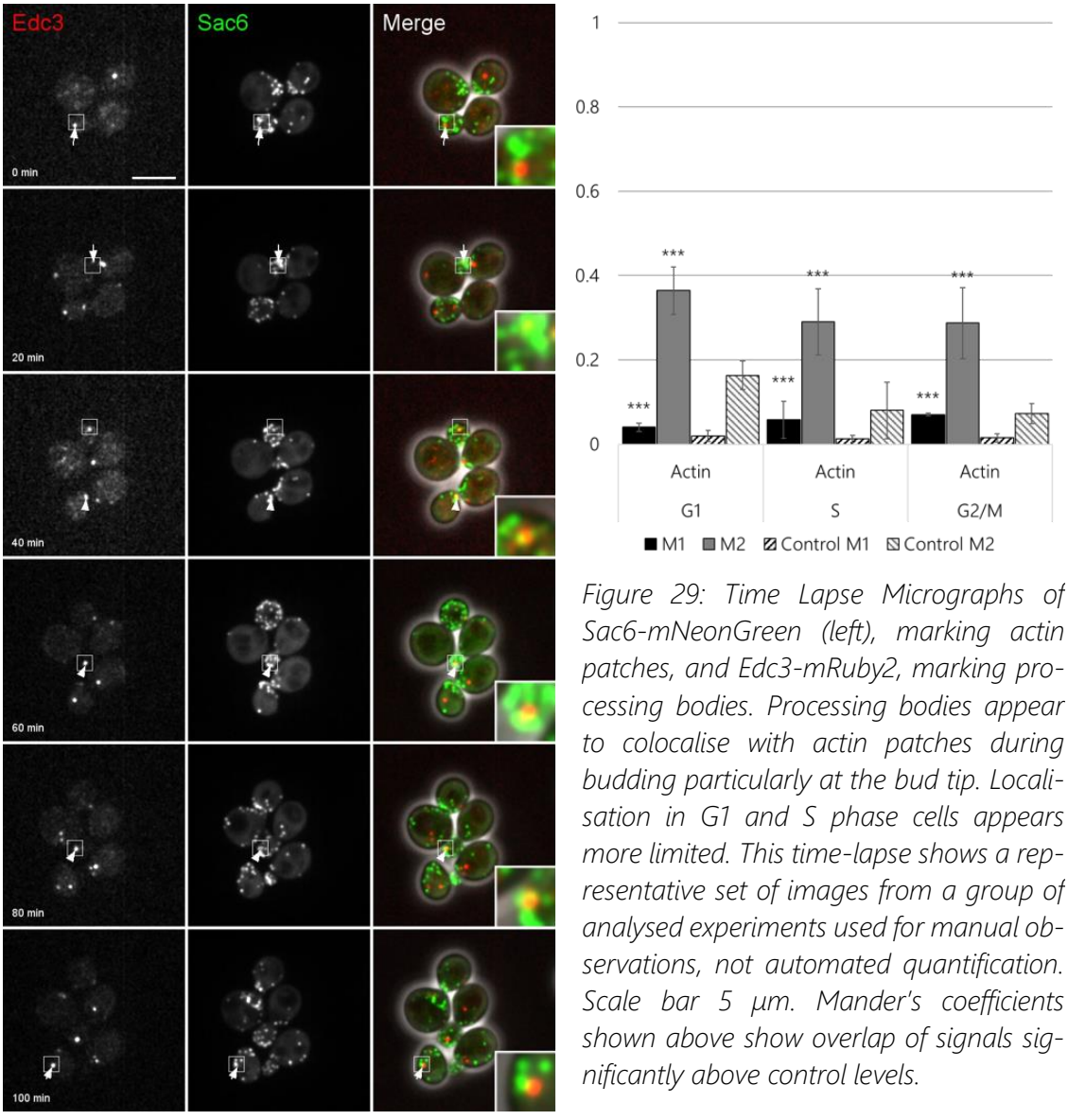

Figure 29: Time Lapse Micrographs of Sac6-mNeonGreen (left), marking actin patches, and Edc3-mRuby2, marking processing bodies. Processing bodies appear to colocalise with actin patches during budding particularly at the bud tip. Localisation in G1 and S phase cells appears more limited. This time-lapse shows a representative set of images from a group of analysed experiments used for manual observations, not automated quantification. Scale bar 5 µm. Mander's coefficients shown above show overlap of signals significantly above control levels.

to move throughout the cytoplasm and interact with their target mRNA. However, p-bodies have also be shown to associate with actin when stationary in mammalian cells, and in plants, actin cables appear to be the main mode of intracellular trafficking of p-bodies (Aizer et al., 2008; Alexandra Steffens et al., 2014). Not only do p-bodies move along actin cables, but yeast Dcp1, a core component of p-bodies, has been shown to directly interact with Myo2, a class V myosin motor, in vitro, with the same true for human and mouse homologs. The major mechanism underpinning of motility in yeast remains uncertain and previous studies indicate that both actin and microtubule cytoskeletons could be used for motility.

To assess the interaction of yeast p-bodies with the actin cytoskeleton, the most prominent yeast actin structures, cortical actin patches (Young et al., 2004) were tagged with mNeonGreen via the actin bundling protein Sac6. Cells were grown as described above and images were analysed for colocalisation through the cell cycle. Figure 29 shows micrographs of cells as they progress through the cell cycle. Manual analysis of micrographs showed association of p-bodies with actin patches during the latter stages of mitosis, identified by bud size of the analysed cells. While complete co-localisation was not observed there was a clear overlap of the fluorescent signals of p-bodies and actin patches that could indicate a physical interaction with the actin cytoskeleton during the budding process in yeast. Previous reports of p-bodies being inherited in budding yeast cells, and this process being dependent on myosin motor proteins, would support the idea that they are trafficked via the actin cytoskeleton.

Contrary to the manual observation of micrographs, the Mander's M2 coefficient shown in Figure 29, which represents the fraction of p-body signal overlapping with Sac6 signal, remained relatively constant throughout the cell cycle, with a slight increase in cells in G1. While manual observation relies upon a lower number of cells due to time taken on analysis, computerised colocalisation calculations do not suffer from this limitation, it is therefore likely that the slight overlap of p-bodies and actin patches observed in micrographs of late G2/M phase cells extends to the rest of the cell cycle. Reports in plants have shown that p-bodies are trafficked within interphase cells along the actin cytoskeleton (A. Steffens

et al., 2014) so this cell-cycle wide association may indicate that the same is true in budding yeast.

5.2.2 Cop1, Anp1, Chc1 / Early, Mid, Late Golgi

The Golgi apparatus is a major part of the protein distribution and maturation network within the cell. Given its major role in protein trafficking and the role of p-bodies in the regulation of protein production, a proximity between these 2 organelles could lead to more efficient management of protein production. In budding yeast, the Golgi apparatus

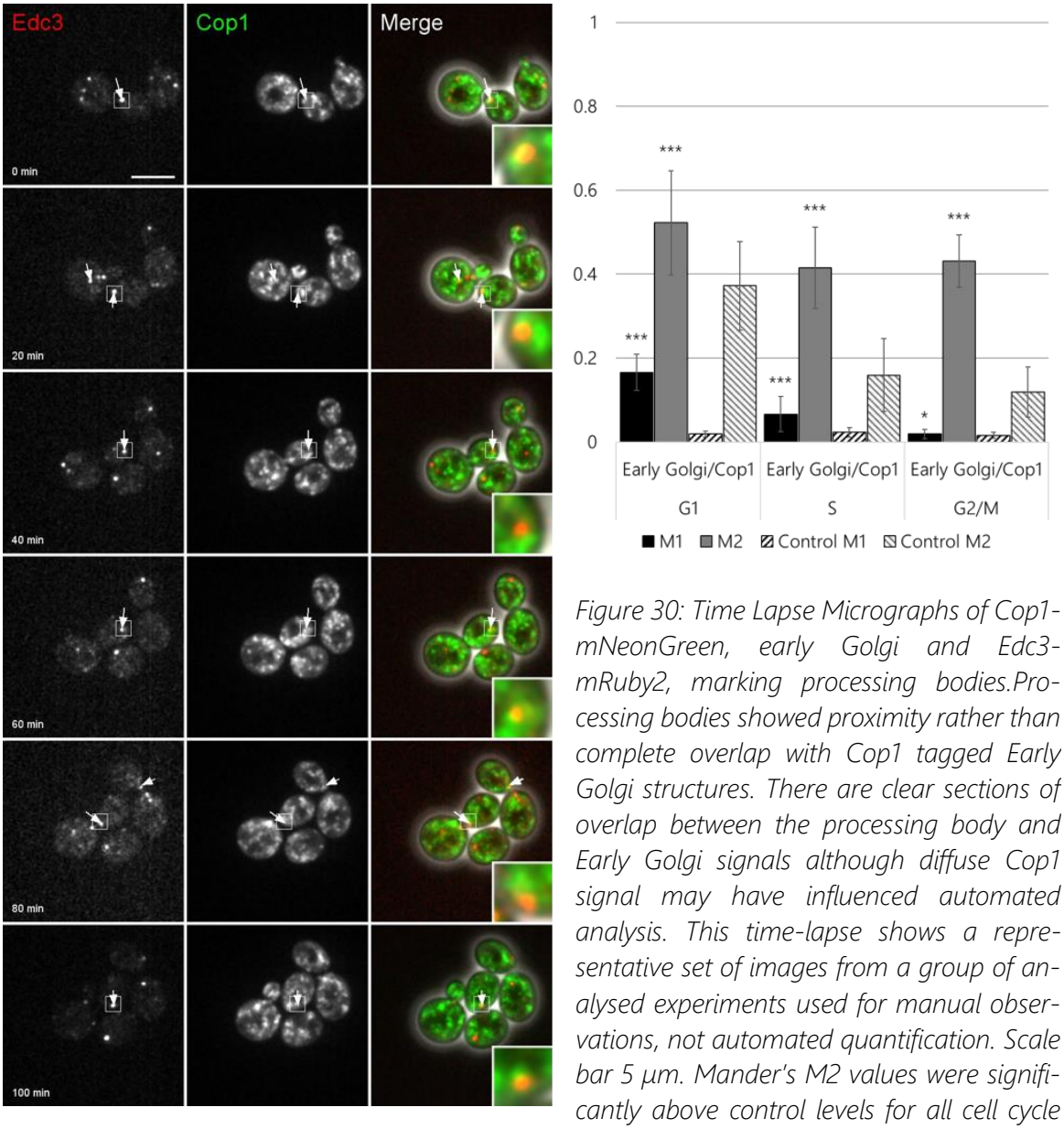

Figure 30: Time Lapse Micrographs of Cop1-mNeonGreen, early Golgi and Edc3-mRuby2, marking processing bodies.Processing bodies showed proximity rather than complete overlap with Cop1 tagged Early Golgi structures. There are clear sections of overlap between the processing body and Early Golgi signals although diffuse Cop1 signal may have influenced automated analysis. This time-lapse shows a representative set of images from a group of analysed experiments used for manual observations, not automated quantification. Scale bar 5 µm. Mander's M2 values were significantly above control levels for all cell cycle stages as shown above.

is separated into early Golgi, Golgi and late Golgi compartments differentiated by their function and protein composition/coating of membranes (Suda & Nakano, 2012), which roughly correspond to the mammalian pre-Golgi, Golgi and trans-Golgi network TGN). In *S. cerevisiae*, cis-Golgi cisterna are generated at endoplasmic reticulum exit sites (ERESs) and mature into later Golgi stages. P-bodies have been shown to associate with ERESs in *Drosophila* (Wilhelm et al., 2005) in a complex associated with a particular subset of

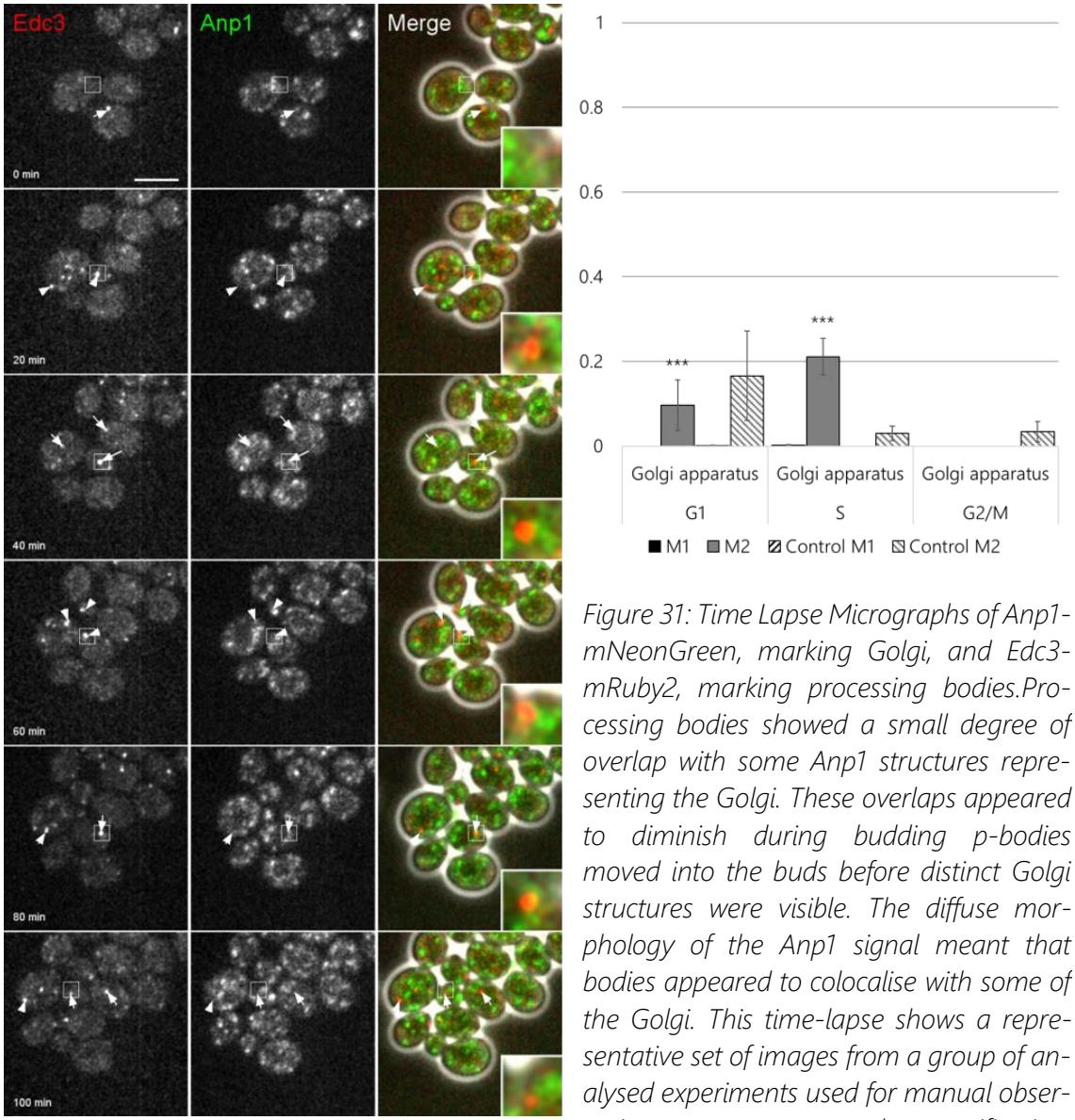

Figure 31: Time Lapse Micrographs of Anp1-mNeonGreen, marking Golgi, and Edc3-mRuby2, marking processing bodies.Processing bodies showed a small degree of overlap with some Anp1 structures representing the Golgi. These overlaps appeared to diminish during budding p-bodies moved into the buds before distinct Golgi structures were visible. The diffuse morphology of the Anp1 signal meant that bodies appeared to colocalise with some of the Golgi. This time-lapse shows a representative set of images from a group of analysed experiments used for manual observations, not automated quantification. Scale bar 5 µm. M2 quantification (shown above) was significant during both G1 and S phases, in line with manual observation of micrographs.

mRNAs. This association may imply a relationship between mRNA storage or release from p-bodies and the localised production of protein at ERESs, and possibly other sites. As well as the previously identified localisation the ERESs, p-bodies also contain a component, Scd6, that both regulates translation via eIF4G and represses the null mutation of clathrin heavy chain Chc1 (Rajyaguru et al., 2012). This dual involvement of a p-body component in both mRNA regulation and trafficking further supports a possible role for bodies within the protein trafficking network.

Each stage of the Golgi network in budding yeast, as well as ER to Golgi vesicles, was visualised with a fluorescent fusion protein incorporating mNeonGreen and co-expressed

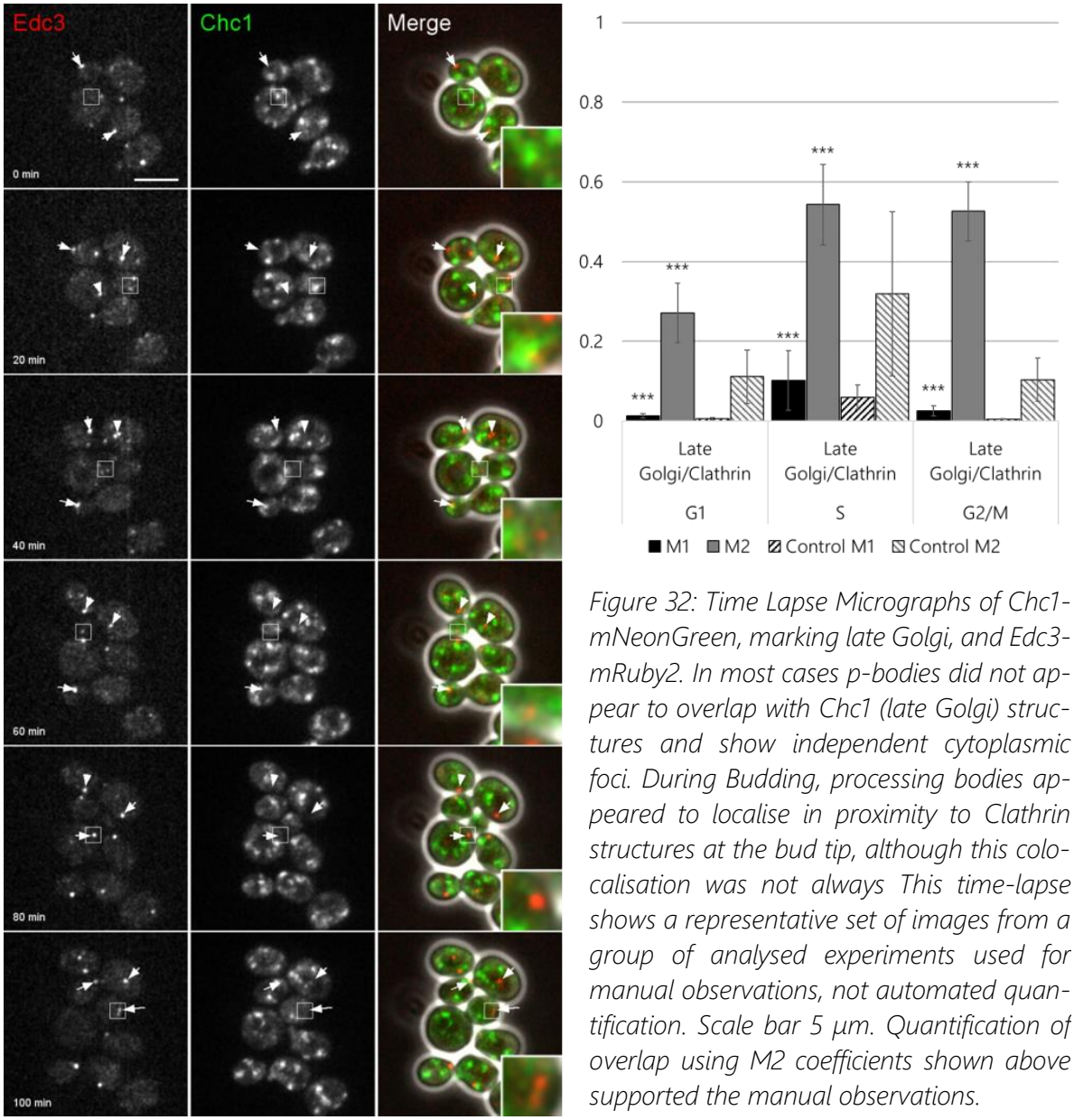

Figure 32: Time Lapse Micrographs of Chc1-mNeonGreen, marking late Golgi, and Edc3-mRuby2. In most cases p-bodies did not appear to overlap with Chc1 (late Golgi) structures and show independent cytoplasmic foci. During Budding, processing bodies appeared to localise in proximity to Clathrin structures at the bud tip, although this colocalisation was not always This time-lapse shows a representative set of images from a group of analysed experiments used for manual observations, not automated quantification. Scale bar 5 µm. Quantification of overlap using M2 coefficients shown above supported the manual observations.

with the p-body marker protein Edc3-mRuby2. ER to Golgi vesicles were tagged with Sec13 a COPII vesicle coat subunit. Early Golgi cisternae were identified by the presence of Cop1, a vesicle coating protein present in early Golgi membranes and vesicles but not in later Golgi membranes (Gomez-Navarro & Miller, 2016). The main Golgi regions were visualised by fusion to Anp1 (Chapman & Munro, 1994) a key protein in the secretory pathway. Finally, the yeast Late Golgi, equivalent to the TGN, was visualised using ChC1, the Clathrin heavy chain.

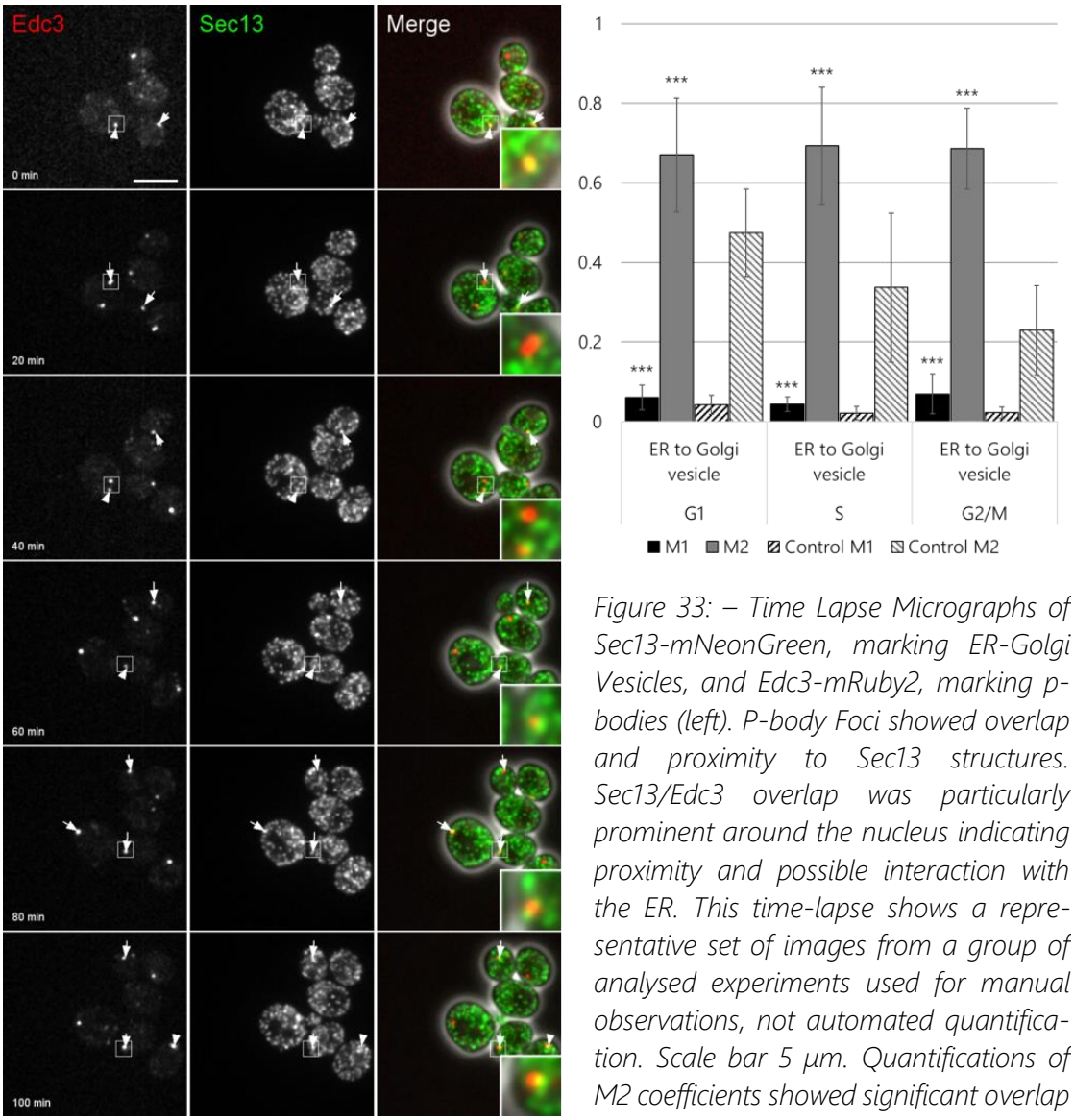

Figure 33: – Time Lapse Micrographs of Sec13-mNeonGreen, marking ER-Golgi Vesicles, and Edc3-mRuby2, marking p-bodies (left). P-body Foci showed overlap and proximity to Sec13 structures. Sec13/Edc3 overlap was particularly prominent around the nucleus indicating proximity and possible interaction with the ER. This time-lapse shows a representative set of images from a group of analysed experiments used for manual observations, not automated quantification. Scale bar 5 µm. Quantifications of M2 coefficients showed significant overlap in all stages of the cell cycle (above)

Visual analysis of micrographs was used to determine initial colocalisation for each of the tagged proteins, followed by computational co-localization analysis for quantification of co-localisation.

Sec13 showed significant but not exclusive overlap with Edc3. Multiple Edc3 foci characteristic of p-bodies were found to overlap with similar Sec13 foci on the same focal plane, although Sec13 coverage was more disperse. Edc3 foci were also found in areas with no Sec13 signal implying Sec13 is not a constituent component of p-bodies. Observation of Edc3 and Sec13 overlap was not limited to any specific cell cycle stage and was observed in nuclear periphery and arbitrary locations within the cell. Automated quantification supported the manual observations, with an M2 coefficient around 0.7 for all cell cycle positions, indicating a significant ($p<0.001$) degree of Edc3 overlap with Sec13. The M1 coefficient was consistently lower around 0.06, confirming the observation of micrographs that Sec13 localisation is independent of p-bodies, unsurprising given its known localisation.

Examination of Cop1-mNeonGreen tagged cell micrographs showed some small areas of overlap between Edc3 foci and Cop1 signal, but no identical overlapping foci as with Sec13. Automated analysis showed an M2 coefficient of around 0.4, rising above 0.5 in G1, meaning roughly 40% of all p-body signal overlapped with Cop1, slightly more during G1. The M1 coefficient showed a similar pattern, its highest proportion of overlap in G1, dropping to lower levels in S and G2/M stages. However, M1 was still significantly lower than M2 due to the dispersed nature of Cop1 localisation.

Unlike with ER-Golgi and Early Golgi structures, p-bodies, visualised by Edc3-mRuby2, showed little overlap with the main Golgi body as visualised by Anp1-mNeonGreen fusion protein. Anp1 signal was diffuse with scattered foci of increased signal, with no clear overlap of Edc3 signal. Automated quantification showed similar results, with insignificant overlap shown via M1 coefficient and only a significant overlap shown via M2 coefficient during S phase, with insignificant overlap in G1 and G2/M.

Late Golgi, visualised by the signal of Clathrin Heavy Chain, showed little overlap with p-bodies. Examination of micrographs showed distinct Edc3 foci independent of Clathrin signal during all stages of the cell cycle. Automated quantification was contrary to manual

observation with M2 coefficients during S and G2/M over 0.5 with a lower overlap during G1. M1 followed the same pattern with a lower coefficient during G1, increasing in S and dropping back again in G2/M. The increased overlap during the latter stages of the cell cycle could be functional, or coincidental due to the fact that both Golgi and p-bodies are trafficked to the bud during asymmetric cell division of budding yeast cells (Suda & Nakano, 2012). The high degree of overlap in automated quantification could also be an artefact due to the diffuse localisation of Clathrin.

The overall pattern of co-localisation, high at the ER-Golgi interface and early Golgi compartments, followed by decreased interaction with the main Golgi body and resurgence in the late Golgi points to a possible role interacting with the protein/vesicle trafficking system during glucose restrictive conditions. Interaction with the main Golgi body is likely limited due to the non-membranous structure of p-bodies, restricting their interaction to the exposed membrane proteins of ER-Golgi and late Golgi Vesicles.

5.2.3 Mitotag / Mitochondria

P-bodies have been identified as sites of mRNA degradation due to their components, but they have also been implicated in RNA interference. In mammalian cell lines, mitochondrial inactivation leads to a decrease in RNA interference efficiency while p-bodies have been shown to associate with mitochondria in live cell imaging (Huang 2011). Although the RNAi machinery is not present in *Saccharomyces cerevisiae*, colocalisation of these organelles may still occur. To verify this interaction in budding yeast, mitochondria were tagged with mRuby2, by fusing this fluorescent protein with the mitochondrial import sequence from the yeast Tom70 protein. This construct was co-expressed with Edc3-mNeonGreen for colocalisation analysis.

Manual observation of micrographs initially indicated positive co-localisation of p-bodies and mitochondria, with Edc3 foci appearing along the length of the mitochondria (Note that the structure of the mitochondria shown in Figure 34 are on a single imaging place, hence the lack of branching). The mitochondria of course extend beyond the p-body foci, so the M1 coefficient is predicted to be significantly lower than M2. Overlap of p-bodies was observed in all cell cycle stages with particular prominence at the bud neck and tip,

indicating a possible link in trafficking into the bud, consistent with previous studies showing a link between mitochondria and the myosin motor protein Myo2 (Westermann, 2014), that has also been identified as a potential component of p-body inheritance (Chang et al., 2008).

Consistent with the idea of shared trafficking apparatus between p-bodies and mitochondria, automated co-localisation quantification showed both progressively increasing M1

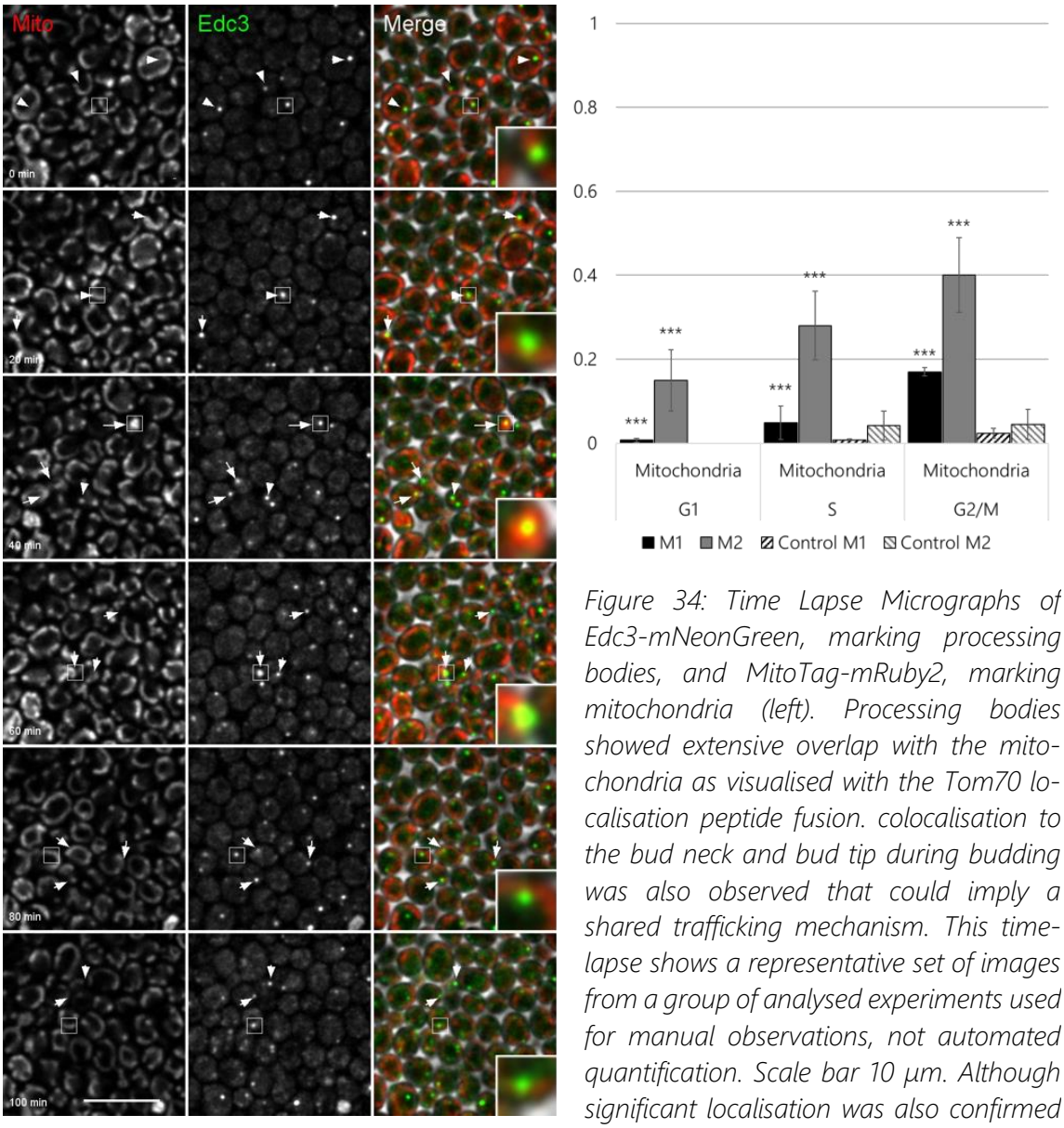

Figure 34: Time Lapse Micrographs of Edc3-mNeonGreen, marking processing bodies, and MitoTag-mRuby2, marking mitochondria (left). Processing bodies showed extensive overlap with the mitochondria as visualised with the Tom70 localisation peptide fusion. colocalisation to the bud neck and bud tip during budding was also observed that could imply a shared trafficking mechanism. This time-lapse shows a representative set of images from a group of analysed experiments used for manual observations, not automated quantification. Scale bar 10 µm. Although significant localisation was also confirmed via Mander's M2 co-efficient as shown above, the M2 values were lower than other membranous organelles.

and M2 coefficients, meaning p-body co-localisation with mitochondria increased to a maximum during G2/M, the stage at which the organelles would be trafficked into the bud. Interestingly the coefficients were not as high as some other organelles, namely early and late Golgi, although this could be due to the disperse nature localisation of these other organelles compared to the organised filamentous structure of the mitochondria. No current evidence points towards the presence of p-bodies within the mitochondria, so the observed overlap likely indicates adjacency to mitochondrial membrane, rather than formation within the mitochondria.

5.2.4 Further organelle markers

To represent a wider range of organelles and uncover any previously unreported localisation, mNeonGreen fusion proteins were created to tag the organelles. Together with the previous tags, this represents a comprehensive coverage of the cellular organelles that might interact with p-bodies.

Peroxisomes, Lipid particles and the myosin contractile ring showed negligible co-localisation with p-bodies based on both manual and automated co-localisation studies, while the spindle pole fusion protein caused a growth abnormality making results unreliable. Interestingly the three remaining fusion proteins did show a small degree of colocalisation, these were the nuclear periphery, nucleolus and endosome.

Endosomes were identified by a fluorescent fusion to Vacuolar-sorting protein Snf7. Micrographs showed some overlap with Edc3 close to the bud site and bud neck during budding, Quantification showed a small degree of colocalisation based on M2 coefficient that was highest in G1, decreased in S and increased again the G2/M, a pattern that was reflected in M1 coefficient.

Micrographs showing the nucleolus, identified by the fusion protein of Nucleolar Protein Nop56, indicated no overlap of Edc3/p-bodies and the nucleolus consistent with previous observations indicating p-bodies are not present within the nucleus (J. Buchan, 2014). However, the quantification of co-localisation showed overlap in the M2 coefficient, which is unusual given the aforementioned lack of Edc3 in the nucleus and most likely due to overlap of fluorescence signals while the two organelles area in close proximity, possible during

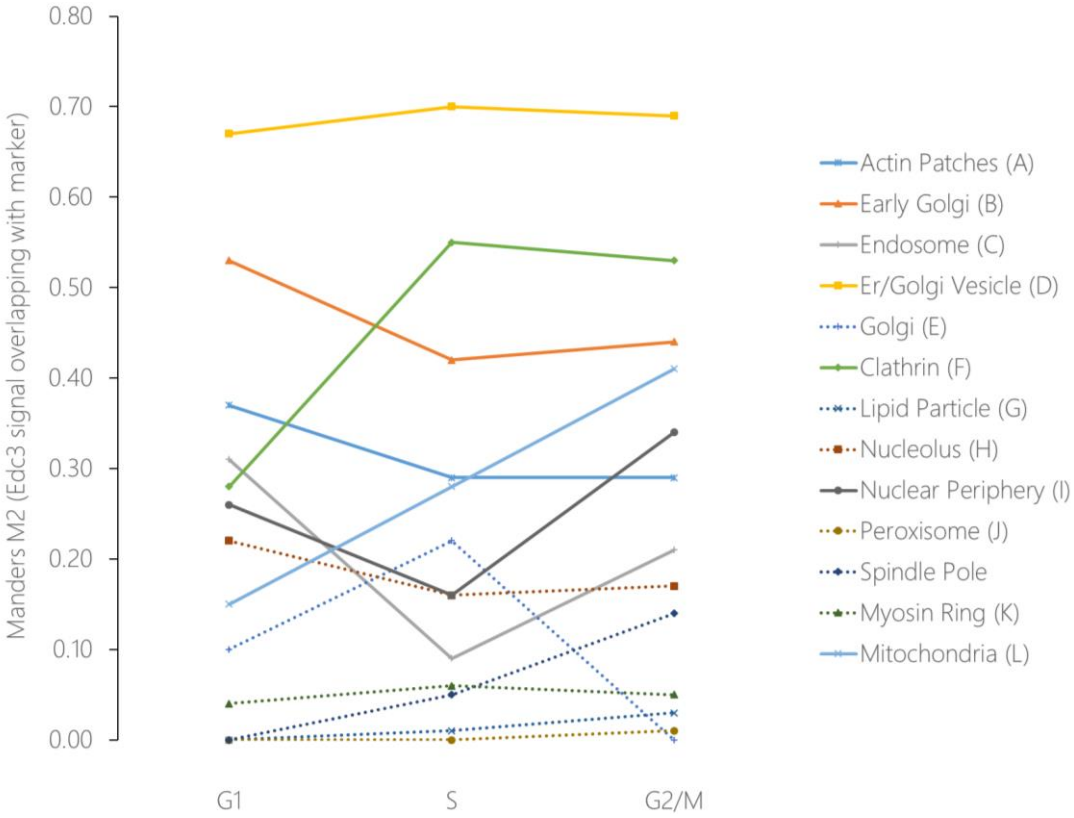

Figure 35: Overview of processing body localisation (Mander's M2 coefficients) for cellular compartments.

cell division. Some p-body constituent proteins such as Dcp1 have previously been shown to shuttle between the cytoplasm and the nucleus (Haimovich et al., 2013), if Edc3 shared this shuttling activity, it could explain the co-localisation results, while still showing minimal overlap in manually assessed images. The signal for the nuclear periphery, which encompasses the nuclear envelope region of the endoplasmic reticulum as well the as nuclear export machinery, showed a similar level of overlap to that of the nucleolus. P-body signal was detected in this region at an increased level during the G2/M phase of the cell cycle which could again be caused by close proximity during cell division or could indicate a closer relationship during budding such as a shared mechanism of inheritance.

The results of the colocalisation analyses are summarised in Figure 35. Although no individual structure shows complete colocalisation with the p-body signal it is clear that p-bodies do not exist in isolation from other cellular compartments. P-body signal showed overlap with the nuclear periphery, as expected given the p-body's role in mRNA triage,

as well as previously unrecorded colocalisation, including the highest level found, with Sec13.

5.3 Age-induced changes in processing body localisation

The progression of replicative ageing in yeast has been shown to cause deterioration of multiple cellular pathways, eventually leading to senescence and cell death. One of the key findings so far, not just in yeast but in multiple organisms, is that dietary restriction appears to increase lifespan. In yeast this manifests itself as an increase in replicative lifespan (RLS) under conditions of reduced nutrients and can be studied in the lab using various methods to measure RLS. The formation of p-bodies is induced under the same conditions shown to increase RLS. Both dietary restriction induced lifespan extension and p-body induction are consequences in a global drop in translation. Given this shared regulatory mechanism, the progression of ageing may impact the dynamics of p-bodies, and p-body function may influence ageing. Understanding how age affects the localisation and interactions of p-bodies is therefore important to determine both how ageing affects p-body function, and how p-body formation due to low glucose conditions might be protective leading to cellular longevity.

To study the localisation of p-bodies in advanced replicative age, single cells of *Saccharomyces cerevisiae* were constrained in a series of traps, in a microfluidic device. This device allowed the removal of daughter cells in media flow, while retaining the mother cells as they advance in age. Each marker strain was loaded into such a device and allowed to grow over a period of several days during which time the devices were imaged using an inverted fluorescence microscope. The cells were grown in synthetic complete media containing 0.1% glucose, a media composition shown to induced p-body formation in yeast while not stopping cell growth. Phase contrast imaging was used to visualise the cells until they reached an age of 15± cell divisions, after which multicolour fluorescence imaging was used to visualise both organelle markers and the p-body constituent protein Edc3.

The organelle markers used in this part of the study were identical to those used in the previous section. The colocalisation procedure used in this section of the study was identical to that used in the previous section. During aging of the mother yeast cells in the

microfluidic chip it was observed that the morphology of several organelle markers was altered with advanced replicative age. The main example of this change in morphology was that of the mitochondria which showed both an increase in size and a lesser degree of fragmentation. Although this observation is not strictly relevant to the current study it may have influenced the quantification of the colocalisation of p-bodies with some organelles due to increased fragmentation.

In cells of advanced replicative age there were some organelles which completely lost colocalisation with p-bodies. These included the nuclear periphery, the endosome, lipid particle and the myosin ring. Of these both the nuclear periphery and the endosome showed an M2 coefficient of above 0.3 during at least one cell cycle point during normal growth. The loss of colocalisation in advanced replicative age could point to the loss of interaction between components of these organelles and p-bodies or could be due to an increase in p-body colocalisation elsewhere within the cell, given that some organelles showed a substantial increase in colocalisation the latter theory is the logical assumption.

5.3.1 Sac6 / Actin Patches

P-bodies showed a decreased overlap with actin patches in cells of advanced replicative age. Micrographs of fluorescently tagged Edc3 and Sac6 showed little overlap on manual inspection, and automated quantification of colocalisation showed a 20% drop in M2 co-efficient compared to young cells meaning insignificant colocalisation vs control during G1, and a 50% drop during S and G2/M. This could again be due to the sequestering of p-bodies in specific locations during advanced replicative age. Given the observed break-down of protein segregation in budding cells of advanced replicative age it could also be that p-bodies lose their link to the actin cytoskeleton during replicative ageing, which may also lead to a breakdown in their segregation.

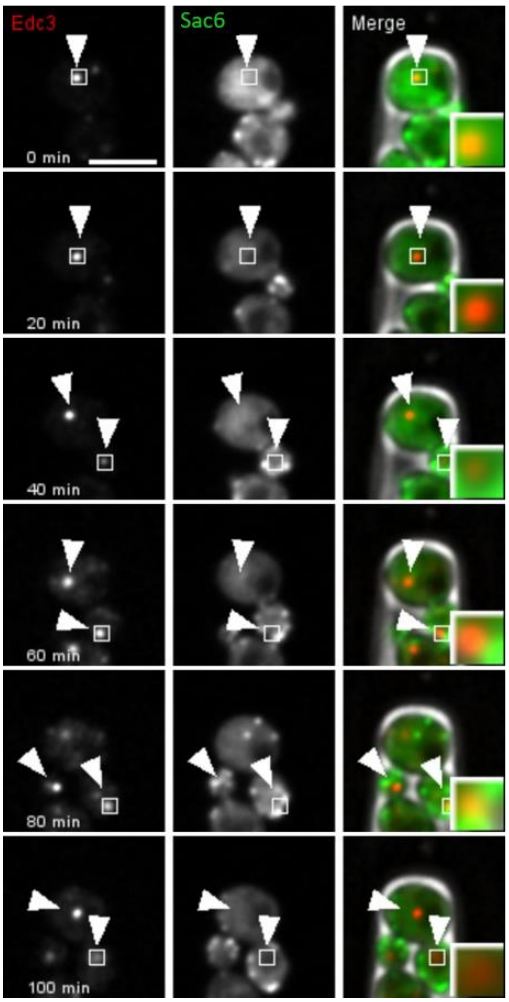

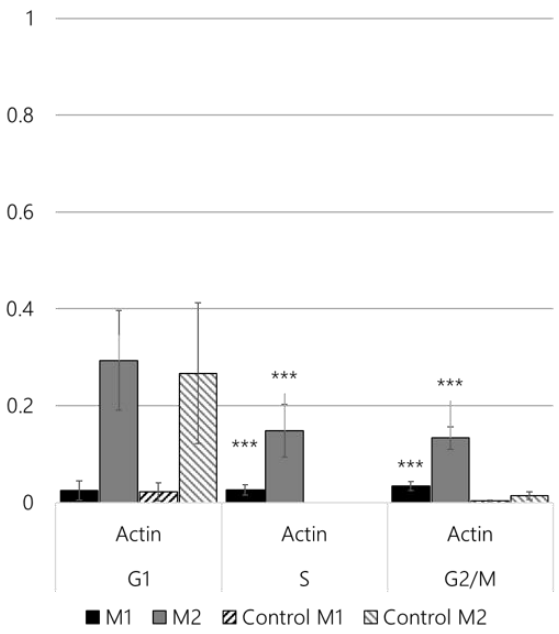

Figure 36: Micrograph of aged cell (top of channel) tagged with Sac6-mNeonGreen and Edc3-mRuby2. Processing bodies showed little overlap with Sac6 in aged cells compared with young cells, although colocalisation was present at the bud tip as observed previously. This time-lapse shows a representative set of images from a group of analysed experiments used for manual observations, not automated quantification. Scale bar 5 µm. Quantification (above) showed that G1 colocalisation was insignificant compared to the control, whereas S and G2/M levels were still significant,

5.3.2 Cop1, Anp1, Chc1 / Early, Mid, Late Golgi

The results for colocalisation of Golgi compartments varied between markers for different sections of the yeast Golgi stages. Localisation of p-bodies to the ER/Golgi vesicle marker Sec13 was reduced by 60% in G1 and S phases and by 90% in G2/M. G1 and G2/m phase colocalisation was insignificant compared to controls. Given the overlap of Sec13 signal with the ER, this drop in colocalisation could imply a reduced association of p-bodies with ERESs in aged cells. Micrographs of Sec13 and Edc3 tagged cells were similar in aged cells to those of young cells, in which P-bodies were clearly distinct in many cases but showed overlap with the ER signal in some cells.

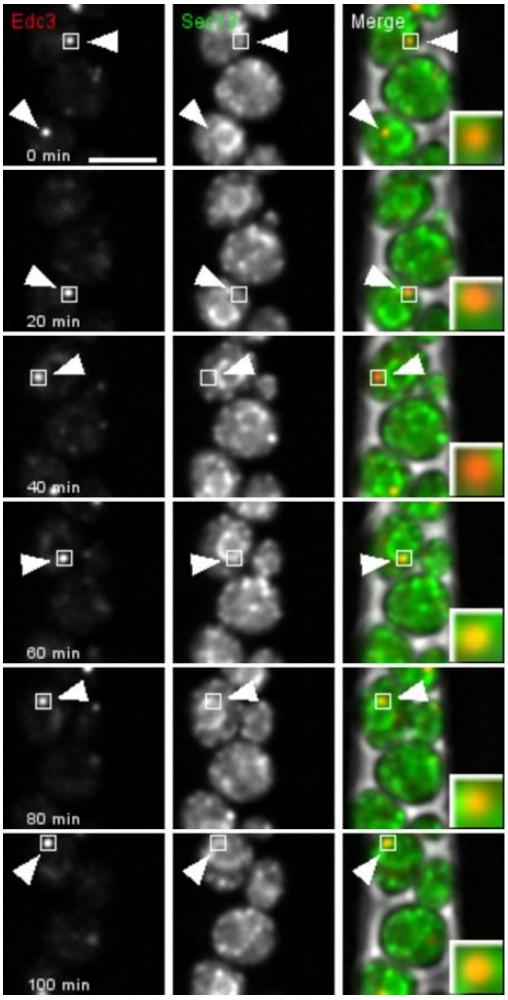

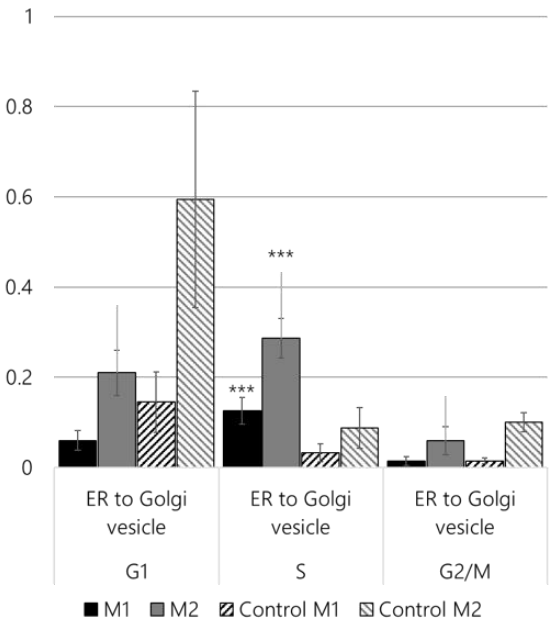

Figure 37: Micrographs of aged cells labelled with Sec13 mNeonGreen and Edc3-mRuby2-. Processing bodies showed a similar overlap with ER-Golgi vesicles in aged cells. Although the morphology of the Sec13 signal became more diffuse, processing bodies were still observed to overlap with distinct Sec13 structures around the nucleus. This time-lapse shows representative set of images from a group of analysed experiments used for manual observations, not automated quantification. Scale bar 5 µm. Quantification of 2 values Showed that G1 localisation was insignificant, as was G2/m localisation, only S phase M2 values were significant (shown above)

Localisation to the Early Golgi compartment, represented by Cop1, was also shown to be reduced during advanced replicative age but still significant compared to controls. M2 coefficient dropped by 47, 66 and 34% for G1, S and G2/M phases respectively. Manual observation of micrographs showed little overlap of the p-body and Cop1 signals during any cell cycle stage. In contrast to the drop in colocalisation with Cop1, Edc3 showed no decrease in localisation with Anp1 in cells of advanced replicative age, although the localisation was low in young cells to begin with. In the G2/M phase, p-bodies showed an increased overlap with Anp1 signal, with an M2 coefficient of 0.18 compared to 0 overlap in young cells. This overlap during the latter stage of the cell cycle could again be due to a breakdown in p-body, or Golgi, trafficking in aged cells leading to dysregulated transport and an increase in random overlap of the signals. In micrographs of Anp1 tagged cells, p-bodies were observed to overlap completely with some Anp1 tagged structures. Whether this overlap is due to an interaction between the 2 compartments or some shared

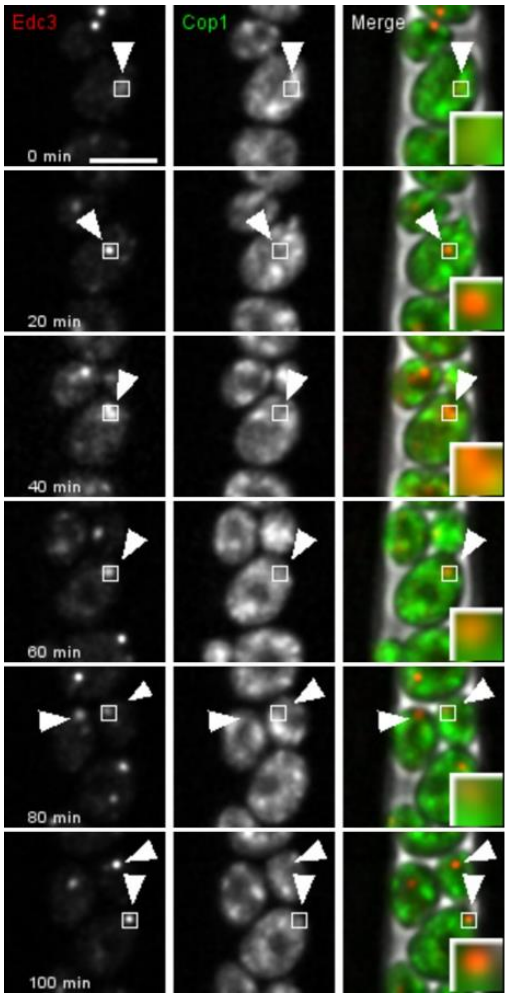

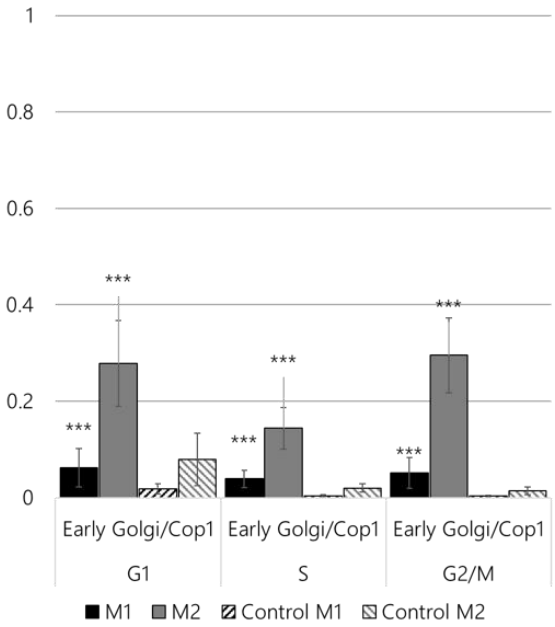

Figure 38: Micrographs of aged cells labelled with Cop1-mNeonGreen and Edc3-mRuby2 No complete overlap of processing bodies with Cop1 structures was observed in aged cells. This time-lapse shows a representative set of images from a group of analysed experiments used for manual observations, not automated quantification. Scale bar 5 µm. M2 values were low but significant compared to controls as shown above.

localisation to a 3rd compartment is not known, and further investigation is required to identify these structures.

Micrographs of Chc1 and Edc3 tagged cells were similar in old cells to those from young cells. Some overlap was seen between Chc1 structures and p-bodies and overlap of identically shaped structures was also observed. Quantification of colocalisation showed an increased M2 coefficient in both G1 and S phases (much larger in G1) but a decrease in G2/M phase cells. The structures observed in micrographs were similar to those observed in Anp1 tagged cells, spherical bodies, that overlapped completely with some foci of Edc3 signal.

5.3.3 Pex3 / Peroxisomes

Automated quantifications of colocalisation of Edc3 with the peroxisome marker Pex3 increased in cells of advanced replicative age. M2 coefficient increased from 0 in al cell-cycle stages to 0.2, 0.65 and 0.43 in G1, S and G2/M respectively. Observation of micrographs showed some overlap in distinct foci of Edc3 and Pex3, although both also formed independent non-overlapping structures. No previous interaction has been shown between p-bodies and peroxisomes, but in plants, peroxisomes, p-bodies and Golgi bodies have been observed to use the same or similar mechanisms of intracellular transport (Hamada et al., 2012) and all pause to interact with the ER. If there is a breakdown in this transport, or the

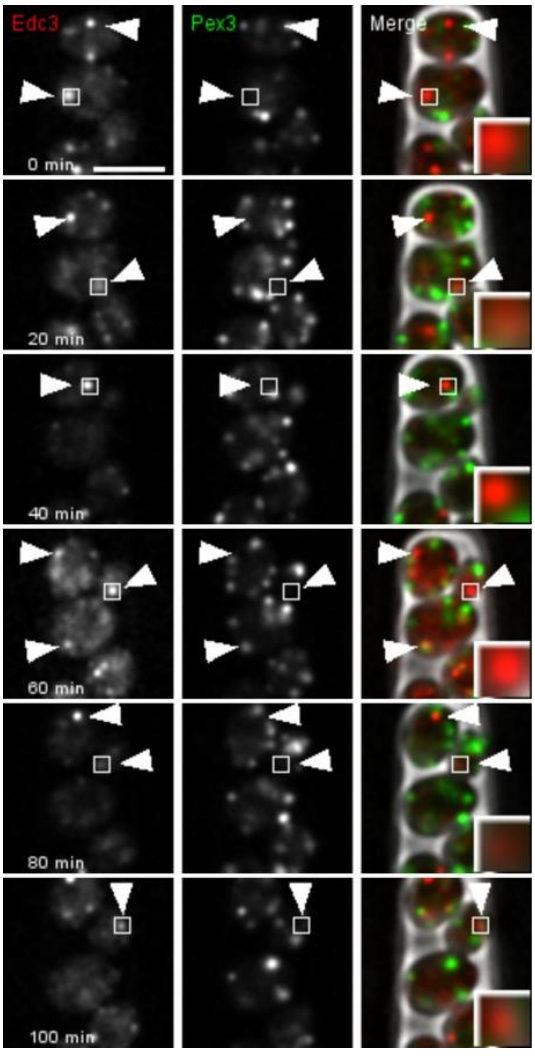

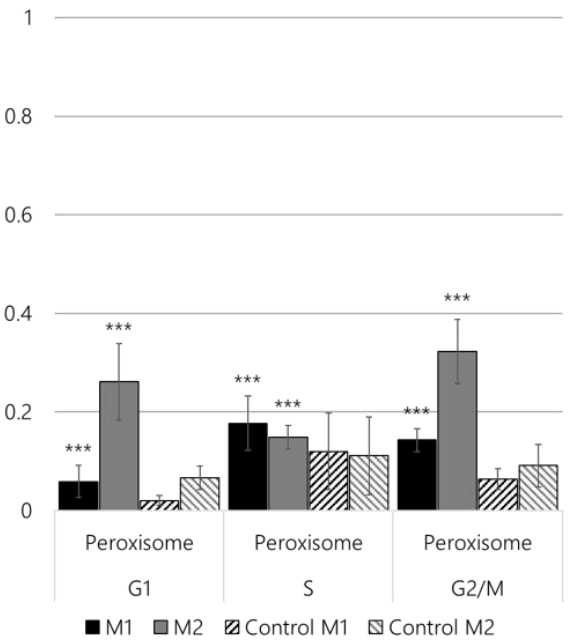

Figure 39: Micrographs of Aged cells tagged with Pex3-mNeonGreen marking peroxisomes and Edc3-mRuby2 marking processing bodies. There was no clear overlap of processing bodies ana peroxisomes in the aged cells at any point during the cell cycle. Both organelles appeared as independent foci. This time-lapse shows a representative set of images from a group of analysed experiments used for manual observations, not automated quantification. Scale bar 5 µm. M2 throughout the cell cycle was significant as shown above.

release from pausing, in aged cells it could cause an accumulation of these organelles at pausing sites leading to a perceived increase in colocalisation.

5.3.4 Mitotag/Mitochondria

The colocalisation of p-bodies with mitochondria showed a large increase based on M2 coefficient in aged cells. In micrographs, individual p-bodies clearly overlapped sections of the mitochondria throughout the cell cycle, although some p-bodies still remained independent. The colocalisation of p-bodies and mitochondria was strongest during G2/M, as with young cells, although in aged cells there was a 100% increase in M2 indicating that the proportion of Edc3 overlapping Mitochondrial signal had doubled. Mitochondria have been shown to control the segregation of some protein aggregates in (Zhou et al., 2014)

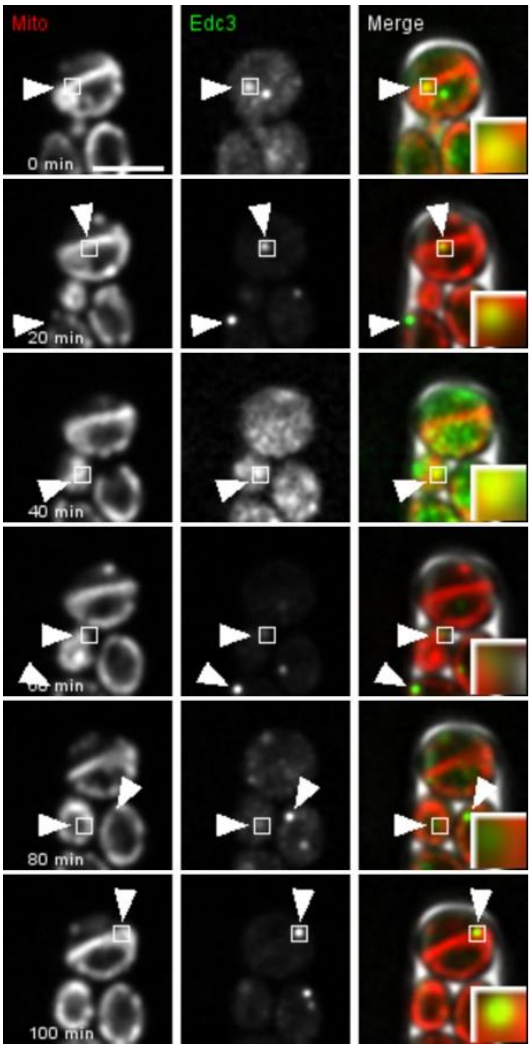

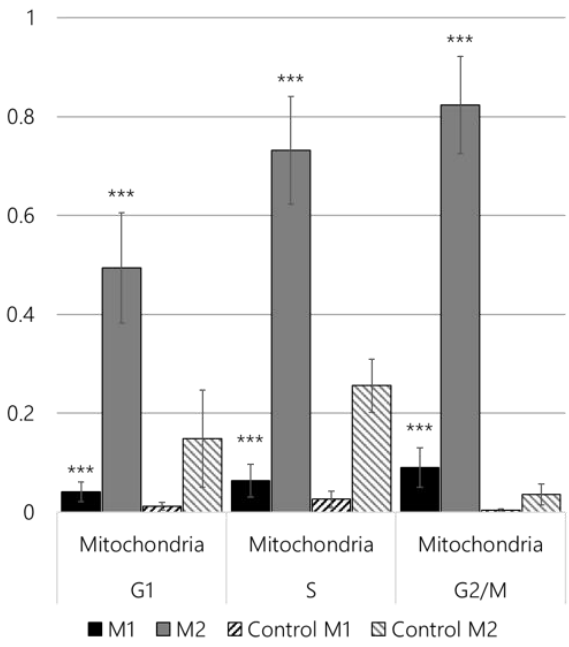

Figure 40: Micrographs of aged yeast cells tagged with MitoTag-mRuby2 and Edc3-mNeonGreen. Processing bodies show consistent overlap with mitochondria throughout the cell cycle in aged cells. Processing bodies were transported through the bud neck to the bud tip alongside mitochondria implying a share transport mechanism. This time-lapse shows a representative set of images from a group of analysed experiments used for manual observations, not automated quantification. Scale bar 5 µm. M2 values were significant compared to controls and higher than for all other organelles in aged cells.

budding yeast, although p-bodies were not investigated. If mitochondria play a role in p-body segregation the increased localisation to mitochondria of p-bodies could be due to changes in this process. In non-inherited aggerates, such as HSp104 chaperones heat induced aggregates, advanced replicative age leads to a decreased association with mitochondria and leakage of aggregates into the daughter cells. P-bodies display an inverse behaviour in young cells, in that they are inherited by daughter cells under conditions of glucose restriction. If this process is regulated by association with mitochondria it is possible that a breakdown in the regulation of association could lead to a failure of p-body inheritance as they remain associated with non-inherited mitochondrial regions. The localisation of p-bodies in aged cells is summarised in Figure 41.

To summarise the results of the colocalisation studies, it was found that the localisation profile of p-bodies, as determined by the marker protein Edc3, was altered in cells of advanced replicative age, these changes are shown in Figure 42. P-bodies showed a decreased association with membranes of the endoplasmic reticulum and Golgi apparatus,

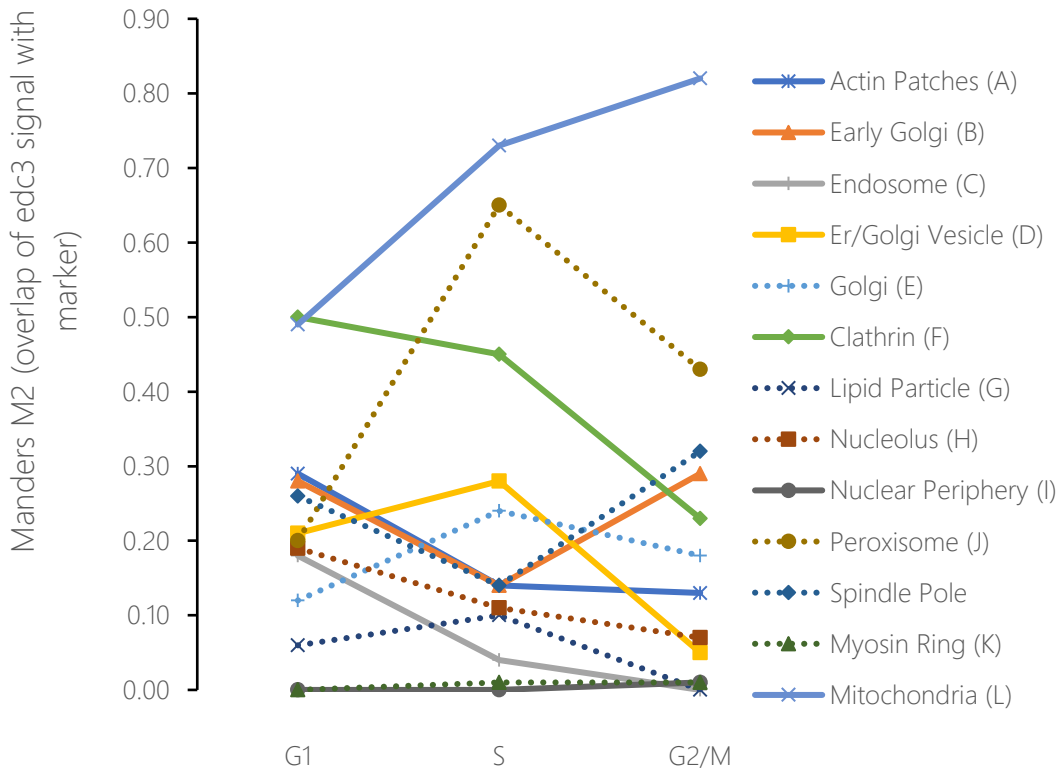

Figure 41: Summary of processing body localisation in aged cells. Figures are summarised as Madners' M2 coefficients during each stage of the cell cycle.

particularly during the G2/M phase of the cell cycle in the case of ER-Golgi vesicles. This drop in colocalisation may indicate a loss of adhesion to, or co-trafficking with these membranes during budding in aged cells, which is known to be present for some mRNA during young cell growth. Conversely p-bodies showed an increased association with the mitochondria in aged yeast cells, possibly indicating a shift in association to the mitochondrial membrane from the ER. The implications of this shift are unclear and require further exploration. The raw changes in Mander's M2 values are summaries in figure 42.

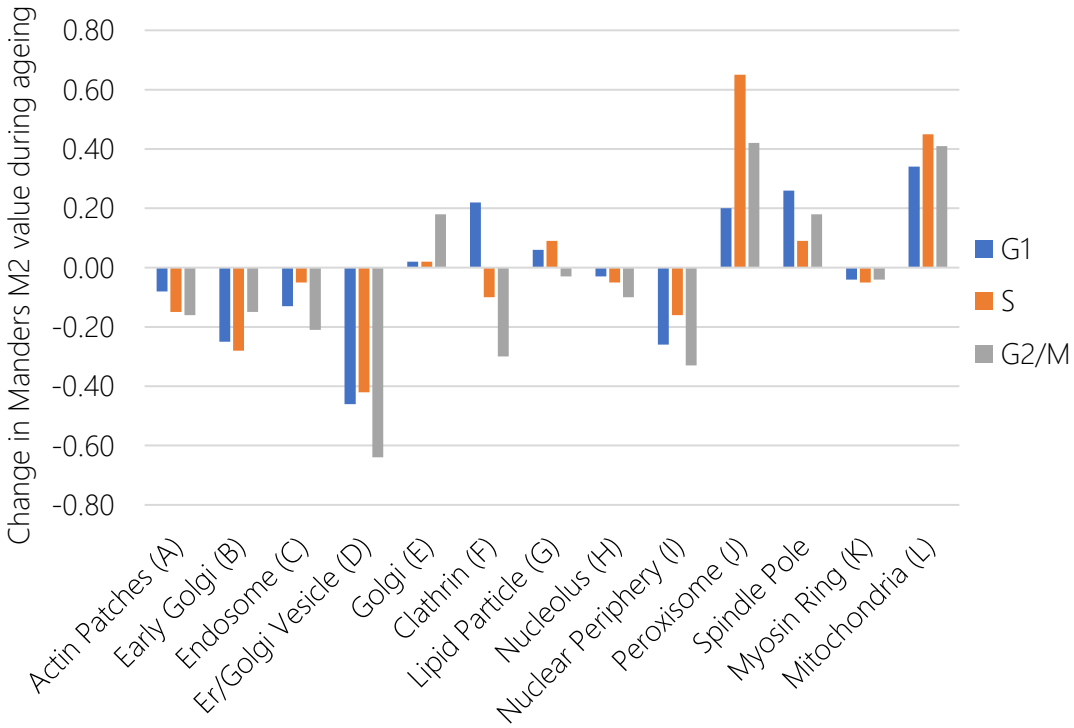

Figure 42: Change in localisation of processing bodies during cellular ageing..Change in Manders M2 represents the change in overlap between the the processing body marker Edc3 and the indicated orgranelle marker.

6 Inheritance and motility of Processing Bodies in *Saccharomyces cerevisiae*

6.1 Movement and inheritance of processing bodies in *Saccharomyces cerevisiae*

While the potential roles of p-bodies in mRNA decay and storage have begun to be uncovered, a third potential role that is yet to be considered has had very little attention. The transport of mRNA in yeast has been well studied and is known to rely on an mRNP complex made up of the class V myosin motor protein Myo4 and the mRNA binding proteins She2 and She3 (Niessing et al., 2018). This complex shuttles a variety of mRNAs into the bud via the actin cytoskeleton for localised translation of proteins important in bud development. This mRNP complex has also been implicated in the early transport of ER into the emerging bud and so its activities are not limited to the transport of mRNAs.

In budding yeast, it has previously been shown that p-bodies, when induced under conditions of glucose deprivation (0.1% glucose in synthetic complete medium), move between mother and daughter cells in a unidirectional manner (Garmendia-Torres et al., 2014) i.e bodies are transported to the daughter cells, and do not return to the mother. The mRNA transport proteins are required for this inheritance of p-bodies, and deletion mutants of Myo4, She2 and She3 all show a loss of unidirectional inheritance during budding. This evidence points towards an expanded definition of p-body function, in which not only mRNA degradation and storage occur in p-bodies, but transport of mRNA as well. The stress specific transport of certain mRNAs to the emerging daughter cell could confer a selective advantage by ensuring an optimised program of gene expression for growth in nutrient restrictive conditions. The same study that identified the inheritance of p-bodies also showed that daughter cells achieve a larger overall size before themselves budding, suggesting that at least as far as cell growth was concerned, inheriting a p-body is advantageous.

P bodies share many similarities with other mRNP and protein aggregates found within eukaryotic cells. Their assembly appears to depend highly on interactions between the low complexity domains of their constituent proteins, leading to a critical concentration at which liquid-liquid phase separation occurs creating the mebraneless granule (Molliex et al., 2015). This reliance on low complexity domains for reversible assembly makes the constituent proteins of mRNP granules susceptible to mutations that could cause aberrant

aggregation, ultimately leading to a cell death. In humans, stress granules, p-body related mRNP granules, have been implicated in the pathology of aggregate-based neurodegenerative diseases, with many of the constituent proteins present as homologues in budding yeast, such as TIA-1 (Pub1) and Ataxin-2 (Pbp1)(Reineke & Lloyd, 2013). It has been suggested that the continuous process of LLPS may lead to a build-up of misfolded proteins with disordered regions that eventually form aggregates of their own, and then self-aggregate, ultimately forming pathological fibrils that cause cell damage, and that this process is enhanced by mutations in the proteins involved. Although p-body proteins have not been shown to be present in human disease state cells in the same way as stress granule proteins, their formation is thought to follow the same process, and multiple p-body proteins have been found to undergo LLPS *in vitro* (Schutz et al., 2017). Given the likely build-up of misfolded proteins associated with any mRNP granule such as a p-body, it would seem counter-intuitive to pass these granules on to a new daughter cell, where the ageing processes is theoretically reset upon budding.

In the case of p-bodies, the evidence that they are inherited for a single generation is clear, although beyond that no data has been published. The general interphase movement of p-bodies has also been largely overlooked, with studies focusing on how cytoskeletal inhibition affects formation and disassembly of the granules (Sweet et al., 2007). In this section, the movement of p-bodies in budding yeast, as well as the inheritance of p-bodies between generations was investigated to gain a greater understanding of how p-bodies carry out their possible function in mRNA transport.

6.2 P bodies are mobile in *S. cerevisiae* and move in a directional manner.

The limited previous studies of p-body motility, in human cells (Aizer & Shav-Tal, 2008) and yeast (Garmendia-Torres et al., 2014) have given little insight into how p-bodies might move around the cell in order to carry out their function. In principle, either mRNAs must be trafficked deliberately to p-bodies, or p-bodies must scan the likely cytoplasmic locations of mRNA (ER, Nuclear exit sites etc) to find and segregate their target mRNAs. In mammalian cells, p-bodies were observed (in a limited study) to remain in small cellular regions, without showing the larger scale directional movement indicative of transport along microtubules (Aizer et al., 2008). In yeast, the localisation of p-bodies to the site of

bud emergence, just before budding has been demonstrated, but the movement in the time periods outside the budding process was not studied in detail (Garmendia-Torres et al., 2014). The exception to this lack of detailed information comes from studies carried out in plants, specifically *Arabidopsis Thaliana*. In *Arabidopsis*, p-bodies have been shown to colocalise with and move in unison with myosin motor proteins, along distinct actin filaments (Alexandra Steffens et al., 2014). This process was reliant on the p-body protein AtDCP1, which was shown to bind to both yeast and mammalian class V myosins, indicating a highly conserved interaction. The same study identified an interaction between yeast Dcp1 and the yeast class V myosin Myo2, a paralog of Myo4, the motor protein involved in mRNA transport.

To investigate the nature of p-body movement in *Saccharomyces cerevisiae*, a brightly fluorescent protein, mNeonGreen, was fused to the yeast p-body component Edc3. The increased intensity and lower photobleaching of this protein allowed images to be captured at high time resolution using a spinning disk fluorescence confocal microscope to track movements of p-bodies in live cells. Images were captured every 100ms with the illuminating laser power set to maximum in order to capture the greatest possible detail. Using this technique, it was also possible to increase the capture speed, up to 70 frames

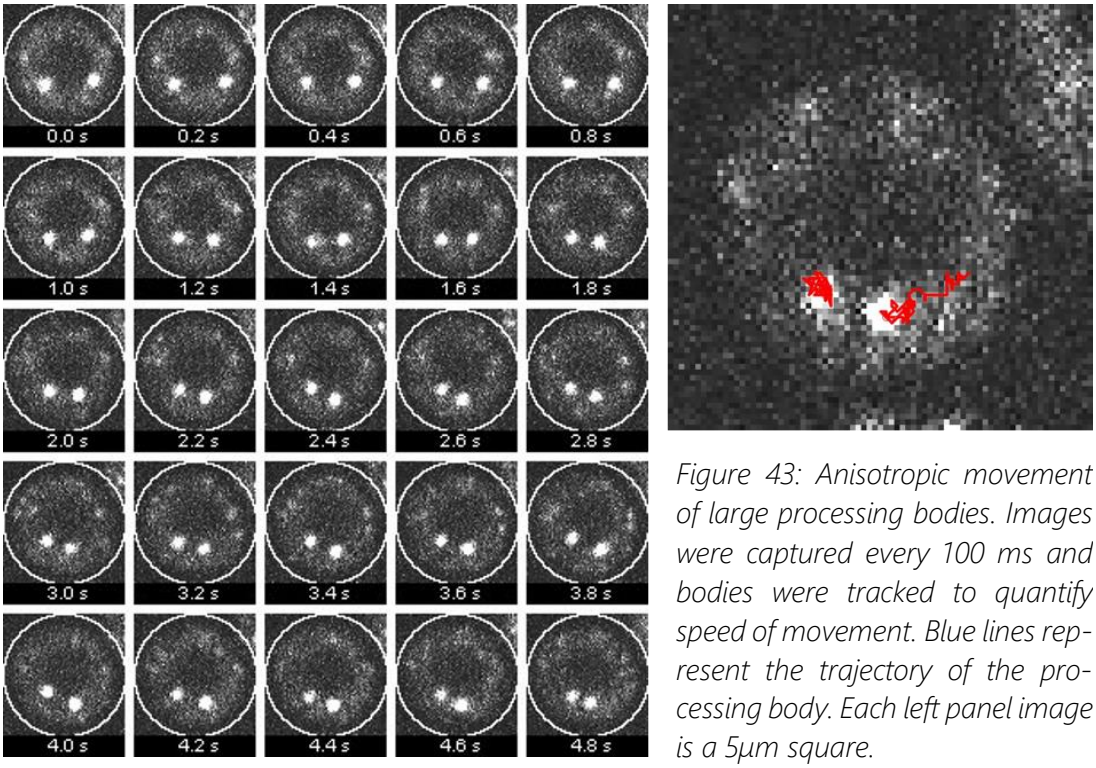

Figure 43: Anisotropic movement of large processing bodies. Images were captured every 100 ms and bodies were tracked to quantify speed of movement. Blue lines represent the trajectory of the processing body. Each left panel image is a 5µm square.

per second, but the loss of signal resulted in noisy images that contained little useful information. 10 frames per second worked well as a compromise between speed of acquisition and signal-to-noise ratio.

Under microscopic observation at 10 frames per second, p-bodies marked by Edc3 showed three main types of movement. Similar to the observations in mammalian cells, large p-bodies showed anisotropic movement without directionality. These p-bodies remained confined to small areas of roughly 4 square microns. Figure 43 shows an example of this movement.

A second class of p-bodies showed clear fast directional movement along linear pathways. These p-bodies were smaller, with a lower total fluorescence intensity, and therefore protein content. Both classes of p-body were present in single cells and the motile p-bodies often appeared to interact with the larger bodies, possibly exchanging material.

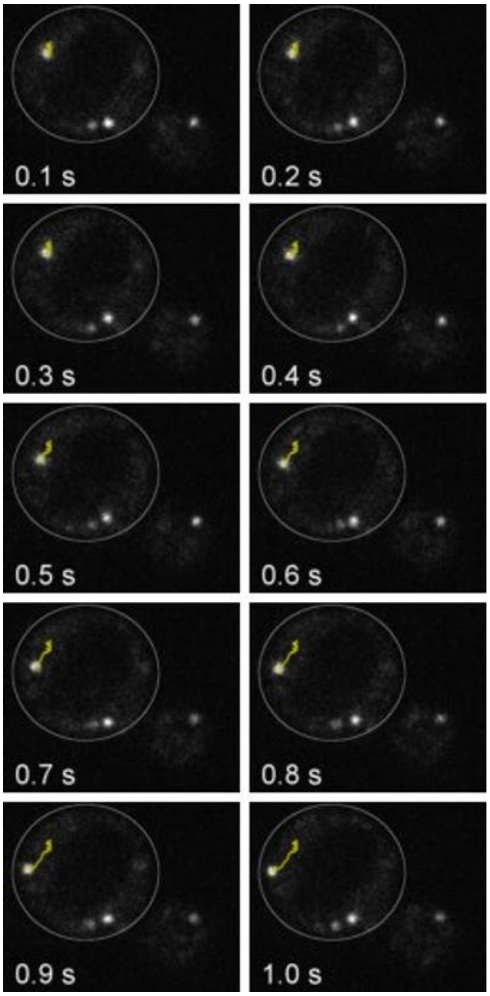

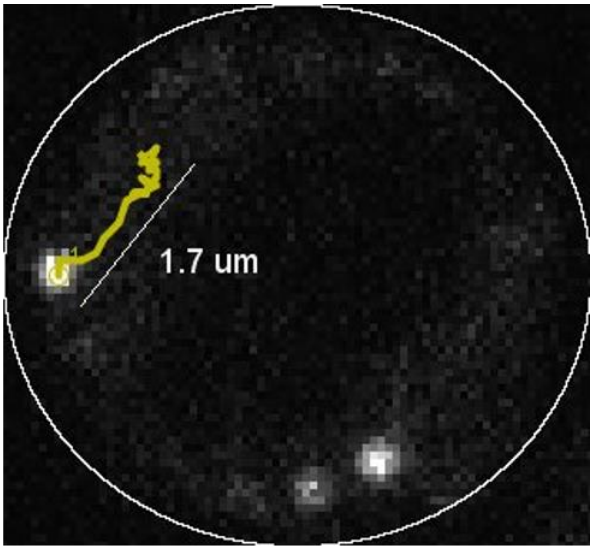

Figure 44: Fast directional movement of processing bodies. Images were captured every 100 ms. Some processing bodies showed fast directional movement of up to 2.5 µm s^{-1}. Trajectory of processing body movement is shown in yellow. Each left panel image is 7 µm tall.

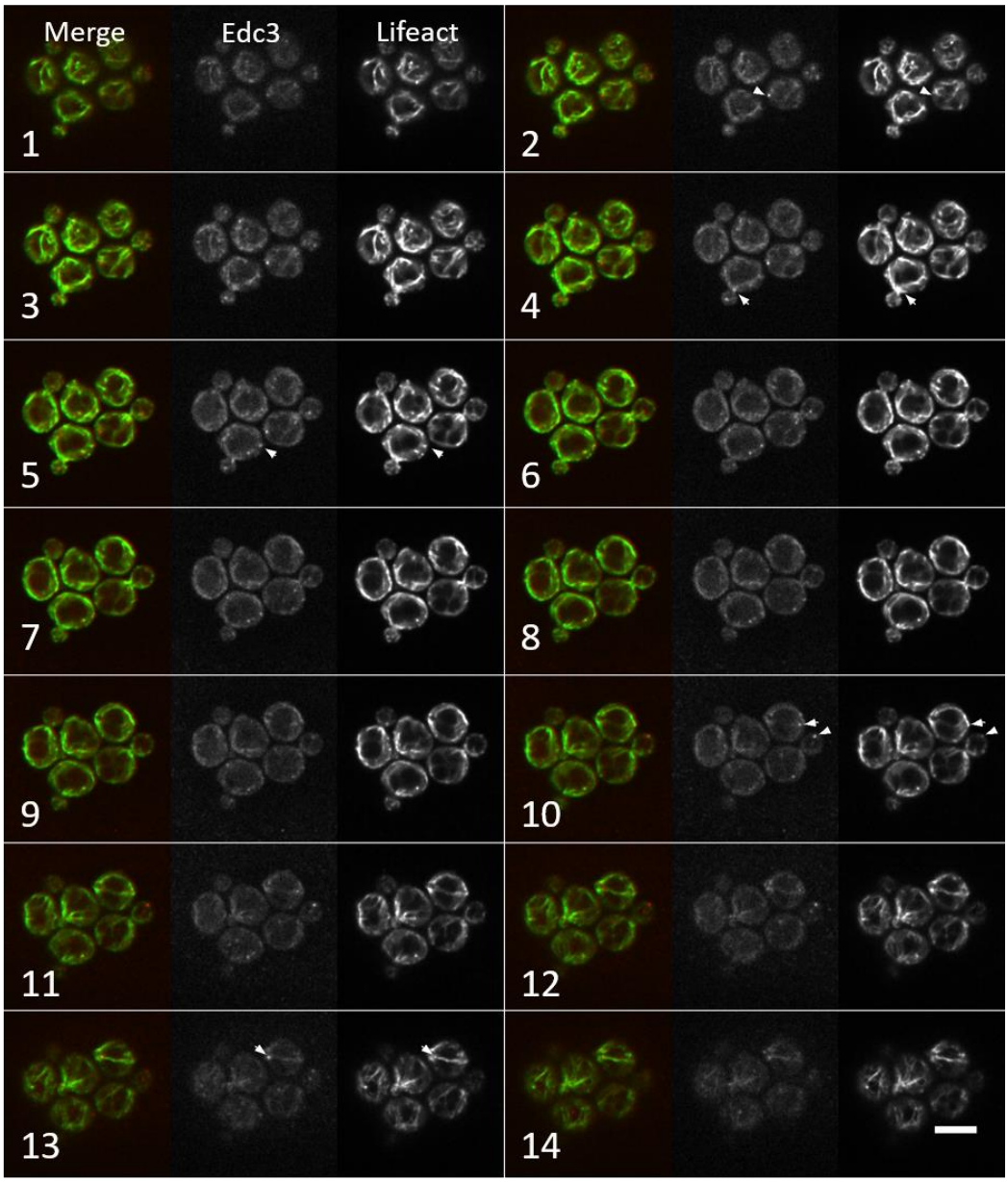

Figure 45 Colocalisation of actin filaments and processing bodies. Actin was visualised with Lifeact-mNeonGreen and processing bodies with Edc3-mRuby2. Each 3-frame section is a 0.5-micron Z section, numbered 1 – 14 from the base of the section to the top. Arrows indicate sites of colocalisation. Scale bar indicated 5 microns. Processing bodies show qualitative overlap with the actin cytoskeleton throughout the cell, and not limited to the coritcal actin cytoskeleton.

Quantification of the speed of movement of these bodies showed an average speed of 2.5 microns/second, consistent with previously observed movement of vesicles along actin filaments facilitated by class V myosins. Although the speed of travel appears consistent with transport along actin filaments, the distance travelled was different to previously observed

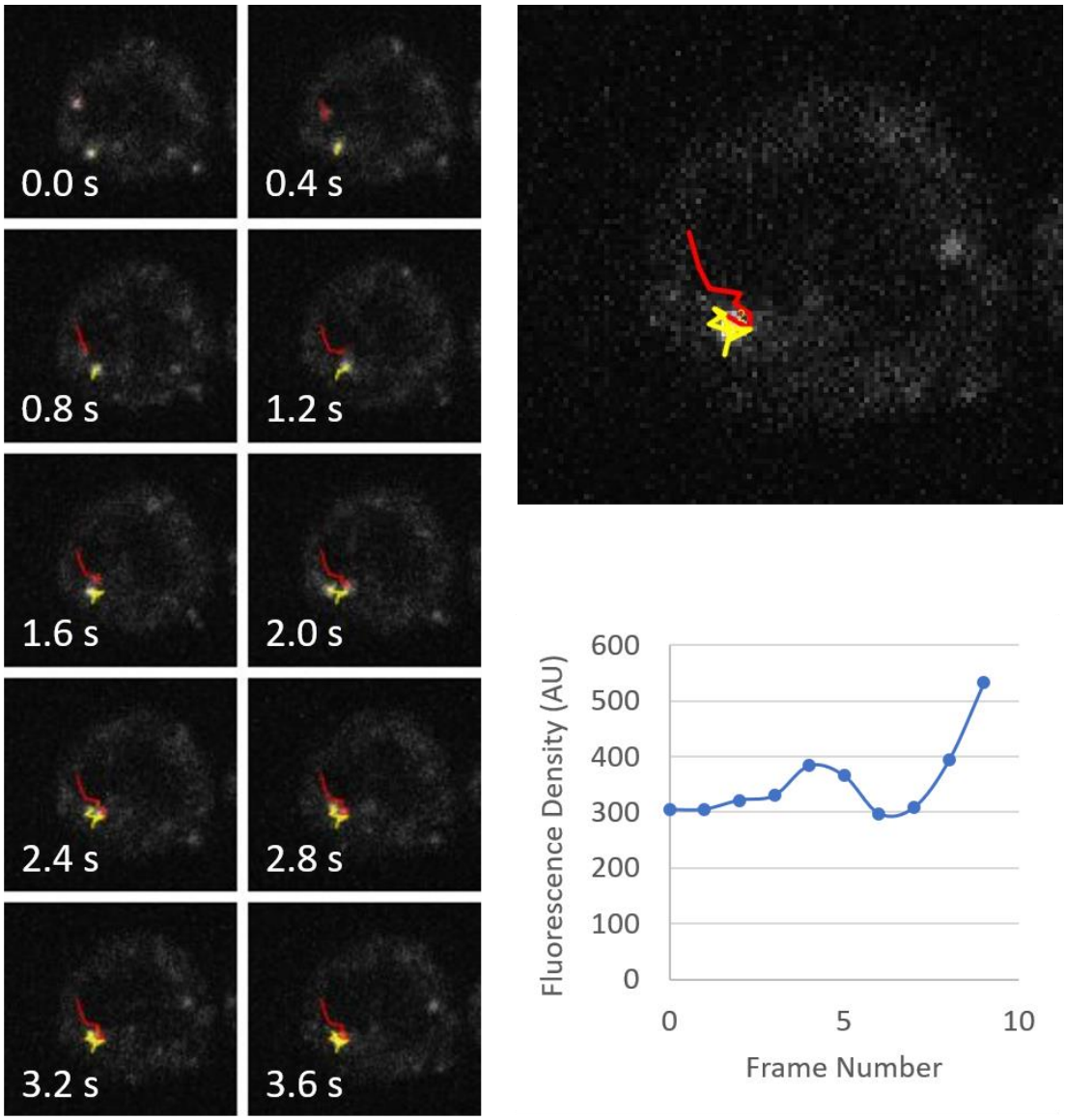

Figure 46: Processing bodies undergo fusion events. Processing bodies appear to interact and undergo fusion events to create larger bodies with higher fluorescence signal. Left – tracks of 2 bodies converging on a single point. Right upper – complete tracks of both bodies. Right lower – Quantification of fluorescence signal for one track showing increased fluorescence upon merge of bodies.

trafficked cargoes. P body movements were shorter, often covering only 1 – 2 microns at a time, although imaging was performed in a single plane and so movement in the 3rd dimension could explain this shortened travel distance. While many p-bodies were observed close to the bud neck in dividing cells, the short time frames of these image sequences (1-4 seconds) did not capture directional movement into the bud. Figure 44 shows an example of the directional movement observed in this class of p-body.

Finally, a third class of bodies was observed to move quickly and directionally, often traversing the inside edge of the cell, perhaps interacting with cortical actin filaments or endoplasmic reticulum. These p-bodies were much smaller and dimmer and were only observed qualitatively and in time-lapse movies rather than single images, as their signal faded quickly due to the intensity of the imaging laser. Whether these p-bodies are in fact present, and not an artefact of imaging noise may be questioned, as inspection of individual images was difficult due to the low signal to noise ratio. Improved imaging technology will be required to validate these observations.

To determine if p-bodies were associated with actin filaments, not just actin patches as quantified in the previous chapter, the actin binding protein ABP-140 was tagged with mNeonGreen via genomic integration and co-expressed with Edc3-mRuby2. ABP-140 signal highlighted clear actin filaments within the cell with which p-bodies were seen to co-localise, although only in certain circumstances. Larger p-bodies did not associate with actin filaments, consistent with their lack of movement, while smaller, dimmer foci more often appeared adjacent to, or overlapping with actin filaments, see Figure 45.

6.2.1 Processing bodies undergo rapid fusion events

While analysing images captured for the purpose of determining p-body movement, an interesting behaviour was observed. Individual p-bodies appear to move to, interact with and fuse with each other to form larger, higher protein content (based on fluorescence signal) granules. This fusing behaviour, as shown in Figure 46, is similar to a previously observed interaction between mammalian p-bodies and mammalian stress granules. It was reported that mammalian stress granules appear to "dock" with p-bodies, but not undergo fusion (J. R. Buchan et al., 2008). This observation that p-bodies can fuse into larger granules is consistent with their structure being the result of liquid-liquid phase separation, as fusion events are expected in such systems (Schutz et al., 2017). These fusion events happen at millisecond timescales, which may be why previous studies, using lower time resolution imaging have failed to identify them *in vivo*.

6.3 P bodies are inherited through multiple generations during caloric restriction

Previous work on the movement of p-bodies during mitosis identified a unidirectional trafficking of individual p-bodies, dependent on the locasome of She2/She3/Myo4. In yeast this activity was observed in cells grown in restrictive glucose conditions of 0.1% glucose, which allows continued cell growth but also induces the formation of p-bodies (Garmendia-Torres et al., 2014). To verify this activity, p-bodies, labelled with Edc3-mNeonGreen were imaged at 1-minute intervals over a 16-hour period, to enable the tracking of p-bodies during several cell divisions.

In agreement with the previously mentioned study, p-bodies were observed moving from mother to daughter cells in a unidirectional manner as shown in Figure 48. To expand upon this observation, individual p-bodies were tracked beyond the initial inheritance, while still under conditions of glucose restriction. Individual p-bodies were observed to be inherited through multiple generations of yeast daughter cells, while the mother cells formed de novo p-bodies at some point between transfer of the existing p-body and exit of mitosis. Although the inheritance of a single p-body may not seem significant, as any mechanism for inheritance will likely act on the p-body if conditions are unchanged, it does reinforce the idea of an active function for the p-body in the stress response, beyond the segregation of existing mRNA. If the contents of the p-body were the functional components, then disassembly of the body should take place upon inheritance to access these contents. It should also be noted that the p-body is essentially a protein aggregate, and in most cases such aggregates are actively retained rather than inherited due to their potential to aggregate further and cause cell damage. The inheritance of the p-body would therefore seem to be counter-intuitive, unless it has an active role in cell growth under glucose restrictive conditions.

6.4 P-body inheritance depends on mRNA transport systems and Dcp1

The inheritance of p-bodies in budding yeast has previously been shown to rely on the "locasome" complex that facilitates mRNA transport. The key components of the locasome

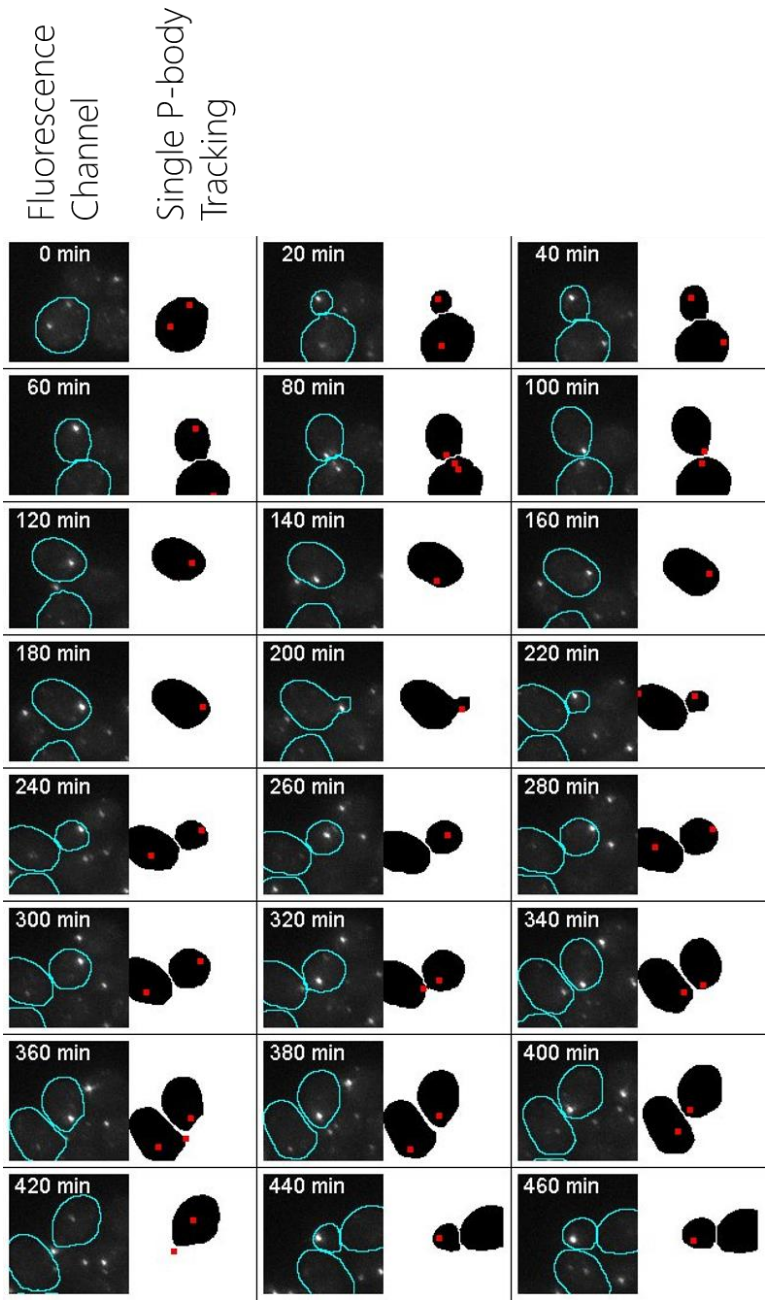

Figure 47: Multigenerational inheritance of processing bodies. Individual processing bodies were tracked across multiple generations of yeast cells. Images were captured every 10 minutes for 16 hours and segmented to identify individual bodies. Individual bodies appear to be inherited through multiple generations without disassembly. Each Image is a 12 µm square. Column 1 shows the fluorescence signal channel of the time lapse capture, column 2 shows image segmentation focused on a single processing body that is trafficked between multiple mother and daughter cells.

are the She2 and She3 mRNA binding proteins and the myosin V motor protein Myo4. Deletion mutants for any of these genes evince loss of p body inheritance and loss of targeted localisation to the bud neck in the time period before budding. A link between

the locasome and p-body in yeast has not yet been validated, although several studies have linked a second myosin V protein Myo2 to the assembly of p-bodies (Chang et al.,

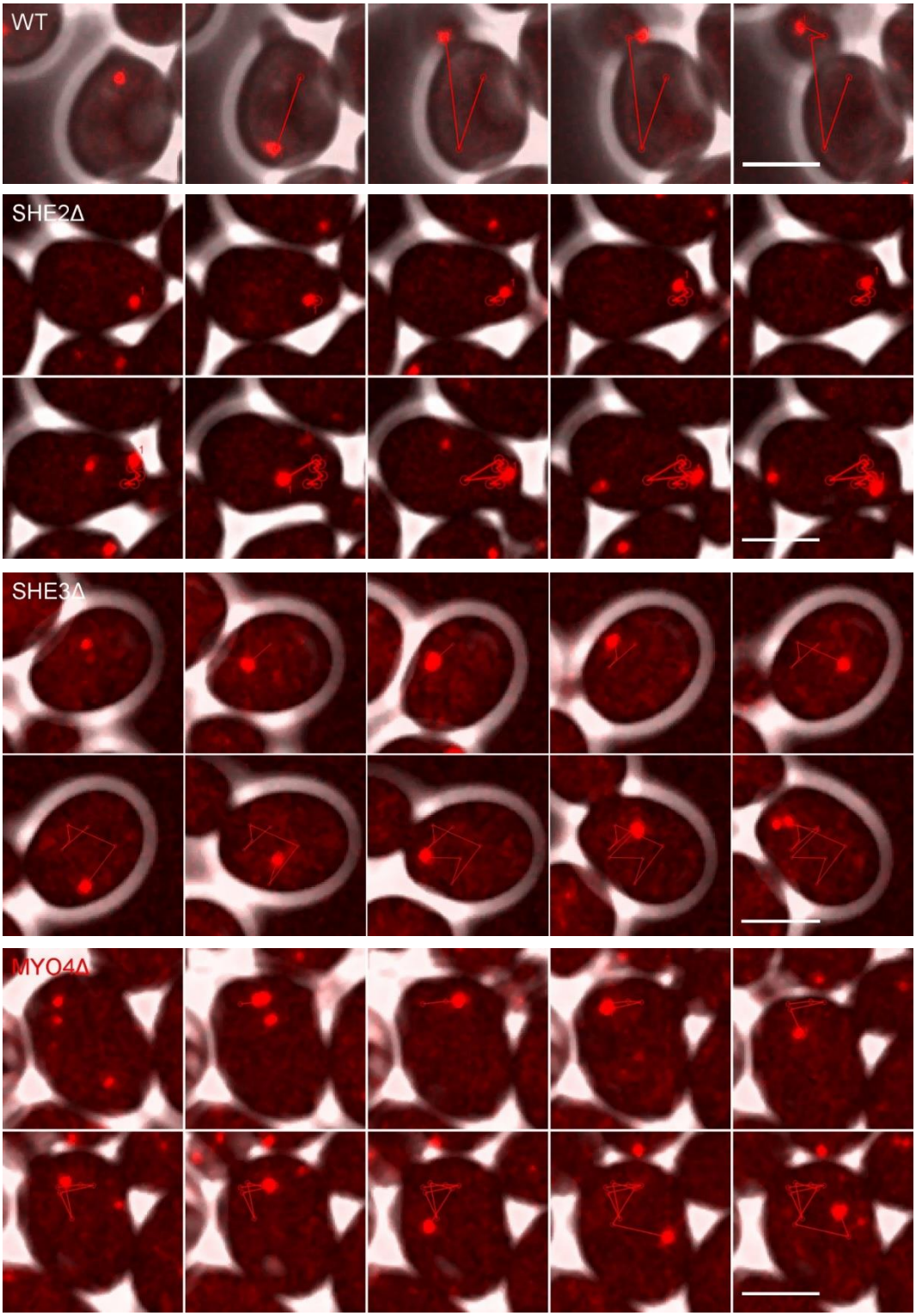

Figure 48: mRNA Transport mutants disrupt processing body inheritance. Deletions of any components of the locasome" complex required for mRNA transport in budding yeast results in a loss of inheritance of processing bodies. Processing bodies were tagged with Edc3-mRuby2. Images were captured every 10 minutes and processing bodies manually tracked. Scale bars represent 5 µm.

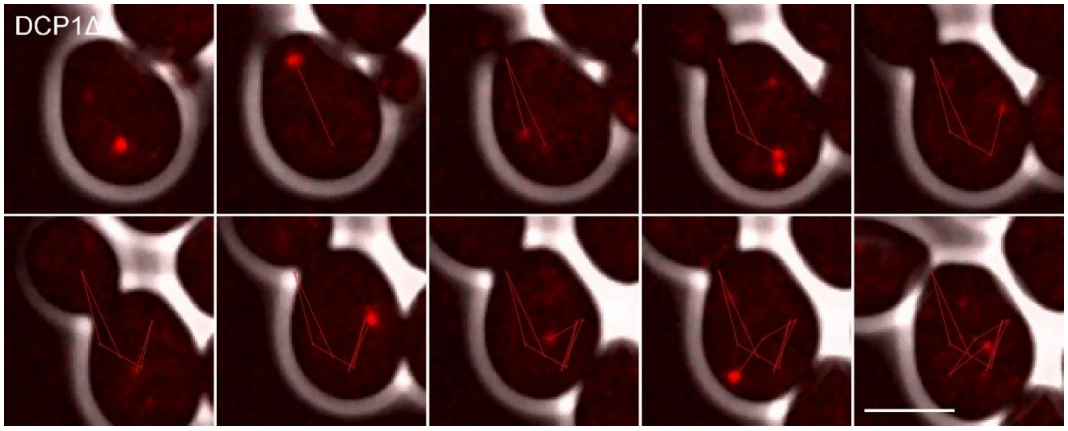

Figure 49: Dcp1 is required for processing body inheritance. Processing bodies were tagged with Edc3-mRuby2 in a Dcp1Δ strain. Images were captured every 10 minutes. Scale bar represents 5 µm.

2008; Alexandra Steffens et al., 2014). In plants the link between movement along actin filaments appears to be the p-body component atDCP1. Yeast Dcp1 has been found to bind Myo2 in vitro.

To test whether yeast Dcp1 might be the link between p-bodies and the locasome in budding yeast, the deletion mutants for the locasome complex published previously were recreated and compared to a deletion of Dcp1. Importantly, during mitosis, p-bodies in the Dcp1 deletion strain show the same loss of inheritance seen in strains deleted for components of the locasome. Whether this loss of activity is due to a loss of interaction between Dcp1 and the locasome is not clear, but it does suggest a potential link between p-bodies and actin filaments that has not previously been identified. The locasome deletion mutants showed a p-body inheritance of 10%, 18% and 5% for Myo4 Δ, She2Δ and She3Δ strains respectively (figure 48), while in the Dcp1Δ strain (figure 49), 8% of total p-bodies were inherited. Interestingly although p-bodies were inherited in wild type cells, there was only a slight change in total Edc3 signal inheritance across the mutant strains, indicating that at least for this protein, the maintenance of protein concentration in the daughter cells does not rely on inheritance of p-bodies.

6.5 P body inheritance is maintained in replicatively aged cells.

Replicative or chronological ageing can cause the breakdown of a number of cellular systems in yeast and other organisms. One such system breakdown is the control of

segregation of protein aggregates. In budding yeast, young mother cells preferentially retain protein aggregates (Dillin et al., 2014) and cell of advanced replicative age progressively lose this ability. To establish whether the inheritance of p-bodies is adversely affected by replicative age, cells tagged with Edc3-mNeonGreen were grown in microfluidic dissection devices to advanced replicative age. Cells were grown to the point of 20 replications (to within one or two generations depending on the age when captured in the device) and imaged over time to visualise the inheritance of p-bodies. Observations of these time lapses videos showed that in advanced replicative age, p-body numbers appear to increase, but in the majority of cells, at least one of these p-body is inherited by the daughter cell. Figure 50 shows the most commonly observed behaviour in which at least one p-bodies continues to be inherited by daughter cells.

From these observations it appears that advanced replicative ageing does not inhibit the inheritance of p-bodies, indicating that this process may be more robustly controlled that the inheritance of protein aggregates. Alternatively, if p-bodies are trafficked while linked

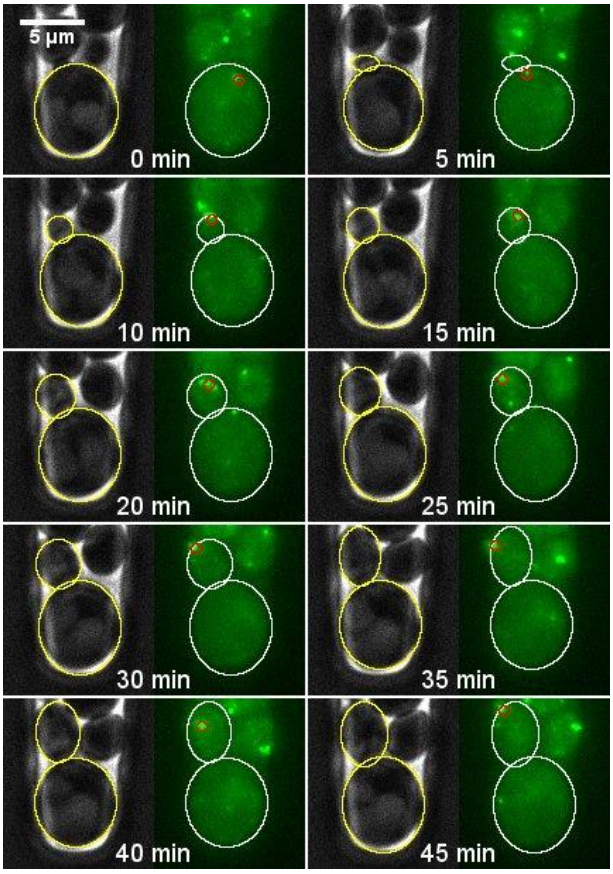

Figure 50: Processing bodies are inherited in cells of advanced replicative age. Cells expressing Edc3-mNeonGreen were grown in CliC2 microfluidic dissection devices in 0.1% glucose media. Images were captured every 5 minutes after 24 hours of growth. The outlines represent individual cells, and red outline an individual p-body. P-bodies continue to be inherited in cells that have undergone multiple budding events. This image shows the 12th bud of the mother cell, in which a processing body is inherited by the daughter cell.

to an existing organelle, it could be that any active mechanism of inheritance does break down over time, but p-bodies continue to be inherited due to their continued association with this organelle.

7 Discussion

7.1 CliC2 microfluidic chips are suitable for analysis of processing bodies during replicative ageing

As established in the introduction to this work, there appears to be a link between the mechanisms and signalling pathways involved in the response to environmental and cellular stress and the progression of ageing. A possible link between these two processes has emerged in the form of cytoplasmic mRNP granules. Types of these granules are formed in response to cellular stresses such as caloric restriction, oxidative stress and increased heat. mRNP granules have also been observed in cells affected by various neurodegenerative disease of ageing, with aberrant aggregation of their constituent proteins a possible cause of such diseases. Investigations of cellular components in human ageing and long-lived animal models is difficult due to the time frames involved and so model organisms are used in which lifespans are significantly shorter. One such ageing model is the replicative lifespan of the asymmetrically dividing budding yeast *Saccharomyces cerevisiae*.

Traditional studies of replicative ageing in yeast utilised physical microdissection in which microdissection needles manually move daughter cells from mothers on agar plates, allowing continued growth of the mother cells. This was a laborious process that required refrigeration of cells for overnight periods potentially impacting analysis of the stress response. More recently, microfluidic platforms have enabled this process to be scaled and integrated into live cell imaging experiments. As the conditions of cellular growth may influence the formation kinetics of p-bodies, any variation must be limited to eliminate bias during imaging experiments. Since there have been no previous studies of yeast p-bodies in replicative ageing, this study first evaluated microfluidic devices for their potential use in the study of p-bodies. Several factors were evaluated to assess the suitability for use in the study of p-bodies during replicative age. When compared with traditional methods of time-lapse imaging, in terms of p body formation and frequency, growth of yeast cells in the CliC 2 microfluidic chip showed both similar induction and frequency of p-bodies. The CliC 2 chip also showed a higher rate of retention when compared with the second tested chip, HYAA. Although the CliC 2 design still suffered from flaws regarding the trapping of yeast cells as demonstrated in chapter 3, it still presents a suitable method for the analysis

of p-bodies in advanced replicative age. This method represents a potentially powerful tool in the study of mRNP granules during ageing, of which there are currently limited models. Future work to refine the designs proposed in this study will improve both the retention and ability to strictly control environmental conditions in these devices.

7.2 Subcellular Localisation and associations of processing bodies

7.2.1 Processing bodies localise to ER and Golgi membranes during log phase growth, implications for function

The various protein and mRNA components of p-bodies in budding yeast have been explored in multiple previous studies although the cellular localisation of these bodies has never been robustly investigated. This previous work has focused on which proteins are recruited to p-bodies, which are important to their formation and disassembly and the associated known roles of these proteins. What is lacking at present is an overview of how the p-body itself acts as an organelle and what its overall function is. Part of refining the understanding of the role of p-bodies is understanding how they behave in the context of other organelles and which organelles they interact with.

P-bodies have been shown in some circumstances to localise to, or in proximity to, organelle membranes in yeast, specifically those of the endoplasmic reticulum (Huch et al., 2016). Several p-body constituent proteins are also suspected to be membrane associated, as demonstrated by membrane flotation assays (Huch et al., 2016). The co-localisation analysis presented in this study identified three markers of the ER and Golgi Apparatus, Sec13, Cop1 and Chc1, representing portions of the ER and early Golgi membranes, as potential sites of p-body localisation. The high degree of localisation with these markers indicated that p-bodies spend significant time associated with ER membranes. This association supports the theory that ER membranes may be sites of p-body formation as previously suggested. Localisation of the constituent factors to ER membranes may act as a catalyst for protein aggregation by bringing together proteins containing low complexity regions in a confined space and limiting diffusion by attachment to membranes. Another possible reason for the association with organelle membranes is to facilitate the trafficking of p-bodies. P-bodies have been shown to be inherited in yeast, and mRNA inheritance has been shown to be possible in association with the endoplasmic reticulum (Fundakowski

et al., 2012). The association of p-bodies with endoplasmic reticulum may therefore indicate a role for p-bodies in the transport of translationally repressed mRNPs. Maintaining an mRNP aggregate between generations during times of cellular stress may help to optimise gene expression in daughter cells by preventing expression of high copy number mRNA not required for maintenance during stress. A visual summary of the colocalisation results is presented in Figure 51.

7.2.2 Replicative age causes a shift in p-body membrane association

The progressive decline in the function of cellular systems over time is one of the main consequences of ageing in eukaryotic cells. The budding yeast Saccharomyces cerevisiae

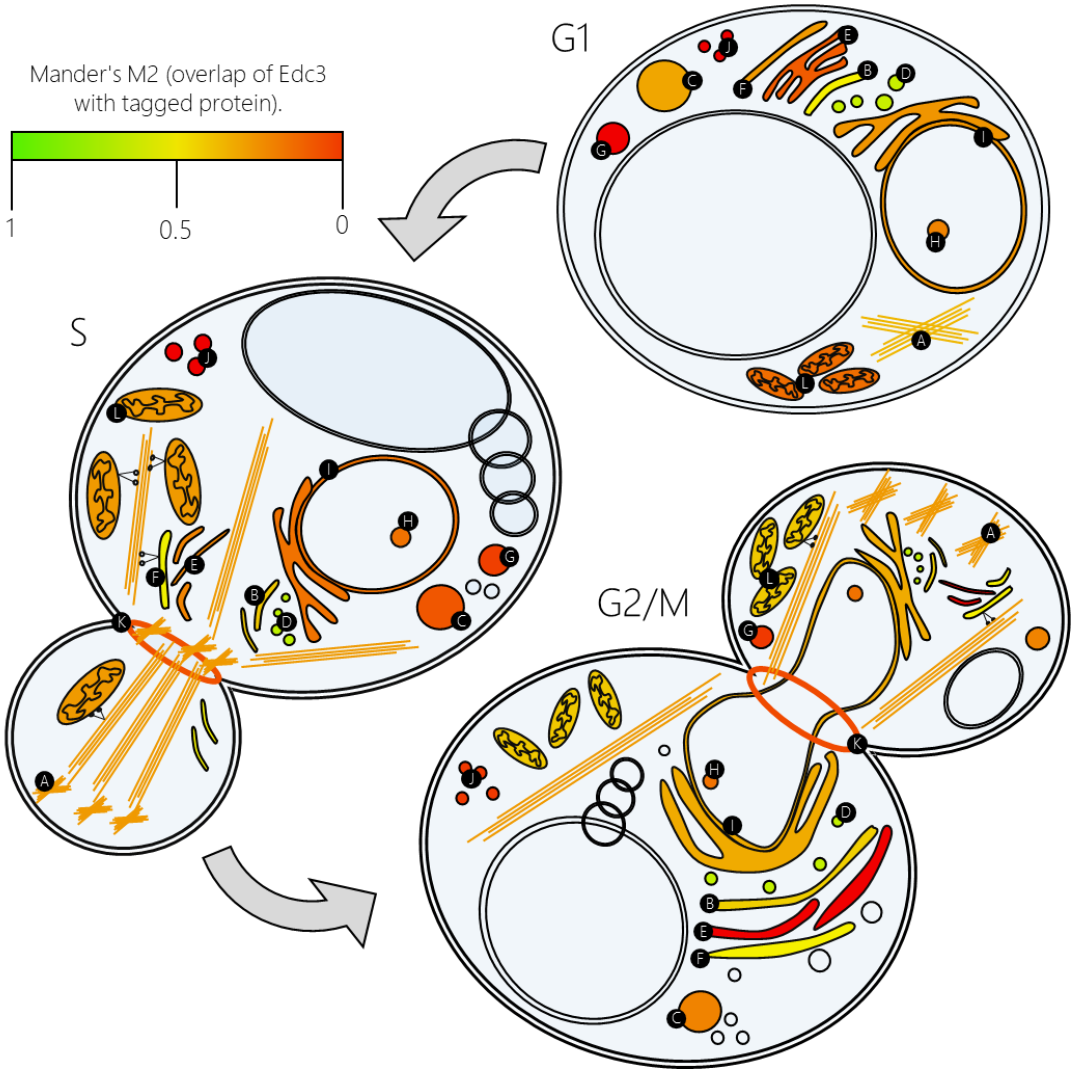

Figure 51: A visual summary of log phase processing body localisation. Actin patches (A), Early Golgi (B), Endosome (C), ER/Golgi vesicle (D), Golgi (E), Clathrin (F), Lipid Particle (G), Nucleolus (H), Nuclear Periphery (I), Peroxisome (J), Myosin ring (K), Mitochondria (L).

is an important model organism in the study of this age-related degeneration due to its easy of growth and asymmetrically cell division, allowing the segregation of components during cell division to be studied. Factors associated with ageing in budding yeast include asymmetric inheritance of damaged or aggregated proteins and extrachromosomal rDNA circles (ERCs) as well as increases in respiration and autophagy. Mitochondrial dysfunction has also been identified as increasing with replicative age in budding yeast (Fehrmann et al., 2013) which can lead to a number of damaging effects including the increased production of reactive oxygen species (Breitenbach et al., 2011). Asymmetric inheritance of dysfunctional mitochondria is therefore important in maintaining daughter cell longevity by restricting damage to the mother. The colocalisation analysis in this study identified a possible link between the progression of ageing in budding yeast and the association of p-bodies with mitochondria.

P-bodies have previously been shown to interact with mitochondria in mammalian cells (Ernoult-Lange et al., 2012) although this interaction has not been observed in budding yeast. This study found that p-bodies associated with mitochondria during log-phase growth, but to a lesser extent than their association with the endoplasmic reticulum. Like the ER, mitochondria are trafficked between mother and daughter yeast cells by an actin/myosin mechanism (Westermann, 2014) and the co-localisation could be a result of shared trafficking pathways along actin filaments. Alternatively, mitochondria, like ER membranes, may also be capable of co-trafficking with p-bodies. The observation that mitochondrial co-localisation with p bodies increases through the cell cycle to the point of cytokinesis would support the idea of shared trafficking for the purpose of inheritance and p bodies localised with mitochondria at the bud site and bud tip together. Association of p-bodies with the endoplasmic reticulum (ER-Golgi region) remained high throughout the cell cycle indicating that it is unlikely that mitochondria are the only inherited organelle to carry p-bodies during inheritance.

The replicative ageing assays carried out in this work identified a shift in colocalisation associated with cells of advanced replicative age. Colocalisation with mitochondria was increased in these cells, although the pattern of increasing colocalisation through the cell cycle remained. None of the pathways known to be affected by replicative ageing in yeast

would explain this change in association between organelles. The segregation of other protein aggregates, including heat induced HSp104 chaperones protein aggregates, has been shown be controlled by mitochondrial attachments (Zhou et al., 2011). These attachments appear to weaken with advanced replicative age resulting in greater inheritance of potentially damaging aggregates. Given that p-bodies are in fact preferentially inherited by daughter cells, rather than retained by mothers, the results of this study raise new questions about how mitochondrial attachments facilitate inheritance, as p-bodies show a contrasting behaviour to other protein aggregates in that they increase, rather than decrease their association with mitochondria during ageing.

Given the breakdown in functional mitochondria inheritance with age and the apparent association of processing bodes with mitochondria, especially with advanced replicative age, it might be expected that the inheritance of p-bodies would break down in aged cells. In fact, this study found that p-bodies continue to be inherited into advanced replicative age of up to 20 generations. In these aged cells p-bodies are also more numerous and its was found that a minimum of one of these bodies was inherited on average. It could be that this lack of deterioration in inheritance is simply due to the higher frequency of p-bodies within the cell allowing for greater probability of inheritance while attached less specifically to mitochondrial membranes. Whether or not the number of p-bodies inherited in cells of advanced replicative age has an effect on the lifespan or fitness of their progeny is yet to be seen and further experimentation will be required to determine this.

7.3 Processing body transport on actin filaments

mRNA transport is known to occur through a Myosin V dependent mechanism along actin filaments. A similar mechanism transports both cortical endoplasmic reticulum and mitochondria in budding yeast (Fundakowski et al., 2012). In plants the link between the actin cytoskeleton and p-bodies has been shown to be the decapping protein Dcp1 (A. Steffens et al., 2014), but limited data are available for yeast. This study uncovered new evidence of p-body transport along the yeast actin cytoskeleton.

In yeast actin forms both filaments and cortical actin patches of bunched actin filaments involved in endocytosis. In this study p-bodies were observed to colocalise with and in

proximity to cortical actin patches in the bud and around the bud neck of dividing yeast cells. This observation alone does not necessarily indicate that p-bodies are trafficked as actin patches are not known to play a role in intracellular trafficking. P-bodies were also observed colocalising with actin filaments qualitatively, although the limitations of current fluorescent proteins meant that dual-colour imaging of yeast actin and p-bodies to confirm connected movement was not possible.

Although dual colour imaging was not possible, fast single colour imaging of p-bodies was found to be possible. This imaging found that p-bodies exhibited a variety of movements. Over very short time spans, p-bodies were found to translocate across limited regions of the cytoplasm with speeds similar to those observed in myosin V (Myo4) mediated actin transport. This movement was directional and suggests that p-bodies are actively transported along actin filaments.

P-bodies are inherited in yeast, in a process dependent on the mRNA "locasome" complex (Garmendia-Torres et al., 2014). This work found that this inheritance is not limited to a single generation, i.e. the p-body is not inherited and disassembled to access the component mRNA and proteins. Instead a single p-body can be inherited through multiple generations when the inducing stress is maintained. Why a yeast cell would pass on this p-body is not clear. Continued regulation of gene expression in the daughter cell is a possibility, as the p-body may rapidly segregate non-essential mRNA and prioritise expression of genes vital for growth under the inducing stress conditions. Similarly, the body may act as a store of potentially valuable mRNA to be released upon release of stress. Alternatively, inheritance of p-bodies may confer an advantage through making essential decay factors available to daughter cells, reducing the burden on translation of these proteins. Given the evolution of this inheritance mechanism, whatever the reason for inheritance is, its benefit must outweigh the risk of inheriting an mRNP composed of multiple proteins with disordered regions with the potential to form larger aggregates.

This study also found a potential link between the actin cytoskeleton and p-bodies in the form of the decapping protein Dcp1. Deletion of Dcp1 mimics the effects of deletions of the mRNA "locasome" complex in terms of p-body inheritance causing asymmetrical

inheritance to be almost completely lost. As Dcp1 was previously shown to bind myosin motor proteins in plants, and *in vitro* to yeast myosins (A. Steffens et al., 2014), this new data suggests that Dcp1 could also be the link between p-bodies and movement along the actin cytoskeleton in *Saccharomyces cerevisiae*. Taken together this new data suggest that p-body can move along actin filaments in a process mediated by myosin motors.

8 Conclusions and future work

The study of ageing in budding yeast has had a recent boost by the introduction of microfluidic dissection devices. In this study, available devices were evaluated for their potential use in the research of p-bodies that require strict control of environmental conditions for their induction and persistence. The Clic2 device was found to sufficiently reproduce the p-body numbers found in existing methodologies and was therefore used for further experimentation. The CliC2 device still had several limitations: retention of cells was limited, and cells were mostly lost before the onset of replicative age induced senescence. Optimisation and further testing of existing and new devices to improve cell retention while maintaining inducing conditions will allow the study of p-bodies further into the replicative lifespan of yeast cells.

The results of this study identify several new potential avenues of research into the role of p-bodies although the question of what the functions=(s) of p-bodies are remains. The localisation of p-bodies at different stages of the cell cycle, summarised in Figure 51, identified a potential role of the mitochondria and endoplasmic reticulum in the trafficking of p-bodies in yeast during mitosis. This link can be explored through further live cell imaging experiments at increased time resolution, to image the inheritance of p-bodies and organelles simultaneously. During the course of this work attempts were made to capture this process by performing automated time-lapse imaging at varying time-resolution, to capture fast time-resolution images of inheritance without causing photodamage. These were ultimately unsuccessful, and optimisation of the imaging protocols may enable this process to be captured in the future.

The component(s) of p-bodies that link them to the mitochondrial or endoplasmic reticulum membranes remain unknown. This study supports Dcp1 as a potential link between p-bodies and actin filaments, but whether Dcp1 acts directly by binding Myosin motors, as it has shown to be capable of, or binds other components linked to organelle membranes is unclear. Further biochemical characterisation of the interactions of Dcp1 will be required to fully elucidate its role in p-body trafficking. Mutation analysis of Dcp1 to determine the

regions required for p-body transport will further develop the understanding of this process.

The overall role of p-bodies in budding yeast remains unclear, while this study lends new evidence to a potential role in mRNA trafficking, functions in mRNA storage and decay remain possible. What is clear is that p-bodies are a significant part of the machinery for post-transcriptional control of gene expression.

9 References

Aizer, A., Brody, Y., Ler, L. W., Sonenberg, N., Singer, R. H., & Shav-Tal, Y. (2008). The Dynamics of Mammalian P Body Transport, Assembly, and Disassembly In Vivo. *Molecular Biology of the Cell*, ***19***(10), 4154–4166.

Aizer, A., Kalo, A., & Kafri, P. (2014). Quantifying mRNA targeting to P bodies in living human cells reveals a dual role in mRNA decay and storage. *Journal of Cell Science*, (August).

Aizer, A., & Shav-Tal, Y. (2008). Intracellular trafficking and dynamics of P bodies. *Prion*, ***2***(4), 131–134.

Anderson, J. S. J., & Parker, R. (1998). The 3′ to 5′ degradation of yeast mRNAs is a general mechanism for mRNA turnover that requires the SK12 DEVH box protein and 3′ to 5′ exonucleases of the exosome complex. *EMBO Journal*, ***17***(5), 1497–1506.

Anderson, P., & Kedersha, N. (2006). RNA granules. *The Journal of Cell Biology*, ***172***(6), 803–808.

Anderson, P., & Kedersha, N. (2008). Stress granules: the Tao of RNA triage. *Trends in Biochemical Sciences*, ***33***(3), 141–150.

Anderson, P., Kedersha, N., & Ivanov, P. (2015). Stress granules, P-bodies and cancer. *Biochimica et Biophysica Acta (BBA) - Gene Regulatory Mechanisms*, ***1849***(7), 861–870.

Ares, M., & Proudfoot, N. J. (2005). The spanish connection: transcription and mRNA processing get even closer. *Cell*, ***120***(2), 163–166.

Baldi, S., Bolognesi, A., Meinema, A. C., & Barral, Y. (2017). Heat stress promotes longevity in budding yeast by relaxing the confinement of age-promoting factors in the mother cell. *ELife*, ***6***, 0–26.

Bashkirov, V. I., Scherthan, H., Solinger, J. A., Buerstedde, J. M., & Heyer, W. D. (1997). A mouse cytoplasmic exoribonuclease (mXRN1p) with preference for G4 tetraplex substrates. *Journal of Cell Biology*, ***136***(4), 761–773.

Beelman, C. A., Stevens, A., Caponigro, G., LaGrandeur, T. E., Hatfield, L., Fortner, D. M., & Parker, R. (1996). An essential component of the decapping enzyme required for normal rates of mRNA turnover. *Nature*, ***382***(6592), 642–646.

Bentley, D. (1999). Coupling RNA polymerase II transcription with pre-mRNA processing. *Current Opinion in Cell Biology*, ***11***(3), 347–351.

Bertrand, E., Chartrand, P., Schaefer, M., Shenoy, S. M., Singer, R. H., & Long, R. M. (1998). Localization of ASH1 mRNA particles in living yeast. *Molecular Cell*, ***2***(4), 437–445.

Bjedov, I., Toivonen, J. M., Kerr, F., Slack, C., Jacobson, J., Foley, A., & Partridge, L. (2010). Mechanisms of Life Span Extension by Rapamycin in the Fruit Fly Drosophila melanogaster. *Cell Metabolism*, ***11***(1), 35–46.

Bobola, N., Jansen, R. P., Shin, T. H., & Nasmyth, K. (1996). Asymmetric accumulation of Ash1p in postanaphase nuclei depends on a myosin and restricts yeast mating-type switching to mother cells. *Cell*, ***84***(5), 699–709.

Boeck, R., Tarun, S., Rieger, M., Deardorff, J. A., Müller-Auer, S., & Sachs, A. B. (1996). The yeast Pan2 protein is required for poly(A)-binding protein-stimulated poly(A)-nuclease activity. *Journal of Biological Chemistry*, ***271***(1), 432–438.

Bohl, F. (2000). She2p, a novel RNA-binding protein tethers ASH1 mRNA to the Myo4p myosin motor via She3p. *The EMBO Journal*, ***19***(20), 5514–5524.

Borja, M. S., Piotukh, K., Freund, C., & Gross, J. D. (2011). Dcp1 links coactivators of mRNA decapping to Dcp2 by proline recognition. *RNA*, ***17***(2), 278–290.

Brachmann, C. B., Sherman, J. M., Devine, S. E., Cameron, E. E., Pillus, L., & Boeke, J. D. (1995). The SIR2 gene family, conserved from bacteria to humans, functions in silencing, cell cycle progression, and chromosome stability. *Genes and Development*, ***9***(23), 2888–2902.

Breitenbach, M., Jazwinski, S., & Laun, P. (2011). *Aging Research in Yeast*.

Brengues, M., & Parker, R. (2007). Accumulation of Polyadenylated mRNA, Pab1p, eIF4E and eIF4G with P-Bodies in Saccharmyces cerevisiae. *Molecular Biology of the Cell*, ***18***(July), 2592–2602.

Brengues, M., Teixeira, D., & Parker, R. (2005). Movement of eukaryotic mRNAs between polysomes and cytoplasmic processing bodies. *Science (New York, N.Y.)*, ***310***(5747), 486–489.

Brown, C. E., & Sachs, A. B. (1998). Poly(A) tail length control in Saccharomyces cerevisiae occurs by message-specific deadenylation. *Molecular and Cellular Biology*, ***18***(11), 6548–6559.

Buchan, J. (2014). mRNP granules: Assembly , function , and connections with disease. *RNA Biology*, (August), 1–12.

Buchan, J. R., Muhlrad, D., & Parker, R. (2008). P bodies promote stress granule assembly in Saccharomyces cerevisiae. *Journal of Cell Biology*.

Buchan, J. R., Yoon, J.-H., & Parker, R. (2011). Stress-specific composition, assembly and kinetics of stress granules in Saccharomyces cerevisiae. *Journal of Cell Science*, ***124***(Pt 2), 228–239.

Cao, D., & Parker, R. (2001). Computational modeling of eukaryotic mRNA turnover. *RNA*, ***7***(9), 1192–1212.

Caponigro, G., Muhlrad, D., & Parker, R. (1993). A small segment of the MAT alpha 1 transcript promotes mRNA decay in Saccharomyces cerevisiae: a stimulatory role for rare codons. *Molecular and Cellular Biology*, ***13***(9), 5141–5148.

Caponigro, G., & Parker, R. (1995). Multiple functions for the poly(A)binding protein in mRNA decapping and deadenylation in yeast. *Genes and Development*, ***9***(19), 2421–2432.

Chang, W., Zaarour, R. F., Reck-Peterson, S., Rinn, J., Singer, R. H., Snyder, M., … Mooseker, M. S. (2008). Myo2p, a class V myosin in budding yeast, associates with a large ribonucleic acid-protein complex that contains mRNAs and subunits of the RNA-processing body. *Rna*, ***14***(3), 491–502.

Chapman, R. E., & Munro, S. (1994). The functioning of the yeast Golgi apparatus requires an ER protein encoded by ANP1, a member of a new family of genes affecting the secretory pathway. *The EMBO Journal*, ***13***(20), 4896–4907.

Chiang, P. Y., Shen, Y. F., Su, Y. L., Kao, C. H., Lin, N. Y., Hsu, P. H., … Chang, C. J. (2013). Phosphorylation of mRNA Decapping Protein Dcp1a by the ERK Signaling Pathway during Early Differentiation of 3T3-L1 Preadipocytes. *PLoS ONE*, ***8***(4), e61697.

Chowdhury, A., Mukhopadhyay, J., & Tharun, S. (2007). The decapping activator Lsm1p-7p-Pat1p complex has the intrinsic ability to distinguish between oligoadenylated and polyadenylated RNAs. *RNA*, ***13***(7), 998–1016.

Cosson, B., Couturier, A., Chabelskaya, S., Kiktev, D., Inge-Vechtomov, S., Philippe, M., & Zhouravleva, G. (2002). Poly(A)-binding protein acts in translation termination via eukaryotic release factor 3 interaction and does not influence [PSI(+)] propagation. *Molecular and Cellular Biology*, ***22***(10), 3301–3315.

Cougot, N., Babajko, S., & Séraphin, B. (2004). Cytoplasmic foci are sites of mRNA decay in human cells. *The Journal of Cell Biology*, ***165***(1), 31–40.

Cougot, N., Cavalier, A., Thomas, D., & Gillet, R. (2012). The dual organization of P-bodies revealed by immunoelectron microscopy and electron tomography. *Journal of Molecular Biology*, ***420***(1–2), 17–28.

Cowart, L. A., Gandy, J. L., Tholanikunnel, B., & Hannun, Y. A. (2010). Sphingolipids mediate formation of mRNA processing bodies during the heat-stress response of Saccharomyces cerevisiae. *Biochemical Journal*, ***431***(1), 31–38.

Crane, M. M., Clark, I. B. N., Bakker, E., Smith, S., & Swain, P. S. (2014). A Microfluidic System for Studying Ageing and Dynamic Single-Cell Responses in Budding Yeast. *PLoS ONE*, ***9***(6), e100042.

Cuervo, A. M. (2008, December). Autophagy and aging: keeping that old broom working. *Trends in Genetics*.

NIH Public Access.

Dang, W., Steffen, K. K., Perry, R., Dorsey, J. A., Johnson, F. B., Shilatifard, A., … Berger, S. L. (2009). Histone H4 lysine 16 acetylation regulates cellular lifespan. *Nature*, ***459***(7248), 802–807.

Decker, C. J., & Parker, R. (2012). P-bodies and stress granules: Possible roles in the control of translation and mRNA degradation. *Cold Spring Harbor Perspectives in Biology*, ***4***(9), 1–16.

Decker, C. J., Teixeira, D., & Parker, R. (2007). Edc3p and a glutamine/asparagine-rich domain of Lsm4p function in processing body assembly in Saccharomyces cerevisiae. *The Journal of Cell Biology*, ***179***(3), 437–449.

Defossez, P. A., Prusty, R., Kaeberlein, M., Lin, S. J., Ferrigno, P., Silver, P. A., … Guarente, L. (1999). Elimination of replication block protein Fob1 extends the life span of yeast mother cells. *Molecular Cell*, ***3***(4), 447–455.

Denoth-Lippuner, A., Krzyzanowski, M. K., Stober, C., & Barral, Y. (2014). Role of SAGA in the asymmetric segregation of DNA circles during yeast ageing. *ELife*, ***2014***(3), 1–33.

Deshmukh, M. V., Jones, B. N., Quang-Dang, D. U., Flinders, J., Floor, S. N., Kim, C., … Gross, J. D. (2008). mRNA Decapping Is Promoted by an RNA-Binding Channel in Dcp2. *Molecular Cell*, ***29***(3), 324–336.

Dever, T. E., Kinzy, T. G., & Pavitt, G. D. (2016). Mechanism and regulation of protein synthesis in Saccharomyces cerevisiae. *Genetics*, ***203***(1), 65–107.

Di Gregorio, S. E., & Duennwald, M. L. (2018). Yeast as a model to study protein misfolding in aged cells. *FEMS Yeast Research*, (August), in press.

Dicarlo, J. E., Norville, J. E., Rios, X., Aach, J., & Church, G. M. (2013). Genome engineering in Saccharomyces cerevisiae using CRISPR-Cas systems. *Nucleic Acids Research*, ***41***(7), 4336–4343.

Dillin, A., Gottschling, D. E., & Nyström, T. (2014). The good and the bad of being connected: the integrons of aging. *Current Opinion in Cell Biology*, ***26***, 107–112.

Doma, M. K., & Parker, R. (2006). Endonucleolytic cleavage of eukaryotic mRNAs with stalls in translation elongation. *Nature*, ***440***(7083), 561–564.

Doma, M. K., & Parker, R. (2007). RNA quality control in eukaryotes. *Cell*, ***131***(4), 660–668.

Dunckley, T., & Parker, R. (1999). The DCP2 protein is required for mRNA decapping in Saccharomyces cerevisiae and contains a functional MutT motif. *EMBO Journal*, ***18***(19), 5411–5422.

Dunckley, T., Tucker, M., & Parker, R. (2001). Two related proteins, Edc1p and Edc2p, stimulate mRNA decapping in Saccharomyces cerevisiae. *Genetics*, ***157***(1), 27–37.

Dunn, K. W., Kamocka, M. M., & McDonald, J. H. (2011). A practical guide to evaluating colocalization in biological microscopy. *American Journal of Physiology. Cell Physiology*, ***300***(4), C723-42.

Edelmann, F. T., Schlundt, A., Heym, R. G., Jenner, A., Niedner-Boblenz, A., Syed, M. I., … Niessing, D. (2017). Molecular architecture and dynamics of ASH1 mRNA recognition by its mRNA-transport complex. *Nature Structural and Molecular Biology*, ***24***(2), 152–161.

Ernoult-Lange, M., Baconnais, S., Harper, M., Minshall, N., Souquere, S., Boudier, T., … Weil, D. (2012). Multiple binding of repressed mRNAs by the P-body protein Rck/p54. *RNA (New York, N.Y.)*, ***18***(9), 1702–1715.

Eyler, D. E., Wehner, K. A., & Green, R. (2013). Eukaryotic release factor 3 is required for multiple turnovers of peptide release catalysis by eukaryotic release factor 1. *Journal of Biological Chemistry*, ***288***(41), 29530–29538.

Fehrmann, S., Paoletti, C., Goulev, Y., Ungureanu, A., Aguilaniu, H., & Charvin, G. (2013). Aging yeast cells undergo a sharp entry into senescence unrelated to the loss of mitochondrial membrane potential. *Cell Reports*, ***5***(6), 1589–1599.

Finkel, T., Deng, C. X., & Mostoslavsky, R. (2009, July 30). Recent progress in the biology and physiology of sirtuins. *Nature*.

Floor, S. N., Jones, B. N., Hernandez, G. A., & Gross, J. D. (2010). A split active site couples cap recognition by Dcp2 to activation. *Nature Structural and Molecular Biology*, ***17***(9), 1096–1101.

Fong, N. (2001). Capping, splicing, and 3′ processing are independently stimulated by RNA polymerase II: different functions for different segments of the CTD. *Genes & Development*, ***15***(14), 1783–1795.

Franks, T. M., & Lykke-Andersen, J. (2008). The Control of mRNA Decapping and P-Body Formation. *Molecular Cell*, ***32***(5), 605–615.

Frydryskova, K., Masek, T., Borcin, K., Mrvova, S., Venturi, V., & Pospisek, M. (2016). Distinct recruitment of human eIF4E isoforms to processing bodies and stress granules. *BMC Molecular Biology*, ***17***(1), 21.

Fundakowski, J., Hermesh, O., & Jansen, R. P. (2012). Localization of a subset of yeast mRNAs depends on inheritance of endoplasmic reticulum. *Traffic*, ***13***(12), 1642–1652.

Gallo, C. M., Munro, E., Rasoloson, D., Merritt, C., & Seydoux, G. (2008). Processing bodies and germ granules are distinct RNA granules that interact in C. elegans embryos. *Developmental Biology*, ***323***(1), 76–87.

Ganley, A. R. D., & Kobayashi, T. (2014). Ribosomal DNA and cellular senescence: New evidence supporting the connection between rDNA and aging. *FEMS Yeast Research*, ***14***(1), 49–59.

Garmendia-Torres, C., Skupin, A., Michael, S. a, Ruusuvuori, P., Kuwada, N. J., Falconnet, D., … Dudley, A. M. (2014). Unidirectional P-body transport during the yeast cell cycle. *PloS One*, ***9***(6), e99428.

Gehlen, L. R., Nagai, S., Shimada, K., Meister, P., Taddei, A., & Gasser, S. M. (2011). Nuclear geometry and rapid mitosis ensure asymmetric episome segregation in yeast. *Current Biology*, ***21***(1), 25–33.

Genz, C., Fundakowski, J., Hermesh, O., Schmid, M., & Jansen, R. P. (2013). Association of the yeast RNA-binding protein She2p with the tubular endoplasmic reticulum depends on membrane curvature. *Journal of Biological Chemistry*, ***288***(45), 32384–32393.

Giaever, G., Chu, A. M., Ni, L., Connelly, C., Riles, L., Véronneau, S., … Johnston, M. (2002). Functional profiling of the Saccharomyces cerevisiae genome. *Nature*, ***418***(6896), 387–391.

Gietz, R. D., & Woods, R. A. (2002). Transformation of yeast by lithium acetate/single-stranded carrier DNA/polyethylene glycol method. *Methods in Enzymology*, ***350***, 87–96.

Gill, T., Aulds, J., & Schmitt, M. E. (2006). A specialized processing body that is temporally and asymmetrically regulated during the cell cycle in Saccharomyces cerevisiae. *Journal of Cell Biology*, ***173***(1), 35–45.

Goldstrohm, A. C., Hook, B. A., Seay, D. J., & Wickens, M. (2006). PUF proteins bind Pop2p to regulate messenger RNAs. *Nature Structural and Molecular Biology*, ***13***(6), 533–539.

Goldstrohm, A. C., Seay, D. J., Hook, B. A., & Wickens, M. (2007). PUF protein-mediated deadenylation is catalyzed by Ccr4p. *Journal of Biological Chemistry*, ***282***(1), 109–114.

Gomez-Navarro, N., & Miller, E. A. (2016). COP-coated vesicles. *Current Biology*, ***26***(2), R54–R57.

Görnemann, J., Barrandon, C., Hujer, K., Rutz, B., Rigaut, G., Kotovic, K. M., … Séraphin, B. (2011). Cotranscriptional spliceosome assembly and splicing are independent of the Prp40p WW domain. *RNA*, ***17***(12), 2119–2129.

Ha, C. W., & Huh, W. K. (2011). Rapamycin increases rDNA stability by enhancing association of Sir2 with rDNA in Saccharomyces cerevisiae. *Nucleic Acids Research*, ***39***(4), 1336–1350.

Haimovich, G., Medina, D., & Causse, S. (2013). Gene expression is circular: factors for mRNA degradation also foster mRNA synthesis. *Cell*.

Hamada, T., Tominaga, M., Fukaya, T., Nakamura, M., Nakano, A., Watanabe, Y., … Baskin, T. I. (2012). RNA

processing bodies, peroxisomes, Golgi bodies, mitochondria, and endoplasmic reticulum tubule junctions frequently pause at cortical microtubules. *Plant & Cell Physiology*, ***53***(4), 699–708.

Harigaya, Y., Jones, B. N., Muhlrad, D., Gross, J. D., & Parker, R. (2010). Identification and Analysis of the Interaction between Edc3 and Dcp2 in Saccharomyces cerevisiae. *Molecular and Cellular Biology*, ***30***(6), 1446–1456.

Harman, D. (2006). Free radical theory of aging: An update - Increasing the functional life span. In *Annals of the New York Academy of Sciences* (Vol. 1067, pp. 10–21).

Harrison, D. E., Strong, R., Sharp, Z. D., Nelson, J. F., Astle, C. M., Flurkey, K., … Miller, R. A. (2009). Rapamycin fed late in life extends lifespan in genetically heterogeneous mice. *Nature*, ***460***(7253), 392–395.

He, C., Zhou, C., & Kennedy, B. K. (2018). The yeast replicative aging model. *Biochimica et Biophysica Acta - Molecular Basis of Disease*, ***1864***(9), 2690–2696.

He, W., & Parker, R. (2001). The yeast cytoplasmic lsm1/pat1p complex protects mRNA 3′ termini from partial degradation. *Genetics*, ***158***(4), 1445–1455.

He, X., & Moore, C. (2005). Regulation of yeast mRNA 3′ end processing by phosphorylation. *Molecular Cell*, ***19***(5), 619–629.

Hempenstall, S., Page, M. M., Wallen, K. R., & Selman, C. (2012). Dietary restriction increases skeletal muscle mitochondrial respiration but not mitochondrial content in C57BL/6 mice. *Mechanisms of Ageing and Development*, ***133***(1), 37–45.

Hilgers, V., Teixeira, D., & Parker, R. (2006). Translation-independent inhibition of mRNA deadenylation during stress in Saccharomyces cerevisiae. *RNA*, ***12***(10), 1835–1845.

Horvathova, I., Voigt, F., Kotrys, A. V., Zhan, Y., Artus-Revel, C. G., Eglinger, J., … Chao, J. A. (2017). The Dynamics of mRNA Turnover Revealed by Single-Molecule Imaging in Single Cells. *Molecular Cell*, ***68***(3), 615–625.e9.

Hsu, C. L., & Stevens, A. (1993). Yeast cells lacking 5′-->3′ exoribonuclease 1 contain mRNA species that are poly(A) deficient and partially lack the 5′ cap structure. *Molecular and Cellular Biology*, ***13***(8), 4826–4835.

Huang, L., Mollet, S., Souquere, S., Le Roy, F., Ernoult-Lange, M., Pierron, G., … Weil, D. (2011). Mitochondria associate with P-bodies and modulate microRNA-mediated RNA interference. *Journal of Biological Chemistry*, ***286***(27), 24219–24220.

Hubstenberger, A., Courel, M., Bénard, M., Souquere, S., Ernoult-Lange, M., Chouaib, R., … Weil, D. (2017). P-Body Purification Reveals the Condensation of Repressed mRNA Regulons. *Molecular Cell*, ***68***(1), 144–157.e5.

Huch, S., Gommlich, J., Muppavarapu, M., Beckham, C., & Nissan, T. (2016). Membrane-association of mRNA decapping factors is independent of stress in budding yeast. *Nature Publishing Group*, (October 2015), 1–16.

Jackson, R. J., Hellen, C. U. T., & Pestova, T. V. (2010). The mechanism of eukaryotic translation initiation and principles of its regulation. *Nature Reviews. Molecular Cell Biology*, ***11***(2), 113–127.

Jamar, N. H., Kritsiligkou, P., & Grant, C. M. (2018). Loss of mRNA surveillance pathways results in widespread protein aggregation. *Scientific Reports*, ***8***(1), 1–10.

Jo, M. C., Liu, W., Gu, L., Dang, W., & Qin, L. (2015). High-throughput analysis of yeast replicative aging using a microfluidic system. *Proceedings of the National Academy of Sciences*, ***112***(30), 9364–9369.

Jo, M. C., & Qin, L. (2016). Microfluidic Platforms for Yeast-Based Aging Studies. *Small*.

Johnson, S. C., Rabinovitch, P. S., & Kaeberlein, M. (2013, January 16). MTOR is a key modulator of ageing and age-related disease. *Nature*.

Jorgensen, P., Nishikawa, J. L., Breitkreutz, B. J., & Tyers, M. (2002). Systematic identification of pathways that couple cell growth and division in yeast. *Science*, ***297***(5580), 395–400.

Kaeberlein, M. (2013). Longevity and aging. *F1000Prime Reports*, ***5***(March), 1–8.

Kaeberlein, M., McVey, M., & Guarente, L. (1999). The SIR2/3/4 complex and SIR2 alone promote longevity in Saccharomyces cerevisiae by two different mechanisms. *Genes and Development*, ***13***(19), 2570–2580.

Kaeberlein, M., Powers, R. W., Steffen, K. K., Westman, E. A., Hu, D., Dang, N., … Kennedy, B. K. (2005). Regulation of yeast replicative life span by TOR and Sch9 in response to nutrients. *Science (New York, N.Y.)*, ***310***(5751), 1193–1196.

Kaganovich, D., Kopito, R., & Frydman, J. (2008). Misfolded proteins partition between two distinct quality control compartments. *Nature*, ***454***(7208), 1088–1095.

Kapahi, P., Zid, B. M., Harper, T., Koslover, D., Sapin, V., & Benzer, S. (2004). Regulation of lifespan in Drosophila by modulation of genes in the TOR signaling pathway. *Current Biology*, ***14***(10), 885–890.

Kedersha, N., Stoecklin, G., Ayodele, M., Yacono, P., Lykke-Andersen, J., Fritzler, M. J., … Anderson, P. (2005). Stress granules and processing bodies are dynamically linked sites of mRNP remodeling. *The Journal of Cell Biology*, ***169***(6), 871–884.

Kenna, M., Stevens, A., McCammon, M., & Douglas, M. G. (1993). An essential yeast gene with homology to the exonuclease-encoding XRN1/KEM1 gene also encodes a protein with exoribonuclease activity. *Molecular and Cellular Biology*, ***13***(1), 341–350.

Kennedy, B. K., Gotta, M., Sinclair, D. A., Mills, K., McNabb, D. S., Murthy, M., … Guarente, L. (1997). Redistribution of silencing proteins from telomeres to the nucleolus is associated with extension of life span in S. cerevisiae. *Cell*, ***89***(3), 381–391.

Kennedy, B. K., Steffen, K. K., & Kaeberlein, M. (2007, June). Ruminations on dietary restriction and aging. *Cellular and Molecular Life Sciences*.

Kiebler, M. A., & Bassell, G. J. (2006, September 21). Neuronal RNA Granules: Movers and Makers. *Neuron*.

Kobayashi, T., Funakoshi, Y., Hoshino, S. I., & Katada, T. (2004). The GTP-binding release factor eRF3 as a key mediator coupling translation termination to mRNA decay. *Journal of Biological Chemistry*, ***279***(44), 45693–45700.

Kroschwald, S., Maharana, S., Mateju, D., Malinovska, L., Elisabeth, N., Poser, I., … Alberti, S. (2015). Promiscuous interactions and protein disaggregases determine the material state of stress-inducible RNP granules. *ELife*, 1–32.

Kshirsagar, M., & Parker, R. (2004). Identification of Edc3p as an enhancer of mRNA decapping in Saccharomyces cerevisiae. *Genetics*, ***166***(2), 729–739.

Kyryakov, P., Gomez-Perez, A., Glebov, A., Asbah, N., Bruno, L., Meunier, C., … Titorenko, V. I. (2016). Empirical verification of evolutionary theories of aging. *Aging*, ***8***(10), 2568–2589.

LaGrandeur, T., & Parker, R. (1999). The cis acting sequences responsible for the differential decay of the unstable MFA2 and stable PGK1 transcipts in yeast include the context of the translational start codon. *RNA*, ***5***(3), 420–433.

Lamming, D. W., Ye, L., Katajisto, P., Goncalves, M. D., Saitoh, M., Stevens, D. M., … Baur, J. A. (2012). Rapamycin-induced insulin resistance is mediated by mTORC2 loss and uncoupled from longevity. *Science*, ***335***(6076), 1638–1643.

Lavut, A., & Raveh, D. (2012). Sequestration of highly expressed mRNAs in cytoplasmic granules, P-bodies, and stress granules enhances cell viability. *PLoS Genetics*, ***8***(2), e1002527.

Lee, S., Avalos, I., Huberts, D. H. E. W., Lee, L. P., & Heinemann, M. (2012). Whole lifespan microscopic

observation of budding yeast aging through a micro fl uidic dissection platform. *Pnas*, 4–8.

Lee, S., Lim, W. A., & Thorn, K. S. (2013). Improved Blue, Green, and Red Fluorescent Protein Tagging Vectors for S. cerevisiae. *PLoS ONE*, ***8***(7), e67902.

Lee, T. I., & Young, R. A. (2000). Transcription of Eukaryotic Protein-Coding Genes. *Annual Review of Genetics*, ***34***(1), 77–137.

Lin, S. J., Defossez, P. A., & Guarente, L. (2000). Requirement of NAD and SIR2 for life-span extension by calorie restriction in saccharomyces cerevisiae. *Science*, ***289***(5487), 2126–2128.

Lindsay, A. J., & McCaffrey, M. W. (2011). Myosin Va is required for P body but not stress granule formation. *Journal of Biological Chemistry*, ***286***(13), 11519–11528.

Lindstrom, D. L., Leverich, C. K., Henderson, K. A., & Gottschling, D. E. (2011). Replicative Age Induces Mitotic Recombination in the Ribosomal RNA Gene Cluster of Saccharomyces cerevisiae. *PLoS Genetics*, ***7***(3), e1002015.

Linz, B., Koloteva, N., Vasilescu, S., & McCarthy, J. E. G. (1997). Disruption of ribosomal scanning on the 5′-untranslated region, and not restriction of translational initiation per se, modulates the stability of nonaberrant mRNAs in the yeast Saccharomyces cerevisiae. *Journal of Biological Chemistry*, ***272***(14), 9131–9140.

Liu, B., Larsson, L., Caballero, A., Hao, X., Öling, D., Grantham, J., & Nyström, T. (2010). The Polarisome Is Required for Segregation and Retrograde Transport of Protein Aggregates. *Cell*, ***140***(2), 257–267.

Liu, B., Larsson, L., Franssens, V., Hao, X., Hill, S. M., Andersson, V., … Nyström, T. (2011, November 23). Segregation of protein aggregates involves actin and the polarity machinery. *Cell*.

Loschi, M., Leishman, C. C., Berardone, N., & Boccaccio, G. L. (2009). Dynein and kinesin regulate stress-granule and P-body dynamics. *Journal of Cell Science*, ***122***(Pt 21), 3973–3982.

Luo, G., Costanzo, M., Boone, C., & Dickson, R. C. (2011). Nutrients and the Pkh1/2 and Pkc1 protein kinases Control mRNA decay and P-body assembly in yeast. *Journal of Biological Chemistry*, ***286***(11), 8759–8770.

Luo, Y., Na, Z., & Slavoff, S. A. (2018). P-Bodies: Composition, Properties, and Functions. *Biochemistry*, ***57***(17), 2424–2431.

McCarthy, J. E. G. (1998). Posttranscriptional control of gene expression in yeast. *Microbiol Mol Biol Rev*, ***62***(4), 1492–1553.

McCormick, M. A., Delaney, J. R., Tsuchiya, M., Tsuchiyama, S., Shemorry, A., Sim, S., … Kennedy, B. K. (2015). A Comprehensive Analysis of Replicative Lifespan in 4,698 Single-Gene Deletion Strains Uncovers Conserved Mechanisms of Aging. *Cell Metabolism*, ***22***(5), 895–906.

Medvedik, O., Lamming, D. W., Kim, K. D., & Sinclair, D. A. (2007). MSN2 and MSN4 link calorie restriction and TOR to sirtuin-mediated lifespan extension in Saccharomyces cerevisiae. *PLoS Biology*, ***5***(10), 2330–2341.

Miller, J. E., Zhang, L., Jiang, H., Li, Y., Pugh, B. F., & Reese, J. C. (2017). Genome-Wide Mapping of Decay Factor-mRNA Interactions in Yeast Identifies Nutrient Responsive Transcripts as Targets of the Deadenylase Ccr4. *G3: Genes|Genomes|Genetics*, ***8***(1), g3.300415.2017.

Miller, S. B., Ho, C.-T., Winkler, J., Khokhrina, M., Neuner, A., Mohamed, M. Y., … Bukau, B. (2015). Compartment-specific aggregases direct distinct nuclear and cytoplasmic aggregate deposition. *The EMBO Journal*, ***34***(6), 778–797.

Molliex, A., Temirov, J., Lee, J., Coughlin, M., Kanagaraj, A. P., Kim, H. J., … Taylor, J. P. (2015). Phase Separation by Low Complexity Domains Promotes Stress Granule Assembly and Drives Pathological Fibrillization. *Cell*, ***163***(1), 123–133.

Mugler, C. F., Hondele, M., Heinrich, S., Sachdev, R., Vallotton, P., Koek, A. Y., … Weis, K. (2016). ATPase activity

of the DEAD-box protein Dhh1 controls processing body formation. *ELife*, ***5***(OCTOBER2016).

Muhlrad, D., Decker, C. J., & Parker, R. (1994). Deadenylation of the unstable mRNA encoded by the yeast MFA2 gene leads to decapping followed by 5′ → 3′ digestion of the transcript. *Genes and Development*, ***8***(7), 855–866.

Muhlrad, D., Decker, C. J., & Parker, R. (1995). Turnover mechanisms of the stable yeast PGK1 mRNA. TL - 15. *Molecular and Cellular Biology*, ***15 VN-r***(4), 2145–2156.

Muhlrad, D., & Parker, R. (1992). Mutations affecting stability and deadenylation of the yeast MFA2 transcript. *Genes and Development*, ***6***(11), 2100–2111.

Muhlrad, D., & Parker, R. (1994). Premature translational termination triggers mRNA decapping. *Nature*, ***370***(6490), 578–581.

Müller, M., Heuck, A., & Niessing, D. (2007, January 29). Directional mRNA transport in eukaryotes: Lessons from yeast. *Cellular and Molecular Life Sciences*.

Müller, M., Heym, R. G., Mayer, A., Kramer, K., Schmid, M., Cramer, P., … Niessing, D. (2011). A cytoplasmic complex mediates specific mrna recognition and localization in yeast. *PLoS Biology*, ***9***(4), e1000611.

Niessing, D., Jansen, R. P., Pohlmann, T., & Feldbrügge, M. (2018). mRNA transport in fungal top models. *Wiley Interdisciplinary Reviews: RNA*, ***9***(1), 1–13.

Nissan, T., & Parker, R. (2008). Analyzing P-bodies in Saccharomyces cerevisiae. *Methods in Enzymology*, ***6879***(08), 507–520.

Nissan, T., Rajyaguru, P., She, M., Song, H., & Parker, R. (2010). Decapping activators in Saccharomyces cerevisiae act by multiple mechanisms. *Molecular Cell*, ***39***(5), 773–783.

Nover, L., Scharf, K. D., & Neumann, D. (1989). Cytoplasmic heat shock granules are formed from precursor particles and are associated with a specific set of mRNAs. *Molecular and Cellular Biology*, ***9***(3), 1298–1308.

Nyström, T., & Liu, B. (2014). Protein quality control in time and space - links to cellular aging. *FEMS Yeast Research*, ***14***(1), 40–48.

Olivas, W., & Parker, R. (2000). The Puf3 protein is a transcript-specific regulator of mRNA degradation in yeast. TL - 19. *The EMBO Journal*, ***19 VN-r***(23), 6602–6611.

Omodei, D., & Fontana, L. (2011, June 6). Calorie restriction and prevention of age-associated chronic disease. *FEBS Letters*.

Parker, R. (2012). RNA degradation in Saccharomyces cerevisae. *Genetics*, ***191***(3), 671–702.

Pilkington, G. R., & Parker, R. (2008). Pat1 contains distinct functional domains that promote P-body assembly and activation of decapping. *Molecular and Cellular Biology*, ***28***(4), 1298–1312.

Rajgor, D., Mellad, J. A., Soong, D., Rattner, J. B., Fritzler, M. J., & Shanahan, C. M. (2014). Mammalian microtubule P-body dynamics are mediated by nesprin-1. *Journal of Cell Biology*, ***205***(4), 457–475.

Rajyaguru, P., She, M., & Parker, R. (2012). Scd6 targets eIF4G to repress translation: RGG motif proteins as a class of eIF4G-binding proteins. *Molecular Cell*, ***45***(2), 244–254.

Ramachandran, V., Shah, K. H., & Herman, P. K. (2011). The cAMP-Dependent Protein Kinase Signaling Pathway Is a Key Regulator of P Body Foci Formation. *Molecular Cell*, ***43***(6), 973–981.

Ramirez, C. V., Vilela, C., Berthelot, K., & McCarthy, J. E. G. (2002). Modulation of eukaryotic mRNA stability via the cap-binding translation complex eIF4F. *Journal of Molecular Biology*, ***318***(4), 951–962.

Rao, B. S., & Parker, R. (2017). Numerous interactions act redundantly to assemble a tunable size of P bodies in Saccharomyces cerevisiae. *Proceedings of the National Academy of Sciences*, ***114***(45), E9569–E9578.

Reijns, M. A. M., Alexander, R. D., Spiller, M. P., & Beggs, J. D. (2008). A role for Q/N-rich aggregation-prone regions in P-body localization. *Journal of Cell Science*, ***121***(15), 2463–2472.

Reineke, L. C., & Lloyd, R. E. (2013). Diversion of stress granules and P-bodies during viral infection. *Virology*, ***436***(2), 255–267.

Riesen, M., & Morgan, A. (2009). Calorie restriction reduces rDNA recombination independently of rDNA silencing. *Aging Cell*, ***8***(6), 624–632.

Robida-Stubbs, S., Glover-Cutter, K., Lamming, D. W., Mizunuma, M., Narasimhan, S. D., Neumann-Haefelin, E., … Blackwell, T. K. (2012). TOR signaling and rapamycin influence longevity by regulating SKN-1/Nrf and DAF-16/FoxO. *Cell Metabolism*, ***15***(5), 713–724.

Rodriguez, A. J., Shenoy, S. M., Singer, R. H., & Condeelis, J. (2006). Visualization of mRNA translation in living cells. *The Journal of Cell Biology*, ***175***(1), 67–76.

Rogina, B., & Helfand, S. L. (2004). Sir2 mediates longevity in the fly through a pathway related to calorie restriction. *Proceedings of the National Academy of Sciences*, ***101***(45), 15998–16003.

Rzeczkowski, K., Beuerlein, K., Müller, H., Dittrich-Breiholz, O., Schneider, H., Kettner-Buhrow, D., … Kracht, M. (2011). c-Jun N-terminal kinase phosphorylates DCP1a to control formation of P bodies. *Journal of Cell Biology*, ***194***(4), 581–596.

Sachs, A. B., Davis, R. W., & Kornberg, R. D. (1987). A single domain of yeast poly(A)-binding protein is necessary and sufficient for RNA binding and cell viability. *Molecular and Cellular Biology*, ***7***(9), 3268–3276.

Sampaio-Marques, B., Felgueiras, C., Silva, A., Rodrigues, M., Tenreiro, S., Franssens, V., … Ludovico, P. (2012). SNCA (α-synuclein)-induced toxicity in yeast cells is dependent on sirtuin 2 (Sir2)-mediated mitophagy. *Autophagy*, ***8***(10), 1494–1509.

Schäfer, I. B., Rode, M., Bonneau, F., Schüssler, S., & Conti, E. (2014). The structure of the Pan2-Pan3 core complex reveals cross-talk between deadenylase and pseudokinase. *Nature Structural and Molecular Biology*, ***21***(7), 591–598.

Schmid, M., Jaedicke, A., Du, T. G., & Jansen, R. P. (2006). Coordination of Endoplasmic Reticulum and mRNA Localization to the Yeast Bud. *Current Biology*, ***16***(15), 1538–1543.

Schutz, S., Noldeke, E. R., & Sprangers, R. (2017). A synergistic network of interactions promotes the formation of in vitro processing bodies and protects mRNA against decapping. *Nucleic Acids Research*, ***45***(11), 6911–6922.

Schwartz, D. C., & Parker, R. (1999). Mutations in translation initiation factors lead to increased rates of deadenylation and decapping of mRNAs in Saccharomyces cerevisiae. *Mol Cell Biol*, ***19***(8), 5247–5256.

Schwartz, D. C., & Parker, R. (2000). mRNA Decapping in Yeast Requires Dissociation of the Cap Binding Protein, Eukaryotic Translation Initiation Factor 4E. *Molecular and Cellular Biology*, ***20***(21), 7933–7942.

Sfakianos, A. P., Mellor, L. E., Pang, Y. F., Kritsiligkou, P., Needs, H., Abou-Hamdan, H., … Whitmarsh, A. J. (2018, March 9). The mTOR-S6 kinase pathway promotes stress granule assembly. *Cell Death and Differentiation*, pp. 1–15.

Shaner, N. C., Lambert, G. G., Chammas, A., Ni, Y., Cranfill, P. J., Baird, M. A., … Wang, J. (2013). A bright monomeric green fluorescent protein derived from Branchiostoma lanceolatum. *Nature Methods*, ***10***(5), 407–409.

Shao, S., & Hegde, R. S. (2011). Membrane Protein Insertion at the Endoplasmic Reticulum. *Annual Review of Cell and Developmental Biology*, ***27***(1), 25–56.

She, M., Decker, C. J., Sundramurthy, K., Liu, Y., Chen, N., Parker, R., & Song, H. (2004). Crystal structure of Dcp1p and its functional implications in mRNA decapping. *Nature Structural and Molecular Biology*, ***11***(3), 249–256.

She, M., Decker, C. J., Svergun, D. I., Round, A., Chen, N., Muhlrad, D., … Song, H. (2008). Structural Basis of Dcp2 Recognition and Activation by Dcp1. *Molecular Cell*, ***29***(3), 337–349.

Sheth, U., & Parker, R. (2003). Decapping and Decay Messenger RNA Occur in Cytoplasmic Processing Bodies. *Science*, ***300***(5620), 805–808.

Sheth, U., & Parker, R. (2003). Decapping and decay of messenger RNA occur in cytoplasmic processing bodies. *Science*, ***300***(5620), 805–808.

Smith, C., Lari, A., Derrer, C. P., Ouwehand, A., Rossouw, A., Huisman, M., … Montpetit, B. (2015a). In vivo single-particle imaging of nuclear mRNA export in budding yeast demonstrates an essential role for Mex67p. *Journal of Cell Biology*, ***211***(6), 1121–1130.

Smith, C., Lari, A., Derrer, C. P., Ouwehand, A., Rossouw, A., Huisman, M., … Montpetit, B. (2015b). In vivo single-particle imaging of nuclear mRNA export in budding yeast demonstrates an essential role for Mex67p. *Journal of Cell Biology*, ***211***(6), 1121–1130.

Smith, E. D., Tsuchiya, M., Fox, L. A., Dang, N., Hu, D., Kerr, E. O., … Kennedy, B. K. (2008). Quantitative evidence for conserved longevity pathways between divergent eukaryotic species. *Genome Research*, ***18***(4), 564–570.

Souquere, S., Mollet, S., Kress, M., Dautry, F., Pierron, G., & Weil, D. (2009). Unravelling the ultrastructure of stress granules and associated P-bodies in human cells. *Journal of Cell Science*, ***122***(20), 3619–3626.

Specht, S., Miller, S. B. M., Mogk, A., & Bukau, B. (2011). Hsp42 is required for sequestration of protein aggregates into deposition sites in Saccharomyces cerevisiae. *Journal of Cell Biology*, ***195***(4), 617–629.

Spokoini, R., Moldavski, O., Nahmias, Y., England, J. L., Schuldiner, M., & Kaganovich, D. (2012). Confinement to Organelle-Associated Inclusion Structures Mediates Asymmetric Inheritance of Aggregated Protein in Budding Yeast. *Cell Reports*, ***2***(4), 738–747.

Stalder, L., & Mühlemann, O. (2009). Processing bodies are not required for mammalian nonsense-mediated mRNA decay. *RNA*, ***15***(7), 1265–1273.

Stanfel, M. N., Shamieh, L. S., Kaeberlein, M., & Kennedy, B. K. (2009, October). The TOR pathway comes of age. *Biochimica et Biophysica Acta - General Subjects*. NIH Public Access.

Steffens, A., Jaegle, B., Tresch, A., Hulskamp, M., & Jakoby, M. (2014). Processing-Body Movement in Arabidopsis Depends on an Interaction between Myosins and DECAPPING PROTEIN1. *Plant Physiology*, ***164***(4), 1879–1892.

Steffens, A., Jaegle, B., Tresch, A., Hülskamp, M., & Jakoby, M. (2014). Processing-body movement in Arabidopsis depends on an interaction between myosins and DECAPPING PROTEIN1. *Plant Physiology*, ***164***(4), 1879–1892.

Steiger, M., Carr-Schmid, A., Schwartz, D. C., Kiledjian, M., & Parker, R. (2003). Analysis of recombinant yeast decapping enzyme. *RNA*, ***9***(2), 231–238.

Stevens, A., & Poole, T. L. (1995). 5′-Exonuclease-2 of Saccharomyces cerevisiae. Purification and features of ribonuclease activity with comparison to 5′-exonuclease-1. *Journal of Biological Chemistry*, ***270***(27), 16063–16069.

Suda, Y., & Nakano, A. (2012). The Yeast Golgi Apparatus. *Traffic*, ***13***(4), 505–510.

Sweet, T. J., Boyer, B., Hu, W., Baker, K. E., & Coller, J. (2007). Microtubule disruption stimulates P-body formation. *RNA*, ***13***(4), 493–502.

Teixeira, D., Sheth, U., Valencia-sanchez, M. A., Brengues, M., & Parker, R. O. Y. (2005). Processing bodies require RNA for assembly and contain nontranslating mRNAs Processing bodies require RNA for assembly and contain nontranslating mRNAs. *Rna*, ***11***, 371–382.

Tessarz, P., Schwarz, M., Mogk, A., & Bukau, B. (2009). The Yeast AAA+ Chaperone Hsp104 Is Part of a Network That Links the Actin Cytoskeleton with the Inheritance of Damaged Proteins. *Molecular and Cellular Biology*, ***29***(13), 3738–3745.

Tharun, S., & Parker, R. (1999). Analysis of mutations in the yeast mRNA decapping enzyme. *Genetics*, ***151***(4), 1273–1285.

Thore, S., Mauxion, F., Séraphin, B., & Suck, D. (2003). X-ray structure and activity of the yeast Pop2 protein: A nuclease subunit of the mRNA deadenylase complex. *EMBO Reports*, ***4***(12), 1150–1155.

Tissenbaum, H. A., & Guarente, L. (2001). Increased dosage of a sir-2 gene extends lifespan in Caenorhabditis elegans. *Nature*, ***410***(6825), 227–230.

Toda, T., Cameron, S., Sass, P., Zoller, M., Scott, J. D., McMullen, B., … Wigler, M. (1987). Cloning and characterization of BCY1, a locus encoding a regulatory subunit of the cyclic AMP-dependent protein kinase in Saccharomyces cerevisiae. *Molecular and Cellular Biology*, ***7***(4), 1371–1377.

Tucker, M., Staples, R. R., Valencia-Sanchez, M. A., Muhlrad, D., & Parker, R. (2002). Ccr4p is the catalytic subunit of a Ccr4p/Pop2p/Notp mRNA deadenylase complex in Saccharomyces cerevisiae. *The EMBO Journal*, ***21***(6), 1427–1436.

Tucker, M., Valencia-Sanchez, M. A., Staples, R. R., Chen, J., Denis, C. L., & Parker, R. (2001). The transcription factor associated Ccr4 and Caf1 proteins are components of the major cytoplasmic mRNA deadenylase in Saccharomyces cerevisiae. *Cell*, ***104***(3), 377–386.

Urban, J., Soulard, A., Huber, A., Lippman, S., Mukhopadhyay, D., Deloche, O., … Loewith, R. (2007). Sch9 Is a Major Target of TORC1 in Saccharomyces cerevisiae. *Molecular Cell*, ***26***(5), 663–674.

Van Dijk, E., Cougot, N., Meyer, S., Babajko, S., Wahle, E., & Séraphin, B. (2002). Human Dcp2: A catalytically active mRNA decapping enzyme located in specific cytoplasmic structures. *EMBO Journal*, ***21***(24), 6915–6924.

Van Dijk, E. L., Chen, C. L., Daubenton-Carafa, Y., Gourvennec, S., Kwapisz, M., Roche, V., … Morillon, A. (2011). XUTs are a class of Xrn1-sensitive antisense regulatory non-coding RNA in yeast. *Nature*, ***475***(7354), 114–119.

Van Hoof, A., Frischmeyer, P. A., Dietz, H. C., & Parker, R. (2002). Exosome-mediated recognition and degradation of mRNAs lacking a termination codon. *Science*, ***295***(5563), 2262–2264.

Vellai, T., Takacs-Vellai, K., Zhang, Y., Kovacs, A. L., Orosz, L., & Müller, F. (2003). Genetics: Influence of TOR kinase on lifespan in C. elegans. *Nature*, ***426***(6967), 620–620.

Vilela, C., Ramirez, C. V., Linz, B., Rodrigues-Pousada, C., & McCarthy, J. E. G. (1999). Post-termination ribosome interactions with the 5′UTR modulate yeast mRNA stability. *EMBO Journal*, ***18***(11), 3139–3152.

Vilela, C., Velasco, C., Ptushkina, M., & McCarthy, J. E. (2000). The eukaryotic mRNA decapping protein Dcp1 interacts physically and functionally with the eIF4F translation initiation complex. *The EMBO Journal*, ***19***(16), 4372–4382.

Vindry, C., Marnef, A., Broomhead, H., Twyffels, L., Ozgur, S., Stoecklin, G., … Standart, N. (2017). Dual RNA Processing Roles of Pat1b via Cytoplasmic Lsm1-7 and Nuclear Lsm2-8 Complexes. *Cell Reports*, ***20***(5), 1187–1200.

Viswanathan, P., Ohn, T., Chiang, Y.-C., Chen, J., & Denis, C. L. (2004). Mouse CAF1 Can Function As a Processive Deadenylase/3′–5′-Exonuclease in Vitro but in Yeast the Deadenylase Function of CAF1 Is Not Required for mRNA Poly(A) Removal. *Journal of Biological Chemistry*, ***279***(23), 23988–23995.

Wang, C., Schmich, F., Srivatsa, S., Weidner, J., Beerenwinkel, N., & Spang, A. (2018). Context-dependent deposition and regulation of mRNAs in P-bodies. *ELife*, ***7***, 1–25.

Wasko, B. M., & Kaeberlein, M. (2014). Yeast replicative aging: A paradigm for defining conserved longevity

interventions. *FEMS Yeast Research*, ***14***(1), 148–159.

Westermann, B. (2014). Mitochondrial inheritance in yeast. *Biochimica et Biophysica Acta - Bioenergetics*, ***1837***(7), 1039–1046.

Wilhelm, J. E., Buszczak, M., & Sayles, S. (2005). Efficient protein trafficking requires trailer hitch, a component of a ribonucleoprotein complex localized to the ER in Drosophila. *Developmental Cell*, ***9***(5), 675–685.

Wilson, J. E., Pestova, T. V, Hellen, C. U. T., & Sarnow, P. (2000). Initiation of protein synthesis from the A site of the ribosome. *Cell*, ***102***(4), 511–520.

Yang, Z. (2004). GW182 is critical for the stability of GW bodies expressed during the cell cycle and cell proliferation. *Journal of Cell Science*, ***117***(23), 5567–5578.

Yoon, J. H., Choi, E. J., & Parker, R. (2010). Dcp2 phosphorylation by Ste20 modulates stress granule assembly and mRNA decay in Saccharomyces cerevisiae. *Journal of Cell Biology*, ***189***(5), 813–827.

Young, M. E., Cooper, J. A., & Bridgman, P. C. (2004). Yeast actin patches are networks of branched actin filaments. *Journal of Cell Biology*, ***166***(5), 629–635.

Zhang, Q., Meng, X., Li, D., Chen, S., Luo, J., Zhu, L., … Gu, W. (2017). Binding of DEAD-box helicase Dhh1 to the 5-untranslated region of ASH1 mRNA represses localized translation of ASH1 in yeast cells. *Journal of Biological Chemistry*, ***292***(23), 9787–9800.

Zhou, C., Slaughter, B. D., Unruh, J. R., Eldakak, A., Rubinstein, B., & Li, R. (2011). Motility and segregation of Hsp104-associated protein aggregates in budding yeast. *Cell*, ***147***(5), 1186–1196.

Zhou, C., Slaughter, B. D., Unruh, J. R., Guo, F., Yu, Z., Mickey, K., … Li, R. (2014). Organelle-based aggregation and retention of damaged proteins in asymmetrically dividing cells. *Cell*, ***159***(3), 530–542.

Zid, B. M., & O'Shea, E. K. (2014). Promoter sequences direct cytoplasmic localization and translation of mRNAs during starvation in yeast. *Nature*, ***514***(7520), 117–121.

Appendix

Table of processing body regulators

Table 1: Regulators of p-body assembly and disassembly in Saccharomyces cerevisiae

NAME	NAME DESCRIPTION	MOLECULAR FUNCTIONS	BIOLOGICAL PROCESSES	REFERENCE
PKH1	Pkb-activating Kinase Homolog	protein serine/threonine kinase activity	cell wall integrity MAPK cascade , endocytosis , late endosome to vacuole transport via multivesicular body sorting pathway , peptidyl-serine phosphorylation , peptidyl-threonine phosphorylation , positive regulation of cytoplasmic mRNA processing body assembly , positive regulation of protein serine/threonine kinase activity , regulation of nuclear-transcribed mRNA poly tail shortening	Luo G, et al. (2011) PMID:21163942
TPK3	Takashi's Protein Kinase	cAMP-dependent protein kinase activity	mitochondrion organization , negative regulation of cytoplasmic mRNA processing body assembly , negative regulation of cytoplasmic translation , protein kinase A signalling , protein phosphorylation , Ras protein signal transduction	Ramachandran V, et al. (2011) PMID:21925385
PAT1	Protein Associated with Topoisomerase II	chromatin binding , mRNA binding , protein binding , RNA binding	cytoplasmic mRNA processing body assembly , deadenylation-dependent decapping of nuclear-transcribed mRNA , formation of translation preinitiation complex , negative regulation of translational initiation , regulation of translational initiation	Buchan JR, et al. (2008) PMID:18981231
BCY1	Bypass of CYclic-AMP requirement	cAMP-dependent protein kinase inhibitor activity	negative regulation of Ras protein signal transduction , positive regulation of adenylate cyclase activity , positive regulation of transcription from RNA polymerase II promoter in response to glucose starvation , positive regulation of transcription from RNA polymerase II promoter in response to nitrogen starvation , protein	Ramachandran V, et al. (2011) PMID:21925385

			localization to bud neck , **regulation of cytoplasmic mRNA processing body assembly**	
TPK2	Takashi's Protein Kinase	cAMP-dependent protein kinase activity , translation initiation factor binding	invasive growth in response to glucose limitation , negative regulation of cytoplasmic mRNA processing body assembly , negative regulation of cytoplasmic translation , protein kinase A signalling , protein phosphorylation , Ras protein signal transduction	Ramachandran V, et al. (2011) PMID:21925385
PKC1	Protein Kinase C	protein kinase C activity	actin filament organization , autophagy of peroxisome , cellular bud neck septin ring organization , intracellular signal transduction , positive regulation of cytoplasmic mRNA processing body assembly , protein phosphorylation , regulation of fungal-type cell wall organization , regulation of nuclear-transcribed mRNA poly tail shortening , signal transduction	Luo G, et al. (2011) PMID:21163942
RAS2	homologous to RAS proto-oncogene	GTP binding , GTPase activity	activation of adenylate cyclase activity , ascospore formation , macroautophagy , positive regulation of adenylate cyclase activity , positive regulation of pseudohyphal growth , positive regulation of transcription by galactose , protein localization by the Cvt pathway , protein localization to bud neck , **regulation of cytoplasmic mRNA processing body assembly** , regulation of protein localization , replicative cell aging	Ramachandran V, et al. (2011) PMID:21925385
CDC39	Cell Division Cycle	ATPase activator activity	negative regulation of cytoplasmic mRNA processing body assembly , nuclear-transcribed mRNA catabolic process, deadenylation-dependent decay , nuclear-transcribed mRNA poly tail shortening , positive regulation of transcription elongation from RNA polymerase II	Mugler CF, et al. (2016) PMID:27692063

			promoter , pseudohyphal growth , regulation of cell cycle , regulation of transcription by RNA polymerase II , response to pheromone triggering conjugation with cellular fusion , transcription elongation from RNA polymerase II promoter	
CAF20	Cap Associated Factor		negative regulation of translation , positive regulation of cytoplasmic mRNA processing body assembly	Ka M, et al. (2008) PMID:18182159
DHH1	DEAD box Helicase Homolog	ATP-dependent RNA helicase activity , chromatin binding , mRNA binding , protein binding , translation regulator activity, nucleic acid binding	cytoplasmic mRNA processing body assembly , deadenylation-dependent decapping of nuclear-transcribed mRNA , negative regulation of translation , negative regulation of translational elongation , regulation of cytoplasmic mRNA processing body assembly , stress granule assembly	Mugler CF, et al. (2016) PMID:27692063
SCD6	Suppressor of Clathrin Deficiency	eukaryotic initiation factor 4G binding , mRNA binding , RNA binding	cytoplasmic mRNA processing body assembly , negative regulation of translational initiation , stress granule assembly	Rajyaguru P, et al. (2012) PMID:22284680
LSM4	Like SM	U6 snRNA binding	cytoplasmic mRNA processing body assembly , mRNA splicing, via spliceosome , nuclear-transcribed mRNA catabolic process	Decker CJ, et al. (2007) PMID:17984320
EDC3	Enhancer of mRNA DeCapping	mRNA binding	cytoplasmic mRNA processing body assembly , deadenylation-independent decapping of nuclear-transcribed mRNA , positive regulation of nuclear-transcribed mRNA catabolic process, deadenylation-dependent decay	Decker CJ, et al. (2007) PMID:17984320
TPK1	Takashi's Protein Kinase	cAMP-dependent protein kinase activity	negative regulation of cytoplasmic mRNA processing body assembly , peptidyl-serine phosphorylation , protein kinase A signalling , protein phosphorylation , Ras protein signal transduction , regulation of	Ramachandran V, et al. (2011) PMID:21925385

			macroautophagy	
PKH2	Pkb-activating Kinase Homolog	protein kinase activity , protein serine/threonine kinase activity	cell wall integrity MAPK cascade , late endosome to vacuole transport via multivesicular body sorting pathway , peptidyl-serine phosphorylation , positive regulation of cytoplasmic mRNA processing body assembly , positive regulation of protein serine/threonine kinase activity , protein phosphorylation , regulation of nuclear-transcribed mRNA poly tail shortening	Luo G, et al. (2011) PMID:21163942

List of Yeast Strains used in this study

Many yeast strains were made for this study, to evaluate specific primers and protein fusions, below are the final strains used for the data presented in this study.

MATING TYPE	DESCRIPTION	STUDY
MATA	*his3-d1 leu2-d0 met15-d0 ura3-d0 Edc3:mRuby3-KanMX*	Chip Evaluation
MATA	*his3-d1 leu2-d0 met15-d0 ura3-d0 Edc3:mRuby3-KanMX Sac6:mNeonGreen-HygMX*	Colocalisation
MATA	*his3-d1 leu2-d0 met15-d0 ura3-d0 Edc3:mRuby3-KanMX Cop1:mNeonGreen-HygMX*	Colocalisation
MATA	*his3-d1 leu2-d0 met15-d0 ura3-d0 Edc3:mRuby3-KanMX Snf7:mNeonGreen-HygMX*	Colocalisation
MATA	*his3-d1 leu2-d0 met15-d0 ura3-d0 Edc3:mRuby3-KanMX Sec13:mNeonGreen-HygMX*	Colocalisation
MATA	*his3-d1 leu2-d0 met15-d0 ura3-d0 Edc3:mRuby3-KanMX Anp1:mNeonGreen-HygMX*	Colocalisation
MATA	*his3-d1 leu2-d0 met15-d0 ura3-d0 Edc3:mRuby3-KanMX Chc1:mNeonGreen-HygMX*	Colocalisation
MATA	*his3-d1 leu2-d0 met15-d0 ura3-d0 Edc3:mRuby3-KanMX Erg6:mNeonGreen-HygMX*	Colocalisation
MATA	*his3-d1 leu2-d0 met15-d0 ura3-d0 Edc3:mRuby3-KanMX Nop56:mNeonGreen-HygMX*	Colocalisation
MATA	*his3-d1 leu2-d0 met15-d0 ura3-d0 Edc3:mRuby3-KanMX Nic96:mNeonGreen-HygMX*	Colocalisation

MATA	*his3-d1 leu2-d0 met15-d0 ura3-d0 Edc3:mRuby3-KanMX Pex3:mNeon-Green-HygMX*	Colocalisation
MATA	*his3-d1 leu2-d0 met15-d0 ura3-d0 Edc3:mRuby3-KanMX Spc42:mNeon-Green-HygMX*	Colocalisation
MATA	*his3-d1 leu2-d0 met15-d0 ura3-d0 Edc3:mRuby3-KanMX MYO1:mNeon-Green-HygMX*	Colocalisation
MATA	*his3-d1 leu2-d0 met15-d0 ura3-d0 Edc3:mRuby3-KanMX ABP140P:mNeonGreen-HygMX*	Colocalisation
MATA	*his3-d1 leu2-d0 met15-d0 ura3-d0 Edc3:mNeonGreen-HygMX*	Dynamics, Inheritance
MATA	*his3-d1 leu2-d0 met15-d0 ura3-d0 Edc3:mRuby2-KanMX dcp1Δ::HygMX*	Inheritance
MATA	*his3-d1 leu2-d0 met15-d0 ura3-d0 Edc3:mRuby2-KanMX she2Δ::HygMX*	Inheritance
MATA	*his3-d1 leu2-d0 met15-d0 ura3-d0 Edc3:mRuby2-KanMX she3Δ::HygMX*	Inheritance
MATA	*his3-d1 leu2-d0 met15-d0 ura3-d0 Edc3:mRuby2-KanMX myo4Δ::HygMX*	Inheritance
MATA	*his3-d1 leu2-d0 met15-d0 ura3Δ::Mitotag:mRuby2 Edc3:mNeonGreen-HygMX*	*Colocalisation*

List of Bacterial strains used in this study

Plasmids for yeast strain construction were stored in bacterial vectors prior to PCR and yeast transformation. The bacterial strains used for the final data in this study are listed below.

STRAIN BACKGROUND	PLASMID	DESCRIPTION
DH5A *E. COLI*	pFA6a-mNeon-Green:hygMX6	Plasmid with mNeonGreen and Hygromycin resistance marker
TOP10 *E. COLI*	pyomRuby2-KanMX	Plasmid with yomRuby2 and Kanamycin resistance marker
DH5A *E. COLI*	pUG6 (KanMX)	Plasmid with Kanamycin resistance marker
DH5A *E. COLI*	pFA6a-hphMX6 (HygMX)	Plasmid with Hygromycin resistance marker
TOP10 E. COLI	pMitoTag	Plasmid with Tom70 localisation signal fused to mRuby2 and URA3 marker

List of Primers for yeast integrations

Yeast strains were constructed by homologous recombination, below is a list of primers used for the final strains in this study.

DESCRIPTION	5' - 3' SEQUENCE

AMPLIFY MNEONGREEN-HYGMX WITH HOMOLOGOUS ENDS FOR ABP140P FUSION	GTACCGCTGCTGGGTACAAGCTGTGTTTGAC-GTTCCTCAAGGTGGTTCTGGTTCTATGGTGAGCAAGGGCGAGGA
	TTAAAGCGACAGATAATATTAAAATGATAGATAGTTTTGACGTTAG-TATCGAATCGACAG
AMPLIFY MNEONGREEN-HYGMX WITH HOMOLOGOUS ENDS FOR SAC6 FUSION	AATTATTACTTTTATCGCTTCGTTAATGACTTT-GAACAAAGGTGGTTCTGGTTCTGGTGG-TATGGTGAGCAAGGGCGAGGA
	GAAAAAAAGTTCACAGGATATATGGCTTAATAAGTAGTTTCGTTAG-TATCGAATCGACAG
AMPLIFY MNEONGREEN-HYGMX WITH HOMOLOGOUS ENDS FOR COP1 FUSION	TAAGATCGGTGCACCTGCATCCGGATTAAGAATACGTG-TAGGTGGTTCTGGTTCTGGTGGTATGGTGAGCAAGGGCGAGGA
	ATATAACTGTTAATTACATAGTCAGTTTTTTTTTTTCACTCGTTAG-TATCGAATCGACAG
AMPLIFY MNEONGREEN-HYGMX WITH HOMOLOGOUS ENDS FOR SNF7 FUSION	TGAAAAAGCATTAAGAGAACTACAAGCAGAAATGGGGCTT-GGTGGTTCTGGTTCTGGTGGTATGGTGAGCAAGGGCGAGGA
	GACAACAAAAAAATAAAAACTATTAATTATGACTTAGCATCGTTAG-TATCGAATCGACAG
AMPLIFY MNEONGREEN-HYGMX WITH HOMOLOGOUS ENDS FOR SEC13 FUSION	TCTTGAGGGTAAATGG-GAACCCGCTGGTGAAGTTCATCAGGGTGGTTCTGGTTCTGGTGG-TATGGTGAGCAAGGGCGAGGA
	ACAAATCTTTAATTGTTATACGTTACTGTACATTATGCGTCGTTAG-TATCGAATCGACAG
AMPLIFY MNEONGREEN-HYGMX WITH HOMOLOGOUS ENDS FOR ANP1 FUSION	TCCTAAAGAAGTTCCATTAGACTTCGACCCTGATAGAAAC-GGTGGTTCTGGTTCTGGTGGTATGGTGAGCAAGGGCGAGGA
	AGTTAAAGACCAAAGAATAGAGGTTTGATATTATTATCGGCGTTAG-TATCGAATCGACAG
AMPLIFY MNEONGREEN-HYGMX WITH HOMOLOGOUS ENDS FOR CHC1 FUSION	GCTGATGAACAGCGCGATGAACGTTCAACCCACAGGATTT-GGTGGTTCTGGTTCTGGTGGTATGGTGAGCAAGGGCGAGGA
	TAAAAGTATATAAATTGAAAAGGCAGTTTCAATCATTTTACGTTAG-TATCGAATCGACAG
AMPLIFY MNEONGREEN-HYGMX WITH HOMOLOGOUS ENDS FOR ERG6 FUSION	CGCCGAAACCCCCTCCCAAACTTCCCAAGAA-GCAACTCAAGGTGGTTCTGGTTCTGGTGG-TATGGTGAGCAAGGGCGAGGA
	ATGCAGTGAATTATAGTTTTTTCTTATTCTGATAGAAAATCGTTAG-TATCGAATCGACAG

AMPLIFY MNEONGREEN-HYGMX WITH HOMOLOGOUS ENDS FOR NOP56 FUSION	TAAAAAGGAAAAGAAGGATAAAAAGAA-GAAAAGTAAGGATGGTGGTTCTGGTTCTGGTGG-TATGGTGAGCAAGGGCGAGGA
	TAATAATATTTCTAAATATACAATATACAGCTTCCAAATCCGTTAG-TATCGAATCGACAG
AMPLIFY MNEONGREEN-HYGMX WITH HOMOLOGOUS ENDS FOR NIC96 FUSION	GGAAACGTACAGCACTTTAATTAATATAGAC-GTCTCTCTAGGTGGTTCTGGTTCTGGTGG-TATGGTGAGCAAGGGCGAGGA
	GACTGAGGCTTTGTACAACGAAAGCCAAAATATTCGATGACGTTAG-TATCGAATCGACAG
AMPLIFY MNEONGREEN-HYGMX WITH HOMOLOGOUS ENDS FOR PEX3 FUSION	CAGCAACTTTGGCGTCTCCAGCTCGTTTTCCTTCAA-GCCTGGTGGTTCTGGTTCTGGTGGTATGGTGAGCAAGGGCGAGGA
	TGCAGGGTAATGTCATGTTACCTATTGCACACTTACTGTACGTTAG-TATCGAATCGACAG
AMPLIFY MNEONGREEN-HYGMX WITH HOMOLOGOUS ENDS FOR SPC42 FUSION	TATGTCAGAAACATTCGCAACTCCCACTCCCAA-TAATCGAGGTGGTTCTGGTTCTGGTGGTATGGTGAGCAAGGGCGAGGA
	CCGATAGCATTAATCCTTACTTATACGTCTATTCGTAGGACGTTAG-TATCGAATCGACAG
AMPLIFY MNEONGREEN-HYGMX WITH HOMOLOGOUS ENDS FOR MYO1 FUSION	AAATATTGATAGTAACAATGCACAGAGTAAAATTTTCAG-TGGTGGTTCTGGTTCTGGTGGTATGGTGAGCAAGGGCGAGGA
	GTACCACCTTTAAGACTACTATCGAAGGATACGGGGTGAACGTTAG-TATCGAATCGACAG
AMPLIFY YOMRUBY2 + MARKER WITH HOMOLOGOUS ENDS FOR EDC3 FUSION	TATACGTATGTATCCAGTTTAGGCTAAAGTAATTCTTGGTgcataggccac-tagtggatctgatatcacc
	TGATCTTTTCGTCACTGACGGGTCCCTGCTATTAGATTTGATCGGTGAC-GGTGCTGGTTTAATTAAC
AMPLIFY MNEONGREEN + MARKER WITH HOMOLOGOUS ENDS FOR EDC3 FUSION	TGATCTTTTCGTCACTGACGGGTCCCTGCTATTAGATTT-GGGTGGTTCTGGTTCTGGTGGTATGGTGAGCAAGGGCGAGGA
	TATACGTATGTATCCAGTTTAGGCTAAAGTAATTCTTGGTgcataggccac-tagtggatctgatatcacc
AMPLIFY MITOTAG-MRUBY2 CONSTRUCT WITH HOMOLO-GOUS ENDS FOR URA3 LOCUS INTEGRATION	CATATTTATGGTGAAGGATAAGTTTTGACCATCAAAGAAGCACTATA-GAACGCGGCCGCC
	GGATAGTTCCTTTTTATAAAGGCCATGAAGCTTTTTCTTTCAC-TATAGGGAGACCGGCAG
	TCTAAAACACAAAAAAACAAAAAAAATCCTATAACCAGTTCTCCCG-CATGATATGGACATATTGTCGTTAGAACG

AMPLIFY A MARKER WITH HOMOLOGOUS ENDS TO REPLACE MYO4	ATTTTCTGTCTAATTTTATAATTTTACTGACAGTAGCTAAGCCCTCTGTATGAGCGAGGAAGCGGAAGAGC
AMPLIFY A MARKER WITH HOMOLOGOUS ENDS TO REPLACE SHE2	GTAAACCCTCCTTAATTTTCCTTTTGCATAATACCAGACACTTAAAAAATATGGACATATTGTCGTTAGAACG GATGCTGAAAATGAGTACGCCAGAATAAGAGCCGATCATCAGTGTTTTGATGAGCGAGGAAGCGGAAGAGC
AMPLIFY A MARKER WITH HOMOLOGOUS ENDS TO REPLACE SHE3	TTATTGATTTGTTGCCATGAGTAGCAGCAGTCTGAAGGGGTTACCAAACGATATGGACATATTGTCGTTAGAACG AAGTGAAAAATATGGATTCGTGTCTATAAAACCTTAGAGGCATCTATTTATGAGCGAGGAAGCGGAAGAGC
AMPLIFY A MARKER WITH HOMOLOGOUS ENDS TO REPLACE DCP1	AGCAAGAAAGAAAAGAAAATTGACGAAAAAACAATAGAGAATATGGACATATTGTCGTTAGAACG TCACTTGGGCATCTCACCTCTGTGCTCAAGCAAAAGAATCTGAGCGAGGAAGCGGAAGAGC

ImageJ Analysis Macros

Macro to select cell outlines manually

```
dir1 = getDirectory("Choose Source Directory");
dir2 = getDirectory("Choose Destination Directory");
list = getFileList(dir1);
setBatchMode(true);
for (i = 0; i < list.length; i++) {
    showProgress(i + 1, list.length);
    filename = dir1 + list[i];
    if (endsWith(filename, ".tif")) {
        open(filename);
        var name = File.name;
        setBatchMode(false);
        waitForUser("Select Cells", "Please select cells using ROIs and press t to add to the list");
        setBatchMode(true);
        roiManager("Save", dir2 + name + ".zip");
        roiManager("Deselect");
        roiManager("Delete");
        run("Close All");
    }
}
```

Macro to segment cells from phase contrast and manually fix

```
setBatchMode(true);
dir1 = getDirectory("Choose Image Directory");
list = getFileList(dir1);
for (i = 0; i < list.length; i++) {
    showProgress(i + 1, list.length);
    if (endsWith(list[i], "/")) {
        subdir = dir1 + list[i];
        name = File.getName(subdir);
        sublist = getFileList(subdir);
        for (j = 0; j < sublist.length; j++) {
```

```
            if (endsWith(sublist[j], "Merge/")) {
                subsubdir = subdir + sublist[j];
                name2 = File.getName(subsubdir);
                subsublist = getFileList(subsubdir);
                for (m = 0; m < subsublist.length; m++) {
                    filename = subsubdir + subsublist[m];
                    if (endsWith(filename, ".tif")) {
                        open(filename);
                        name3 = File.nameWithoutExtension;
                        rename("image");
                        run("Split Channels");
                        selectWindow("C2-image");
                        run("Despeckle", "stack");
                        run("Smooth", "stack");
                        run("Enhance Contrast...", "saturated=5 normalize pro-
cess_all");
                        run("Auto Threshold", "method=Otsu white stack");
                        run("Watershed", "stack");
                        if (roiManager("count") > 0) {
                            roiManager("Deselect");
                            roiManager("Delete");
                        }
                        setBatchMode(false);
                        waitForUser("Fix Errors manually then press OK");
                        setTool("ROI Tool");
                        waitForUser("Add ROI every 5 divisons");
                        selectWindow("C1-image");
                        roiManager("Save", dir1 + File.separa-
tor + name + File.separator + name2 + File.separator + "maskset.zip");
                        if (roiManager("count") > 0) {
                            roiManager("Deselect");
                            roiManager("Delete");
                        }
                        selectWindow("C1-image");
                        saveAs("TiFF", dir1 + File.separator + name + File.separa-
tor + name2 + File.separator + name3 + "Fluor");
                        run("Close All");
                    }
                }
            }
        }
    }
}
```

Macro to crop image and mask files

```
setBatchMode(true);
dir1 = getDirectory("Choose Image Directory");
dir2 = getDirectory("Choose Mask Directory");
dir3 = getDirectory("Choose Save Directory");
list = getFileList(dir1);
for (i = 0; i < list.length; i++) {
    showProgress(i + 1, list.length);
    if (endsWith(list[i], "/")) {
        subdir = dir1 + list[i];
        subdir2 = dir2 + list[i];
        name = File.getName(subdir);
        name2 = File.getName(subdir2);
        sublist = getFileList(subdir);
        sublist2 = getFileList(subdir2);
```

```
        for (j = 0; j < sublist.length; j++) {
            filename = subdir + sublist[j];
            if (endsWith(filename, ".tif")) {
                open(filename);
                name2 = File.nameWithoutExtension;
                mask = subdir2 + name2 + "_mask_mask.tif";
                rename("image");
                open(mask);
                name3 = File.nameWithoutExtension;
                rename("mask");
                run("Analyze Particles...", "add");
                selectWindow("mask");
                close();
                selectWindow("image");
                run("Split Channels");
                selectWindow("C1-image");
                roiManager("Select", 0) run("Make Inverse");
                run("Colors...", "foreground=black background=black selection=yel-
low");
                run("Fill", "slice");
                selectWindow("C2-image");
                roiManager("Select", 0) run("Make Inverse");
                run("Colors...", "foreground=black background=black selection=yel-
low");
                run("Fill", "slice");
                run("Merge Channels...", "c1=C1-image c2=C2-image c4=C3-image cre-
ate");
                path = dir3 + name;
                File.makeDirectory(path);
                saveAs("TiFF", dir3 + File.separator + name + File.separa-
tor + name2);
                roiManager("Deselect");
                roiManager("Delete");
                run("Close All");
            }
        }
    }
}
```

Macro to select individual cell masks for further analysis

```
dir1 = getDirectory("Choose Source Directory");
dir2 = getDirectory("Choose Mask Directory");
list = getFileList(dir1);
for (i = 0; i < list.length; i++) {
    showProgress(i + 1, list.length);
    if (endsWith(list[i], "/")) {
        subdir = dir1 + list[i];
        sublist = getFileList(subdir);
        for (j = 0; j < sublist.length; j++) {
            filename = subdir + sublist[j];
            if (endsWith(filename, ".tif")) {
                open(filename);
                var name = File.nameWithoutExtension;
                rename("image");
                doWand(100, 100);
                setTool("wand");
                waitForUser("Select Cells");
                run("Analyze Particles...", "  show=Masks");
                selectWindow("image");
```

```
                close();
                selectWindow("Mask of image");
                path = dir2 + list[i];
                File.makeDirectory(path);
                saveAs("TiFF", dir2 + list[i] + name + "_" + "mask" + "");
                run("Close All");
            }
        }
    }
};
```

Macro to extract p body sizes and densities from masked cells

```
// turn on batch processing
setBatchMode(false);
run("Set Measurements...", "area integrated redirect=None decimal=3"); // ask for directories
dir1 = getDirectory("Choose Image Directory");
dir2 = getDirectory("Choose Mask Directory");
dir3 = getDirectory("Choose Results Save Directory"); // extract file lists
imagelist = getFileList(dir1);
maskdirlist = getFileList(dir2); // start loop of images
for (i = 0; i < imagelist.length; i++) {
    showProgress(i + 1, imagelist.length); // set up subdirectories and get image lists, get mask lists of the same
    if (endsWith(imagelist[i], "/")) {
        subdir = dir1 + imagelist[i];
        maskdir = dir2 + imagelist[i];
        sublist = getFileList(subdir);
        masklist = getFileList(maskdir);
        for (j = 0; j < sublist.length; j++) {
            filename = subdir + sublist[j];
            mask = maskdir + masklist[j]; //open file
            run("Bio-Formats Importer", "open=filename color_mode=Default specify_range view=Hyperstack stack_order=XYCZT c_begin=2 c_end=2 c_step=1 t_begin=1 t_end=1 t_step=1");
            rename("image"); // process image for analysis
            run("Enhance Contrast", "saturated=0.35");
            run("Despeckle");
            run("Smooth");
            open(mask);
            rename("mask");
            selectWindow("mask");
            if (roiManager("count") > 0) {
                roiManager("Deselect");
                roiManager("Delete");
            }
            run("Analyze Particles...", "add");
            if (roiManager("count") > 0) {
                maskset = maskdir + "maskset " + i + ".zip";
                roiManager("Save", maskset);
                selectWindow("mask");
                close(); // cycle through ROIs
                n = roiManager("count");
                for (m = 0; m < n; m++) {
                    roiManager("Deselect");
                    roiManager("select", m);
                    run("Measure");
                    saveAs("Results", dir3 + "Cell " + i + "-" + m + " size");
                    run("Clear Results");
```

```
                        selectWindow("image");
                        run("Find Maxima...", "noise=50 output=[Single Points]");
                        selectWindow("image Maxima");
                        run("Watershed");
                        if (roiManager("count") > 0) {
                            roiManager("Deselect");
                            roiManager("Delete");
                        }
                        run("Analyze Particles...", "add");
                        selectWindow("image Maxima");
                        close();
                        dotset = maskdir + "dotset " + i + "-" + m + ".zip";
                        if (roiManager("count") > 0) {
                            roiManager("Save", dotset);
                        } //record number of bodies per cell
                        x = roiManager("count");
                        print(x);
                        selectWindow("Log");
                        saveAs("Text", dir3 + "Body Count Cell " + i + "-" + m);
                        print("\\Clear");
                        if (x > 0) { // cycle through ROIs and meas-
    ure p body size and intensity
                            for (y = 0; y < x; y++) {
                                roiManager("Deselect");
                                selectWindow("image");
                                roiManager("select", y);
                                run("Enlarge...", "enlarge=8 pixel");
                                run("Duplicate...", "title=image-1");
                                selectWindow("image-1");
                                run("Select None");
                                run("Duplicate...", "title=image-2");
                                selectWindow("image-2");
                                run("8-bit");
                                run("Auto Local Threshold", "method=Otsu radius=15 pa-
    rameter_1=0 parameter_2=0 white");
                                run("Invert LUT");
                                if (roiManager("count") > 0) {
                                    roiManager("Deselect");
                                    roiManager("Delete");
                                }
                                saveAs("TiFF", dir3 + "Cell " + i + "-" + m + "-
    " + y + "mask");
                                rename("image-2");
                                doWand(8, 8);
                                roiManager("Add");
                                selectWindow("image-2");
                                close();
                                selectWindow("image-1");
                                roiManager("Select", 0);
                                run("Measure");
                                selectWindow("image-1");
                                saveAs("TiFF", dir3 + "Cell " + i + "-" + m + "-
    " + y);
                                close();
                                if (roiManager("count") > 0) {
                                    roiManager("Deselect");
                                    roiManager("Delete");
                                }
                                roiManager("Open", dotset);
                            } // end of analyse single body loop – open next body
                                saveAs("Results", dir3 + "Cell " + i + "-" + m);
                                run("Clear Results");
```

```
                            } // end of analyse all bod-
    ies in a cell loop – open next cell
                            if (roiManager("count") > 0) {
                                roiManager("Deselect");
                                roiManager("Delete");
                            }
                            selectWindow("image");
                            roiManager("Open", maskset);
                        } // end of entire image loop, close im-
    age and open next one
                    }
                    run("Close All");
                } // goes to next image
            } // goes to next folder
        } // end of script
```

Buffer Compositions

TAE Buffer 50X

Composition:

2.0 M Tris acetate

0.05 M EDTA

pH 8.2 – 8.4 (at 25°C)

TAE Buffer 1X

Composition:

40 mM Tris acetate

1 mM EDTA

pH 8.2 – 8.4 (at 25°C)

CCMB80 Buffer

10 mM KOAc pH 7.0 (10 ml of a 1M stock/L)

80 mM CaCl2.2H2O (11.8 g/L)

20 mM MnCl2.4H2O (4.0 g/L)

10 mM MgCl2.6H2O (2.0 g/L)

10% glycerol (100 ml/L)

adjust pH DOWN to 6.4 with 0.1N HCl if necessary, add dH20 to desired volume, sterile filter and store at 4°C

SOB Medium

0.5% (w/v) yeast extract

2% (w/v) tryptone

10 mM NaCl

2.5 mM KCl

20 mM MgSO4

Adjust to pH 7.5 prior to use with NaOH

Yeast Synthetic Complete (SC) Medium

Ammonium Sulphate	5

Vitamins µg/l		Supplements mg/l	
Biotin	2	Adenine Sulphate	18
Ca-Panthotenate	400	Alanine	76
Folic Acid	2	Arginine	76
Inositol	2000	Asparagine	76
Nicotinic Acid	400	Aspartic Acid	76
p-Aminobenzoic Acid	200	Cysteine	76
Pyridoxine HCl	400	Glutamine	76
Riboflavin	200	Glutamic Acid	76
Thiamine HCl	400	Glycine	76
Trace Elements µg/l		Histidine	76
		Inositol	76
Boric Acid	500	Isoleucine	76
Copper Sulfate	40	Leucine	360
Potassium Iodide	100	Lysine	76
Ferric Chloride	200	Methionine	76
Manganese Sulfate		PABA	8
Sodium Molybdate	200	Phenylalanine	76
Zinc Sulfate	400	Proline	76
Minerals g/l		Serine	76
		Threonine	76

KH2PO4	1	Tryptophan	76
Magnesium Sulphate.anh	0.5	Tyrosine	76
Sodium Chloride	0.1	Uracil	76
Calcium Chloride.anh	0.1	Valine	76

Omit Amino acids for drop out medium.

Low fluorescence medium

As above SC medium, omitting Folic Acid and Roboflavin.

YPD Yeast Media

Reagent	Amount to add (per 1 L final volume)	
	Liquid	Agar plates
Bacto agar	--	24 g
Bacto peptone	20 g	20 g
Yeast extract	10 g	10 g
Water	950 mL	950 mL

Autoclave and add sterile filtered glucose to 2%.

YPD+G418 (for 1L)

Same recipe as above.

After autoclaving let cool until 55°C

Add G418 to have a final concentration of 200mg/L

(1 mL of 200mg/mL G418 in 1L of YPD)

YPAD Yeast Media

Bacto-peptone, 20 g

Bacto-yeast extract, 10 g

glucose, 20 g

Adenine sulfate, 40 mg

Bacto-agar, 20 g

Distilled H2O, to 1000 ml

Autoclave

Yeast transformation Stocks

Stocks:

10x LiAc = 1M LiAc pH 7.5

10x TE = 0.1M Tris, 0.01M EDTA pH 7.5

50% PEG

Salmon sperm (carrier DNA)

For chromosomal integration - prepare fresh:

LiAc/TE (in sterile tube)

1 ml LiAc

1 ml TE

8 ml d[H20]

40% PEG/LiAc/TE (in sterile tube)

0.5 ml LiAc

0.5 ml TE

4 ml 50% PEG

Yeast Lysis Buffer

200 mM LiOAc/1% SDS